



Nucleotide Excision Repair: New Approaches to investigate its exceptionally broad substrate specificity

Anna Seck

► To cite this version:

Anna Seck. Nucleotide Excision Repair: New Approaches to investigate its exceptionally broad substrate specificity. Structural Biology [q-bio.BM]. Université Grenoble Alpes [2020-..], 2021. English. NNT : 2021GRALV002 . tel-03536511

HAL Id: tel-03536511

<https://theses.hal.science/tel-03536511>

Submitted on 20 Jan 2022

HAL is a multi-disciplinary open access archive for the deposit and dissemination of scientific research documents, whether they are published or not. The documents may come from teaching and research institutions in France or abroad, or from public or private research centers.

L'archive ouverte pluridisciplinaire **HAL**, est destinée au dépôt et à la diffusion de documents scientifiques de niveau recherche, publiés ou non, émanant des établissements d'enseignement et de recherche français ou étrangers, des laboratoires publics ou privés.

THÈSE

Pour obtenir le grade de

DOCTEUR DE L'UNIVERSITÉ GRENOBLE ALPES

Spécialité : **Biologie Structurale et Nanobiologie**

Arrêté ministériel : 25 mai 2016

Présentée par

Anna SECK

Thèse dirigée par **Joanna TIMMINS**
et codirigée par **Jean-Luc RAVANAT**

Préparée au sein de l'**Institut de Biologie Structurale**
dans l'**École Doctorale Chimie et Sciences du Vivant**

Nucleotide Excision Repair: New approaches to investigate its exceptionally broad substrate specificity

Thèse soutenue publiquement le **19 janvier
2021**, devant le jury composé de :

Monsieur Eric DE FRANCO

Professeur, Université Grenoble Alpes, Président du jury

Monsieur Bertrand CASTAING

Directeur de recherche, CNRS, Rapporteur

Monsieur Nicolaas DE GROOT

Ingénieur Chercheur, CEA, Rapporteur

Madame Anna CAMPALANS

Ingénieur Chercheur, CEA, Examinatrice

Madame Sylvie SAUVAIGO

Présidente LXRepair, Examinatrice

Madame Joanna TIMMINS

Directrice de recherche, CNRS, Directrice de thèse



Remerciements

Tout d'abord, je remercie tous les membres du jury d'avoir accepté d'évaluer mes travaux de thèse : Bertrand Castaing, Nicolaas De Groot, Eric De Francq, Anna Campalans et Sylvie Sauvaigo. Je remercie aussi les membres de mon CSI, Pablo Radicella et Jean-François Constant.

Je remercie Joanna Timmins et Jean-Luc Ravanat de m'avoir donné l'opportunité d'effectuer ma thèse dans leur équipe. Je n'ai pas assez de mots pour exprimer ma gratitude à votre égard. Merci de m'avoir encadrée aussi bien tout au long de cette thèse. Merci pour votre temps et l'accompagnement que j'ai eu. Merci pour votre gentillesse, votre positivité et vos encouragements (surtout quand les manip n'étaient pas les meilleurs). J'ai vraiment apprécié d'avoir travaillé avec vous. Merci pour votre investissement, votre soutien et surtout votre patience. J'ai appris énormément de choses. Je ne pouvais pas espérer mieux comme encadrants. Merci.

Un énorme merci à Salvatore Debonis pour sa grande aide sur mon projet, j'ai beaucoup aimé travailler avec toi. Merci aussi à Sylvain Caillat pour son aide, sa bonne humeur et les chocolats cachés dans son tiroir.

Je remercie tous les membres des groupes VIC et CIBEST avec qui j'ai aimé interagir. Vous m'avez tous mis à l'aise dès mon arrivée. J'ai adoré passer tous ces moments de partage de gâteaux avec vous. C'étaient mes moments préférés après (Ou avant :D) mes manip. Merci à toute l'équipe de Joanna, notamment à Fabienne pour les conseils pour l'après-thèse.

Merci à Anne-Sophie pour ton amitié et ton soutien, Kaiyao, Guillaume pour les pauses café et les mardis KFC entre autres, Laura pour ta super bonne humeur, Kevin qui essaie encore de me torturer à distance, Müge pour son accueil à mon arrivée, ma Rida pour les Green Mango qui requignent, Rana et Rime pour leur gentillesse.

Ibrahima, je te remercie infiniment d'avoir été là, ton soutien a été très précieux.

Merci à mes trois familles Seck, Gueye et Ndiaye. Merci à mes trois Mamans et mes trois Papas. Merci Aby - Chérie, Ousmane, Alioune, Aissatou, Oumou, Diouma, Adjì, Marème. Merci à Léna, Françoise, Elisa, Didi, Sandy, Rachelle, Saoudatou, Fatou, Khadija, Marième, Dido, Sophie.

Cette dernière partie, je la consacre à deux personnes spéciales et chères à mon cœur, Ndeye Sokhna Tall et Maury Tall Seck. Merci pour tout. Merci d'être là, de m'encourager, de me soutenir, de croire en moi. Je te dédie ce manuscrit mon Papa chéri.

TABLE OF CONTENTS

| | |
|---|-----------|
| Introduction..... | 15 |
| 1. Description of DNA, its composition and structure | 16 |
| 2. Sources of DNA damage | 18 |
| 3. DNA repair pathways | 19 |
| 3.1 Double strand break repair | 20 |
| 3.2. Single-strand repair pathways | 24 |
| 3.2.1. Mismatch repair | 24 |
| 3.2.2. Base excision repair | 27 |
| 3.2.3. Direct repair | 31 |
| 3.3. Nucleotide excision repair | 32 |
| 3.3.1. Substrate specificity | 32 |
| 3.3.2 Mechanism of action of NER | 34 |
| 3.3.3. Uvr proteins | 37 |
| 3.3.3.1. UvrA | 37 |
| 3.3.3.2 UvrB | 46 |
| 3.3.3.3. UvrC | 51 |
| 3.3.3.4. UvrD | 57 |
| 3.3.4. Choice of bacterial models for the study of prokaryotic NER | 59 |
| 3.3.4.1. <i>E. coli</i> NER as a model system | 59 |
| 3.3.4.2. Use Uvr proteins from thermophilic bacteria | 59 |
| 3.3.4.3. Alternative: the NER system from the radiation-resistant bacterium <i>Deinococcus radiodurans</i> | 61 |
| 4. <i>Deinococcus radiodurans</i> | 62 |
| 4.1. General presentation and features | 62 |
| 4.2. <i>D. radiodurans</i> NER | 65 |
| Aim of the thesis | 69 |
| Materials and methods | 73 |
| 1. Cloning and mutagenesis | 74 |
| 1.1 Cloning of <i>Deinococcus radiodurans</i> genes | 74 |
| 1.1.1. PCR amplification of the genes | 74 |
| 1.1.2. Digestion of the plasmid | 75 |
| 1.1.3. Ligation reaction | 75 |

| | |
|---|-----------|
| 1.1.4. Transformation of <i>E. coli</i> DH5a cells | 76 |
| 1.1.5. Miniprep DNA extraction, construct verification and DNA sequencing | 76 |
| 1.2. Mutagenesis of UvrC | 77 |
| 2. Protein purification | 78 |
| 2.1. Transformation and expression | 78 |
| 2.2. Protein purification | 78 |
| 2.2.1. UvrA1 | 79 |
| 2.2.2. UvrB | 79 |
| 2.2.3. UvrC | 80 |
| 2.2.3.1. Full-length UvrC, UvrC Δ HhH and the mutants..... | 80 |
| 2.2.3.2. UvrC-NEndo | 81 |
| 2.2.3.3. UvrC-N, UvrC-C | 81 |
| 3. DNA material | 83 |
| 3.1. Oligonucleotides | 83 |
| 3.2. Plasmids | 84 |
| 3.2.1. UVC light treatment | 84 |
| 3.2.2. BPDE treatment | 84 |
| 3.2.3. Cisplatin treatment | 85 |
| 3.2.4. KMnO ₄ treatment | 85 |
| 3.2.5. Riboflavin treatment | 85 |
| 3.2.6. Abasic site treatment | 86 |
| 4. Incision assay | 86 |
| 5. Analysis methods | 87 |
| 5.1. Gel electrophoresis | 87 |
| 5.2. Quantification of DNA bands on TBE-Urea polyacrylamide gels | 88 |
| 6. HPLC-MS/MS | 90 |
| 6.1. Principle | 90 |
| 6.2. Separation of the excised oligonucleotide from the plasmid | 91 |
| 6.3. Sample Preparation | 91 |
| 6.4. Sample analysis | 92 |
| 7. MALDI-TOF | 93 |
| 7.1. Principle | 93 |
| 7.2. Sample preparation | 93 |
| Results | 95 |

Chapter I: Reconstitution of *D. radiodurans* NER in vitro

| | |
|---|-----|
| 1. Principle of the NER incision assay | 96 |
| 1.1. Components of the incision assay | 96 |
| 1.2. Analysis of incision products by electrophoresis on urea polyacrylamide gels | 96 |
| 2. Purification of the UvrA1, UvrB and UvrC proteins from <i>D. radiodurans</i> | 98 |
| 2.1. Purification of drUvrA1 | 98 |
| 2.2. Purification of drUvrB | 99 |
| 2.3. Optimisation of the purification of drUvrC | 100 |
| 3. Optimisation of the incision assay | 105 |
| 3.1. Minimal components of the incision reaction | 105 |
| 3.2. Optimization of UvrB and UvrC concentrations | 107 |
| 3.3. Optimization of the DNA substrate concentration | 110 |
| 3.4. Optimization of the salt concentration and the protein dilution buffer | 111 |
| 3.5. Optimization of the magnesium concentration | 114 |
| 3.6. Optimization of the ATP concentration and Mg ²⁺ / ATP ratio | 116 |
| 3.7. Optimized incision assay conditions | 117 |
| 4. Probing the NER activity using the incision assay | 119 |
| 4.1. 5' and 3' incision reactions: order and sites of cleavage | 119 |
| 4.2. Kinetics of the incision reaction..... | 123 |
| 4.3. Role of ATP in the incision assay | 124 |
| 4.4. Role of divalent cations..... | 126 |
| 4.5. Role of iron and other divalent ions..... | 130 |
| 5. Substrate specificity | 134 |
| 6. Deciphering the role of UvrC and its domains in the incision reaction | 143 |
| 6.1. Characterisation of different UvrC constructs..... | 143 |
| 6.1.1. Preparation of the different constructs | 143 |
| 6.1.2. Activity of UvrC constructs and domains in the incision assay | 145 |
| 6.2. Characterisation of UvrC mutants | 149 |
| 6.2.1. Preparation of UvrC mutants | 149 |
| 6.2.2. Incision activity of UvrC mutants | 150 |

Chapter II: Substrate specificity studies on plasmid DNA

| | |
|---|-----|
| 1. Preparation of the various DNA substrates | 153 |
| 1.1. Separation of the different states of the purified pUC19 plasmid | 153 |
| 1.2. Plasmid treatments | 154 |

| | |
|--|------------|
| 1.2.1. UV-C treatment | 154 |
| 1.2.2. BPDE treatment | 156 |
| 1.2.3. Cisplatin treatment | 156 |
| 1.2.4. KMnO ₄ treatment | 157 |
| 1.2.5. Riboflavin treatment | 157 |
| 1.2.6. Sodium citrate treatment | 158 |
| 2. Optimization of the incision assay using UV-C-irradiated plasmid DNA | 158 |
| 2.1. Optimization of the experimental set-up using agarose gel electrophoresis | 158 |
| 2.2. Kinetics of repair of UV-C treated plasmid DNA | 162 |
| 3. Quantitative analysis of the repair efficiency by HPLC-MS/MS | 164 |
| 4. Analysis of the substrate specificity of <i>D. radiodurans</i> NER | 170 |
| 4.1. Repair of BPDE-conjugated DNA | 170 |
| 4.2. Repair of cisplatin-treated plasmid DNA | 171 |
| 4.3. Repair of plasmid DNA containing BER substrates | 173 |
| 4.3.1. Thymine Glycols | 173 |
| 4.3.2. Abasic sites | 175 |
| 4.3.3. 8-oxodG | 176 |
| 5. Repair efficiency of the substrates by the <i>D. radiodurans</i> NER | 178 |
| 6. Kinetic analysis of the repair of lesion containing plasmid by HPLC MS/MS | 180 |
| 6.1. New conditions of repair for UV-C-pUC19 by UvrABC..... | 182 |
| 6.2. New conditions of repair for cisplatin-pUC19 by UvrABC | 183 |
| 6.3. New conditions of repair for KMnO ₄ -pUC19 by UvrABC | 183 |
| 6.4. New conditions of repair for BPDE-pUC19 by UvrABC | 184 |
| DISCUSSION | 189 |
| 1. Development of a functional NER incision assay | 190 |
| 2. Influence of salt on the incision assay | 190 |
| 3. Roles of UvrA1, UvrA2 and UvrB in the incision assay | 191 |
| 4. Roles of divalent ions in the incision assay | 192 |
| 5. Role of ATP binding and hydrolysis in the incision assay | 194 |
| 6. Characterization of the UvrC protein | 194 |
| 7. Sites of incision..... | 198 |
| 8. Substrate specificity | 198 |
| BIBLIOGRAPHY | 203 |

INTRODUCTION

1. Description of DNA, its composition and structure

DNA stores all the biological information that will be maintained through the cell's life in order to ensure a safe and identical transfer to the next generations. The four different bases composing the DNA molecule Adenine (A), Guanine (G), Cytosine (C) and Thymine (T) ensure a large variability. However, DNA bases always pair up in a specific combination as A-T and G-C (Figure 1.1). The sugar and phosphate moieties form the backbone of the chain by means of the 5'-3' phosphodiester bonds between the nucleotides. A pair of two strands linked by hydrogen bonds between the complementary bases and oriented in an antiparallel conformation makes up the double helix structure: one strand is oriented in the 5'-3' direction and the other one in the 3'-5' direction. This specific pairing plays a major role in the maintenance of genetic information for the reason that a strand can serve as a template for the repair of a damaged base. In eukaryotic cells, this genetic material is found in the nucleus in the form of chromosomes, a complex of DNA and proteins. Unfortunately, live species are exposed to various stresses, both endogenous and exogenous, that can damage and destabilize their genome. DNA is a chemical molecule which can react with other chemicals, or absorb energy from irradiation. Such events introduce a large variety of lesions into the DNA (Table 1.1). If not repaired, the DNA may not be able to replicate or be transcribed, and persisting lesions can also turn into a mutation (permanent change) thus to a change in DNA sequence that may impact gene regulation, affect heredity, or trigger cell death or cancer (Travers and Muskhelishvili, 2015).

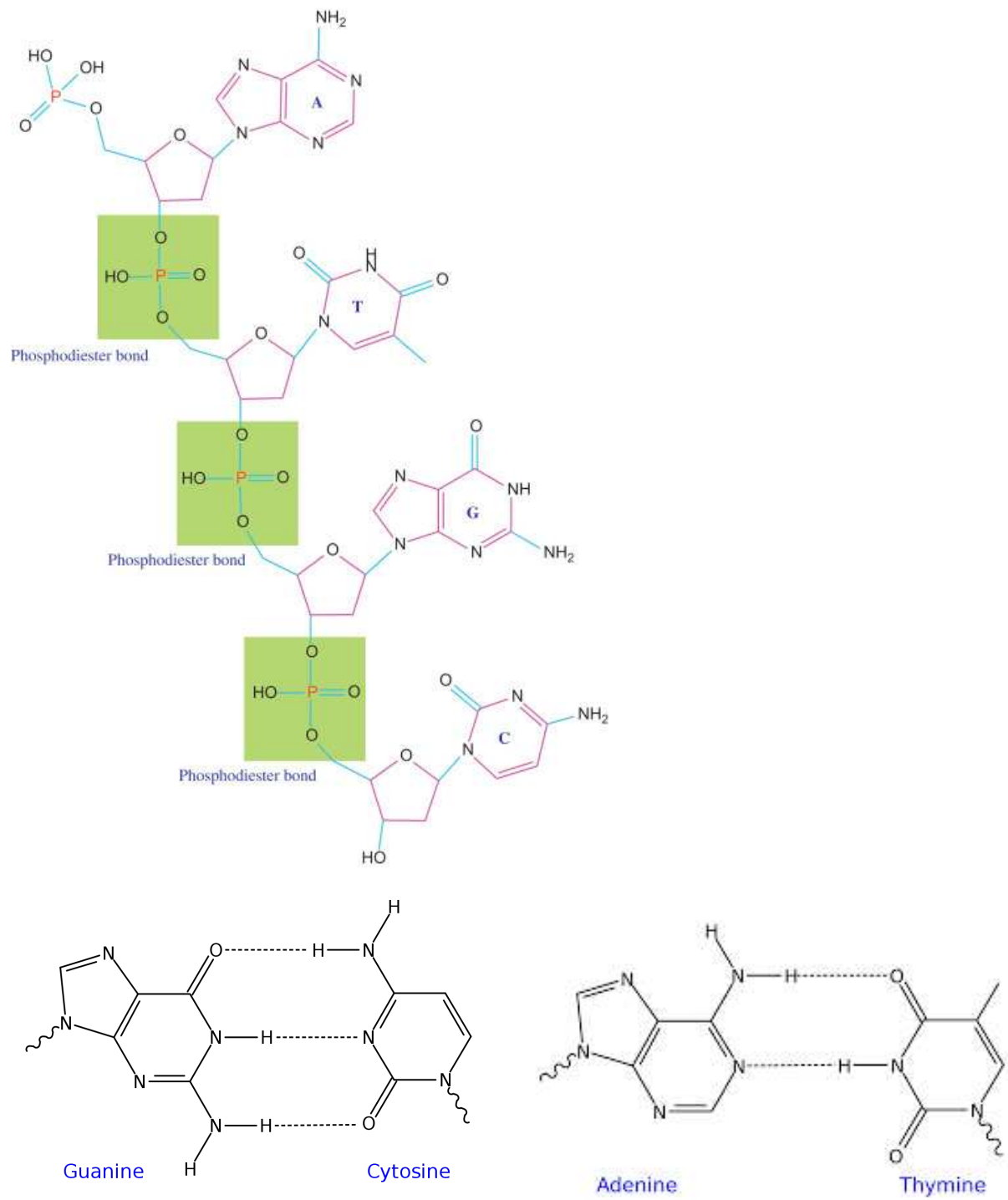


Figure 1.1: Biochemical structure of the DNA and base pairing.

2. Sources of DNA damage:

In cells, oxygen reacts with different families of electron donors, can trap electrons and trigger a cascade of reactions leading to oxidative stress and the production of reactive oxygen species (ROS: superoxide, hydrogen peroxide...). These ROS, together with the activity of enzymes like topoisomerases, are responsible for the formation of endogenous DNA damages that occur naturally in cells. These spontaneous lesions can be found in the form of deamination, hydrolysis, methylation, or oxidation of bases, but also as single and double strand breaks caused by topoisomerases or AP endonucleases or replication fork collapse. Modifying the properties of the base can be genotoxic, but can also alter the base complementarity during rounds of replication. Additionally, during the latter process, errors can arise as a result of polymerase activity and escape the proofreading steps (Chatterjee and Walker, 2017).

In addition to the damage caused by the cellular metabolism, the cell is also exposed to exogenous agents, which encompass the numerous environmental attacks that can be physical (ultraviolet and ionizing radiation) or chemical (benzopyrene, alkylating agents, platinum compounds and psoralens). The damages and their mechanisms are presented in Table 1.

Table 1.1: Sources of damages of the DNA and lesions that can be caused.

| | Damaging agent | Mode of action | Type of damage |
|--|--|---|---|
| E N D O G E N O U S | Hydrolysis (H ₂ O, High temperature...) | Attacks on DNA backbone Hydrolysis of N-glycosylic bond Deamination of base - Cytosine - Guanine - Adenine | SSB Abasic sites Uracil Xanthine Hypoxanthine |
| | Oxidative stress (Reactive Oxygen Species •O ⁻² , H ₂ O ₂ , •OH, ...) | Hydroxyl radicals Attacks on DNA backbone (phosphodiester bond) | 8-oxo-guanine Thymine Glycols SSB DSB |
| | Methylation (S-adenosylmethionine, methylnitrosourea) | Addition of methyl groups on purines | 7-methylguanine 3-methyladenosine O ₆ -methylguanine |
| | Errors of enzyme (Polymerases, topoisomerases) | Base substitution | Mismatches SSB |

| | | | |
|---|--|---|---|
| E X O G E N O U S | Ionizing radiation (ROS↗) | Hydroxyl radicals | 8-oxo-guanine Thymine Glycols SSB DSB |
| | Ultraviolet radiation UVA (320-400 nm), UVB (290-320 nm), UVC (190-290nm) | Cycloaddition between adjacent pyrimidines | UV-bipyrimidine photoproducts (CPDs, 6-4PPs) SSB DSB |
| | Alkylating agents (MMS, MNNG...) | Methyl groups | O ₆ -methylguanine N ₆ -methyl adenine |
| | Cisplatin | Addition of monoadducts, intrastrand/interstrand cross-links. | intrastrand N7- N7 cross-links (GpG. ApG) |
| | Aromatic Hydrocarbons Aromatic AmineS (Cigarettes smoke, other pollutants) | Electrophilic epoxide adducts Arylnitrenium adducts | dGuo-BPDE dG-AF dG-AAF |

SSB: single strand breaks, DSB: double strand breaks, ROS: reactive oxygen species, CPD: cyclobutane pyrimidine dimers, 6-4PP: 6-4 photoproducts, MMS: methyl methanesulfonate, MNNG: Methylnitronitrosoguanidine, BPDE: Benzo(a)pyrene diol epoxide, AF: N-2-Acetylaminofluorene, AAF: 2-Aminofluorene. Data from (Abbotts and Wilson, 2017; Chatterjee and Walker, 2017; Davies, 2005; Hawkins and Davies, 2001; Lindahl, 1993; Madian and Regnier, 2010; Nikitaki et al., 2015; Tubbs and Nussenzweig, 2017).

Following these attacks, preserving the genome becomes vital for organisms. Prokaryotes and eukaryotes engage in DNA repair mechanisms to survive and restore the integrity of the genetic information. Even though prokaryotic systems are more minimal, the repair pathways from prokaryotes and eukaryotes share a number of conserved features to overcome the disruptive events.

3. DNA repair pathways

To maintain the integrity of DNA, cells must rapidly find lesions and trigger repair pathways that are specific for each category of lesion (Figure 1.2). However repair proteins can be involved in multiple pathways and some lesions may require the action of different pathways (Schofield and Hsieh, 2003). Here we present an overview of the

different bacterial repair systems responsible for removing damage affecting either one or both strands of the DNA duplex.

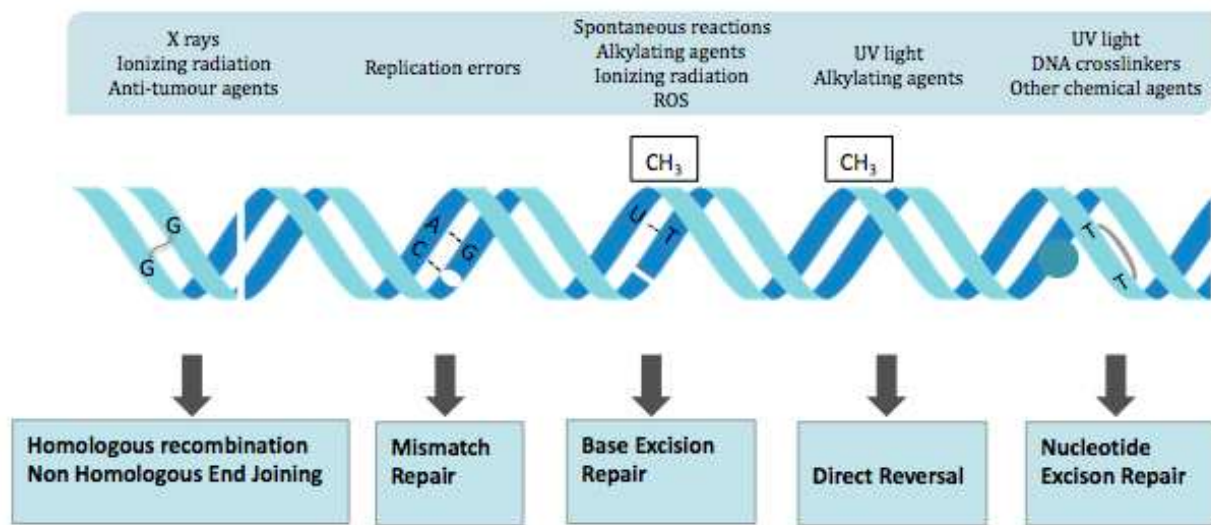


Figure 1.2: Schematic diagram illustrating the main DNA repair pathways present in bacteria. Double-strand breaks are largely repaired by homologous recombination and non-homologous end joining; mismatches, insertions and deletions are repaired by the mismatch repair pathway; single-strand breaks and base modifications are repaired by the base excision repair pathway; damages caused by alkylating agents are repaired by Direct reversal, the photolyases are involved in the repair caused by UV light. Bulky lesions inserted by UV light or DNA crosslinkers are repaired by the NER.

3.1. Double strand break repair

In bacteria, double strand breaks (DSB) are essential for exchange and incorporation of DNA from their environment. However, besides the endogenous sources (recombination or DNA replication fork collapse), DSB can also be caused by external sources, such as ionizing radiation, leading to DNA fragmentation, which is highly hazardous for cells. The pathways responsible for the repair of DSBs are: homologous recombination (HR), non-homologous end joining (NHEJ), extended synthesis-dependent strand annealing (ESDSA) and single strand annealing (SSA), with HR and NHEJ being the major DSB repair pathways (Figure 1.3).

HR requires a second copy of the chromosome carrying the undamaged sequence. This copy will be used as a template for the repair process. In *E. coli*, RecBCD is a helicase-nuclease complex that has been found to bind the dsDNA at the broken spot (blunt or nearly blunt ends) (Lovett, 2011). RecB and RecD are DNA helicases that unwind the DNA duplex. Once RecC hits the Chi sequence (crossover hotspot instigator), the RecB nuclease domain inserts a nick within the Chi site to generate a 3' ssDNA overhang. The protein RecA is then loaded on the overhanging ssDNA to start the strand displacement and exchange with the intact strand and generate Holliday junctions. The junctions are resolved into linear DNA by the RuvABC complex (Dillingham and Kowalczykowski, 2008). The repair presented here is not dependent on replication (replication fork collapse) (White et al., 2018). In *E. coli*, a second pathway, known as the RecFOR system acts as a backup mechanism for HR as shown in *recBC sbcB* mutants (Sandler and Clark, 1994). While RecBCD works on dsDNA, the RecFOR pathway requires the helicase RecQ and the ssDNA exonuclease RecJ in order to first remove nucleotides in the 5' to 3' direction and leave an overhanging 3' ssDNA strand (Ayora et al., 2011; Ivancic-Bace et al., 2003; Lovett, 2011; Lovett and Clark, 1984; Lovett and Kolodner, 1989; Rocha et al., 2005). RecFOR binds the gapped ssDNA, displaces the single-stranded DNA binding (SSB) protein coating the overhanging strand and loads RecA for strand exchange. Nevertheless, as shown by Rocha et al, many bacteria including *Deinococcus radiodurans* do not have the *recBC* genes. Hence, RecFOR is the main pathway for HR in such bacteria (Bentchikou et al., 2010; Cox et al., 2010; Rocha et al., 2005).

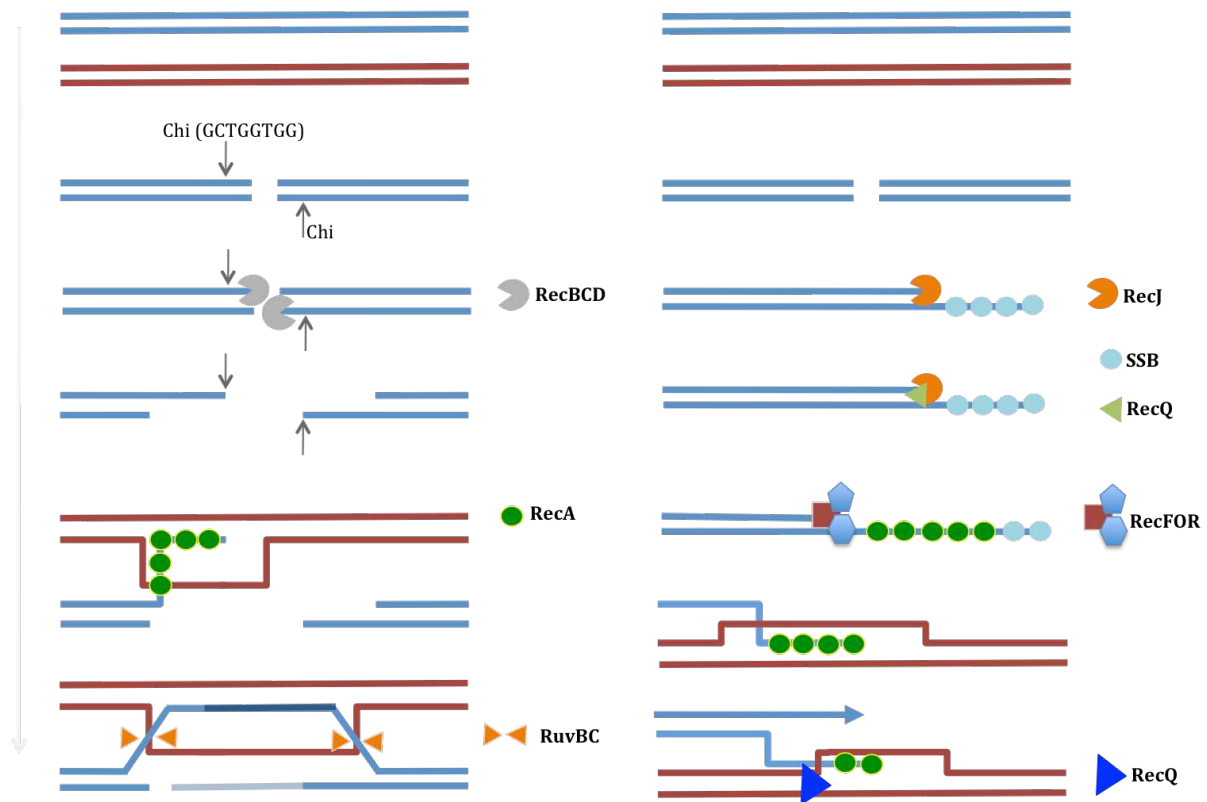


Figure 1.3: Schematic representation of the homologous repair. Left: RecBCD unwinds DNA and nicks one strand at Chi site. The newly generated end is elongated by continued unwinding and is bound by RecA protein which forms a D-loop with another parental duplex. Cutting of the displaced strand in the D-loop allows that strand to pair with the gap in the Chi-containing parent to form a Holliday junction. DNA polymerase extends the end of the filament. After the damaged strand is sufficiently extended, the Holliday junction is cleaved by RuvBC. Right: the double-stranded end is processed by RecQ helicase in combination with RecJ. The single-stranded DNA generated by DNA end-resection is rapidly bound by SSB. RecFOR binds the junction between single-stranded DNA and double-stranded DNA where it displaces SSB and recruits RecA. The RecA-ssDNA filament searches for homology. It forms a D loop, where one strand of the template DNA is displaced by the RecA-ssDNA nucleoprotein filament. After DNA synthesis, to restore the genetic information at the break site, the Holliday junction intermediate may be dissolved by the action of a RecQ helicase.

The second system, the NHEJ repairs DSBs when an intact copy of the chromosome is not available (Figure 1.4). It does not require a template and is thus error-prone. There must be a resection of the ends followed by an extension of the strands. The essential proteins in this system in eukaryotes are the Ku proteins, Ku70 and Ku80 that work as a

heterodimer, for the end binding along with DNA ligase. The bacterial NHEJ studies are more recent than the eukaryotic pathway (Shuman and Glickman, 2007).

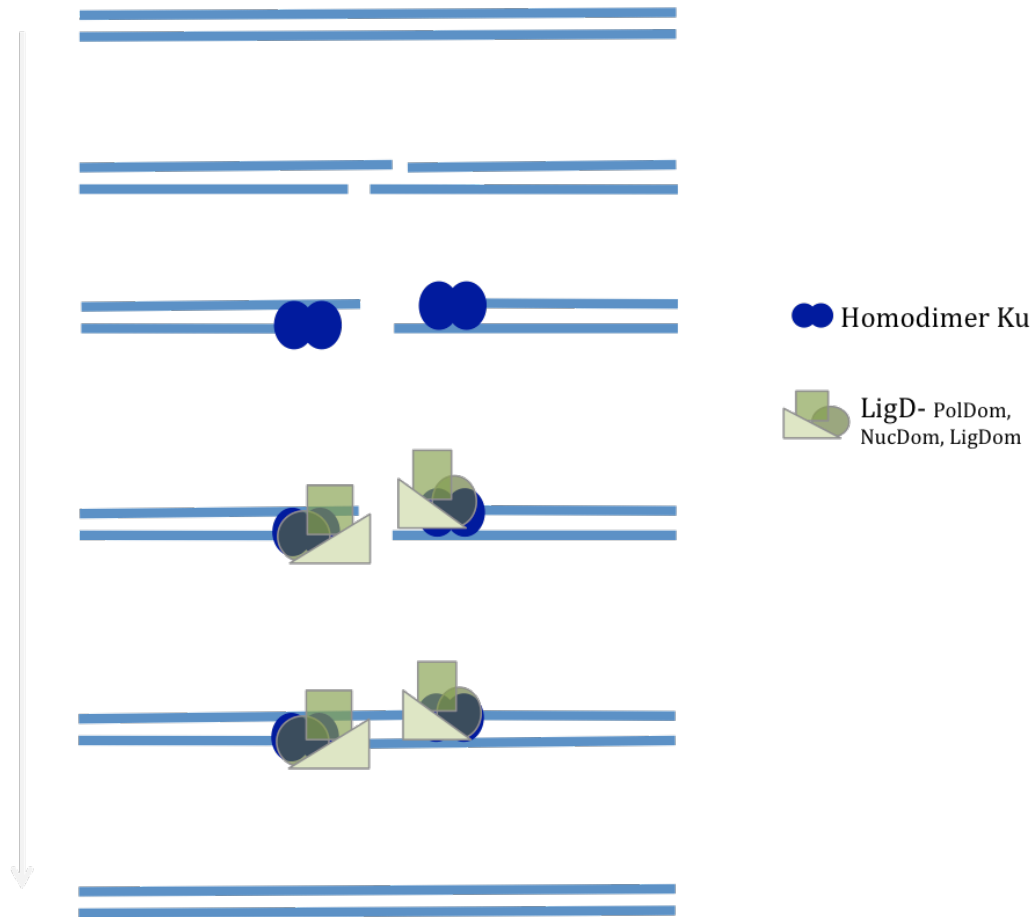


Figure 1.4: Schematic representation of the non-homologous end joining (NHEJ) pathway. NHEJ recruits a homodimer of Ku and LigD for the protection, maturation and synapsis of DNA ends.

In fact, this pathway is not present in all bacteria (not present in *E. coli* for example), but Ku-like proteins have been identified in some bacterial genomes. In bacteria, the Ku is a 30 to 40 kDa protein and is functional as a homodimer with a central ring-like structure around the DNA ends to protect from any non-specific degradations (Pitcher et al., 2007). In *Mycobacteria*, the operons carrying the Ku-like proteins also support the conserved ATP-dependent DNA ligase, LigD. Lig D has three distinct domains: 1) PolDom, a polymerase that is able to extend one strand in a template-dependent way when the paired 5'→3' strand has its overhang, or synthesize nucleotides independently when a template is not available (blunt ends). 2) NucDom, a nuclease that removes the left over

3' phosphate during the DNA breakage to allow the addition of nucleotides and the ligase activity (Glickman, 2014; Shuman and Glickman, 2007). It is a highly regulated domain to avoid excessive resectioning of the 3' end. 3) LigDom, an ATP-dependent ligase domain that seals the breaks. Depending on the nature of the ends following the DSB, they are brought together by the end joining protein Ku then sealed by the ligase activity of LigD (Glickman, 2014). The NHEJ can be mutagenic when it seals blunt ends with the risk of having lost genetic information. Thus, to reduce the loss of information, PolDom and/or NucDom remodel the imprecise ends prior to sealing (Bertrand et al., 2019; Brissett and Doherty, 2009; Weller et al., 2002). In *Deinococcus radiodurans*, this pathway may be present even though Ku-like proteins have not been identified. The protein PprA might play a similar role to Ku proteins (Bowater and Doherty, 2006).

3.2. Single-strand repair pathways

This section deals with repair pathways involved in the elimination of lesions occurring on one of the two strands of DNA. The damage is usually cut out of the strand then polymerases and ligases fill the gap and seal the patch. These processes use the complementary strand as a template. They include mismatch repair (MMR), base excision repair (BER), direct reversal and nucleotide excision repair (NER), the focus of this manuscript.

3.2.1. Mismatch repair

DNA replication is a crucial process for the cell and should be kept error free to avoid any mutation. During this process, the DNA helix is destabilized prior to the copy of each parental strand. The initial double helix is unwound from a specific spot, known as the origin of replication, and the DNA polymerases start the synthesis of new complementary nucleotides, using the parental strands as a template. This critical process comprises multiples events including a proofreading mechanism to minimize replication errors (mismatches, insertions or deletions) (Li, 2008). When an error is inserted in the chain, for instance a nucleotide C, G or A paired with an A in place of a T, a mismatch is detected and DNA replication stops. A 3' exonuclease, DnaQ, then cuts the phosphodiester bond of this misincorporated nucleotide so that it can be replaced (Lovett, 2011).

Unfortunately, some errors occasionally escape the editing functions of the DNA polymerase during the replication and an incorrect base is incorporated into the newly synthesized strand. To differentiate the misincorporated base in the new strand from the correct one, but not matched in the parental DNA, the repair in *E. coli* relies on the state of methylation of the DNA strand. Indeed, it becomes important during this repair process to guide the proteins in order to avoid the removal of the nucleotide in the parental DNA strand that would be replaced to match the wrong base. This event would be a mutation that changes the sequence of the gene and proteins but also the heredity.

The pathway that repairs mismatched bases is the Mismatch Repair pathway (MMR) presented in Figure 1.5 (Shanabruch et al., 1981). In *E. coli*, the enzyme deoxyadenosine methylase (Dam methylase) adds methyl groups to the symmetric sequence GATC/CTAG on the parental strand. This methylation is delayed for the new strand. Hence, this feature will regulate the MMR (Au et al., 1992). In a majority of bacteria, instead of the methyl-directed repair, the strands are discriminated thanks to the discontinuity of the new synthesized strand (Fishel, 2015; Guarné and Charbonnier, 2015; Lacks et al., 1982; Simmons et al., 2008). The mismatch will make a blister caused by the weakened base pairing. This in turn will be detected by a clamp constituted of a dimer of the protein MutS (Wang et al., 2003). In the homodimer of MutS, only one subunit binds the mismatch. The affinity of MutS for the error differs with the sequence: there is a higher affinity for the mismatched base pair G-T or single unpaired bases, which are frequent errors, than for the C-C base pair that is one of the rarest errors (Brown et al., 2001; Dohet et al., 1985; Fazakerley et al., 1986; Kramer et al., 1984; Kunkel and Erie, 2005). This binding step initiates the MMR. MutS motion on the DNA strand is a diffusion-driven slide (Gorman et al., 2007; Jiang et al., 2005). It locates the kink due to the mismatch, binds to the blister and then bends the DNA at a $\sim 60^\circ$ angle. The protein then undergoes conformational changes thanks to ATP-ADP exchanges (Junop et al., 2001). MutS-mismatch forms a complex with a dimer of MutL (Acharya et al., 2003; Junop et al., 2001; Pang et al., 1985). The complex will later activate the endonuclease activity of the protein MutH in *E. coli*. MutH will cleave the new unmethylated strand at the nearest sequence GATC. In the bacteria lacking *mutH* gene, the C-terminus of MutL carries an endonuclease domain that is regulated by the presence of MutS-mismatch complex and ATP (Fukui, 2010; Guarné and Charbonnier, 2015; Simmons et al., 2008). MutL is then responsible for the incisions

in the new strand. The helicase UvrD, driven by SSB protein, unwinds the DNA helix from the cut to slightly further than the mismatch, whilst exonucleases, ExoVII or RecJ for the 5'-3' direction and Exoi and ExoX for the 3'-5' direction, hydrolyze the released fragments. The DNA polymerase III then fills the gap and the ligase links the nick (Au et al., 1992; Burdett et al., 2001; Dao and Modrich, 1998; Fishel, 2015; Fukui, 2010; Hu et al., 2017; Lovett and Kolodner, 1989; Nestmann, 1977; Welsh et al., 1987).

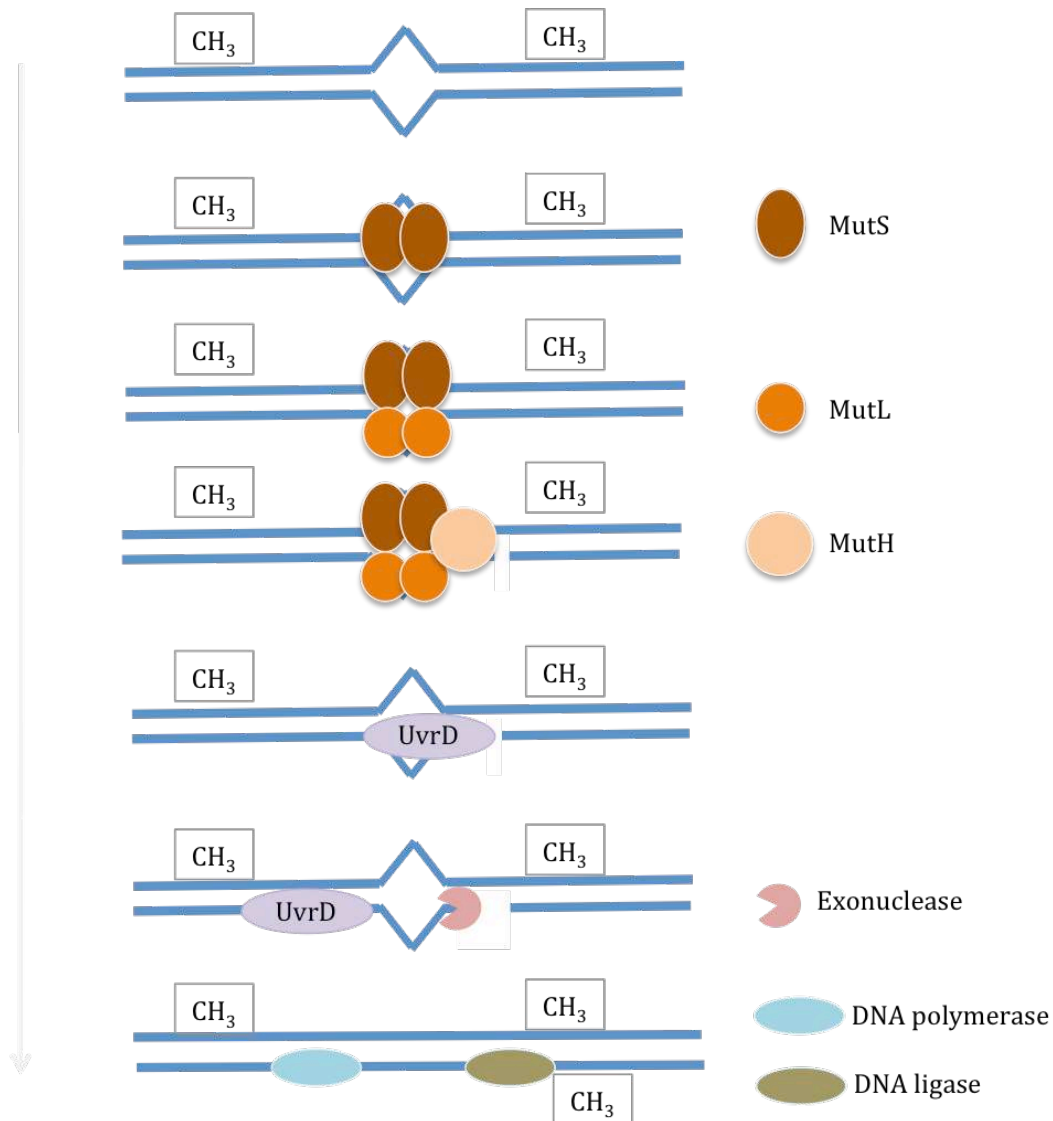


Figure 1.5: Schematic representation of the methyl-directed mismatch repair in *E. coli*. The mismatch recognition by a dimer of MutS (MutS₂) will allow the recruitment of a dimer of MutL (MutL₂). MutH is then activated and cleaves the new unmethylated strand at the nearest GATC sequence. The helicase UvrD unwinds the DNA before the intervention of the exonucleases, ExoVII or RecJ for the 5'-3' direction and Exoi and ExoX for the 3'-5' direction. DNA Pol III fills the gap and DNA ligase seals the remaining nick to finalise the repair.

This pathway is not specific: it repairs any damage that causes a slight distortion in the helix. Those can be base substitution mismatches caused by base analogs or insertion-deletion mismatches of up to four nucleotides causing frameshift mutations for example (Kunkel and Erie, 2005). Furthermore, MutS and MutL participate in the very-short-patch repair (VSP) in order to remove G:T mismatches resulting from the deamination of the methylated cytosine into a thymine (Lieb, 1987).

3.2.2. Base excision repair

Sources of damages, like ROS or ionizing radiation, can alter bases, deoxyribose, free nucleotides, proteins, lipids, or generate abasic sites (Lu et al., 2001). They are able to trigger hydrolysis, alkylation or oxidation of DNA bases. The issue is that during the subsequent round of DNA replication, a damaged base will be incorrectly paired, causing a substitution that could generate transversions from A-T to C-G for example (Figure 1.6).

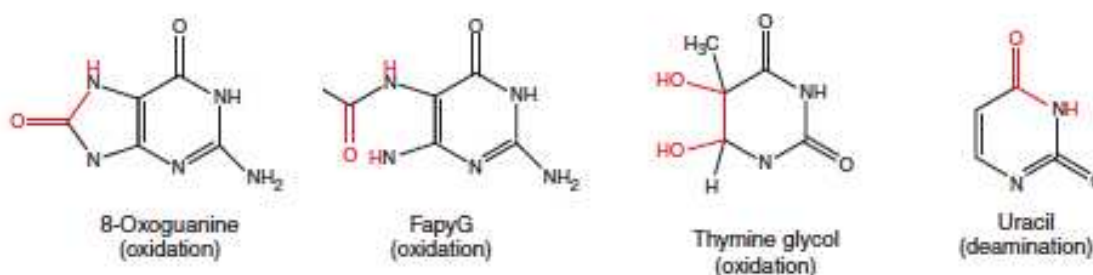


Figure 1.6: Chemical structures of some modified bases repaired by the base excision repair.

These transitions change the information encoded by the sequence. Hence, there is a need to delete damaged bases, a process that is taken care of by the base excision repair (BER) pathway (Figure 1.7).

First, a DNA glycosylase recognizes the lesion and hydrolyzes the N-glycosylic bond between the damaged base and the sugar, which is part of the backbone, thereby creating an apurinic/apyrimidic (AP) abasic site. The next step is performed by an AP endonuclease, which cuts the phosphate-sugar backbone on the 5' side of the abasic site, leaving a 3'OH group and a 5'-deoxyribosephosphate (dRP) which will be removed by a dRPase. Some DNA glycosylases, known as bifunctional, possess an additional AP lyase activity, giving them the ability to remove the lesion and also incise the backbone on the

3' side of the abasic site, leaving a 3'-unsaturated aldehyde or a 3'-phosphate and a 5'-phosphate group at the ends of the DNA (Dianov and Lindahl, 1994; McCullough et al., 1999).

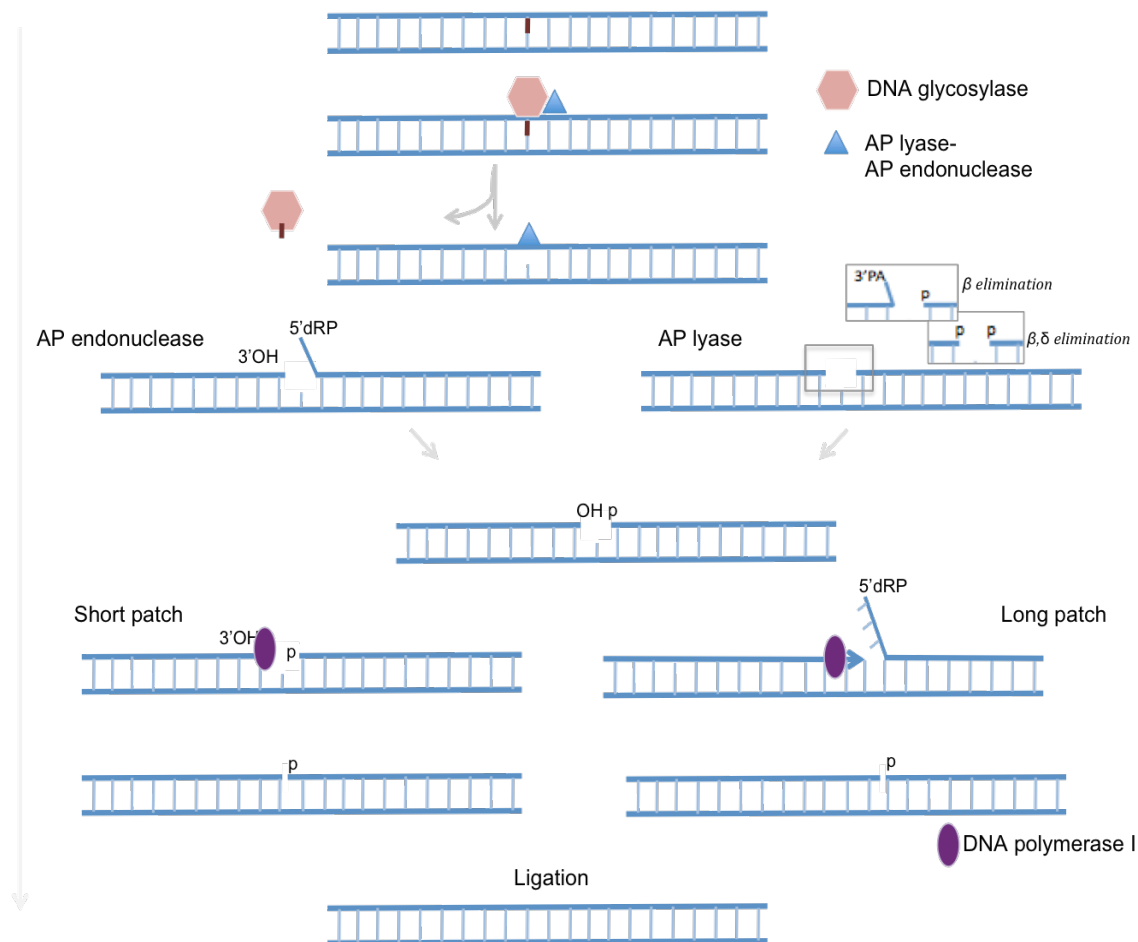


Figure 1.7: Schematic representation of the base excision repair. The damaged base is removed by the DNA glycosylase (salmon). AP endonuclease (blue) nicks on the 5' side of the AP site through a hydrolytic reaction to generate a 3'-OH and 5'-deoxyribosephosphate (dRP). The latter is removed by deoxyribophosphodiesterase (dRPase). When the AP lyase incises an AP site, it produces a 3' unsaturated aldehyde (by β elimination) or 3' phosphate (by β / δ elimination) and a 5'-phosphate. These 3' blocking groups must be removed by 3' phosphoesterase to allow DNA polymerase activity. The DNA polymerase I (purple) can fill the gap with one single nucleotide (short patch BER) or 5 to 10 nucleotides (long patch BER). A DNA ligase seals the repaired strand to finalize the repair.

To complete the repair, an AP endonuclease processes the 3' cleaved abasic site for it to become a DNA polymerase primer. In *E. coli*, the DNA polymerase I fills the gap with one single nucleotide (short patch BER) or synthesizes more ~5 to 10 nucleotides- while a 5'

exonuclease associated with the polymerase degrades the strand ahead (long patch BER). A DNA ligase subsequently seals the nick to finalize the repair (Dalhus et al., 2009; Kow, 1994).

DNA glycosylases can be classified based on their structure or their functions (Denver et al., 2003; McCullough et al., 1999; Thayer et al., 1995). There are either monofunctional or bifunctional DNA glycosylases and there are almost as many DNA glycosylases as there are types of damaged bases (Table 1.2). Most bacteria possess around 10 DNA glycosylases (Aravind et al., 1999). The most common ones being Formamidopyrimidine DNA glycosylase (Fpg), and MutY for the repair of 8-oxo-7,8-dihydroguanine (8oxoG) for example.

Table 1.2: Bacterial DNA glycosylases and their main substrates. Bifunctional DNA glycosylases are highlighted with a grey background. Adapted from (Brooks et al., 2013; Jacobs and Schar, 2012; Kurthkoti et al., 2020; Lee et al., 2010; Morita et al., 2010).

| DNA glycosylases | Substrates |
|------------------|---|
| UNG | Uracil |
| AlkA | 3-Methyladenine, ethenoA |
| MUG | Hydroxymethyluracil, ethenoC, Xanthine |
| Nfi (Endo V) | Hypoxanthine |
| MutY | Adenine from A:G, A:C and A:GO mispair |
| Fpg (Mut M) | Formamidopyrimidine and 8-oxoguanine from 8oxoG:C |
| Endo III (Nth) | Pyrimidine adducts such as thymine glycol, urea, uracil glycol, FapyG |
| EndoVIII (Nei) | Pyrimidine adducts, TGs, FapyG, FapyA |

Many products can result from base oxidation, but 8-oxo-7,8-dihydroguanine (8oxoG) is the most studied one. It can be paired with C or A that can lead to transversions. It can be repaired by different DNA mechanisms:

- Fpg (or MutM) is a bifunctional DNA glycosylase that acts on oxidative lesions. To operate, Fpg bends the DNA and then processes the lesion in a recognition pocket that has been demonstrated to be flexible enough to allow the repair of 8oxoG, but also Fapy-dG and Fapy-dA (Boiteux et al., 1992; Hamm et al., 2007; Tchou et al., 1994). Fpg removes the

damaged base, cleaves the abasic site on both the 3' and 5' sides through a beta/delta elimination reaction and processes the 3' unsaturated aldehyde end into a 3' phosphate. An AP endonuclease then further processes the 3' phosphate.

- The monofunctional DNA glycosylase MutY is able to recognize an 8oxoG:A mispair. It removes the intact base A from 8oxoG:A before the DNA polymerase I introduces the correct C in front of G to prevent mutation (Fromme et al., 2004; Johnson et al., 1996; Krokan et al., 1997; Manuel et al., 2004; McCann and Berti, 2008).

- MutT is a protein that will remove the 8oxo-dGTP from the nucleotide pool by hydrolyzing it into 8oxo-dGMT so that 8oxoG cannot be incorporated during DNA synthesis (Akiyama et al., 1989).

Another group of abundant oxidative products are the cytotoxic lesions, thymine glycols (TGs). TGs are processed by Endonuclease III (EndoIII), a bifunctional DNA glycosylase that removes oxidized pyrimidines (Dizdaroglu, 2005; Sarre et al., 2019). Another bifunctional N-glycosylase, Nei, can also act on TGs (Zhang et al., 2000).

The detection and recognition process by DNA glycosylases have been the focus of numerous studies (Banerjee et al., 2006, 2005; Bellamy et al., 2007; Blainey et al., 2006; Cao et al., 2004). First, the DNA glycosylase has been shown to bind non-damaged DNA and move using either a 1D diffusion (sliding) or a 3D motion (hopping). A hypothesis is that the recognition of the lesion is both intrahelical and extrahelical (requiring base flipping). There is a partial intrahelical detection: while the DNA glycosylase scans the strand, it also applies a conformational strain (pinching, bending); this way, the enzyme detects a local flexibility due to the presence of the lesion (Banerjee et al., 2006; Mol et al., 1999; Parikh et al., 1999). The conformational change will ease the base flipping out of the helix (Banavali and MacKerell, 2002; Priyakumar and MacKerell, 2006; Qi et al., 2009). This process is necessary to discriminate the damaged base. The flipped base is able to access the enzyme recognition pocket. For instance, the base flipping is essential for Ung to distinguish thymine from uracil (Parker et al., 2007). The base will go through different checkpoints on its way to be inserted into the recognition pocket of the DNA glycosylase (Stivers, 2008; Wagenknecht, 2006). Some recognition pockets can be more specific than others, they will process a various range of damaged lesions (Hollis et al., 2000; O'Brien and Ellenberger, 2004; Stivers and Jiang, 2003; Xiao et al., 1999).

Atomic Force Microscopy studies answered the detection question with MutY (Bangalore et al., 2020). The poor base stacking due to the presence of the lesion causes an instability of the helix that is accentuated with the action of the DNA glycosylase which inserts a hairpin, or a finger residue during DNA interrogation (Yang, 2008). The lower energy barrier and the strain on the DNA backbone makes the lesion a preferential target for base flipping (Bangalore et al., 2020; Yin et al., 2014). Depending on their structure, DNA glycosylases bind to the DNA strand upstream and downstream of the lesion, and interact with both the modified base and the estranged base (Dalhus et al., 2009; Fromme and Verdine, 2003; Sarre et al., 2019). In the case of MutY binding to 8oxoG:A containing DNA, MutY causes a 55° bend in the DNA, whilst the non-damaged DNA displays an average bending angle of 34° during damage searching. This larger angle is interpreted as the flipping of the adenine into the catalytic pocket of the protein (Bangalore et al., 2020).

3.2.3. Direct repair

Other pathways are also involved in base repair such as direct reversal of the damage by photolyases or alkyltransferases. These mechanisms need both energy and electron transfer (Dalhus et al., 2009; Park et al., 1995). Following their activation by blue or near-UV light, photolyases are effective on UV-induced lesions such as CPD and (6-4) photoproducts. The absorbed photons are transferred to excite an anionic FADH⁻ that emits an electron to split the pyrimidine dimer and restore the undamaged DNA. The catalytic cycle is completed after the transfer of the electron to the catalytic cofactor of the photolyases. In organisms lacking photoreactivation activity like *D. radiodurans*, the UV-induced lesions are repaired by the NER.

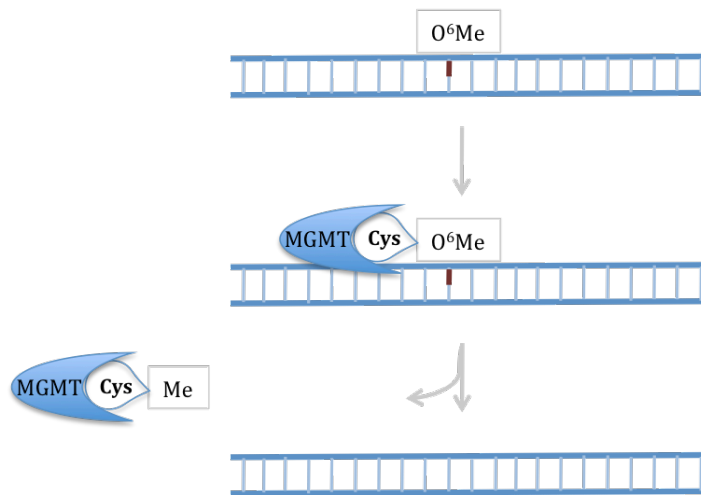


Figure 1.8: Schematic representation of a direct repair pathway: Action of the suicidal DNA repair protein O⁶-methylguanine-DNA-methyltransferase (MGMT). The methyl group of O⁶-alkylguanine (O⁶Me-G) is added to the conserved catalytic cysteine thereby rendering the enzyme inactive.

Alkyltransferases are a group of repair proteins that are consumed during the repair: they repair the mutagenic lesion O⁶-alkylguanine by transferring the alkyl group of the damaged base to themselves whereupon they become inactive (Figure 1.8). The alkyl group is accepted on a catalytic cysteine residue in its active site. It is the case of the protein O⁶-methylguanine-DNA-methyltransferase (MGMT) in *E. coli* (Pegg, 2000). Some bacteria like *D. radiodurans* carry this *mgmt* gene but it is classified as an alkyltransferase-like because it is able to bind O⁶-alkylguanine without the possibility to repair the lesion. It is missing the active site cysteine responsible for the removal of the methyl group. In such cases, these lesions are repaired by an alternative pathway, generally the NER pathway, described in the next section (Rill et al., 2020; Tubbs and Tainer, 2010).

3.3. Nucleotide excision repair

3.3.1. Substrate specificity

NER is one of the single-strand repair pathways. It repairs a broad range of lesions that are structurally and chemically unrelated, but have been proposed to more or less distort the DNA helix (Figure 1.9). Many lesions resulting from the DNA treatment with various damaging agents were identified as substrates of this repair pathway (Table 1.3).

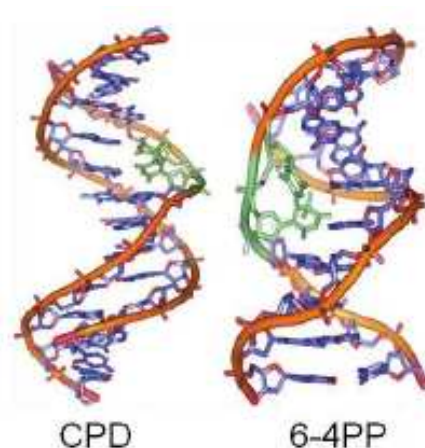


Figure 1.9: Structures of dsDNA molecules holding pyrimidine dimers: CPD (left) and 6-4PP (right), illustrating the distortions in the DNA duplex caused by such lesions (Rastogi et al., 2010).

Some well-known substrates of the NER are generated by UV-damage (Cyclobutane pyrimidine dimers and 6-4-photoproducts), benzo[a]pyrene diol epoxide (BPDE-guanine) and anticancer agents (Guanine *cis*-platinum adducts) (Chatterjee and Walker, 2017; Truglio et al., 2006a). In addition to these substrates, there is also adducts that are synthetically prepared and are mimics for bulky DNA damage (fluorescein-modified thymine). These lesions generally block normal replication and transcription.

Table 1.3: Damaging agents and corresponding DNA lesions repaired by the Nucleotide Excision Repair (Truglio et al., 2006a).

| Damaging agent | Lesions generated- Adduct description |
|---|---|
| Ionizing radiation | Thymine glycol HO-C ⁵ , C ⁶ -thymine DNA-protein crosslinks |
| Anthramycin | N ² -guanine |
| UV irradiation | Cyclobutane pyrimidine dimers, 6-4-photoproducts DNA-protein crosslinks |
| Cisplatin | Guanine <i>cis</i> -platinum adducts |
| N-acetoxy-2-acetylaminofluorene (AAF),N-hydroxyaminofluorene (AF) | C ⁸ -guanine |
| N-methyl-N-nitronitrosoguanidine (MNNG) | O ⁶ -methyl guanine |
| Polycyclic aromatic hydrocarbons (PAHs) | Benzo[a]-pyrene- guanine, N ² -guanine, methylchrysene/C ⁸ -guanine, 1-nitropyrene |

| | |
|-------------|---|
| Psoralen | 8-methoxypsoralen (8-MOP), 4,5',8-trimethylpsoralen (TMP) C ⁵ , C ⁶ -thymine |
| Fluorescein | Synthetically prepared fluorescein adducted thymine |
| Cholesterol | Synthetically prepared cholesterol adducted base |
| Menthol | Synthetically prepared menthol adducted base |

3.3.2 Mechanism of action of NER

Unlike the BER that is initiated by a DNA glycosylase specific for each type of base modification, the prokaryotic NER involves four proteins, UvrA, UvrB, UvrC and UvrD, that act sequentially to repair all NER substrates irrespective of their structure (Kisker et al., 2013) (Figure 1.10). The system in eukaryotes is much more complex with 30 proteins (Gillet and Schärer, 2006; Goosen and Moolenaar, 2008; Kisker et al., 2013; Spivak, 2015). However, some similarities exist between the prokaryotic and eukaryotic processes. In both cases, NER includes substrate recognition, followed by a dual incision of the DNA to release an oligonucleotide containing the lesion, the synthesis of a new DNA strand by DNA polymerase I to fill the gap and a final sealing step performed by a ligase. This pathway can be initiated during two processes: the global genome repair (GGR) and the transcription coupled repair (TCR). As its name implies, the GGR subpathway is recruited during the whole genome inspection to detect the lesions, whilst the TCR is tightly coupled to transcription and is recruited through a transcription factor when the RNA polymerase encounters a discontinuity during its procession along the template strand. This might be the reason why TCR-NER is recruited faster to the lesion on transcribed strands. GGR and TCR rely on the same four Uvr proteins, but in TCR, an additional protein, Mfd, is also needed (Figure 1.10) (Kisker et al., 2013).

Mfd is a protein able to displace the RNA polymerase only when the latter is stopped by a lesion, while processing the transcribed strand (Ganesan et al., 2012). Without *Mfd*, the cells cannot engage into the TCR pathway showing that this protein initiates it. Structurally, Mfd carries a region at its N-terminus, which shares a sequence homology with UvrB, and interacts with UvrA. However this homology does not allow Mfd to participate in the damage recognition process (Assenmacher et al., 2006; Manelyte et al.,

2010). The next region in Mfd is the RNA polymerase interaction domain (RID) followed by helicase motifs involved in DNA binding and a regulatory domain. When Mfd binds the RNA polymerase stalled at the lesion, it triggers an opened conformation of the protein to allow ATP binding by Mfd then DNA binding. The hydrolysis of ATP in the helicase domains of Mfd helps the withdrawal of the DNA from the RNA polymerase that will fall off the DNA strand that is still interacting with Mfd to keep the open conformation. The DNA is wrapped around Mfd. The protein then recruits an UvrA dimer that will then associate with UvrB for damage recognition. From this step, the GG-NER and TC-NER converge. In TCR, the loading of the Uvrs releases Mfd (Selby, 2017).

In GG-NER, UvrA scans the DNA and binds the damaged DNA with a higher affinity than a non-damaged DNA (Orren and Sancar, 1989; Pakotiprapha et al., 2012; Stracy et al., 2016). UvrB is then loaded onto the lesion to form a pre-incision complex and UvrA is released. UvrB then recruits UvrC that is responsible for the incisions of the DNA backbone upstream and downstream of the lesion to release a 12 or 13mer oligonucleotide containing the lesion. UvrD is a helicase that unwinds the DNA, dissociates the UvrBC complex and releases the proteins and the incised DNA fragment. The Polymerase I unhooks UvrB and synthesizes the new nucleotides and the DNA ligase seals the strand (Figure 1.10) (Caron et al., 1985; Husain et al., 1985; Kisker et al., 2013; Orren et al., 1992; Sancar and Rupp, 1983; Truglio et al., 2006a; Van Houten et al., 1988; Verhoeven et al., 2000).

Through single-molecule approaches, the motions of the Uvr proteins during this sequential repair have been analysed to understand how the proteins scan the genome, detect, verify and eliminate the lesions, and how the DNA is handed over to the next protein (Kad et al., 2010; Kad and Van Houten, 2012; Stracy et al., 2016). *In vitro* assays suggest that the search mechanism may involve sliding and/or hopping (*in vitro* assays), while single-molecule *in vivo* imaging indicates that the UvrA dimer or the UvrA-UvrB complex can jump from one strand to another (intersegmental transfer). This process requires the presence of ATP and the ATPase activities of the proteins guide the scanning.

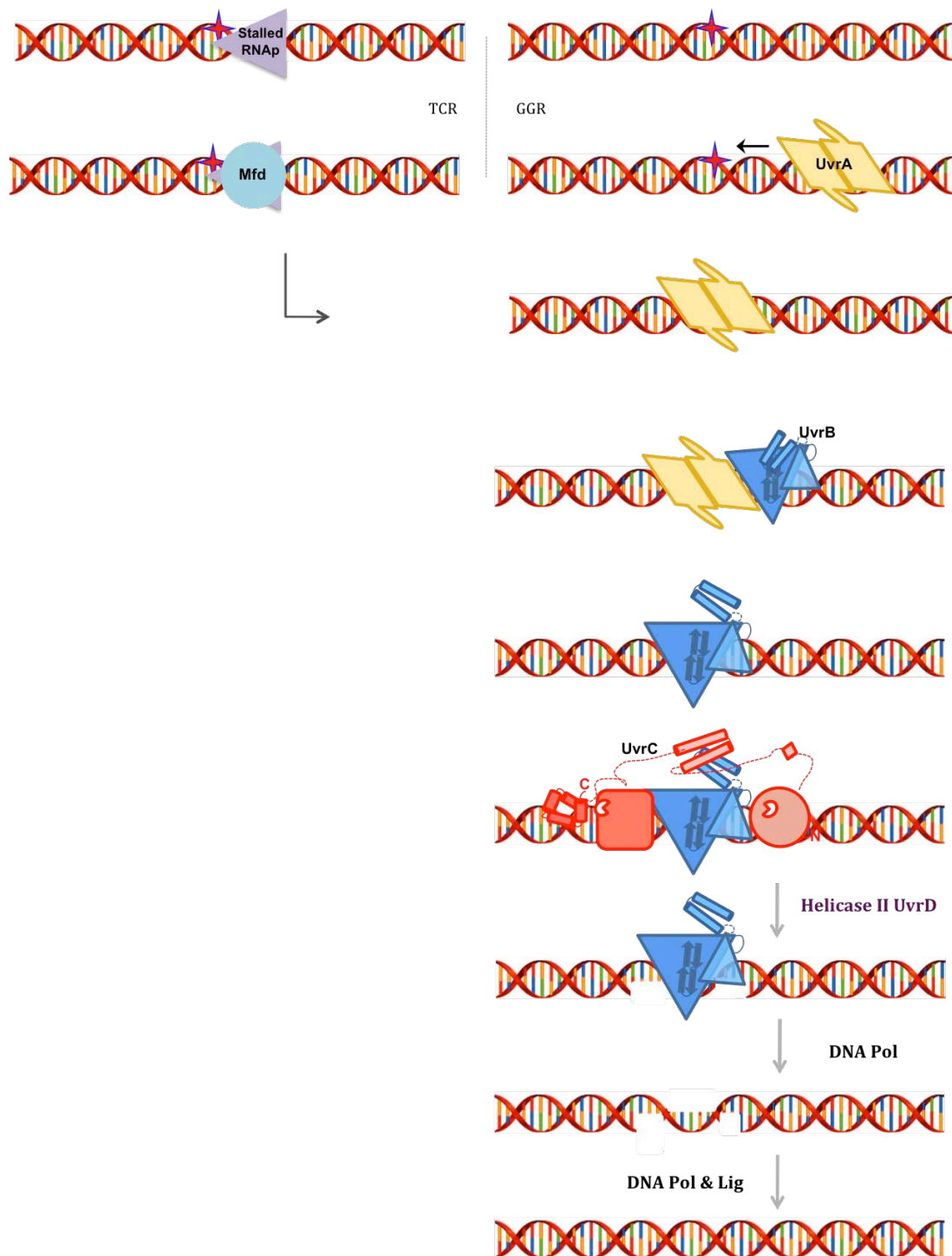


Figure 1.10: Schematic diagram of the nucleotide excision repair pathway. In TCR-NER (left): Mfd (light blue) is recruited at the site of the stalled RNA polymerase. In GG-NER, UvrA (yellow) scans the genome in an ATP-dependent manner in search of lesions. After damage verification UvrB (dark blue) is loaded onto the DNA and a stable UvrB-DNA pre-incision complex is formed, which recruits UvrC (red) to incise the DNA upstream and downstream of the DNA lesion using its two endonuclease domains in order to produce a 12mer fragment containing the modified nucleotide. Finally, UvrD unwinds the DNA duplex to release the DNA fragment and the UvrBC complex to allow the polymerase I to fill the gap and the DNA ligase to seal the nicks.

The abundance of UvrA and UvrB has been shown to increase following exposure to damaging agents. In *E. coli*, these proteins are regulated by the SOS system: after the SOS response is triggered, their levels can rise by 10-fold. UvrC is not under the SOS control. While UvrA levels increase from 25 to 250 copies and UvrB levels increase to around 1000 copies, UvrC levels remain constant at around 10 molecules per cell (Van Houten, 1990). This observation confirms that there is an extensive damage searching by UvrA and UvrB and the protein UvrC intervenes only after verification of the lesion to incise the damaged fragment (Van Houten, 1990). Some bacteria, like *D. radiodurans*, do not possess a SOS response system. In *D. radiodurans*, the regulation occurs instead through transcriptional regulators encoded by the genes *IrrE* and *DdrO* or *DrRRA* and *DdrI* that are upregulated in response to DNA damage and regulate various pathways. *IrrE* is overexpressed 3.77-fold following oxidative stress. Its overexpression might be due to the increase in the level of ROS. *IrrE* is a metalloprotease that cleaves the transcriptional regulator *DdrO*, which is bound to a Radiation Desiccation Response (RDR) motif upstream of a RDR regulon to repress it. Thus, the cleavage induces the expression of the RDR regulon that comprises ~20 genes including *recA*, *uvrA*, *uvrB* and *uvrD* genes (Blanchard et al., 2017; de la Tour et al., 2013; Devigne et al., 2015; Gao et al., 2020).

3.3.3. Uvr proteins

3.3.3.1. UvrA

UvrA is a protein of the ATPase-binding cassette (ABC) family that functions as a dimer (Figure 1.11) (Doolittle et al., 1986; Junop et al., 2001; Locher, 2004; Myles and Sancar, 1991). This assembly relies mostly on hydrophobic forces and the interaction depends on ATP binding and hydrolysis (Zou et al., 1998a). There are five classes of UvrAs, but class I UvrA (UvrA1) is the most studied one and it is present in all bacteria (except *chlamydiae*) (Figure 1.12). This class was first characterized in *E. coli* and is involved in NER. It is a well-conserved protein as can be seen in the sequence alignment presented in Figure 1.13, which shows that UvrAs from different bacterial species share between 50% and 70% sequence similarity.

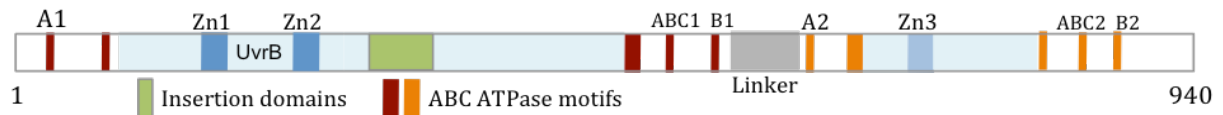


Figure 1.11: Schematic representation of the domain structure of UvrA1. The two nucleotide binding domains (NBD; blue) are separated by a protease sensitive linker (grey). Each NBD possesses the following ATP binding motifs: Walker A (A1 and A2), Walker B (B1 and B2) and ABC signature (ABC1 and ABC2) motifs. UvrA also possesses three Zn binding motifs (dark blue), a UvrB interaction domain (labelled UvrB) and an insertion domain (green).

UvrA1 is a 105kDa protein composed of two tandem ABC-like ATPase domains, also known as nucleotide binding domains, or NBDs, separated by a protease sensitive linker (Figure 1.11). Several additional motifs and subdomains are inserted into each of these NBDs. The amino-terminal NBD I holds two inserted zinc binding domains, while the carboxy-terminal NBD II holds a short zinc-finger (Figure 1.11) (Navaratnam et al., 1989). As shown in Figure 1.14, each NBD is composed of a Walker A motif, a Walker B motif and Q-, D-, H- loops. Between the Walker A and Walker B, there is an ABC signature sequence, Leu-Ser-Gly-Gly and also the cysteine-rich zinc binding motifs (Smith et al., 2002). The other classes of UvrAs are either missing one or several of these subdomains (Class II and Class III), or have duplicated NBDs (Class IV) or a combination of both (Class V) (Figure 1.12). Different classes of UvrA or different UvrAs from a same class can coexist in a given organism (Goosen and Moolenaar, 2008), as is the case in *D. radiodurans*.

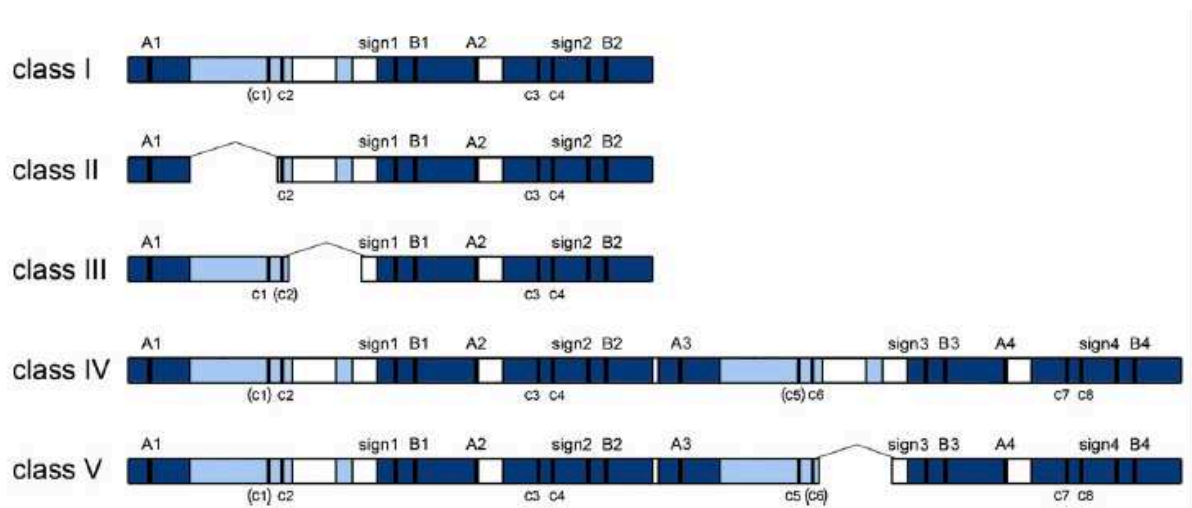


Figure 1.12: Classes of UvrA proteins found in bacteria. Dark blue areas represent domains that are 65–75% conserved among all UvrA proteins. Light blue regions are 30–40% conserved and white regions are 10–15% conserved. Taken from (Goosen and Moolenaar, 2008).

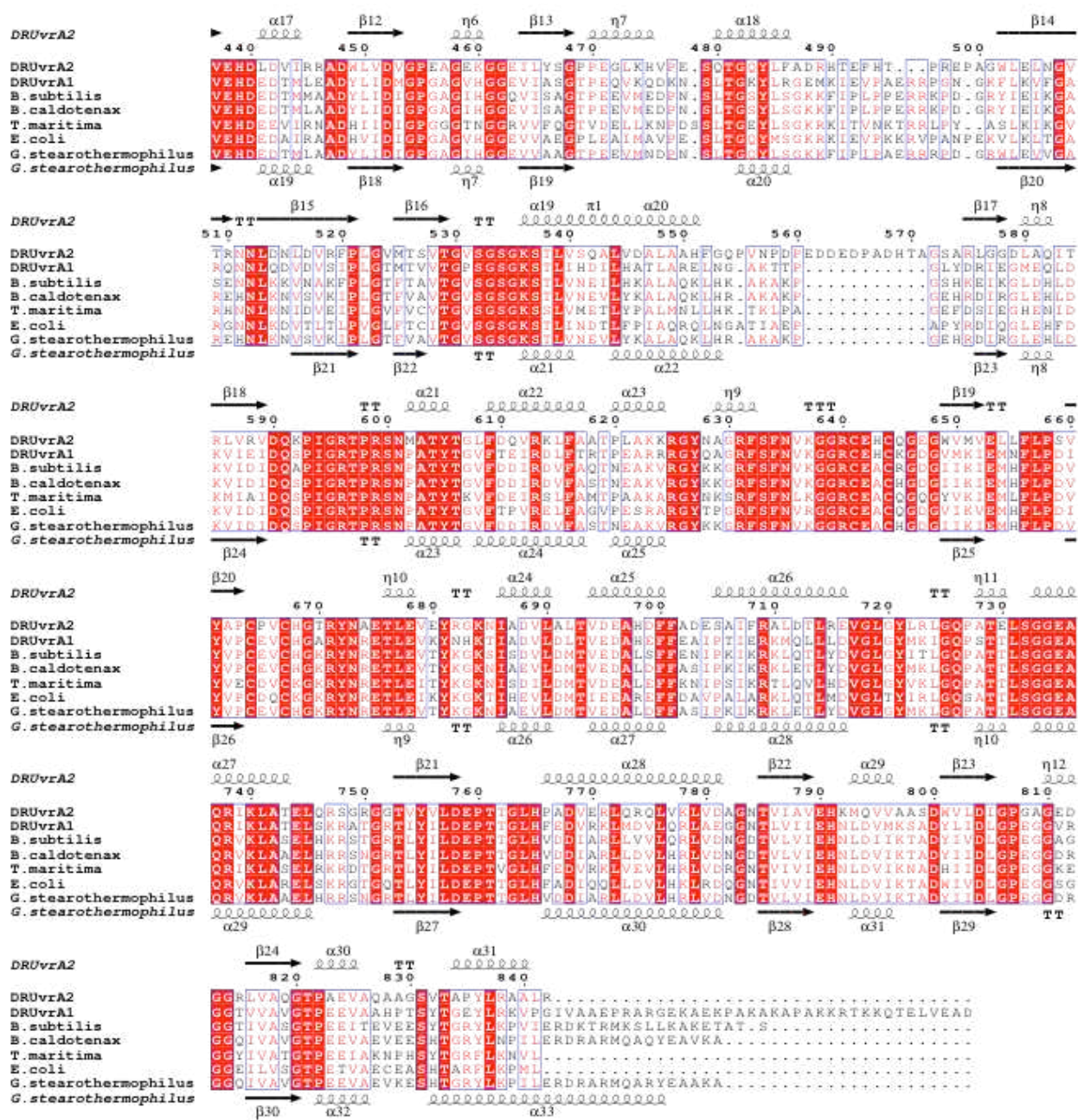


Figure 1.13: Sequence alignment of UvrAs from *D. radiodurans* (UvrA1 and UvrA2), *B. subtilis*, *B. caldotenax*, *T. maritima*, *E. coli* and *G. stearothermophilus*.

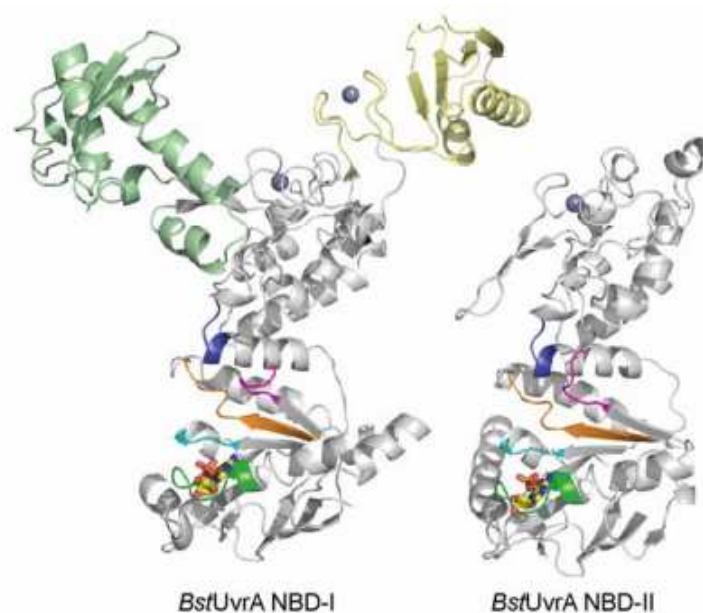
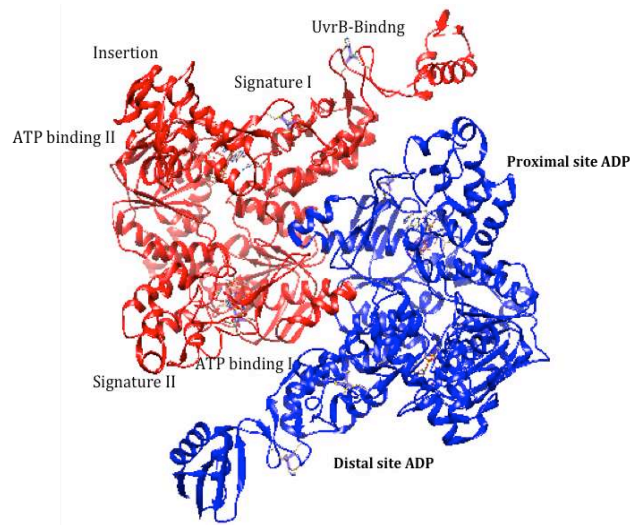


Figure 1.14: Crystal structures of the nucleotide-binding domains of *Bacillus stearothermophilus* UvrA. The conserved ATPase motifs are colored as follows: Walker A, green; Walker B, orange; ABC signature motif, blue; Q-loop, magenta; and H-loop, cyan, Zn atoms, as spheres. The UvrB-binding domain and the insertion domain, which are inserted in the NBD-I of UvrA, are shown in pale yellow and pale green, respectively. Taken from (Pakotiprapha et al., 2008).

The dimer interface is formed by the two NBD-I subunits. Structural data shows that the nucleotides were not found at the interface between the two subunits (Pakotiprapha et al., 2008). The UvrA1 dimer possesses four ATP binding sites: two proximal sites (interface between ATP binding domain I and signature domain II) and two distal sites (interface between ATP binding domain II and signature domain I) (Figure 1.15.A). Each ATP molecule is bound by the Walker A motif, Q-loop, Walker B motif and H-loop from one NBD and the signature motif and D-loop from the second NBD (Figure 1.15.B) (Hopfner and Tainer, 2003; Smith et al., 2002). The Q-loop linking the NBDs is the switch that triggers the rearrangements following nucleotide binding (Hopfner and Tainer, 2003). Without DNA, the proximal sites bind ATP weakly and hydrolyse it slowly, while the distal sites bind more firmly and hydrolyse it rapidly. (Case et al., 2019) The presence of nucleotides stabilizes the UvrA dimer and its structure during DNA binding. The hydrolysis of ATP is required to power the conformational changes (Case et al., 2019; Goosen and Moolenaar, 2001; Pakotiprapha et al., 2012, 2008).

A)



B)

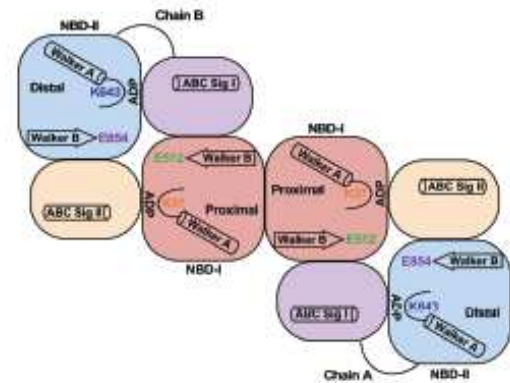


Figure 1.15: A) *Geobacillus stearothermophilus* UvrA structure (two subunits: one red and one blue) (PDB code: 2R6F). B) Schematic illustration of the composite ATP binding sites, showing the two NBDs in each monomer (chains A, B). (Case et al., 2019)

As mentioned previously, the repair is initiated when UvrA locates the damage in the DNA helix. DNA footprinting studies performed with UvrA reveal that the protein covers 32 bases of DNA (Van Houten et al., 1988, 1987). UvrA binds non-damaged DNA as well, but with a lower affinity (Mazur and Grossman, 1991; Timmins et al., 2009). The binding of the protein is presented on Figure 1.16 with palindromic 32-mer with a fluorescein conjugated base in position 14 (Jaciuk et al., 2011).



Figure 1.16: Structure of *Thermotoga maritima* UvrA dimer in complex with a palindromic 32 mer oligonucleotide containing a fluorescein-conjugated thymine in position 14. (Jaciuk et al., 2011)

These findings are supported by further studies of UvrA from *Bacillus stearothermophilus* and also class II UvrA from *D. radiodurans* (Jaciuk et al., 2011; Timmins et al., 2009). UvrA generates a bubble of repair by unwinding the damaged DNA in close proximity to the lesion. This bubble will be necessary for UvrB interaction with the damage strand (Moolenaar et al., 2000a; Zou et al., 2001, 1997; Zou and Van Houten, 1999). Depending on the lesion, there will be different angles in which the DNA helix will be bent and already unwound and it has been proposed that UvrA is able to detect the unstable region as a substrate (Jaciuk et al., 2011). DNA binding involves residues from different regions of the protein: the signature domains, the insertion domains and the zinc fingers (Croteau et al., 2008, 2006; Timmins et al., 2009; Truglio et al., 2006b). These interactions between UvrA and the DNA are affected by temperature, salt, protein concentration and the nucleotide bound state.

Specific residues have been identified as being strongly involved in DNA binding. The structures of the protein showed that the insertion domains are able to allow an open or closed conformation that will give access to the positively charged groove on the ventral side of the protein for DNA binding (Pakotiprapha et al., 2012; Timmins et al., 2009). Mutations in each half of UvrA1 were made to assess the roles of the N-terminal and C-terminal regions. Mutations inserted into the central region of the insertion domain (conserved Lys and Arg mutated to Ala in *Bacillus caldotenax* and *Geobacillus stearothermophilus* UvrA or Glu in *Deinococcus radiodurans* Class II UvrA) disrupt DNA binding or reduce the affinity for DNA (Croteau et al., 2008; Pakotiprapha et al., 2008; Timmins et al., 2009). In *B. caldotenax*, Lys-680-Ala and Arg-691-Ala lessen the binding of a damage-containing substrate by 37-fold. The deletion of eleven highly conserved amino acids (substituted with Gly) in the C-terminal zinc finger did not impede the DNA binding, but affected the damage-specific binding (Croteau et al., 2008, 2006). In *E. coli*, the Cys-763-Phe or Cys-763-Ser mutations in the C-terminal zinc-binding motif resulted in UvrA defective in NER, while the mutations Cys-253-Ser or Cys-256-Ser in the N-terminal zinc-binding domain did not affect the repair (Moolenaar et al., 2000c; Visse et al., 1993; Wang et al., 1994).

The same goes for the residues of the signature domain in the C-terminus (*Thermotoga maritima* UvrA: residues Gly-670, Thr-679, Tyr-680, Arg-688, Lys-704, Ser-705, Ser-708,

and Asn-710) that have the most interaction with the DNA fragment. In fact, these residues allow the binding of four consecutive nucleotides on the DNA. UvrA is mostly found to interact with the DNA backbone (Truglio et al., 2006b). These data show the involvement of the different domains of the C-terminus besides its zinc finger motif mentioned above, which is necessary for damage recognition (Caron and Grossman, 1988; Croteau et al., 2006; Grossman and Thiagalingam, 1993; Moolenaar et al., 2000a; Navaratnam et al., 1989; Timmins et al., 2009; Truglio et al., 2006b; Wang et al., 1994).

The nature of the DNA solicits different ATPase sites activity during the protein binding (Case et al., 2019). Mutations in the zinc finger of the NBD II as well as the NBD I and the helix-turn-helix motif stop UvrA from differentiating damaged DNA and non-damaged DNA due to the destabilization of the ATPase domain (Case et al., 2019; Croteau et al., 2006; Kraithong et al., 2017; Wang et al., 1994; Wang and Grossman, 1993). When used instead of ATP, ADP and non-hydrolysable homologs triggered a tight nonspecific binding to DNA (Van Houten et al., 1988). The conformational changes, induced by ATP binding and hydrolysis at proximal and distal sites, will favour either the processivity of UvrA along the DNA when there is no lesion in the helix or instead block the dimer once the lesion is located (Case et al., 2019). The motion of UvrA needs ATP to move along the DNA until it hits the lesion and binds the area. Although UvrA alone can discriminate between damaged and undamaged DNA, at present, it is unclear whether both UvrA and UvrB are needed for damage recognition as proposed in the helicase scanning model (Koo et al., 1991; Oh et al., 1989; Oh and Grossman, 1987; Rossi et al., 2011). There is substantial evidence for a heterotetrameric UvrA₂UvrB₂ complex. A crystallographic study of the minimal domains needed for UvrA-UvrB complex formation and hydrodynamic studies indicate a 1:1 protein ratio (Pakotiprapha and Jeruzalmi, 2013). Several electron microscopy, fluorescence resonance energy transfer, atomic force microscopy and Q-dot technology-based studies have also confirmed the existence of a heterotetramer composed of two UvrAs and two UvrBs: UvrA₂UvrB₂ (Jaciuk et al., 2020; Kad et al., 2010; Malta et al., 2007; Pakotiprapha et al., 2012; Shi et al., 1992; Van Houten et al., 2005).

To study the damage search strategy of UvrA, single molecule techniques like optical tweezers, magnetic tweezers and direct imaging of the DNA have been used successfully, but have also showed some limitations. The elevated DNA platforms making use of

quantum dots (Qdot) were found to be more suitable for the analysis of the motion of UvrA (Kad and Van Houten, 2012). The advantage of Qdots is that they are brighter and much more photostable. The proteins UvrA and UvrB were labelled with distinct fluorophores and the Qdots did not affect the activity of the proteins. UvrA was biotinylated and conjugated with one molecule of Qdot per dimer and UvrB was labelled with a HA tag and the conjugation with the Qdot was done with an antibody sandwich (Kad et al., 2010). The DNA was stretched between 5 μ M beads (Figure 1.17). The UvrA dimer alone showed a 3D motion and was able to jump to a nearby strand after 7 seconds of residence time on the DNA. When UvrB was added the complex UvrA₂UvrB₂ switched to three possible motions: a random diffusion, an ATP-directed motion and a diffusion interrupted by pauses. The latter might correspond to a strand interrogation during the damage sensing. Each encounter of UvrA₂UvrB₂ and the DNA lasted approximately 40 seconds (Kad et al., 2010; Kad and Van Houten, 2012).

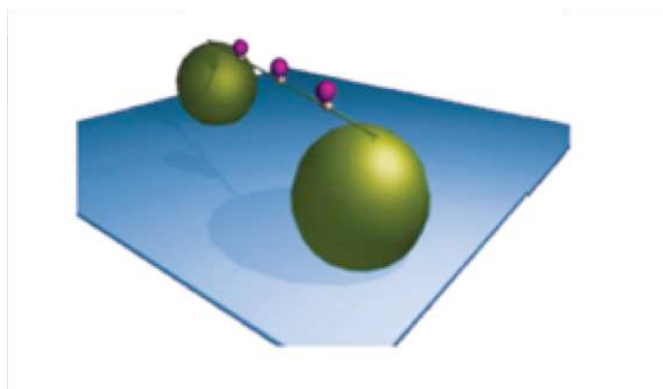


Figure 1.17: Illustration of a DNA tightrope showing three Qdot-labeled protein complexes bound to a single tightrope of DNA suspended between two 5 μ m silica beads (Hughes et al., 2013).

Damage recognition by the UvrA₂UvrB₂ complex is achieved with the damage-specific DNA binding site of UvrB. The following step in the repair is the damage verification by the second protein UvrB that will help distinguish the strand to incise after the indirect readout by UvrA (DellaVecchia et al., 2004). UvrA recruits UvrB via its first N-terminal zinc-binding insertion domain (Claassen and Grossman, 1991). This induces a conformational change that allows damage verification and loading of UvrB onto the DNA to form the preincision complex. Therefore, in principle two UvrB molecules can be bound by a UvrA dimer. However, the stoichiometry of the UvrA-UvrB complex involved in damage verification is still unclear. Recent SEC-MALS analyses suggest that two molecules of UvrB are present on the DNA, but only one will loaded onto the lesion (Jaciuk et al.,

2020). This action requires the ATPase activity of both ATP sites of UvrA (Case et al., 2019; Stracy et al., 2016). The recruitment of UvrB is compromised when the walker A motifs of the N- or C- terminus are mutated. ATP hydrolysis releases UvrA from the DNA for the handover to UvrB. This ATP hydrolysis occurs in UvrA, but maybe also in UvrB (Case et al., 2019; Goosen and Moolenaar, 2001; Mazur and Grossman, 1991; Oh et al., 1989; Pakotiprapha et al., 2012, 2008; Stracy et al., 2016).

3.3.3.2. UvrB

UvrB is the protein that interacts with all the other Uvr proteins during NER, the first interaction being with UvrA for the damage verification prior to the formation of the preincision complex (Orren and Sancar, 1990). It has recently been proposed that the recruited UvrB is loaded 18bp away from the lesion, and thanks to its helicase activity, it reaches UvrA and the damaged DNA (Figure 1.10) (Jaciuk et al., 2020).

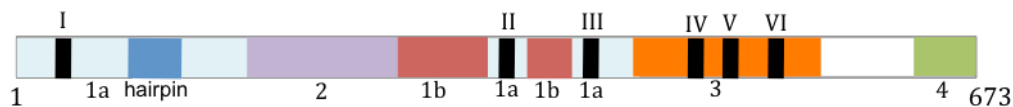


Figure 1.18: Schematic representation of the domain structure of UvrB.

UvrB is a 75kDa protein belonging to the helicase superfamily II that has weak helicase and ATP activities and acts more as a duplex destabiliser. Many structures of UvrB have been solved from *B. subtilis*, *B. caldotenax*, *T. thermophilus* and *E. coli*. (Alexandrovich et al., 2001, 1999; Eryilmaz et al., 2006; Machius et al., 1999; Nakagawa et al., 1999, 1997; Sohi et al., 2000; Theis et al., 1999; Truglio et al., 2006b, 2004; Waters et al., 2006). The C-terminus of UvrB is flexible and was thus purified separately in order to determine its structure. UvrB carries five domains in the following orders: 1a, 2, 1b, 3, a flexible linker then 4. Domains 1a and 3 are structurally similar to SF2 helicases (RecA like domains) (Figure 1.18).

A flexible β -hairpin, located in domain 1a, is responsible for damage verification (Figure 1.19). The verification involves the rotation of the base located 3' to the lesion on the damaged strand, into a pocket of UvrB or away from the protein when the lesion is

voluminous (Jaciuk et al., 2020; Moolenaar et al., 2001; Sancar et al., 1984; Skorvaga et al., 2002). The hairpin carries highly conserved hydrophobic and aromatic residues. The tip of the hairpin interacts with domain 1b. The “padlock model” predicts that this tip of the β -hairpin is inserted into the DNA double helix and clamps one strand between the hairpin and domain 1b that interacts with DNA. A recent reconstitution of the UvrA-UvrB-DNA complex has shown that the damaged strand is the one locked under the β -hairpin. Depending on its size, the lesion can be positioned either behind the β -hairpin leading to a flipping of the base inside the hydrophobic pocket of the protein, or located at the base of the β -hairpin, in the case of bulky lesions, while the other strand is at the surface of the lesion (Truglio et al., 2006b) (Jaciuk et al., 2020). Translocation of UvrB along the DNA will be stalled upon reaching the DNA lesions (Jaciuk et al., 2020).

Deletion of the β -hairpin tip (residues Gln 97 to Asp112, replaced with a Gly) in *B. caldotenax* UvrB results in a protein that is recruited by UvrA, but is not able to verify the lesion. As a result, the DNA helix is not destabilised. The ATPase activity is increased at the site because UvrB still hydrolyses the ATP in order to translocate along the DNA, but the verification step is lost (Skorvaga et al., 2002). The highly conserved aromatic residues at the base of the β -hairpin were also studied. Specific mutations of Tyr101 and Phe108 to Ala also disrupt the damage verification properties of UvrB (Moolenaar et al., 2001).

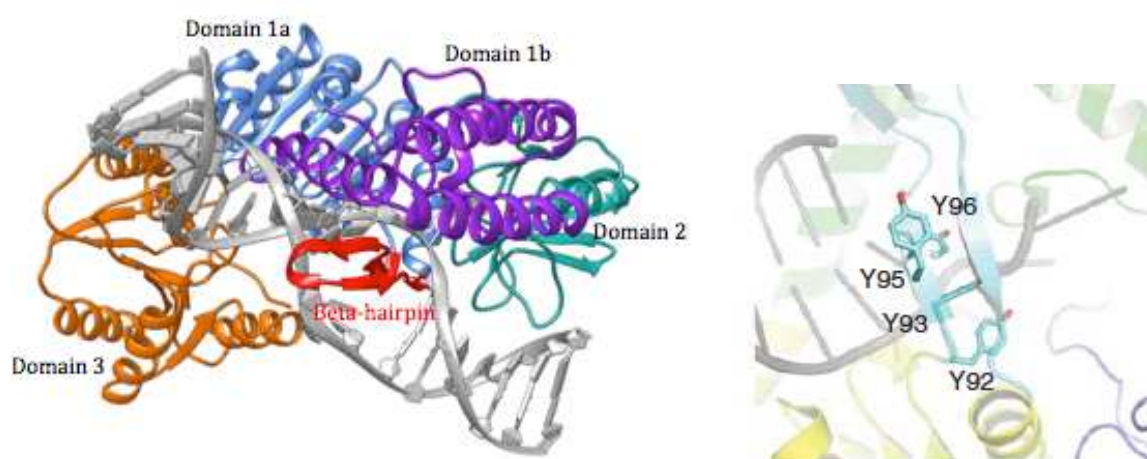


Figure 1.19: Crystal structure of UvrB. Left: The different domains of *Bacillus caldotenax* UvrB (PDB entry 6o8g). The hairpin is indicated in red. Right: Strictly conserved and functionally critical tyrosine residues located on the inner face of the β -hairpin occupy the space vacated by the extrahelical nucleoside (PDB entry 2FDC). (Kisker et al., 2013; Lee et al., 2019).

When the lesion is flipped out of the helix, which occurs when the lesions are small enough to fit into the hydrophobic pocket of UvrB, the vacant position in the DNA helix is filled by one of the residues Tyr92 and/or Tyr93, the lesion interacts with Tyr95 and the nucleotide next to the lesion binds Tyr96 (Figure 1.19) (Kisker et al., 2013; Lee et al., 2019). The mutations Tyr92 Ala and Tyr93 Ala display an inability to distinguish damaged from non-damaged DNA, forming preincision complexes with both (Moolenaar et al., 2001). The residues Tyr92 and Tyr93 thus protect the non-damaged DNA from incision. In the presence of damaged DNA, Tyr95 and Tyr96 mutants were not able to destabilize the helix to transition to the preincision complex, thereby blocking incision by the UvrABC system. The same behaviour of the protein was observed when the charged residues Arg123 and Glu99 were mutated (Skorvaga et al., 2004; Van Houten et al., 2005).

Once the presence of the lesion is confirmed, the conformation of the β -hairpin changes in order to allow the binding of the DNA to domain 1b of UvrB. In the preincision complex, the DNA strand is bent and wrapped around the protein (Shi et al., 1992; Verhoeven et al., 2001). The helicase motifs in domain 3 maintain the DNA conformation prior to incision by UvrC. A nucleotide is bound at the interface of domains 1a and 3 in between the six helicase motifs. UvrB ATPase activity is triggered by UvrA and damaged DNA or the cleavage of domain 4 (Caron and Grossman, 1988; Oh et al., 1989; Seeley and Grossman, 1989). Since UvrA and UvrB both have potential ATPase activities, their activities were assessed using mutations in either the walker A motif or in the helicase motifs, or alternatively by using GTP (UvrB can only use ATP, while UvrA can utilize ATP and GTP). The mutation Lys45Ala in UvrB Walker A motif affects its ATP hydrolysis (Seeley and Grossman, 1990), but the formation of the UvrB:DNA complex is unaffected, indicating that the ATPase activity of UvrB is not necessary for the loading of UvrB onto the DNA by UvrA. During the incision, UvrC can also bind to the UvrB:DNA preincision complex in the presence of non-hydrolysable nucleotide, ATP γ S (Moolenaar et al., 2000b), but the hydrolysis of ATP is necessary to perform the incision (Seeley and Grossman, 1990, 1989). After this hydrolysis, a new round of ATP binding is needed to change the conformation of UvrB and allow the 3' incision.

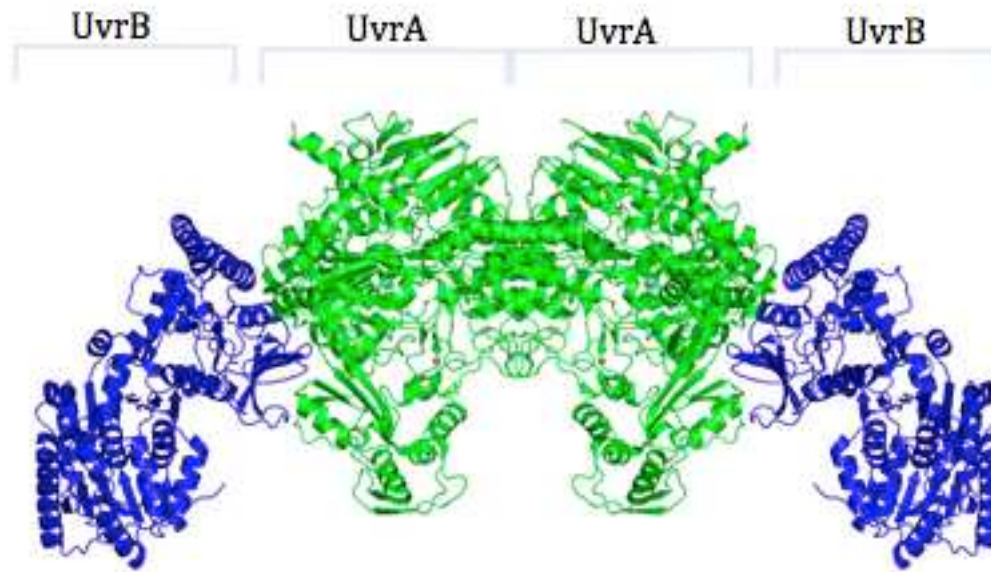


Figure 1.20: Crystal structure of the UvrA₂ (green)-UvrB₂ (blue) complex from *Geobacillus* sp. (PDB entry: 3uwx). The complex has been shown to be able to adopt different conformations while passing the damaged DNA from UvrA to UvrB (Pakotiprapha et al., 2012; Rossi et al., 2011).

UvrA is required for the interaction of UvrB with dsDNA. Structures of UvrA in complex with UvrB show interactions between the UvrB-binding domain in UvrA and domain 2 of UvrB, but also between the second signature domain of UvrA and domain 1b of UvrB that binds the DNA (Figure 1.20) (Jaciuk et al., 2020; Pakotiprapha et al., 2012, 2009). UvrA and UvrB interact through electrostatic interactions (Hsu et al., 1995). The point mutant Tyr96Ala in *B. caldotenax* UvrB helped with the crystallisation of this disordered domain 2 (Truglio et al., 2004) and its structure reveals that it shows similarities with the UvrA binding domain of Mfd implicated in TCR-NER (Assenmacher et al., 2006; Zou et al., 1998a). Some residues present at the surface of this domain are close to the β -hairpin and participate in the UvrB:DNA preincision complex formation. Single and double mutations of arginine and glutamine residues in domain 2 of UvrB showed changes in the net charge of the protein, and unsurprisingly also affected the interaction with UvrA (Truglio et al., 2004). These mutants of UvrB along with the proteins UvrA and UvrC, display a less effective NER system compared to the wild-type UvrB (Skorvaga et al., 2004; Zou et al., 2004). When domain 2 is entirely deleted in UvrB, no incision by the UvrABC could be detected. This could be due to either a decrease in the specificity of the system or the incapacity of UvrA to recruit UvrB to the damaged site (Truglio et al., 2004). It has been

proposed that UvrB may take part in UvrA dissociation from non-damaged DNA, along with ATP. If UvrB detects no lesion in the area bound by UvrA, both proteins are released from the strand (Truglio et al., 2006a). This hypothesis implies that UvrB is present during the binding of both damaged and non-damaged DNA by UvrA. If the lesion is present on the other hand, only UvrA is released because its interaction with UvrB is weakened. UvrB is then loaded onto the lesion in order to form the pre-incision complex. Pakotiprapha and colleagues suggested a model presented in Figure 1.21, in which the two molecules of UvrB are loaded on the opposite strands and translocate towards the lesion. The asymmetry of the dimer caused by the presence of the lesion on one strand directs the loading of UvrC, while one of the units of the dimer is displaced (Jaciuk et al., 2020; Pakotiprapha et al., 2012). Another model suggests that the binding of UvrC may be required for the release of UvrA (Kisker et al., 2013).

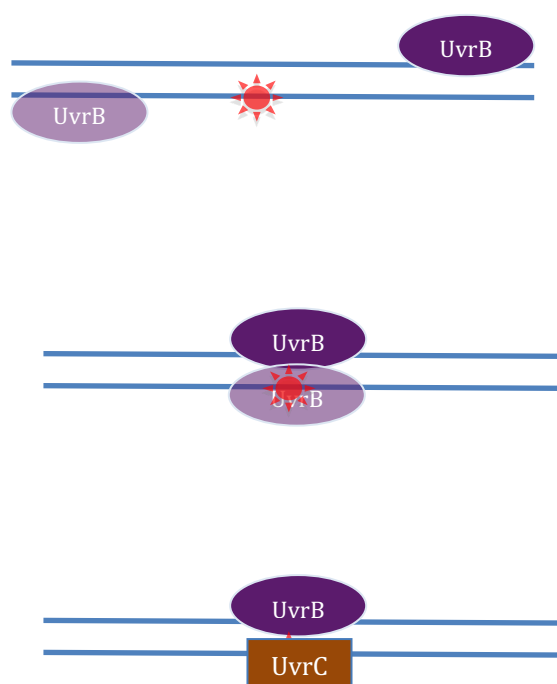


Figure 1.21: Model of DNA damage search and verification by UvrB. This model proposes that two molecules of UvrB are loaded by UvrA on opposite strands of the DNA duplex approximately 80Å away from the lesion. UvrB then translocates from this peripheral location to the site of damage in the 5'→3' direction powered by its single-strand DNA translocase activity. Two nearby UvrB molecules on opposite strands may be stabilized around the lesion site. The intrinsic asymmetry of damaged DNA could direct the final UvrB-DNA configuration and the loading of UvrC onto the correct strand, with the loss of one of the two UvrBs (Pakotiprapha et al., 2012).

The C-terminus of UvrB contains a helix-loop-helix (HhH) motif that is needed for UvrB dimerisation. In the UvrA-UvrB complex, this domain lies in the vicinity of the DNA-binding region of UvrA (Hsu et al., 1995; Jaciuk et al., 2020). This helix-loop-helix is also the interaction site with UvrC, which carries a similar domain. In earlier studies, it had also been proposed to be involved in the interaction with UvrA, but its deletion showed that it was not essential for UvrA binding (Moolenaar et al., 1998a, 1997, 1995; Nakagawa et al., 1997). The deletion of this domain, however, impairs the incision step of the repair pathway. The tight binding of UvrB to DNA ensures a precise intervention of UvrC during the incision process (Goosen and Moolenaar, 2001; Skorvaga et al., 2002).

3.3.3.3. UvrC

UvrC is responsible for the dual incision on the 5' and 3' sides of the lesion thanks to its two endonuclease domains located respectively at the C- and N-termini of UvrC. These two domains can be inactivated independently (Karakas et al., 2007; Lin and Sancar, 1992; Truglio et al., 2005; Verhoeven et al., 2000).

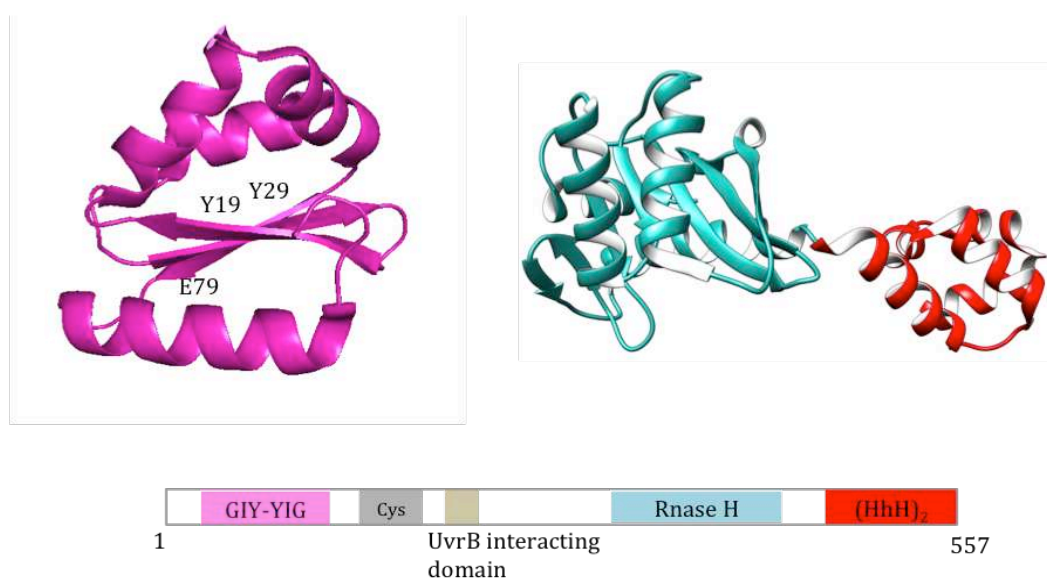


Figure 1.22: Schematic representation of the domain structure of UvrC along with structures of the N-terminal GIY-YIG endonuclease domain (pink) and the C-terminal RNase H endonuclease (blue) and HhH₂ (red) domains from *T. maritima*. (PDB entries: 1YCZ, 2NRT).

The N-terminal region of UvrC carries a GIY-YIG endonuclease (or GVV-YVG in some bacteria), followed by a cysteine-rich region, (CX₆₋₁₆)CX₇CX₃C, and the UvrB binding domain that is structurally similar to the UvrB C-terminal HhH motif in domain 4. This interaction is needed for the 3' incision (Hsu et al., 1995; Moolenaar et al., 1998b, 1995; Truglio et al., 2005). The C-terminal half of UvrC holds an RNase H endonuclease domain connected to one or two HhH motifs known to bind DNA (Singh et al., 2002) (Figure 1.22). The cysteine residues are not conserved in all UvrC homologs indicating that this sequence may not be necessary for the repair system.

Structures of the GIY-YIG domains of *B. caldopenax* and *T. maritima* UvrC have been determined (Truglio et al., 2005). The domain consists of a three-stranded β -sheet surrounded by four α -helices. A highly conserved patch of residues was identified on the surface of the GIY-YIG endonuclease, forming a concave surface suitable for binding dsDNA and necessary for the activity. Mutations of these residues (Tyr19, Tyr29, Gly31, Lys32, Arg39, Tyr43, Glu76, Asn88 in *T. maritima* UvrC) decrease substantially the cleavage activity on the 3' side of the lesion. Among these residues, a conserved glutamate, Glu76 in *T. maritima* UvrC (corresponding to Glu72 in *D. radiodurans* UvrC, shown in Figure 1.23) and five water molecules coordinate a divalent cation, Mg^{2+} or Mn^{2+} (Truglio et al., 2005). Tyr29 that is located close to the divalent cation acts as a general base. It strips a proton from a nucleophilic water molecule and transfers its own proton to a metal bound hydroxide. The cation is the Lewis acid and a metal-bound water protonates the 3' OH leaving group of the phosphate as a general acid (Figure 1.24).

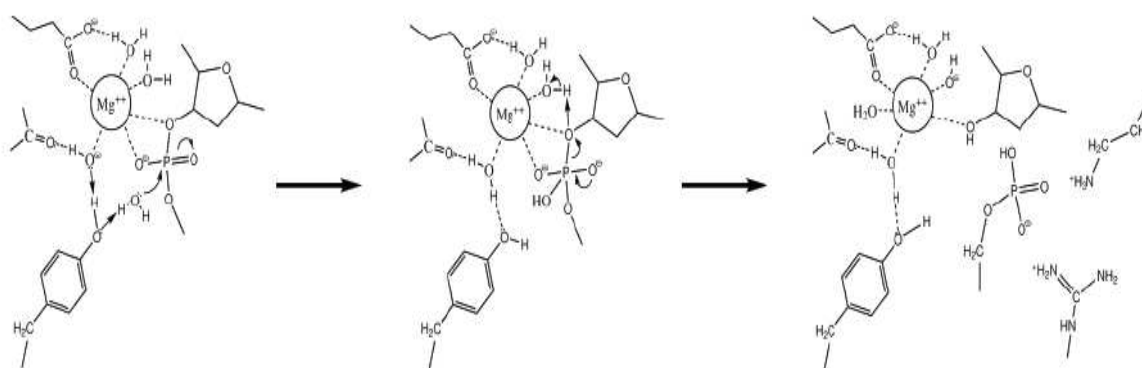


Figure 1.24: Coordination of a divalent cation (here, Mg^{2+}) in the active site of the GIY-YIG endonuclease domain of *T. maritima* UvrC (Truglio et al., 2005). The Mg^{2+} ion is coordinated by a glutamic acid and five water molecules. The function of the Lewis acid is fulfilled by the divalent cation. One of the coordinating water molecules assumes the role of the general acid and donates its proton to the 3' OH leaving group of the phosphate, and the general base is a tyrosine residue.

A structure of the C-terminal half of *T. maritima* UvrC, composed of the RNase H domain and the dual (HhH)₂ motif has also been determined (Karakas et al., 2007) (Figure 1.22). In the active site of the RNase H-like endonuclease domain, there is a DDKH motif that holds two conserved Asp and a His or an additional Asp that are essential for cleavage on the 5' side of the lesion. Mutating these residues in the following mutants completely

abolishes 5' cleavage activity: His538Phe, His538Tyr, Asp399Ala, Asp438Ala, Asp466Ala, Asp399Asn (corresponding to Asp391 in *D. radiodurans*, shown in Figure 1.23), Asp438Asn and Asp466Asn (Lin and Sancar, 1992). In addition, the mutation His495Glu shows the importance of the side chain of the histidine in the incision (Karakas et al., 2007). The aspartic acids also play a role in the catalytic activity and in addition, they have been suggested to coordinate one or two metal ions as well (Karakas et al., 2007; Lin and Sancar, 1992). The surface opposite the active site carries a conserved patch of positively charged residues in which mutations can compromise both 3' and 5' incisions.

The (HhH)₂ motif maintains a conformation of the incision complex that will allow the dual incision. Its deletion results in mutants that are not able to bind ssDNA and the 5' incision efficiency was reduced drastically (Moolenaar et al., 1998b). This motif has a strong affinity for the repair bubble such as the one generated by UvrA and UvrB in the previous step of the NER (Singh et al., 2002; Truglio et al., 2006b). Depending on the DNA substrate (type of lesion introduced into the DNA duplex and sequence) tested, the (HhH)₂ motif appears to be needed either for the 5' incision or for both the 5' and 3' incisions, because it participates in the flexibility of the repair system (Verhoeven et al., 2002). In some bacteria, the UvrC protein is lacking a (HhH)₂ motif and yet it is still involved in NER, suggesting that this region is in some cases dispensable. In these cases, UvrC stabilisation by UvrB has been proposed to be sufficient to ensure proper incision (Goosen and Moolenaar, 2008).

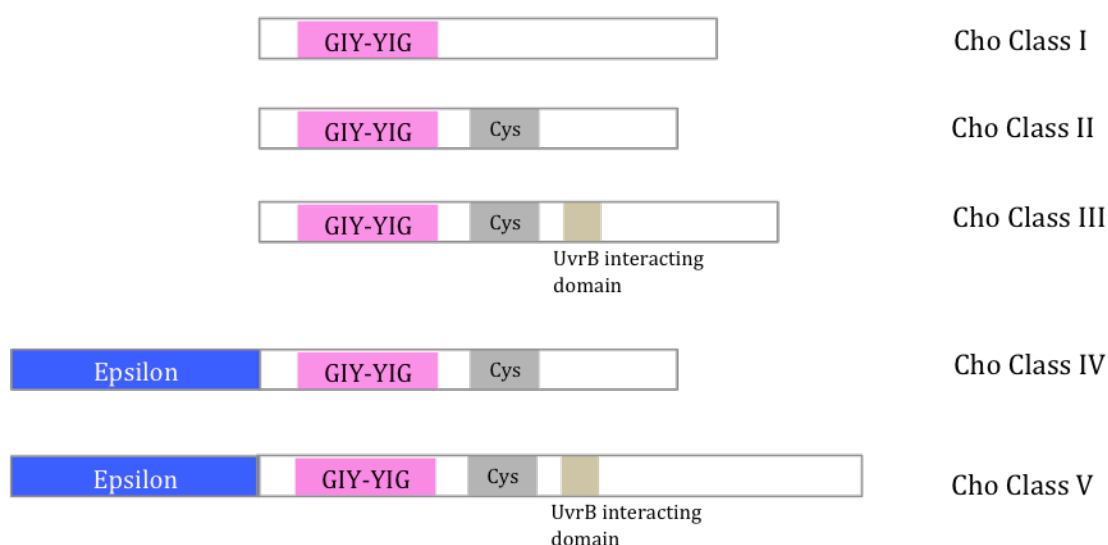


Figure 1.25: Schematic representations of the domain structure of C-homolog (Cho) proteins.

Unlike UvrC, in certain bacterial strains, there is a C-homolog (Cho) protein that is inducible by the SOS response. In bacteria containing both *UvrC* and *Cho* genes, Cho acts as a backup mechanism. Cho proteins are highly similar to the N-terminal half of UvrC (Moolenaar et al., 2002). The domain composition of Cho varies from the GIY-YIG endonuclease only to an extension to more domains of the region, the cysteine-rich consensus sequence plus the UvrB-interaction site. Cho proteins that contain the endonuclease and cysteine-rich region can function in NER, which suggests that the UvrB interacting domain is dispensable in these cases. The activities and specificities of UvrC and Cho are different: although the N-terminal GIY-YIG domain is responsible for the 3' incision in both cases, Cho incises the ninth phosphodiester bond on the 3' side, while UvrC incises the fourth or the fifth (Goosen and Moolenaar, 2008). This additional mechanism can be triggered in case of very bulky lesions that require a larger incision. Different classes of Cho proteins are found in bacteria. *E. coli* Cho is a class II protein with a GIY-YIG endonuclease domain and a cysteine cluster, and it can incise on the 3' side of the lesion, when UvrC is unable to process the substrate (Figure 1.25). No Cho homologs are encoded in the genome of *D. radiodurans*.

The two incisions by the N-terminal and the C-terminal endonuclease domains of UvrC produce a 12-13 nucleotide fragment. The first assays with UvrABC from *E. coli* showed that depending on the substrates used (thymine-thymine dimers, thymine-cytosine dimers, cytosine-cytosine dimers or psoralen adduct), the site of incision by the N-terminal GIY-YIG domain of UvrC on the 3' side of the lesion varies (Sancar and Rupp, 1983). It takes place at either the fourth or fifth phosphodiester bond 3' to the lesion and leaves a 3'-OH terminus, while the 5' cut occurs eight phosphodiester bonds 5' to the lesion and produces a 5'-P terminus regardless of the nature of the lesion (Sancar and Rupp, 1983). In addition, a defined order for the incisions was confirmed with the use of UvrC mutants or UvrC-homolog Cho of *E. coli* (Lin and Sancar, 1992; Moolenaar et al., 2002; Verhoeven et al., 2000). The activity of UvrC-Asp399Ala and Cho, which perform the incision on the 3' side only, and of UvrC-Arg42Ala, which only incises on the 5' side, were assessed. These experiments revealed that the first incision occurs on the 3' side, which is then followed by a second incision reaction on the 5' side (Moolenaar et al., 2002; Zou et al., 1997).

3.3.3.4. UvrD

UvrD is known to participate in several repair processes and thus contributes to UV-resistance (Arthur and Lloyd, 1980; Bentchikou et al., 2010; Bruand and Ehrlich, 2000; Caron et al., 1985; Matson and Robertson, 2006; Veaute et al., 2005). In NER, it unwinds the DNA helix following the dual incision by UvrC to release the 12-13mer fragment containing the lesion and the UvrB and UvrC proteins. The helicase activity of UvrD requires the presence of the proteins UvrB and UvrC on the site (Atkinson et al., 2009; Manelyte et al., 2009). In fact, it was demonstrated that when the DNA duplex was nicked but naked, without any proteins, UvrD was not able to unwind the helix. The presence of the previous proteins and the conformational change already present in DNA facilitates UvrD recruitment and DNA unwinding (Atkinson et al., 2009; Manelyte et al., 2009).



Figure 1.26: Schematic representation of the domain structure of UvrD. UvrD is composed of 4 domains, 1A (green), 1B (beige), 2A (orange), 2B (blue), and a flexible C-terminal extension (white).

UvrD is a type A Superfamily I helicase with a 3'-5' unwinding polarity (Gorbalenya and Koonin, 1993). It carries two RecA-like domains and unwinds the DNA duplex thanks to its ATPase activity. UvrD is composed of 4 domains, 1A, 1B, 2A, 2B, and a flexible C-terminal extension (Figure 1.26). Structural studies of UvrD show that the nucleotide-binding sites are identified at the interface of the RecA-like domains (domains 1A and 2A), while domains 1B and 2B are involved in DNA binding (Figure 1.26) (Lee and Yang, 2006; Stelter et al., 2013; Yang, 2010). Depending on the nucleotide-bound state, the protein binds differently the ssDNA and the dsDNA (Lee and Yang, 2006). The C-terminal portion interacts with UvrB domains 1a and 2, however it is not essential for NER activity, since C-terminally truncated-UvrD are fully functional (Manelyte et al., 2009). In these cases, UvrD still interacts with UvrB via its N-terminal region.

A monomer of UvrD is able to bind a dsDNA with a 3' ssDNA tail and barely interacts with blunt ended dsDNA. In order to unwind the DNA helix, UvrD has been shown to function as a dimer and maybe also as a trimer (Yokota et al., 2013). One monomer binds the 3' ssDNA tail and the other is found at the ss-dsDNA junction. The tail has to be at least 4nt long for *E. coli* UvrD to bind and 12nt long for unwinding. The longer it gets, the more monomers are needed on the site (Ali et al., 1999; Sun et al., 2008). A monomer of *D. radiodurans* UvrD is capable of binding a 7nt ssDNA tail and displays a helicase activity on such a substrate (Figure 1.27) (Stelter et al., 2013). *D. radiodurans* UvrD, unlike *E. coli* UvrD, was also shown to bind a 5' ssDNA tail with the same affinity as the 3' end and to perform a 5'→3' helicase activity (Stelter et al., 2013). In addition to unwinding DNA, UvrD is also able to translocate along a ssDNA strand in the 3'→5' direction. The binding of UvrD to the ssDNA triggers a movement of its domain 2B and the new setting of the interface between 1B and 2B allows the interaction with the DNA duplex (Singleton et al., 2007)

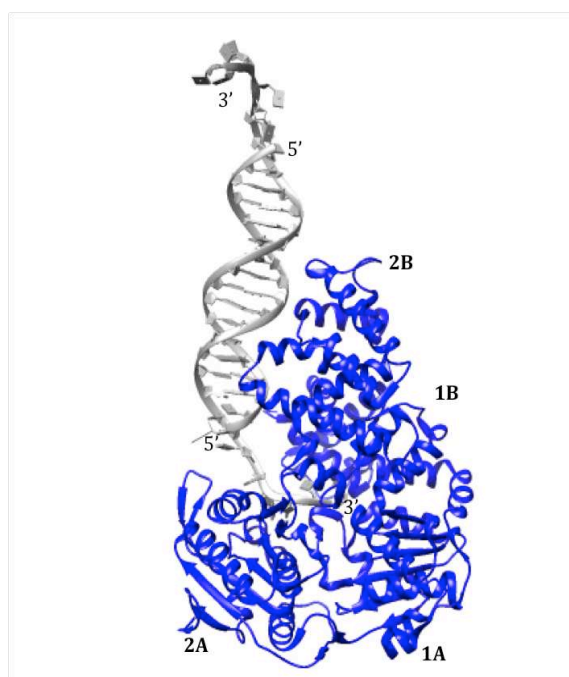


Figure 1.27: Crystal structure of *D. radiodurans* UvrD (blue) bound to a DNA duplex (grey) with a 7nt ssDNA tail (PDB entry 4c2u) (Stelter et al., 2013).

In the presence of both ATP and ATP γ S, UvrD is able to bind DNA tightly. The binding of the nucleotide triggers the closing of the 1A-2A interface around ATP, causing a movement of domains 1B and 2B that destabilises the base pairing in the DNA duplex. The

ATP binding and hydrolysis allow the mechanical movement of the protein and alternated tight and loose interactions between the protein and the DNA (Matson and George, 1987; Singleton et al., 2007; Stelter et al., 2013; Yang, 2010). In the dimer of UvrD, each subunit has to carry an active ATP binding site (N. K. Maluf et al., 2003; Yokota et al., 2013).

3.3.4. Choice of bacterial models for the study of prokaryotic NER

Over the past 40 years, researchers worldwide have developed incision assays in order to assess and determine the activity of each Uvr protein, wild-type or mutant, in the NER repair process. Many bacterial models have been used for this purpose with their advantages and disadvantages.

3.3.4.1. *E. coli* NER as a model system

Among these organisms, we can cite the most studied system from *Escherichia coli*. The first data on the mechanism of the NER pathway were indeed established with *E. coli* proteins (Beck et al., 1985; Kow et al., 1990; Lin and Sancar, 1992; Malta et al., 2007; Sancar and Rupp, 1983; Thomas et al., 1988; Yeung et al., 1983; Zou et al., 2004). However, the reconstitution of the NER displays a disadvantage: the UvrA and UvrC proteins present a thermal instability. Zou et al showed that *E. coli* UvrA lost its activity irreversibly after 30 min at 37°C in the absence of chaperones. The heat shock proteins (DnaK, DnaJ, and GrpE) were essential for the stability of UvrA in an effective incision assay with UvrB and UvrC (Zou et al., 1998b). There was therefore a need to reconstitute the NER pathway with more stable proteins.

3.3.4.2. Use of Uvr proteins from thermophilic bacteria

More recently, other NER systems have been successfully reconstituted using Uvr proteins from thermophilic bacteria, including *Bacillus caldotenax*, *Thermus thermophilus* and *Thermotoga maritima*. Unfortunately, the UvrA, UvrB and UvrC were usually mixed from different sources in order to have an efficient and functional system. For example, an efficient assay has been reconstituted using UvrA and UvrB from *B. caldotenax*

combined with UvrC from *T. maritima*. This is because the purified *B. caldotenax* UvrC was found not to perform any incision on the 3' side of the lesion when used in an incision on DNA treated with BPDE in the presence of *B. caldotenax* UvrA and UvrB proteins. Only the incision on the 5' side of the lesion was performed. Both incisions were restored when *B. caldotenax* UvrA and UvrB was instead combined with *T. maritima* UvrC (Jiang et al., 2006). The temperature for these experiments with the interspecies combination of UvrABC was first a pre-incubation at 65°C then 55°C for an hour (Croteau et al., 2008, 2006; Jaciuk et al., 2020, 2011; Jiang et al., 2006; Verhoeven et al., 2002; Wirth et al., 2016). These temperatures and conditions are not necessarily the optimal parameters for all the proteins used. Examples of previously determined incision assays are presented in Table 1.4.

Table 1.4: Examples of incision assays reconstituted using different bacterial Uvr proteins

| Substrates | Uvr proteins | Conditions of the incision assay* | References |
|---|---|---|--|
| 50 bp dsDNA oligos containing centered fluorescein-conjugated thymine (FIdT) | UvrA and UvrB from <i>B. caldotenax</i> UvrC from <i>T. maritima</i> | Preheat the proteins for 10 min at 65°C Reaction at 55°C | (Croteau et al., 2008; Wirth et al., 2016) |
| 50 bp dsDNA oligos containing centered FIdT | UvrA, UvrB, UvrC from <i>T. maritima</i> | Pre-incubation with UvrA and DNA- 25 min at 25°C or 37°C Reaction at 65°C | (Jaciuk et al., 2020, 2011) |
| 50 bp dsDNA oligos containing <i>cis</i> - or <i>trans</i> -BPDE | UvrA and UvrB from <i>B. caldotenax</i> UvrC from <i>T. maritima</i> | Pre-incubation with UvrA and UvrB and DNA- 30 min at 60°C Reaction at 60°C | (Jiang et al., 2006) |
| - 50 bp dsDNA oligos containing centered FIdT - 50 bp dsDNA oligos containing CPD dimer | UvrA, UvrB and UvrC from <i>E. coli</i> | Reaction at 37°C | (Zou et al., 2004) |
| - 50 bp dsDNA oligos containing <i>cis</i> -Pt-GG - 50 bp dsDNA oligos containing N3-menthol | UvrA, UvrB and UvrC from <i>E. coli</i> | Reaction at 37°C | (Malta et al., 2007; Verhoeven et al., 2002) |

| | | | |
|---|--|---|--|
| - 50 bp dsDNA oligos containing cholesterol | | | |
| - Plasmid containing 4-NQO adducts - Plasmid containing psoralen adducts - UV- irradiated plasmid | UvrA, UvrB and UvrC from <i>E. coli</i> | Reaction at 37°C | (Sancar and Rupp, 1983; Sibghat-Ullah et al., 1990; Thomas et al., 1988) |
| - UV- irradiated plasmid | UvrA, UvrB and UvrC from <i>Mycobacterium tuberculosis</i> | Sequential addition: 37°C UvrA for 10 min + UvrB for 20 min + UvrC for 30 min | (Mazloum et al., 2011) |

*The incision assay buffer was generally composed of 50 mM Tris-HCl pH 7.5, 50 mM/ 100 mM KCl, 10 mM MgCl₂, 0.1 µg/µl BSA, 5 mM dithiothreitol and 1 mM ATP.

3.3.4.3. Alternative: the NER system from the radiation-resistant bacterium *Deinococcus radiodurans*

Deinococcus radiodurans carries all the proteins of the NER pathway, which show high sequence conservation with their homologs from model bacteria, such as *E. coli*. Moreover, all the Uvr proteins from *D. radiodurans* can be efficiently overexpressed in *E. coli* and purified for biochemical and structural studies (Stelter et al., 2013; Timmins et al., 2009; Timmins and Moe, 2016). The purified proteins are stable and active. The purification protocols of *D. radiodurans* Uvr proteins were established by J. Timmins and colleagues at ESRF between 2006 and 2011. Structural studies are being performed in J. Timmins' team on these same proteins in order to complement the biochemical studies and obtain a detailed picture of how NER locates and incises DNA lesions. In addition, unlike its thermophilic counterparts, *D. radiodurans* is a mesophile that grows at an optimum temperature of 30°C, but is perfectly active and functional at 37°C. For all these reasons, the NER system of *D. radiodurans* was our model of choice for this study.

4. *Deinococcus radiodurans*

4.1. General presentation and features

Deinococcus radiodurans is a mesophilic and gram-positive bacterium from the *Deinococcus* genus (Figure 1.28). It is well-known for its high resistance to irradiation and desiccation, which can severely shatter its genome. *D. radiodurans* was compared to *E. coli* based on the D_{37} values, the irradiation dose needed to inactivate 63% of the bacterial population. It shows a dose around 6 kGy for *D. radiodurans* and 0.03kGy for *E. coli* (Figure 1.29). Also *D. radiodurans* is able to repair 200 DSB and 190 crosslinks within 3 to 4 hours (Figure 1.30) (Battista, 1997; Blasius et al., 2008; Harsojo et al., 1981; Moseley and Copland, 1975) and is able to continue growing under a constant exposure of 60 Gy/h (Eltsov and Dubochet, 2005; Venkateswaran et al., 2000).

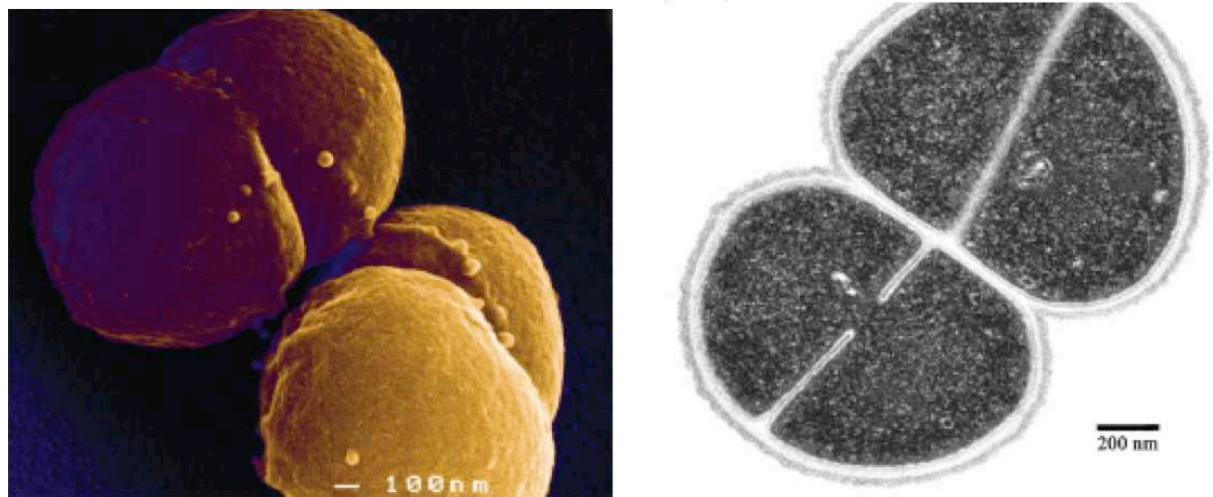


Figure 1.28: Electron micrographs of four *Deinococcus radiodurans* cells forming a tetrad (Rothfuss et al., 2006). Left: scanning electron micrograph. Right: transmission electron micrograph of a sliced *D. radiodurans* tetrad.

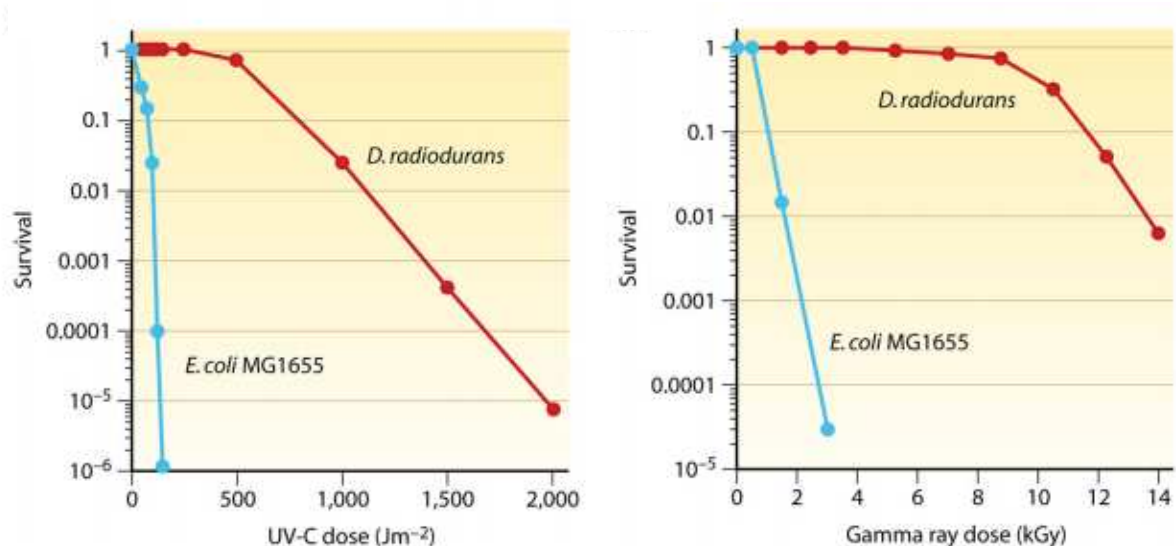


Figure 1.29: Resistance of *D. radiodurans* (red) to UV-C radiation (left) and gamma rays (right) in comparison with *E. coli* (blue). Taken from (Slade and Radman, 2011).

D. radiodurans has been isolated from different sites on earth and it is a non-pathogenic bacterium (Slade and Radman, 2011). *D. radiodurans* grows as dyads and tetrads (Figure 1.28), it has a diameter of 1-3 μm and harbours a pink colour due to carotenoid pigments. The analysis of its genome revealed that it is organised into two chromosomes of respectively 2,65Mbp and 412kbp, a megaplasmid of 177kbp and a plasmid of 45,7kbp with 3195 genes coding for over 2000 proteins (White et al., 1999). Each cell can contain 4 to 10 copies of its genome. These copies may help during the repair steps following irradiation by providing intact templates for the repair process (Hansen, 1978; Harsojo et al., 1981). The high survival rate of *D. radiodurans* to stress was originally postulated to be associated with its ability to protect its genome, but since it was demonstrated that this genome can be shattered after being exposed to irradiation (Figure 1.30), other hypotheses have been made (Cox and Battista, 2005; Gerard et al., 2001; Munteanu et al., 2015).

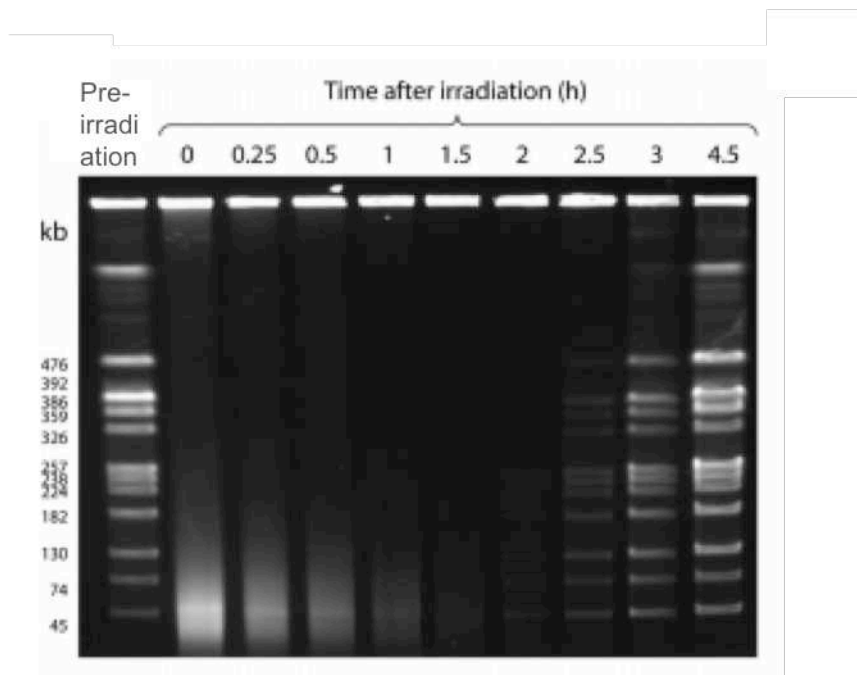


Figure 1.30: Kinetics of DNA fragment joining in *D. radiodurans* after 7 kGy of gamma rays visualized by pulsed-field gel electrophoresis. Non-irradiated and irradiated cells were taken to prepare DNA plugs, which were digested with NotI, generating 12 visible fragments in the lane “pre-irradiation”. The lane “0” shows the NotI restriction pattern of DNA from irradiated cells immediately after irradiation, and subsequent lanes show the NotI restriction patterns of DNA from cells at different time points after irradiation. Taken from (Slade and Radman, 2011).

The main factors that are now believed to contribute to the remarkable radiation resistance of *D. radiodurans* are: 1) its ability to protect its proteome (anti-ROS strategies: carotenoids, catalases & SODs, Mn etc), 2) a conventional, but highly efficient DNA repair machinery (Timmins & Moe, 2016), 3) an expanded set of BER DNA glycosylases compared to *E. coli* (Timmins and Moe, 2016), 4) a highly compact nucleoid (Blasius et al., 2008; Cox and Battista, 2005; Slade and Radman, 2011) and 5) its polyploidy. *D. radiodurans* can carry multiple copies of its genome and this feature enables a more accurate repair during DSB. In addition, the repair proteins are also well protected in the cell. This protection might be explained by the presence of three catalases and four superoxide dismutases that are in charge of the elimination of ROS from the cell environment. ROS levels are also maintained to the lowest thanks to the enrichment in Mn^{2+} , which facilitates cellular repair processes after irradiation or desiccation by providing protection from metabolism-induced ROS. The reduction of the proteins containing Fe-S is also involved (Daly, 2009; Daly et al., 2007, 2004; Ghosal et al., 2005;

Krisko and Radman, 2013; Lipton et al., 2002; Makarova et al., 2001; Sharma et al., 2013; Slade and Radman, 2011). Lastly, alternative pathways were found to repair UV-induced damage when the UvrABC was not available. This characteristic allows a quicker reaction to the bacteria facing cell death (Daly et al., 2010, 2007, 2004; Timmins and Moe, 2016).

4.2 *D. radiodurans* NER

As mentioned above, *D. radiodurans*' genome encodes for a complete set of Uvr proteins, including two UvrA variants, a class I (UvrA1) and a class II UvrA (UvrA2) (Eisen and Wu, 2002; Friedberg et al., 2006; Liu et al., 2003). *E. coli* and *D. radiodurans* have similar NER systems since *ecUvrA* can partially replace *drUvrA* and restore Mitomycin C resistance (Agostini et al., 1996; Slade and Radman, 2011). UvrA2 shares a high sequence and structural identity with homologs from class I (~41%) and shows similar NBD organisation and DNA binding preferences (Timmins et al., 2009). The main difference is that UvrA2 is missing a UvrB binding domain. Thus, UvrA2 may not be able to participate in NER. Although the role of the class II UvrA is not completely elucidated, the expression of the gene was shown to be upregulated following irradiation. One of the hypotheses was that UvrA2 is able to bind damaged DNA to eliminate it from the cell (White et al., 1999). In *D. radiodurans*, the efficient elimination of damaged DNA is an essential step to avoid the incorporation of damaged nucleotides into newly synthesised DNA. Other enzymes and chaperones, including the expanded Nudix hydrolysase family that have been identified as "house-cleaning" enzymes, also contribute to the elimination of modified proteins and damaged DNA (Bessman et al., 1996; Makarova et al., 2001; Tanaka et al., 2004; Xu et al., 2001). In the absence of UvrA1, UvrA2 was shown to be involved in the repair of DNA in *Pseudomonas putida* (Tark et al., 2008). It might be involved in UV resistance and resistance to antibiotics (Lomovskaya et al., 1996; Tanaka et al., 2004; Ylihonko et al., 1996).

As already mentioned, no SOS response has been identified in *D. radiodurans*. Following exposure to DNA damaging agents, the Uvr proteins of *D. radiodurans* are all upregulated (Table 1.5) (Liu et al., 2003; Mattimore and Battista, 1996; Ott et al., 2017; Slade and Radman, 2011; Tanaka et al., 2004).

Table 1.5: Proteins of the NER pathway in *D. radiodurans*. (Liu et al., 2003; White et al., 1999)

| Proteins | Locus tag | Gene induced after ionizing radiation | Level of up- or down regulation after ionizing radiation (folds induction) |
|----------|-----------|---------------------------------------|--|
| UvrA1 | DR1771 | YES | 3.5 |
| UvrA2 | DRA0188 | YES | 2.0 |
| UvrB | DR2275 | YES | 4.9 |
| UvrC | DR1354 | YES | 3.8 |
| UvsE | DR1819 | NO | 1.0 |
| Mfd | DR1532 | NO | 0.7 |
| UvrD | DR1775 | YES | 3.3 |

Interestingly, the *D. radiodurans* *uvrA1uvrA2* double mutant retains full UV-resistance because of the presence of an alternate UVDE (UV damage endonuclease or UvsE) repair pathway for the repair of bipyrimidine photoproducts (Earl et al., 2002). UVDE from *Thermus thermophilus* shows structural similarities with the endonuclease IV AP endonuclease, and displays a large substrate specificity. In addition to processing photoproducts, it processes AP sites, uracil, dihydrouracil and is involved in mismatch repair pathway where it acts on insertion –deletion loops (Doetsch et al., 2005; Paspaleva et al., 2007). It introduces a nick immediately 5' to a UV-lesion that is then processed by other proteins for damage excision and repair. The respective contributions of NER and the UVDE pathways to eliminate pyrimidine dimers from UV-irradiated DNA in *D. radiodurans* has been evaluated: UVDE efficiently removes both cyclobutane pyrimidine dimers (CPDs) and pyrimidine (6-4) pyrimidone dimers (6-4 PPs), whereas NER seems more specific for 6–4 PPs (Tanaka et al., 2005). Moreover, inactivation of the two pathways does not completely abolish the ability to eliminate CPDs and 6-4 PPs from DNA suggesting the presence of another back-up pathway (Tanaka et al., 2005).

Aim of the thesis

The data collected over the past decades on bacterial NER have shed light on this essential pathway, however, a lot of questions remain to be addressed, notably regarding the nature and common features of the diverse lesions repaired by the NER pathway and the role of UvrC in the repair process.

The aim of my thesis was thus to improve our understanding of the molecular mechanisms underlying this complex pathway and to further decipher the substrate specificity of bacterial NER by establishing an efficient incision assay using the UvrABC proteins from *D. radiodurans*.

The key objective was therefore to set-up a functional incision assay *in vitro* using purified recombinantly expressed *D. radiodurans* UvrA, UvrB and UvrC proteins, which could be used to assess the repair of DNA substrates either in the form of short DNA oligonucleotides containing synthetic lesions, such as the well-studied fluorescein-conjugated thymine, but also plasmid DNA treated with different protocols so as to produce a wide diversity of DNA lesions. The UvrD was not included since it is not needed for the incision reaction *in vitro*. Repair would be assessed by gel electrophoresis in the case of oligonucleotide substrates and by both gel electrophoresis and HPLC coupled to tandem mass spectrometry, making use of the dual expertise of J. Timmins' and J.-L. Ravanat's laboratories.

The development of such an assay would then allow us to (i) better understand the nature of NER substrates and common properties of NER substrates in particular in terms of DNA duplex distortion, and (ii) decrypt the precise role of each of the three Uvr proteins and their respective subdomains in the repair process. UvrA and UvrB have been the focus of numerous studies in the recent years that have shed light on their combined action in damage identification and verification. In contrast, the mode of action of the dual endonuclease, UvrC, in processing the damaged DNA still remains largely elusive. To investigate the role of UvrC in NER, our goal was to produce different truncation and point mutants of UvrC and evaluate their respective activities in our reconstituted incision assay.

Materials and methods

1. Cloning and mutagenesis

The *uvrA1* (DR_1771), *uvrA2* (DR_A0188), *uvrB* (DR_2275) and *uvrC* (DR_1354; UvrC-full-length, UvrC-ΔHhH, UvrC-N and UvrC-C) genes had already been cloned into an ampicillin resistance plasmid (pET151 or pProexHtB) for expression in *E. coli* with a TEV cleavable N-terminal His-tag before my arrival in the laboratory. The cloning of additional constructs and genes is described below. Table 3.1 provides a complete list of the clones used in this work.

Table 3.1: List of constructs used in this study

| Name | Construct | Residue range | Plasmid |
|------------|-----------------------------------|---------------|-----------|
| UvrA1 | Full-length | 1-1016 | pProexHtB |
| UvrA2 | Full-length | 81-922 | pLX-02 |
| UvrB | Full-length | 60-730 | pProexHtB |
| UvrC | Full-length | 1-617 | pET151d |
| UvrC-ΔHhH | C-terminally truncated UvrC | 1-547 | pProexHtB |
| UvrC-NEndo | N-terminal GIY-YIG domain of UvrC | 1-93 | pProexHtB |
| UvrC-N | N-terminal half of UvrC | 1-365 | pProexHtB |
| UvrC-C | C-terminal half of UvrC | 366-617 | pET151d |

1.1 Cloning of *Deinococcus radiodurans* genes

1.1.1. PCR amplification of the genes

Using polymerase chain reaction (PCR), the *uvrC-NEndo* genes was amplified from *Deinococcus radiodurans* genomic DNA extracted using the NucleoSpin kit for extraction of DNA from cells and tissues (Macherey-Nagel) for cloning into pProexHtB (EMBL; see vector map in Annex). The primers used to perform the mutagenesis reactions are shown in Table 3.2. A typical PCR reaction included the following reagents:

| |
|---|
| 20 μL Phusion Master Mix (including Phusion polymerase, dNTPs, MgCl ₂ and GC buffer) |
| 17 μL H ₂ O |
| 1 μL 1:25 diluted <i>D. radiodurans</i> genomic DNA |
| 1 μL primer Forward 20pmol/ μL containing restriction enzyme site BamHI |
| 1 μL primer Reverse 20pmol/ μL containing restriction enzyme site XhoI |
| 40 μL |

The PCR reaction cycles used were:

- Step 1 – Complete denaturation - 98°C- 3 min
- Step 2 – Denaturation - 98°C- 30 sec
- Step 3 – Annealing - 58°C- 30 sec
- Step 4 – Elongation - 72°C – 1kbp/min
- Step 5 – Final elongation - 72°C -3 min
- Step 6 – End of reaction - 10 °C hold.
- } 30 cycles

The PCR products were analyzed on a 1% Tris-Borate-EDTA (TBE) agarose gels. The PCR bands were gel purified using the DNA gel extraction kit (Macherey-Nagel) and eluted in 30 µL of elution buffer. The PCR products were then digested with the two enzymes (BamHI or NcoI and XhoI) in 10x CutSmart buffer (New England Biolabs) at 37 °C for 2h and further purified with the PCR clean-up kit (Macherey-Nagel).

Table 3.2: List of primers used to amplify *D. radiodurans* UvrC-NEndo

| Gene | Primers | Restriction sites | Plasmid |
|-------------------|---|-------------------|-----------|
| <i>uvrC-NEndo</i> | For: AAGGATCCATGCATTTTCGACGACCTGCCCCGTG Rev: TTCTCGAGTCAATAGTGCTTGTCGTCCTTGAGCAG | BamHI XhoI | pProexHtB |

1.1.2. Digestion of the plasmid

In parallel, 0.5 µg pProexHtB plasmid was digested with the two enzymes (BamHI and XhoI) in 10x CutSmart buffer (New England Biolabs) at 37 °C for 2h and subsequently separated on a 1% TBE agarose gel, purified with the DNA gel extraction kit (Macherey-Nagel) and eluted in 50 µL of elution buffer.

1.1.3. Ligation reaction

Prior to setting up the ligation reaction, the relative amounts of purified and digested PCR products and plasmid were evaluated on a 1% TBE agarose gel. A three-fold molar excess of PCR product was mixed with digested plasmid for the ligation reaction. A typical reaction included the following reagents:

1 μ L linearized plasmid pProexHtB
2 μ L 5x buffer Rapid DNA ligation (Fermentas)
0.5 μ L T4 Ligase (Fermentas)
3 μ L PCR product
3.5 μ L H₂O

10 μ L

The ligation reaction was performed at room temperature for 30 min. A control ligation containing only the digested plasmid was performed in parallel to evaluate the cloning efficiency.

1.1.4. Transformation of *E. coli* DH5 α cells

3 μ L of each ligation reaction were then added to 15 μ L of thawed *E. coli* DH5 α cells (New England Biolabs) and were incubated on ice for 30 min. DNA uptake was induced by a heat shock at 42°C for 45 sec, after which the tubes were placed on ice again for 1-2 min. 0.5 mL SOC medium (see Annex for details) was added to the transformation before incubating them at 37°C for 1h. After spinning down the cell suspension, the entire transformation was plated on LB agar supplemented with 100 μ g/mL ampicillin.

1.1.5. Miniprep DNA extraction, construct verification and DNA sequencing

Typically, 4 or 5 colonies from each cloning reaction were used to inoculate 5 mL LB cultures supplemented with ampicillin for DNA extraction the following morning after an overnight growth at 37°C. The plasmid DNA was extracted using a DNA miniprep kit (Macherey-Nagel) and the DNA was eluted in 50 μ L of elution buffer. 5 μ L of this miniprep DNA was digested with the two enzymes BamHI and XhoI in 10x CutSmart buffer for 1h at 37°C. The digested plasmid reactions were analyzed on 1% agarose gel and the plasmids containing inserts of the expected size (usually two positive clones) were sent for DNA sequencing (Genewiz). When the sequencing results were available, they were compared to that of the databank and if no mutations were detected, we proceeded with these clones.

1.2. Mutagenesis of UvrC

UvrC mutants were generated from the plasmid carrying the *uvrC* of interest using PCR. The templates were pET151d-*uvrC* full-length for the mutants UvrC^{E72A} and UvrC^{D391A}, pET151d-*uvrC-C* for UvrC-C^{D391A} and pProexHtB-*uvrC-N* for UvrC-N^{E72A}. The primers used to perform the mutagenesis reactions are shown in Table 3.3.

A typical mutagenesis PCR reaction included the following reagents:

20 µL Phusion Master Mix (including Phusion polymerase, dNTPs, MgCl₂ and GC buffer)
 17 µL H₂O
 1 µL template DNA plasmid (20-50ng)
 1 µL Mut primer Forward 20pmol/ µL
 1 µL Mut primer Reverse 20pmol/ µL

40 µL

The PCR reaction cycles used were:

Step 1 – Complete denaturation - 98°C- 3 min
 Step 2 – Denaturation - 98°C- 30 sec
 Step 3 – Annealing – 55 to 58°C- 30 sec
 Step 4 – Elongation - 72°C – 7 min
 Step 5 – Final elongation - 72°C - 10 min
 Step 6 – End of reaction - 10 °C hold.

} 18 cycles

An annealing temperature of 58°C was used for mutants UvrC^{D391A} and UvrC-N^{E72A}, while a lower annealing temperature of 55°C was needed to efficiently amplify PCR products for mutants UvrC^{E72A} and UvrC-C^{D391A}.

Table 3.3: List of primers used for mutagenesis of UvrC

| Mutant | Primers |
|------------|---|
| UvrC_E72A | For: GAGGCACTCGTGCTCGCAGCCAACCTCATCAAG Rev: CTTGATGAGGTTGGCTGCGAGCACGAGTGCCTC |
| UvrC_D391A | For: CGCATCGAGGGCTACGCCAACTCGAACCTGTTT Rev: AAACAGGTTTCGAGTTGGCGTAGCCCTCGATGCG |

The parental DNA was digested using DpnI (1 µL of DpnI for 1h-37°C, twice). We transformed 15 µL of *E. coli* DH5α cells with 1 µL of the digested PCR product. After the

miniprep and the sequencing to check the presence of the mutation, *E. coli* BL21 (DE3) cells were transformed for the expression of the proteins.

2. Protein purification

2.1. Transformation and expression

For protein expression, all clones used in this study were transformed into *E. coli* BL21 (DE3) cells (for UvrA2, UvrB, UvrC, UvrC-NEndo, UvrC-ΔHhH, UvrC-C, UvrC-N) or BL21 (DE3) pLysS (for UvrA1) as described above, except that only 100 μL of the transformation was plated on LB agar plates supplemented with ampicillin. Glycerol stocks of these different transformants were prepared by inoculating 1 mL of LB + ampicillin with one colony and growing the culture to an OD₆₀₀ of 0.6 after which 0.8 mL of culture was mixed with 0.2 mL of 100% sterile glycerol and flash frozen in liquid nitrogen for long-term storage at -80°C.

For all proteins, 2 to 6L of BL21 cultures were prepared in baffled flasks (1L of culture per 2L flask) and protein expression was induced using 1mM of IPTG (Euromedex) at 20°C overnight after the culture reached an OD₆₀₀ of 0.6-0.8. The cells were pelleted by centrifugation at 6,000 x g for 20 min and the cell pellets were resuspended in 20mL of resuspension buffer (see below for details) supplemented with an EDTA-free protease inhibitor tablet (Roche).

2.2. Protein purification

For all the proteins, the presence of the 6x His-tag allowed the first step of purification to be a Nickel column (Histrap Fast Flow from GE healthcare or Ni-IDA from Macherey Nagel). This step was typically followed by at least two or three additional steps:

- TEV cleavage at 4°C to remove the His-tag, followed by a second Nickel affinity column to remove traces of uncleaved protein and the His-tagged TEV protease.
- An anion exchange or heparin column to remove protein contaminants and more importantly DNA contamination.
- A final size exclusion chromatography column to remove the last contaminants, eliminate protein aggregates and verify that homogeneity of the protein preparation.

2.2.1. UvrA1

For UvrA1, the cell pellet was resuspended in buffer A1 composed of 30 mM Na-Phosphate buffer pH 8, 1 M NaCl, 1 mM β -mercaptoethanol (β ME), 2 mM MgCl_2 supplemented with protease inhibitors (Roche). DNase I and lysozyme (Roche) were added to the cell suspension prior to lysis by five freeze/thaw cycles. The cell lysate was centrifuged 30 min at 20,000 rpm at 4°C to separate the cell debris from the supernatant containing the protein. The first purification step was performed on a 5 mL Histrap FF column (GE Healthcare) equilibrated in buffer A to isolate the His-tagged protein. The supernatant was loaded onto the column with a syringe, after which the column was washed with buffer A, and then with buffer A supplemented with 20 mM and 50mM imidazole to eliminate the contaminants. The protein was eluted from the Ni^{2+} column with buffer A supplemented with 200 mM imidazole. The fractions containing UvrA1 were pooled and TEV protease was added to the protein at a 1:20 w/w ratio prior to dialysis at 4°C overnight into buffer A2 composed of 30 mM Na-Phosphate buffer pH 8.0, 2 mM MgCl_2 , 150 mM NaCl, 1 mM tris(2-carboxyethyl)phosphine (TCEP) to reduce the NaCl and remove the imidazole. The cleaved UvrA1 was loaded on 1 mL of Ni-IDA resin (Macherey-Nagel) equilibrated in buffer A2 to remove uncleaved UvrA1 and the his-tagged TEV protease, and was recovered in the flow-through. It was then loaded on a 5 mL HiTrapQ column (GE Healthcare) equilibrated in buffer A2 and eluted with a NaCl gradient from 150 mM to 1 M in buffer A2. Finally, UvrA1 was separated by size exclusion chromatography on a SEC650 column (BioRad) in buffer A3 composed of 50 mM Tris-HCl pH 8, 2 mM MgCl_2 , 150 mM NaCl, 1 mM TCEP and 5% glycerol.

2.2.2. UvrB

For UvrB, the cell pellet was resuspended in buffer B1 composed of 50 mM Tris-HCl pH 8, 2 M NaCl, 10 % glycerol supplemented with protease inhibitors (Roche). DNase I and lysozyme (Roche) were added to the cell suspension prior to lysis by sonication (5 min; 15 sec ON/ 30 sec OFF; intensity 70 %). The cell lysate was centrifuged 30 min at 20,000 rpm at 4°C to separate the cell debris from the supernatant containing the protein. The first purification step was performed on a 5 mL Histrap FF column (GE Healthcare) equilibrated in buffer B2 composed of 20 mM Tris-HCl pH 8, 300 mM NaCl, 5 mM MgCl_2

and 2 mM β ME. The supernatant was loaded onto the column with a syringe, after which the column was washed with buffer B2, and then with buffer B2 supplemented with 30 mM imidazole to eliminate the contaminants. The protein was eluted from the Ni^{2+} column with buffer B2 supplemented with 250 mM imidazole. The fractions containing UvrB were pooled and TEV protease was added to the protein at a 1:20 w/w ratio prior to dialysis at 4°C overnight into buffer B3 composed of 50 mM Tris-HCl pH 8, 150 mM NaCl, 1 mM MgCl_2 and 1 mM TCEP to reduce the NaCl and remove the imidazole. The cleaved UvrB was loaded on a 5 mL HiTrapQ column (GE Healthcare) equilibrated in buffer B3 and eluted with a NaCl gradient from 150 mM to 1 M in buffer B3. Finally, UvrB was separated by size exclusion chromatography on a SEC650 column (BioRad) in buffer B2 supplemented with 10% glycerol.

2.2.3. UvrC

2.2.3.1. Full-length UvrC, UvrC ΔHhH and the mutants

For UvrC full-length, UvrC ΔHhH and the two mutants UvrC^{E72A} and UvrC^{D391A}, cell pellets were resuspended in buffer C1 composed of 50 mM Tris-HCl pH 8, 2 M NaCl, 10 % glycerol supplemented with protease inhibitors (Roche). DNase I, lysozyme (Roche) and S7 nuclease were added to the cell suspension prior to lysis by sonication (5 min; 15 sec ON/ 30 sec OFF intensity 70 %). The cell lysate was centrifuged 30 min at 20,000 rpm at 4°C to separate the cell debris from the supernatant containing the protein. The first purification step was performed on a gravity-flow 2 mL Ni-IDA resin (Macherey-Nagel) equilibrated in buffer C2 composed of 50 mM Tris-HCl pH 8, 1 M NaCl, 10 % glycerol and 2 mM β ME. After loading the supernatant, the resin was washed extensively with buffer C2 to eliminate the contaminants, and the UvrC protein was eluted with buffer C2 supplemented with 500 mM imidazole. The fractions containing UvrC wild-type or mutants were pooled, diluted to lower the NaCl concentration to 300 mM and loaded on a 5 mL Heparin (GE Healthcare) column equilibrated in buffer C3 composed of 50 mM Tris-HCl pH 8, 300 mM NaCl, 10 % glycerol and 2 mM β ME to eliminate DNA contamination. After loading the diluted protein, the column was washed with buffer C3 and the protein was eluted with a NaCl gradient from 300 mM to 1 M in buffer C3. Fractions containing the UvrC protein were pooled and TEV protease was added to the

protein at a 1:20 w/w ratio and incubated with UvrC at 4°C overnight. The cleaved UvrC was then concentrated and separated by size exclusion chromatography on a SEC650 column (BioRad) in buffer C4 composed of 50 mM Tris-HCl pH 8, 500 mM NaCl, 10 % glycerol, 5 mM MgCl₂ and 2 mM βME.

2.2.3.2. UvrC-NEndo

For UvrC-NEndo, the cell pellet was resuspended in buffer D1 composed of 50 mM Tris-HCl pH 7, 1 M NaCl, 10 % glycerol, 1 mM MgCl₂, 2 mM βME supplemented with protease inhibitors (Roche). DNase I, lysozyme (Roche) and S7 nuclease were added to the cell suspension prior to lysis by sonication (5 min; 15 sec ON/ 30 sec OFF; intensity 70 %). The cell lysate was centrifuged 30 min at 20,000 rpm at 4°C to separate the cell debris from the supernatant containing the protein. The first purification step was performed on a 5 mL HisTrap FF column (GE Healthcare) equilibrated in buffer D1. The supernatant was loaded onto the column with a syringe, after which the column was washed with buffer D1, and then with buffer D1 supplemented with 50 mM imidazole to eliminate the contaminants. The protein was eluted from the Ni²⁺ column with buffer D1 supplemented with 250 mM imidazole. UvrC-NEndo was separated on a SEC 70 column in buffer D2 composed of 50 mM Tris-HCl pH 7, 500 mM NaCl, 10 % glycerol, 1 mM MgCl₂, 2 mM βME. The fractions containing the protein were pooled and TEV protease was added to the protein at a 1:20 w/w ratio and incubated at 4°C overnight. The cleaved UvrC-NEndo was loaded on a gravity-flow 1 mL Ni sepharose resin (Macherey-Nagel), equilibrated in buffer D1 to remove uncleaved UvrC-NEndo and the His-tagged TEV protease, and was recovered in the flow-through and in the washes performed with buffer D1 supplemented with 25 mM imidazole. Finally, UvrC-NEndo was separated by size exclusion chromatography on a SEC70 column (BioRad) in buffer D2.

2.2.3.3. UvrC-N, UvrC-C

For UvrC-N, the cell pellet was resuspended in buffer E1 composed of 50 mM Tris-HCl pH 8, 1 M NaCl, 10 % glycerol, 1 mM MgCl₂, 2 mM βME supplemented with protease inhibitors (Roche). DNase I, lysozyme (Roche) and S7 nuclease were added to the cell suspension prior to lysis by sonication (5 min; 15 sec ON/ 30 sec OFF; intensity 70 %). The cell lysate

was centrifuged 30 min at 20,000 rpm at 4°C to separate the cell debris from the supernatant containing the protein. The first purification step was performed on a 5 mL Histrap FF column (GE Healthcare) equilibrated in buffer E1. The supernatant was loaded onto the column with a syringe, after which the column was washed with buffer D1, and then with buffer D1 supplemented with 25 mM and 50 mM imidazole to eliminate the contaminants. The protein was eluted from the Ni²⁺ column with buffer E1 supplemented with 250 mM imidazole. UvrC-N was separated on a SEC 650 column in buffer E1. The fractions containing the protein were pooled and TEV protease was added to the protein at a 1:20 w/w ratio and incubated at 4°C overnight. The cleaved UvrC-N was loaded on a gravity-flow 1 mL Ni sepharose resin (Macherey-Nagel), equilibrated in buffer E1 to remove uncleaved UvrC-N and the His-tagged TEV protease, and was recovered in the flow-through and in the washes performed with buffer E1 supplemented with 20 mM imidazole. Finally, UvrC-N was separated by size exclusion chromatography on a SEC650 column (BioRad) in buffer E2 composed of 50 mM Tris-HCl pH 8, 500 mM NaCl, 10 % glycerol, 1 mM MgCl₂, 2 mM βME.

For UvrC-C, the cell pellet was resuspended in buffer E1 supplemented with protease inhibitors (Roche), DNase I and lysozyme (Roche) prior to lysis by sonication (4 min; 15 sec ON/ 30 sec OFF; intensity 70 %). The cell lysate was centrifuged 30 min at 20,000 rpm at 4°C to separate the cell debris from the supernatant containing the protein. The first purification step was performed on a 5 mL Histrap FF column (GE Healthcare) equilibrated in buffer F1 composed of 50 mM Tris-HCl pH 8, 1M NaCl and 2.5 mM MgCl₂. The supernatant was loaded onto the column with a syringe, after which the column was washed with buffer F1, and then with buffer F1 supplemented with 25 mM imidazole to eliminate the contaminants. The protein was eluted from the Ni²⁺ column with a buffer composed of 50 mM Tris-HCl pH 8, 200 mM NaCl, 2.5 mM MgCl₂ and 50 mM imidazole. The fractions containing the protein were pooled and TEV protease was added to the protein at a 1:20 w/w ratio and the mix was dialysed at 4°C overnight against 1L of 50 mM Tris-HCl pH 8 and 100 mM NaCl. The cleaved UvrC-C was loaded on a gravity-flow 1 mL Ni sepharose resin (Macherey-Nagel), equilibrated in 50 mM Tris-HCl pH 8 and 200 mM NaCl to remove uncleaved UvrC-C and the his-tagged TEV protease, and was recovered in the flow-through. Finally, UvrC-C was separated by size exclusion chromatography on a SEC650 column (BioRad) in buffer F2 composed of 50 mM Tris-HCl pH 8 and 200 mM NaCl.

3. DNA material

3.1. Oligonucleotides

The DNA substrates used in the incision assay are all double-stranded DNAs 50 base pairs in length with different sequences and/or different modifications. The sequences of these oligonucleotides and their features are shown in Table 3.4. All DNA oligonucleotides were synthesised by Eurofins MWG and were prepared in DNA resuspension buffer (10 mM Tris-HCl pH 8.0, 50 mM NaCl, 0.5 mM EDTA) at a concentration of 100 μ M. The 50mer DNA substrates are only labelled on one strand that contains a fluorophore (ATTO633, red or a FAM, green) at the 5' end, and a thymine in position 26 conjugated to either biotin or fluorescein. Fluorescein- and biotin-conjugated thymines are known substrates of bacterial NER (Truglio et al., 2006a). The modified nucleotide is located in the centre of the upper strand of the duplex. dsDNA substrates presented in Table 3.5 were prepared by annealing 1 volume of labelled oligonucleotide with a slight excess (1:1.1 ratio) of non-labelled complementary strand. The annealing reactions were heated to 98°C for 5 minutes and transferred directly into a 1 L of water at 100°C, which was left at room temperature for slow cooling. The final concentration of annealed substrate was 50 μ M. The DNA substrates were later diluted in DNA resuspension buffer to 250 nM for use in the incision assay.

Table 3.4: List of oligonucleotides used in this study









| Name | Sequence | Modification(s) |
|---------------------|---|--|
| 5'-ATTO633-seq1 | 5'-  - GAC TAC GTA CTG TTA CGG CTC CAT CTC TAC CGC AAT CAG GCC AGA TCT GC -3' | X = ATTO633 |
| 5'-FAM-seq1 | 5'-  - GAC TAC GTA CTG TTA CGG CTC CAT CTC TAC CGC AAT CAG GCC AGA TCT GC -3' | X = FAM |
| 5'-ATTO633-F26-seq1 | 5'-  - GAC TAC GTA CTG TTA CGG CTC CAT  C TAC CGC AAT CAG GCC AGA TCT GC -3' | X = ATTO633 Y = Fluo-dT |
| 5'-ATTO633-F26-seq2 | 5'-  - GTT AGC GAA CGA TAC CTT CAG TAG  C AAG TCC TAG CTG ACC GGT TCG GC -3' | X = ATTO633 Y = Fluo-dT |
| 5'-FAM-B26-seq1 | 5'-  - GAC TAC GTA CTG TTA CGG CTC CAT  C TAC CGC AAT CAG GCC AGA TCT GC -3' | X = FAM Y = Biotin-dT |
| Rev-seq1 | 5'- GCA GAT CTG GCC TGA TTG CGG TAG AGA TGG AGC CGT AAC AGT ACG TAG TC -3' | |
| Rev-seq2 | 5'- GCC GAA CCG GTC AGC TAG GAC TTG A T CTA CTG AAG GTA TCG TTC GCT AAC -3' | |

Table 3.5: List of dsDNA substrates used in the incision assay

| Name | Oligo 1 | Oligo 2 |
|---------------------------|-------------------------|----------------|
| 5'red-50merF26-seq1 | 5'-ATTO633-F26-seq1 | Rev-seq1 |
| 5'red-50merF26-seq2 | 5'-ATTO633-F26-seq2 | Rev-seq2 |
| 5'red-50merB26-seq1 | 5'-FAM-B26-seq1 | Rev-seq1 |
| 5'red-50mer-seq1 | 5'-ATTO633-seq1 | Rev-seq1 |
| 5'green-50mer-seq1 | 5'-FAM-seq1 | Rev-seq1 |
| 5'red-50merB26-strep-seq1 | 5'-FAM-B26-seq1 + strep | Rev-seq1 |

To generate streptavidin-bound DNA substrate, we incubated the dsDNA substrate containing biotin with streptavidin. 20 μ L reactions containing 0.5 μ M dsDNA 50mer B26 oligonucleotide and 10 μ M streptavidin (Sigma) in DNA resuspension buffer were incubated at 25°C for 30 min. Coupling of streptavidin to the biotin was verified by electrophoresis on a 10% TBE native polyacrylamide gel.

3.2. Plasmids

Supercoiled pUC19 plasmid DNA was extracted from 300 mL cultures of *E. cloni*® *E. coli* cells (Euromedex) with a DNA Maxiprep kit (Macherey-Nagel). The purified DNA was resuspended in sterile water at a final concentration of 1 μ g/ μ L. The harvested plasmids were subsequently treated with UV-C light, BPDE, Cisplatin, KMnO₄ or riboflavin as described below to introduce respectively pyrimidine dimers, BPDE-conjugates, inter- and intrastrand crosslinks, thymine glycols and 8-oxo-guanine into the plasmid according to protocols previously developed by Jean-Luc Ravanat and colleagues. After DNA treatments, the plasmid integrity was verified on a 0.8% TBE agarose gel to ensure the plasmid was still largely supercoiled.

3.2.1. UV-C light treatment

We diluted the plasmid to 40 ng/ μ L in water. Drops of 1 μ g pUC19 were frozen on a petri dish. We placed the petri dish under a UV-C light (254 nm) and a radiometer connected to a UVC probe allowed to quantify the doses of irradiation. Three doses were used 0.03 J/cm², 0.15 J/cm², 0.3 J/cm².

3.2.2. BPDE treatment

The damaging agent Benzo[a]pyrene-7,8-dihydrodiol-9,10-epoxyde (BPDE) was dissolved in a solvent composed of 95% THF and 5% TEA to obtain a stock solution of

7.6mM. We incubated 50 µg pUC19 with 5 µL DMSO and 150µM of BPDE for 2 hours at 37°C. The plasmid was then precipitated with 1/10V of 4M NaCl and 2.5V of ethanol 100%, rinsed with ethanol 70% and resuspended in 50µL H₂O at a final concentration of 904 ng/µL.

3.2.3. Cisplatin treatment

We incubated 150 µg pUC19 with 15 µL of cisplatin (1mg/mL) for 2 hours at 37°C. The plasmid was then precipitated with 1/10V of 4M NaCl and 2.5V of ethanol 100%, rinsed with ethanol 70% and resuspended in 150 µL H₂O at a final concentration of 1 µg/µL.

3.2.4. KMnO₄ treatment

150 µg pUC19 were precipitated with 1/10V of 4M NaCl and 2.5V of ethanol 100%, rinsed with ethanol 70% and resuspended in 200 µL of 0.4 M potassium phosphate prior to the addition of 20 µL of 0.4 M KMnO₄. After five minutes of incubation at 4°C, we added 5 µL of allyl alcohol and kept it at 4°C. We centrifuged the reaction 10 minutes at 10,000 rpm and the supernatant was loaded on a NAP 5 column to separate the plasmid. After the load penetrated the resin of the column, we added ~ 300 µL of 10 mM sodium phosphate and eluted the plasmid with 500 µL of sterile water. A new precipitation of the DNA was performed and the plasmid DNA was resuspended in 150 µL H₂O at a final concentration of 1 µg/µL.

3.2.5. Riboflavin treatment

10 mg of riboflavin were dissolved in 150 mL of H₂O and filtered on a 0.22 µm membrane, 3 hours prior to the reaction. 400 µg pUC19 (in 400 µL H₂O) were oxygenated with a pipette during 15 min before addition of 128 µL of filtered riboflavin (32 µl per 100 µg of oxygenated plasmid). We then irradiated the mix for 2 minutes with a halogen light. The DNA was precipitated with 1/10V of 4M NaCl and 2.5V of ethanol 100%, rinsed with ethanol 70% and resuspended in 100 µL H₂O at a final concentration of 1 µg/µL.

3.2.6. Abasic site treatment

To generate abasic sites, we incubated a mix containing 100 µg pUC19 (at 1 µg/µL), 5 µL 0.5 M sodium citrate pH 4.8 and 12 µL 2 M KCl pH 7.9 at 70°C for 1h, 2h, 3h and 4h. 6 µL 0.5 M EDTA and 10 µL 1.5 M Tris-HCl pH 7.5 were added to stop the reaction. The DNA was precipitated with 1/10V of 4M NaCl and 2.5V of ethanol 100%, rinsed with ethanol 70% and resuspended in 100 µL H₂O at a final concentration of 1 µg/µL.

4. Incision assay

The incision assays were performed on either 50mer dsDNA substrates or on treated plasmids. The optimal reaction contained the following reagents:

- 10x buffer composed of 0.5 M Tris pH 7.5, 0.5 M KCl, 50 mM DTT, 20 µM BSA and 25mM MgCl₂
- 2.5 mM ATP prepared in 50 mM Tris-HCl pH 8.0
- DNA substrate: 25 nM 50mer dsDNAs (Table 8) or 120 – 360 ng pUC19 treated plasmid
- 1 µM UvrA1, 0.5 µM UvrB and 2 µM UvrC diluted in a common buffer (50 mM Tris pH 8, 150 mM NaCl, 5% glycerol, 2 mM βME freshly added)

10 µL reactions containing the 10x buffer, DNA, Uvr proteins and water were preincubated at 37°C for 5 min before starting the reaction by the addition of ATP. The incision assay was performed at 37°C for up to 2h.

1 reaction: 10µL

4.5 µL H₂O

1 µL 10x buffer

0.5 µL ADN 0.5µM

1 µL UvrA 10µM

1 µL UvrB 5µM

1 µL UvrC 20µM

----- 3 minutes- 37°C

1 µL ATP 25mM

To stop the reaction, 10 µL of 2x urea loading buffer (composed of 2x TBE, 8 M urea, 0.025% Bromophenol blue and 0.1% SDS) were added to 10 µL incision reaction.

For time course experiments, larger mixes were prepared and incubated at 37°C, and at each timepoint, 10 µL of reaction were retrieved from the mix and added to Eppendorf tubes containing 10 µL of 2x urea loading buffer to stop the reaction.

The incision assay was also performed on plasmid DNA treated as described above. For this, the following reactions were prepared:

1 reaction: 10µL

3 µL H₂O
 1 µL 10x buffer
 2 µL ADN 40 ng/µL
 1 µL UvrA (250 nM- 10 µM)
 1 µL UvrB (250 nM- 5 µM)
 1 µL UvrC (250 nM- 20 µM)
 ----- 3 minutes- 37°C
 1 µL ATP 25mM then incubation at 37°C

The reactions were stopped with the addition of 1µL 10x DNA loading buffer (0.1 M EDTA, 0.5% SDS, 25% glycerol, 0.1% bromophenol blue). The state of the plasmid DNA after the incision assay was assessed on 0.8% TBE agarose gels.

5. Analysis methods

5.1. Gel electrophoresis

Various types of gel electrophoresis were used during this study, which are summarized in Table 3.6. Visualization of these gels was performed on a multifunctional imager, the Chemidoc MP imager from Biorad. The images obtained could be further analyzed and the bands quantified using the software ImageLab (Biorad) as described below.

Table 3.6: Summary of the different types of electrophoresis performed during this work.

| Sample type | Gel type | Acrylamide (%) | Electro-phoresis conditions | Purpose | Visualization mode |
|-------------|----------|----------------|-----------------------------|--|--------------------|
| Proteins | SDS page | 15% | 200 V 45 min room temp | Instant blue staining for smaller proteins | Colorimetric |

| | | | | | |
|-------------------|---|-----------|--|--|--|
| | TGX Stain free (Biorad; no need for staining post migration) | 10% - 12% | 250-300 V 20-30 min room temp | Visualization of proteins | Activation of stain free dye in gel by UV and detection of fluorescence signal |
| Oligo-nucleotides | TBE native polyacrylamide | 15% | 100 V 2h 4°C | Integrity of the oligonucleotide Verification of the annealing | Detection of fluorescence signal |
| | 8M Urea TBE polyacrylamide | 20% | 5W/gel 35 min room temp (gels are pre-run for 30 min at 5W/gel) | Analysis of incision assay products. | Detection of fluorescence signal in either the green (fluorescein and FAM) or the red (ATTO633) channel. |
| Plasmids | Agarose | 0.8% | 100 V 1h 4°C | Verification of conformation of supercoiled plasmid after treatments and incision assay. | Gel red staining after electrophoresis |
| | | 1% | 100 V 30 min room temp | Verification of minipreps | Gel green stain incorporated in the gel |

5.2. Quantification of DNA bands on TBE-Urea polyacrylamide gels

The incision efficiency by UvrABC was evaluated by quantifying the fragments resulting from the incision assay. TBE-urea gels were visualized on the ChemiDoc™ MP Imaging system using two filters: Alexa 647 and Fluorescein. With Image Lab 6.0, the quantification of each band of a lane was made using the lane profile tool as shown in Figure 3.1. This allows to locally correct for the background signal of the gel, which is not uniform. Adjustments were made to the lane profile so that all bands were suitably

integrated. Since the first well on the gel is often the DNA alone, background values from the control lane were subtracted from the values obtained for the equivalent bands in the adjacent wells and the fluorescence signal corresponding to each band was then exported into an Excel file for further processing.

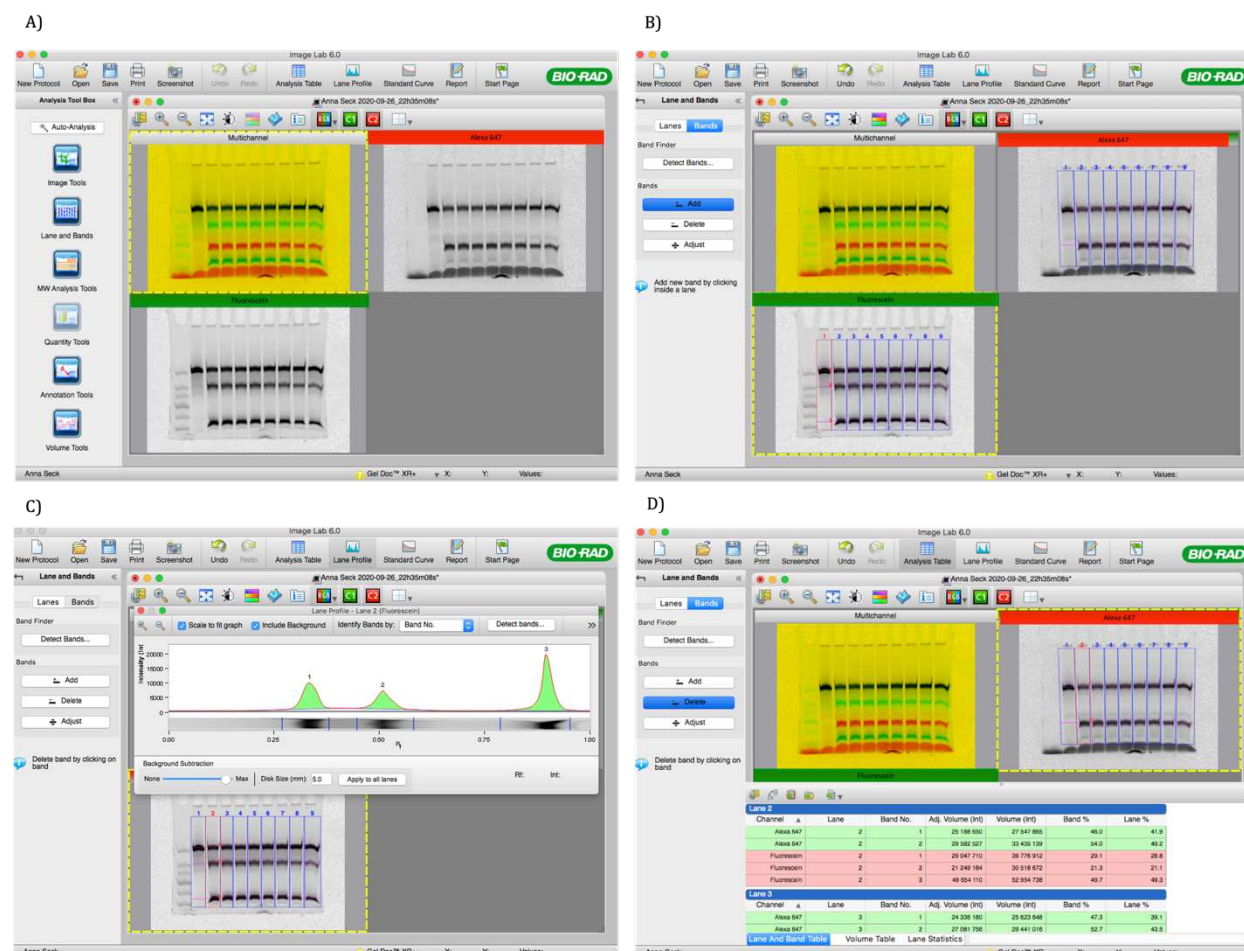


Figure 3.1: Data processing using Image Lab 6.0. The TBE- urea polyacrylamide gel is visualized with the filters Alexa 647 (red bands) and Fluorescein (green bands). A) The multichannel image of the gel is the merged image showing overlaid red and green signals (with yellow background). The 50 mer DNA substrate is visible on both filters, red and green, and the overlay appears in black in the multichannel image. The 32 mer and the 12 mer fragments are only visible with the green filter, whereas the 18 mer fragment is only seen with the red filter. B) Lanes and bands are analyzed for the quantification of fragments in each reaction. The number of lanes corresponds to the number of reactions. The software automatically detects the bands. C) Adjustments are made on the lane profile to have the accurate quantification of each band and the best possible subtraction of background signal. D) The analysis table is generated and exported into Excel for further data analysis and preparation of graphs in Excel and GraphPad Prism 6. Values corresponding to the adjusted volumes and the percentage of bands were used for the analysis.

6. HPLC MS MS

6.1. Principle

The method allows the sensitive and specific detection of DNA lesions. Following enzymatic digestion of DNA, the resulting nucleosides are separated by HPLC onto a C18 reverse-phase chromatography column and eluted with a mixture of an aqueous buffer and acetonitrile allowing separation of nucleosides according to their polarity. The output of the HPLC column is connected through electrospray ionization to a tandem mass spectrometer that is used to detect the DNA lesions using the so-called multiple reaction monitoring (mrm) mode. The first quadrupole selects the pseudomolecular ion of the nucleoside (protonated $[M+H]^+$ or deprotonated $[M-H]^-$ in the positive and negative mode, respectively) that is produced during ionization. This ion is then fragmented in the second quadrupole that is a collision cell and the third quadrupole selects a specific daughter ion of the nucleoside to be detected. Each nucleoside is thus detected using a specific transition, corresponding to its specific parent and daughter ions, such as 284→168 for 8-oxodGuo. Quantification is performed by external calibration. The different transitions that have been used to detect the studied DNA lesions are given in Table 3.7.

Table 3.7: Transitions used to detect different DNA lesions.

| Lesions | Ionisation mode | Transitions |
|---------------------------|-----------------|------------------------------------|
| TT CPD | Neg | 545→447 |
| TT 64PP | Neg | 545→432 |
| 8 oxodGuo | Pos | 284 → 168 |
| BPDE-N ² -dGuo | Pos | 570 → 454 570→ 285 570 → 257 |
| Thymine Glycol | Neg | 275→116 |
| Cisplatin | Neg | 745-513 |

6.2. Separation of the excised oligonucleotide from the plasmid

HPLC MS/MS analysis was only performed on the plasmids. After the different treatments, 120 ng pUC19 was incubated with UvrABC as shown in the following reaction:

1 reaction: 10 μ L

1 μ L 10x buffer
2 μ L H₂O
3 μ L ADN 40 ng/ μ L
1 μ L UvrA (250 nM- 10 μ M)
1 μ L UvrB (250 nM- 5 μ M)
1 μ L UvrC (250 nM- 20 μ M)
----- 3 minutes- 37°C
1 μ L ATP 25mM then incubation at 37°C

For the plasmids treated with UV-C light and BPDE, three reactions were grouped to have enough DNA for efficient detection during the HPLC- MS/MS (360 ng of pUC19 equivalent of 3 reactions). Only one reaction was necessary for the detection of TGs and cisplatin lesions (120 ng of pUC19).

These reactions were stopped by placing the tubes on ice. For a 10 μ L reaction, 90 μ L of sterile water was then added to facilitate the separation on the filter and heated 5 minutes at 95°C. The filters Nanosep - 30k Omega (Pall-vwr) were used to separate the plasmids from the released 12 mer fragments in order to analyse both fractions resulting from the repair by UvrABC.

6.3. Sample Preparation

After separating the repaired plasmids into two fractions (remaining plasmids + 12 mer fragment) on the filter, the two compartments were digested into nucleosides. This digestion of the plasmids includes two steps: first, there is a 2-hour incubation at 37°C with 0.025 U Phosphodiesterase II (P9041, Sigma), 2.5 U DNase II (D4138, Sigma), 0.5 U Nuclease P1 (N8630, Sigma) and 2.5 μ L MNSPDE buffer 10X (200 mM succinic acid, 100 mM CaCl₂, pH 6); the second part is a 2-hour incubation at 37°C after adding 0.015 U Phosphodiesterase I (P3243, Sigma), 2 U Alkaline phosphatase (P6774, Sigma) and 6 μ L of buffer (500 mM Trizma. base, 1 mM EDTA, pH 8). The reaction is then neutralized with 3.5 μ L of 0.1N HCl, centrifuged for 5 minutes at 5000 g, lyophilised and finally

resuspended in the HPLC solvent. This lyophilisation step helps reduce the volume for a more sensitive analysis.

6.4. Sample analysis

During the HPLC MS/MS analysis, the chromatograms obtained will illustrate the different transitions following the fragmentation of the adducts as shown in Figure 3.2. The data collected were analysed using the program Analyst.

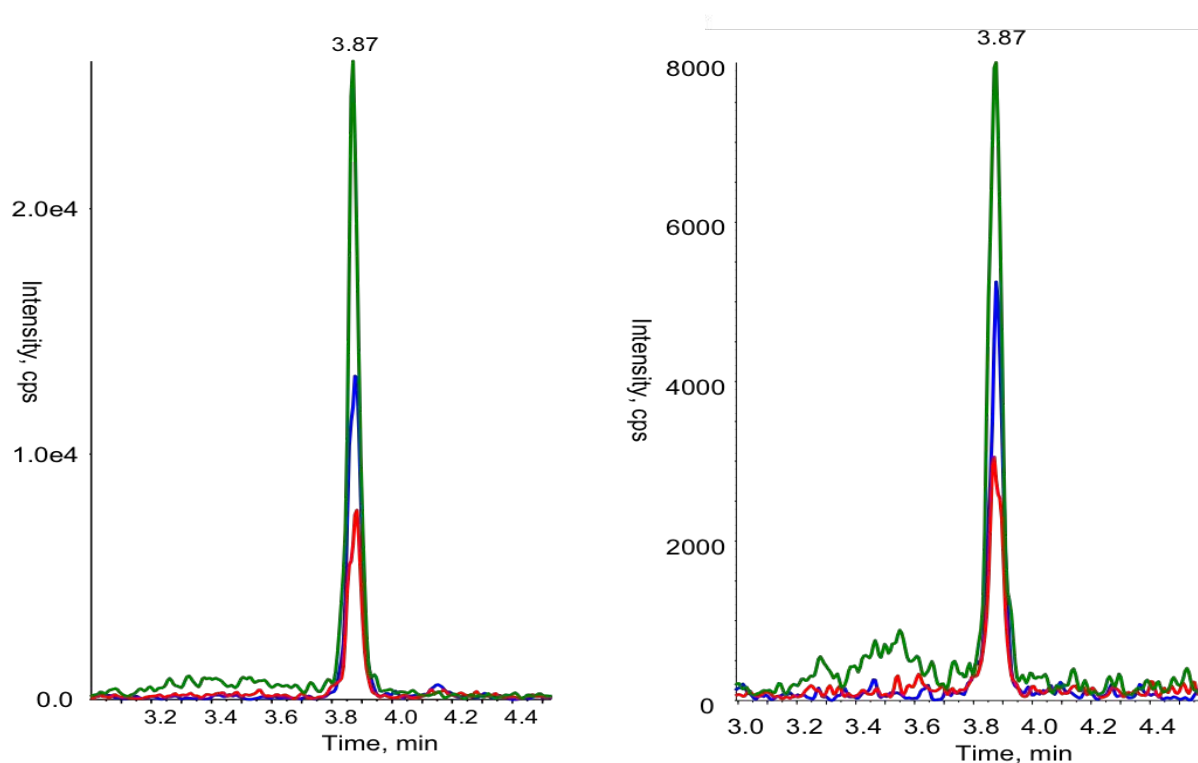


Figure 3.2: Typical chromatograms obtained for the detection of dG-BPDE adducts by HPLC-MS/MS in hydrolysed plasmid (left) and hydrolysed isolated 12mer oligonucleotide (right). 3 transitions were used to detect dG-BPDE adducts: 570 → 454 (blue), 570 → 285 (red), 570 → 257 (green).

7. MALDI-TOF

7.1. Principle

This technique was used to precisely determine the sites of cleavage of the incision reaction by the NER system on oligonucleotide substrates. After processing by the UvrABC proteins the reactions were co-crystallized with a matrix, 3-hydroxypicolinic acid, 3HPA. This matrix allows a strong laser absorption. The mix of matrix and sample was dried on a plate and then exposed to short laser pulses that desorb the matrix and ionize the sample thanks to a charge transfer. The laser energy of the crystal molecules is converted to vibrational oscillation and it leads to the breakdown of the crystal. The ions are accelerated to the detector and are sorted based on their m/z ratio.

7.2. Sample preparation

The incision reactions with UvrABC and the oligonucleotides were performed with the minimum amount of glycerol possible to facilitate the first step of the sample preparation. In fact, 10 pmoles of DNA processed or not by the UvrABC were collected on a Ziptip column C18 and then eluted with 10 μ L 50% acetonitrile. 1 μ L of the sample and 1 μ L of 3HPA were then co-crystallised under vacuum. Next, the plate is placed in the spectrometer for analysis and lasers are focused on different places of the well (Figure 3.3).

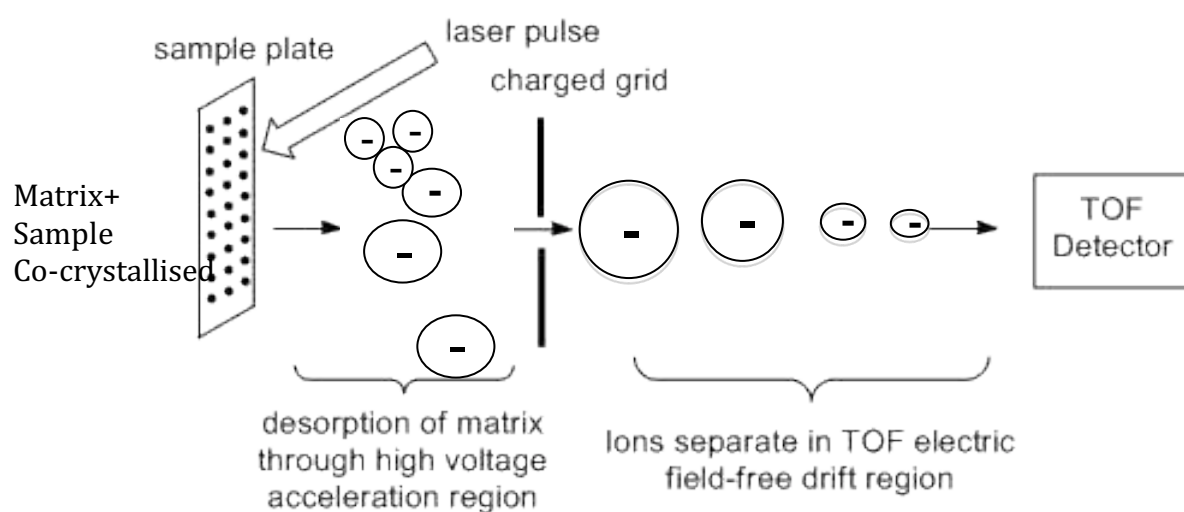


Figure 3.3: Scheme of the ionization of analytes.

Results

Chapter I: Reconstitution of *D. radiodurans* NER *in vitro*

1. Principle of the NER incision assay

1.1. Components of the incision assay

The incision assay was set up with the UvrA1, UvrB and UvrC proteins and a 50 mer dsDNA substrate, 5'red-50merF26-seq1, composed of an oligonucleotide containing a red fluorophore (ATTO633) at the 5' end and a fluorescein-conjugated thymine (FdT) in position 26 that is recognized as a substrate by bacterial NER systems (Truglio et al., 2006a), annealed with its unlabelled complementary strand. In addition, the reaction is buffered at pH 7.5, and contains bovine serum albumin (BSA) to stabilise the proteins and minimise non-specific interactions within the reaction. As described below, a number of parameters needed to be optimized in order to achieve efficient release of the short DNA fragment containing FdT: (i) the purity and stability of the Uvr proteins, (ii) the exact composition of the reaction and the concentrations of each of the constituents (substrate, Uvr proteins, salt, divalent cations, reducing agent etc.), (iii) the temperature of the reaction, and (iv) the order in which the reaction mixture was prepared.

1.2. Analysis of incision products by electrophoresis on urea polyacrylamide gels

Thanks to the presence of the two fluorophores on the dsDNA substrate, we could track the different fragments resulting from the incision. The different fragments produced during the repair are presented in Figure 4.1. Depending on the order of the cuts occurring in the substrate, we can visualize different intermediate fragments on the gel prior to the release of the 12 mer fragment containing the lesion, either a 32 mer if 5' incision occurs first (Figure 4.1.A) or a 30 mer fragment if 3' incision occurs first (Figure 4.1.B).

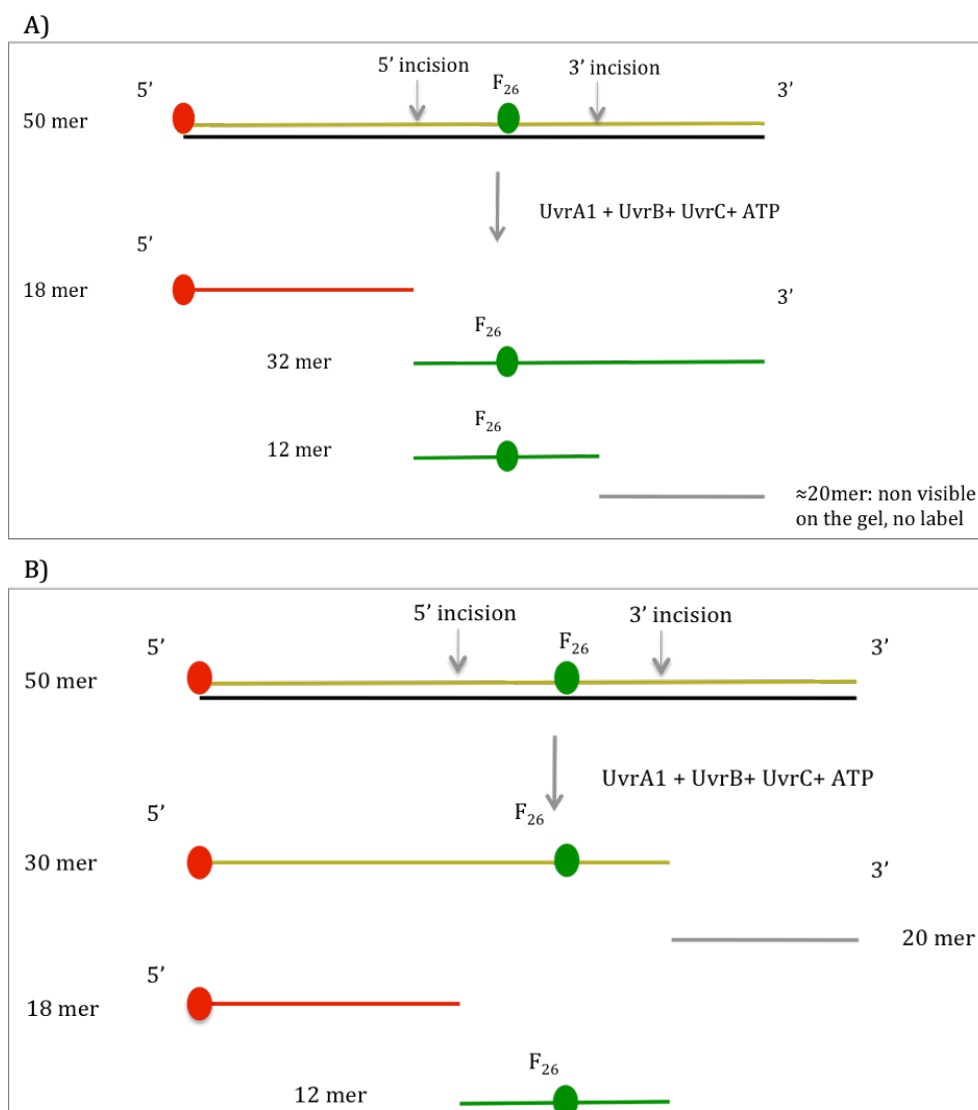


Figure 4.1: Possible schemes of the repair of the 50 mer dsDNA substrate analysed on a urea polyacrylamide gel: A) If the 5' incision occurs first, an 18 mer fragment is released containing an ATTO633 at its 5' end, monitored with the Alexa 647 red filter on the Chemidoc MP imager, and a 32 mer fragment is also produced that carries the fluorescein-conjugated thymine (mimicking the lesion), which can be monitored with the Fluorescein green filter on the Chemidoc MP imager. The 32 mer fragment is then further incised on the 3' side of the lesion to release a 12 mer fragment that contains the lesion that can also be monitored with the Fluorescein filter. The 20 mer fragment produced by this second cleavage step (as well as the complementary strand) does not carry any fluorophore, and is therefore not visible on the gel. B) If the 5' incision occurs first a 20 mer fragment not visible on the gel and a 30 mer fragment containing an ATTO633 at its 5' end and the fluorescein-conjugated thymine, are released. The 30 mer fragment can be monitored on both Alexa 647 and Fluorescein filters. The 30 mer fragment is then incised on the 5' side of the lesion to release the 12 mer that contains the lesion and the 18 mer fragment with the ATTO633 at its 5' end.

2. Purification of the UvrA1, UvrB and UvrC proteins from *D. radiodurans*

The experiments described in this thesis were conducted using different batches of proteins. The purification protocols for the UvrA1, UvrA2 and UvrB proteins were already established in the laboratory, while the purification of UvrC required some optimisation. All Uvr proteins were expressed in *E. coli* with a cleavable N-terminal His-tag.

A detailed description of the different chromatographic steps used to purify the Uvr proteins is provided in the Materials and Methods. Below is a brief overview of the purifications of drUvrA1 and drUvrB, and a more detailed account of the optimisation of the purification of drUvrC.

2.1. Purification of drUvrA1

drUvrA1 is a ~110 kDa protein forming a dimer. Its purification involves three chromatographic steps: nickel-affinity, anion exchange and size-exclusion chromatography. TEV protease cleavage of the His-tag was performed after the anion exchange and traces of His-tagged drUvrA1 and His-tagged TEV protease were removed by a second nickel-affinity step. Figure 4.2 presents the chromatograms from each step. The fractions containing the protein were gathered (indicated in red). After the final size-exclusion chromatography column, two pools were made and tested in the incision assay to determine the fractions to keep for the following experiments (Figure 4.2.C). The aggregated protein (in blue on Figure 4.2.D), was not suitable/functional for the incision assay. The typical yield of drUvrA1 protein was 2.5 mg/L culture.

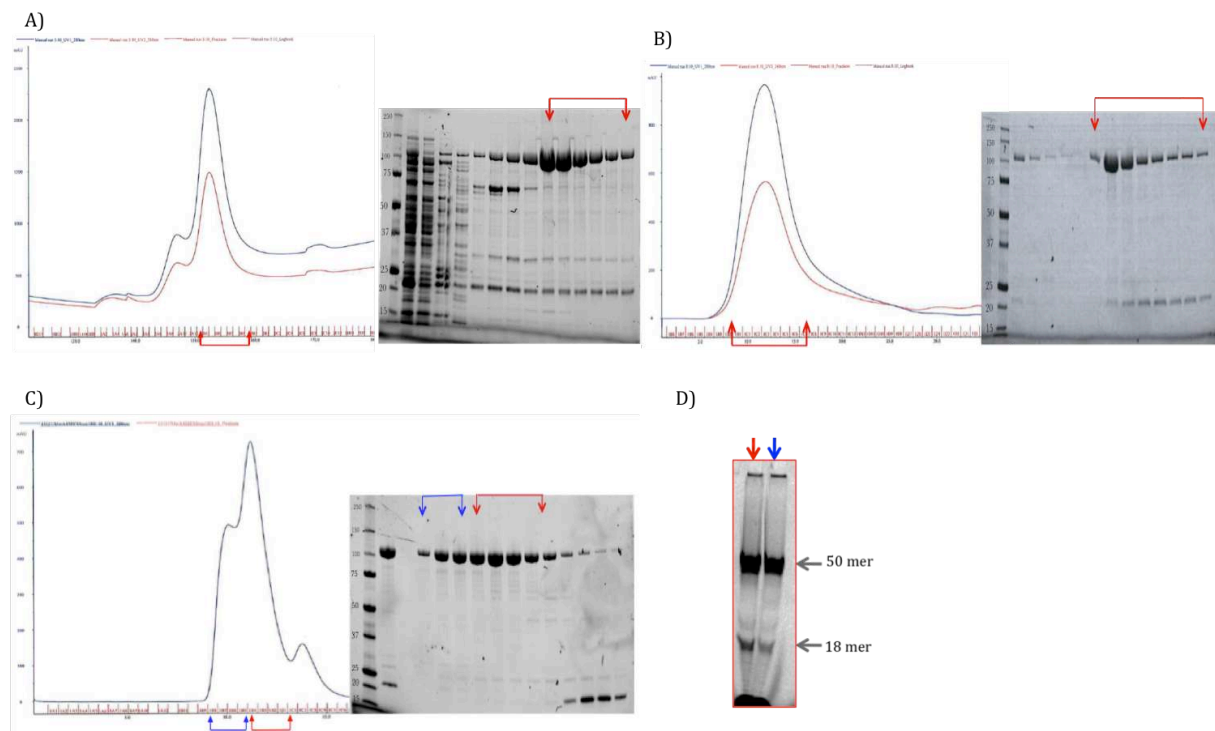


Figure 4.2: Purification steps of UvrA1 from *Deinococcus radiodurans*: A) Chromatogram of the HisTrap FF column with the SDS-PAGE gel of the fractions gathered after the purification, indicated with the red arrow. B) Chromatogram of the HisTrap Q column with the SDS-PAGE gel of the fractions gathered after the purification, indicated with the red arrow. C) Chromatogram of the SEC 650 column and its SDS-PAGE gel. The fractions of the peaks are indicated with blue (corresponding to aggregated UvrA) and red (dimeric UvrA) arrows. D) The fractions from the two peaks obtained after the last step of purification were tested during the incision assay with the substrate 5'red-50merF26-seq1. The incision activity was more efficient with the UvrA from the red fractions.

2.2. Purification of drUvrB

drUvrB is ~80 kDa. Its purification involves three chromatographic steps: nickel-affinity, anion exchange and size-exclusion chromatography (Figure 4.3). The TEV protease cleavage of the His-tag was performed after the nickel-affinity column. The cut was 100% effective, the His-tagged TEV protease was removed during the size-exclusion column. The yield of drUvrB protein was 3.5 mg/L culture. Each new batch of protein was tested to confirm the functionality of the protein in the incision assay.

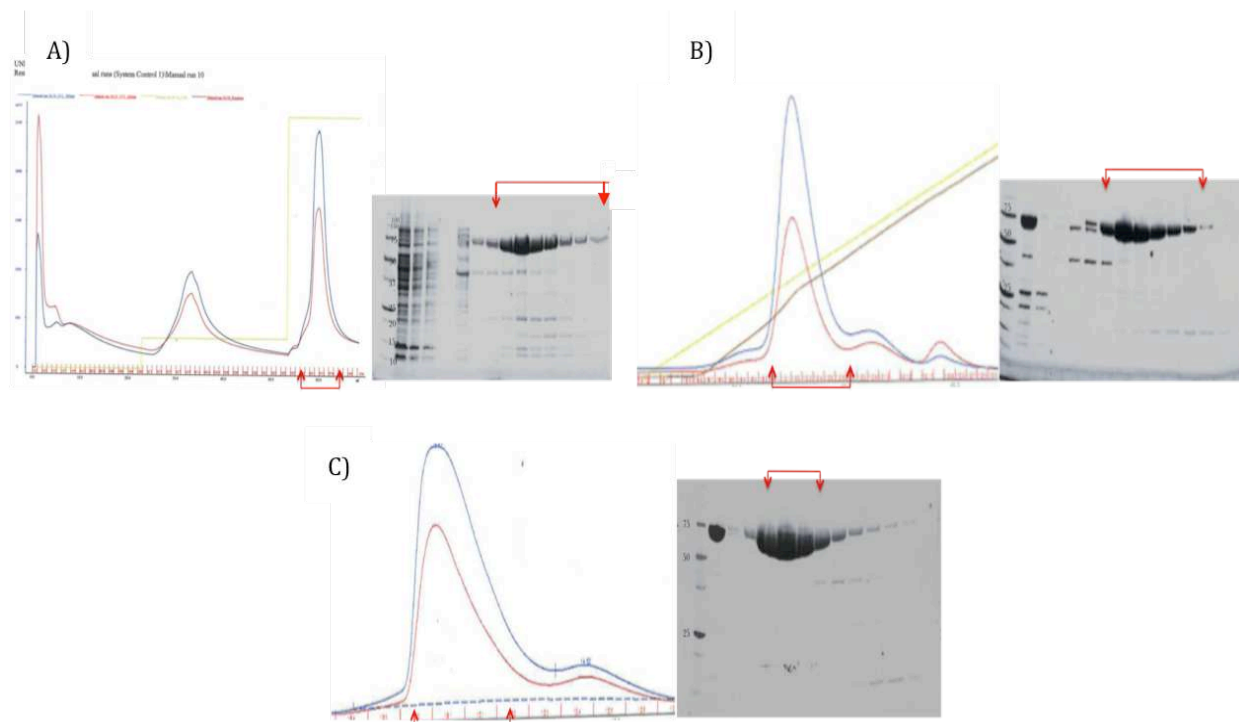


Figure 4.3: Purification steps of UvrB from *Deinococcus radiodurans*: A) Chromatogram of the HisTrap FF column with the SDS-PAGE gel of the fractions gathered after the purification, indicated with the red arrow. B) Chromatogram of the HiTrap Q column with the SDS-PAGE gel of the fractions gathered after the purification, indicated with the red arrow. C) Chromatogram of the SEC 650 column and SDS-PAGE gel of the fractions gathered after the purification, indicated with the red arrow.

2.3. Optimisation of the purification of drUvrC

drUvrC is a 69 kDa protein. Its purification involves three chromatographic steps: nickel-affinity, heparin affinity and size-exclusion chromatography (Figure 4.4).

The first purification was performed as follows:

- A HisTrap FF column to collect the His-tag-UvrC:
- An overnight dialysis along with TEV cleavage at 4°C
- A heparin column to eliminate DNA contamination.
- A final gel filtration using a SEC650 column to remove the last impurities and have the protein in a storage buffer

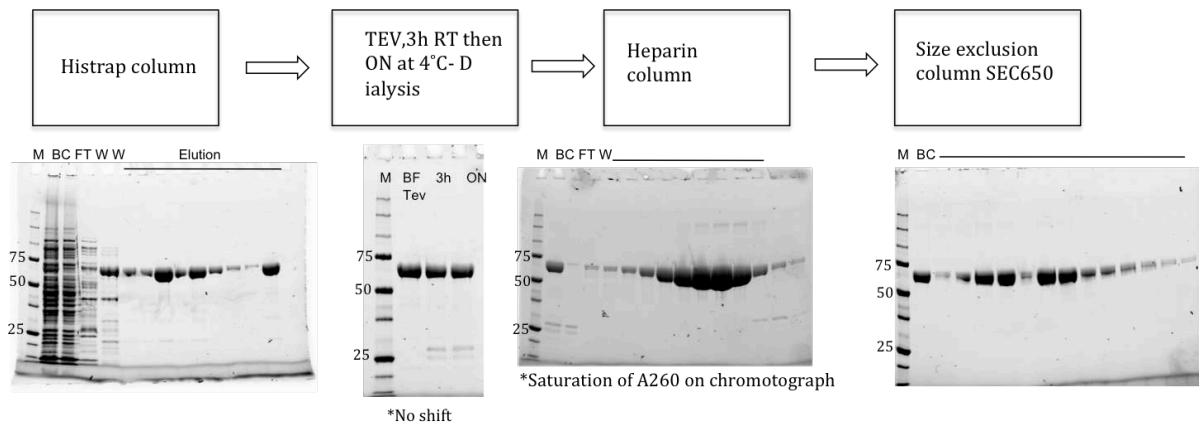


Figure 4.4: Purification steps of UvrC from *Deinococcus radiodurans* using the protocol available at the start of my PhD.

Unfortunately, this protocol did not give a functional protein. The incision assay with 5'red-50merF26-seq1, UvrA1 and UvrB did not show an efficient cut (Figure 4.5).

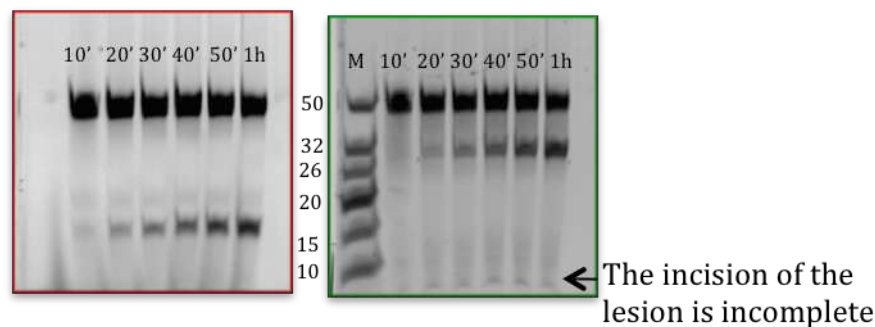


Figure 4.5: Urea polyacrylamide gel presenting the kinetics of the incision assay with the substrate 5'red-50merF26-seq1. The reaction was performed with the protein UvrC purified with the protocol presented in Figure 4.4. On the red filter, the presence of a band around 18 mer shows that the protein can perform the incision on the 5' side of the lesion. On the green filter, no 12 mer fragment is visible, which suggests that the cleavage on the 3' side is not occurring. The repair is thus incomplete.

Incision on the 5' side of the lesion by the C-terminal endonuclease domain of UvrC was functional, but the 3' incision by the N-terminal domain of UvrC was non-existent. In the available purification protocol, the reducing agent used was β ME. During the purification presented in Figure 4.4, the reducing agent used was TCEP, which is known to be more stable. Since the activity of the protein was partly disrupted, we attempted to replace the

TCEP with the β ME in this batch during a step of gel filtration, but this did not improve the incision activity.

A new purification was performed using β ME only as a reducing agent throughout all the process, but the result was the same (Figure 4.6).

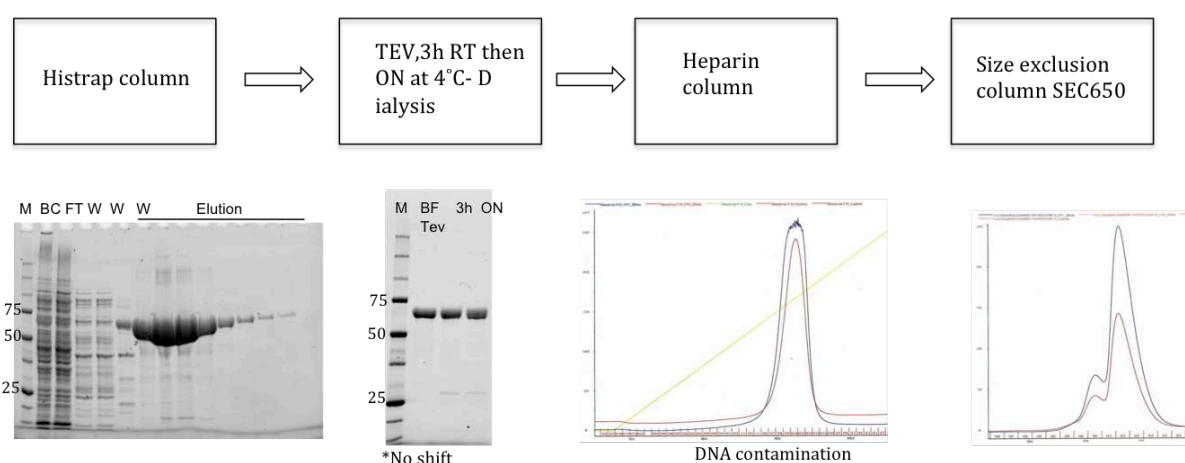


Figure 4.6: Purification steps of UvrC from *Deinococcus radiodurans*. The protein was eluted from the Histrap column and the fractions were gathered. The TEV cleavage was not effective. The chromatogram from the heparin column also showed a high DNA ratio monitored with the absorbance at 260 nm (red curve) compared to the protein monitored with the absorbance at 280 nm (blue curve).

A western blot performed on this protein batch showed the presence of the His-tag at the end of the purification. In fact, the TEV cleavage was not efficient: the gel following the cleavage during the purification did not show a clear shift between the His-tag UvrC and the cleaved UvrC (Figure 4.6). This could be due to the DNA contamination visible on the chromatogram obtained during the heparin column. For the subsequent purifications, the heparin column was performed prior to the TEV cleavage to eliminate more DNA and facilitate the removal of the His-tag. As shown in Figure 4.7.A, this modification enabled an efficient cut of the tag.

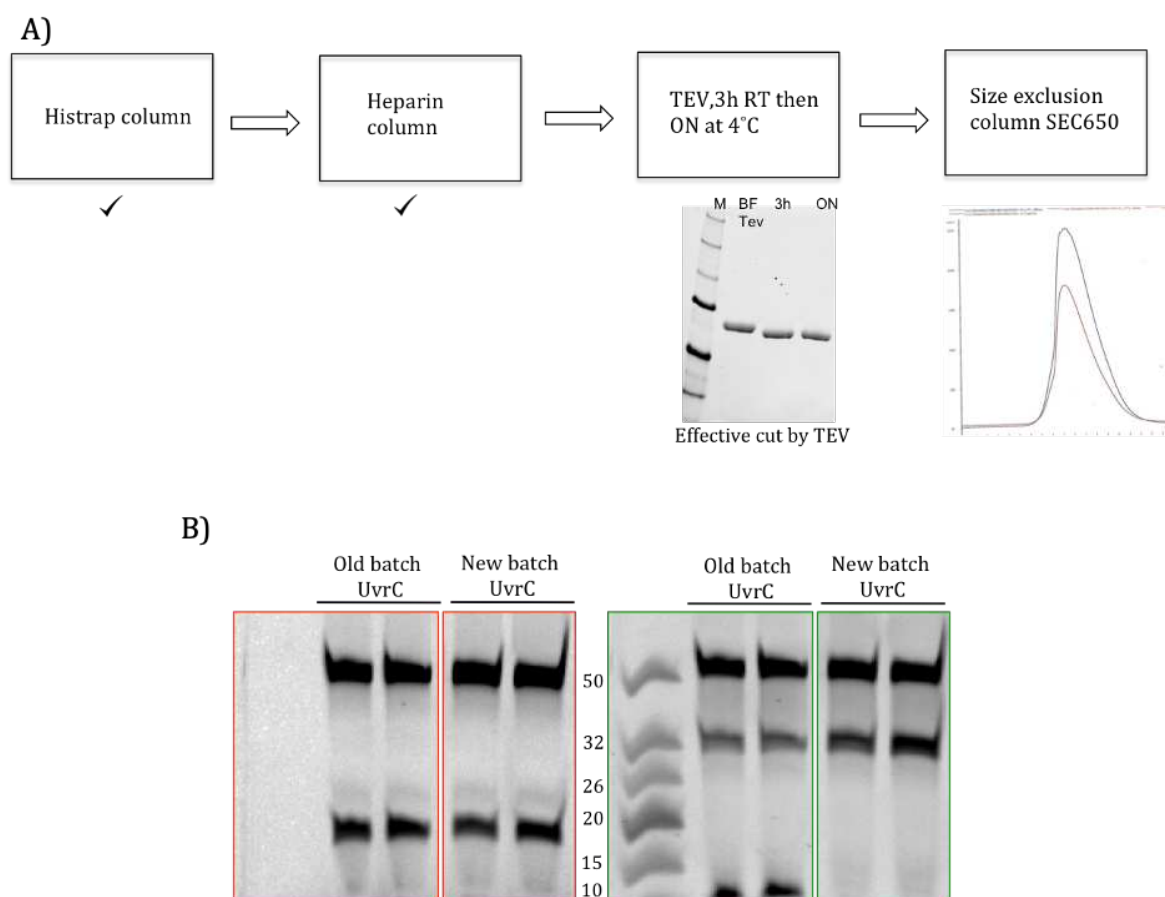


Figure 4.7: Purification steps of UvrC from *Deinococcus radiodurans*. A) In this protocol, the heparin column was performed after the nickel affinity column. The TEV cleavage was more effective. B) The activity of the new batch was compared to the batch already present in the lab. The gel was visualised with the red filter (gel contoured in red) and the green filter (gel contoured in green). The substrate 5'red-50merF26-seq1, is visible on both filters. In the red filter, the 18 mer released after the incision on 5' side of the lesion is present. The intermediate fragment 32 mer is also present in the green filter but unlike the old batch, the incision on 3' side to release the fragment containing the lesion was not present. The protein produced with this protocol was not effective.

The UvrC protein from this batch was tested in the incision assay. The assay showed that the repair was still incomplete even though the His-tag was well cleaved Figure 4.7.B. Once again no incision was being performed on the 3' side of the lesion.

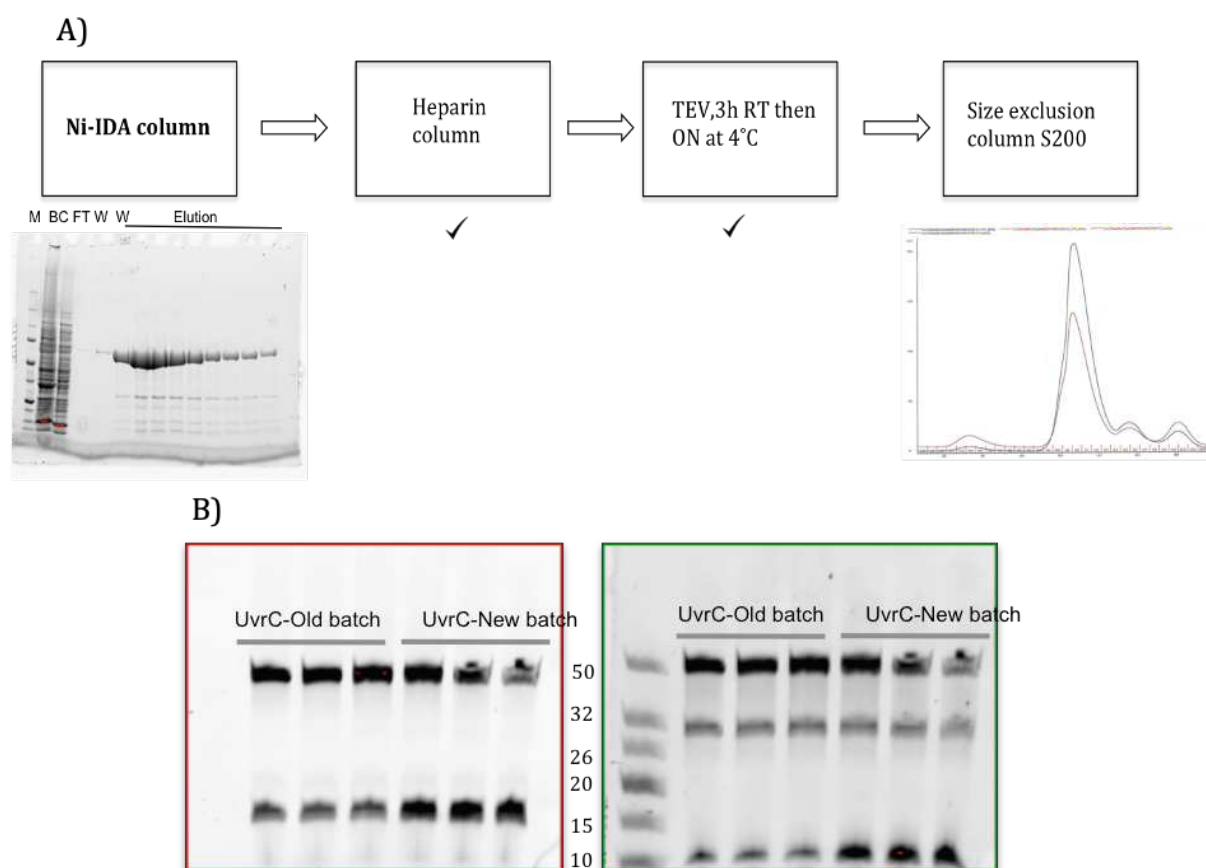


Figure 4.8: Ultimate purification protocol of UvrC from *Deinococcus radiodurans*: A) Purification steps of UvrC. B) The activity of the new batch was compared to the batch already present in the lab. The gel was visualised with the red filter (gel contoured in red) and the green filter (gel contoured in green). The substrate 5'-red-50merF26-seq1, is visible on both filters. In the red filter, the 18 mer released after the incision on the 5' side of the lesion is present. In the green filter, the intermediate fragment 32 mer and the 12 mer fragment containing the lesion were also present. The protein produced with this protocol was active and could efficiently perform the dual incision reaction.

To further improve the purification protocol, the nickel affinity chromatography was performed with a Ni-IDA column instead of a HisTrap FF column. We had observed that the column had lost its blue color (due to the nickel) at the end of the purification, indicating that UvrC may possibly be stripping the nickel from the column. UvrC possesses a cysteine-rich region that could potentially act as a metal binding site. We had indeed observed that the protein displays a brown colour, which was rapidly lost when using a HisTrap column or Nickel Sepharose, as opposed to Ni-IDA resin, in which the nickel ions

are tightly associated with the IDA resin. With a Ni-IDA column, the stripping of Ni²⁺ ions from the column was minimized. The yield of drUvrC was 9 mg/L of culture. The incision assay with this new batch showed an efficient repair of 5'red-50merF26-seq1 (Figure 4.8.B).

3. Optimization of the incision assay

3.1. Minimal components of the incision reaction

First, different combinations of the UvrA1, UvrA2, UvrB, UvrC proteins and ATP were tested in the reaction to determine the minimal elements needed for incision and the conditions that were the most favourable for the efficient release of the 12 mer DNA fragment containing the lesion (Figure 4.9).

When taken alone the proteins UvrA1, UvrA2, UvrB and UvrC did not show any incision activity on the dsDNA substrate (wells 2-4). In wells 5 to 10, when mixing two Uvr proteins, DNA incision was only observed for UvrB and UvrC in the presence of ATP (well 8, fragments indicated with a purple arrow). Several non-specific small fragments could be seen using the red filter meaning that they correspond to fragments of the 5' end of the labelled oligonucleotide.

The condition 11 showed that the specific repair of 50nM 5'red-50merF26-seq1 requires the presence of UvrA1, UvrB, UvrC as well as ATP as confirmed by the well 12 that did not contain any nucleotide and in which no product was seen. The 18 mer fragment is indicated with a red arrow and the 12 mer fragment is indicated with a green arrow. The condition containing UvrA2, UvrB and UvrC showed no incision, which indicates that UvrA1 is necessary for incision activity and the release of the 12 mer fragment (Wells 13-14). drUvrA2 can therefore not substitute for drUvrA1 in the incision reaction.

One of the small fragments present in the condition 8 when UvrB and UvrC were incubated with the oligonucleotide was also observed in the condition 11. Following this observation, we tried to perform the incision at room temperature instead of 37°C to reduce this non-specific activity. The Figure 4.10 shows that incubation at 37°C was clearly more efficient than the room temperature incubation for the incision assay.

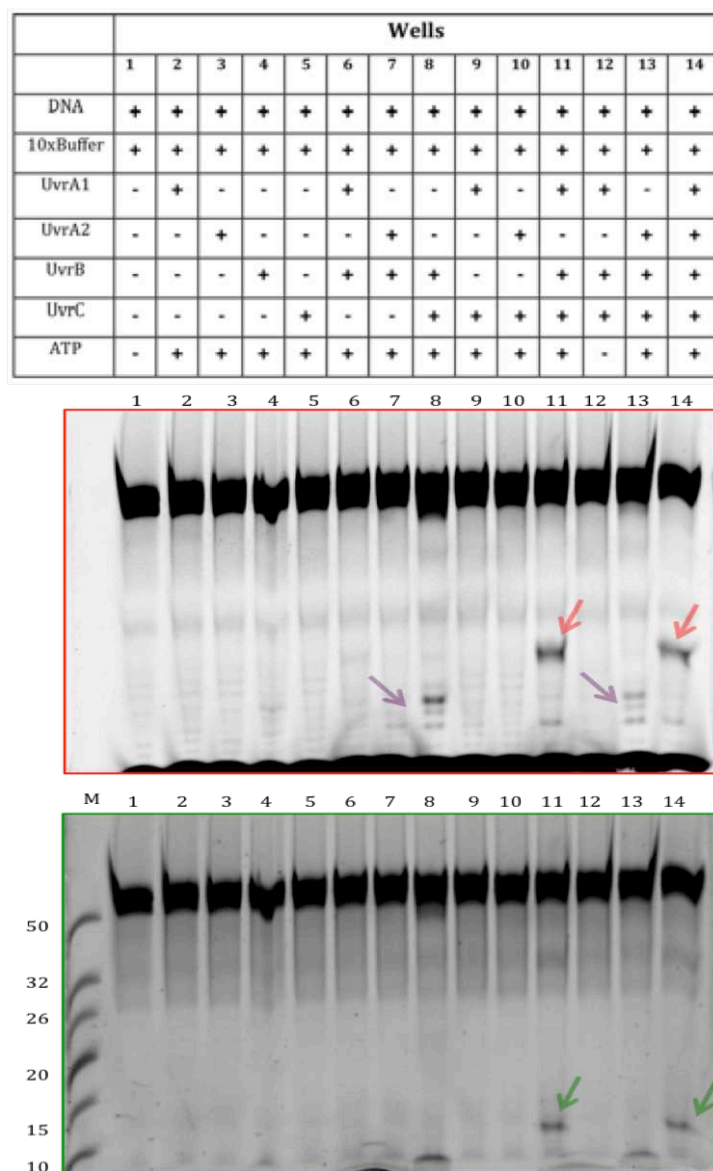


Figure 4.9: Combinations of different components of the incision assay incubated for 1h at 37°C. The gel was visualised with the red filter (top, gel contoured in red) and the green filter (bottom, gel contoured in green). All reactions contained the 5′red-50merF26-seq1 DNA substrate and 10x buffer (0.5 M Tris pH 7.5, 0.5 M KCl, 50 mM DTT, 100 mM MgCl₂). Well 1: DNA alone. Wells 2-5: incision reactions in the presence of ATP and either UvrA1, UvrA2, UvrB or UvrC. Well 6: incision reaction in the presence of ATP, UvrA1 and UvrB. Well 7: incision reaction in the presence of ATP, UvrA2 and UvrB. Well 8: incision reaction in the presence of ATP, UvrB and UvrC. Well 9: incision reaction in the presence of ATP, UvrA1 and UvrC. Well 10: incision reaction in the presence of ATP, UvrA2 and UvrC. Well 11: incision reaction in the presence of ATP, UvrA1, UvrB and UvrC. Well 12: incision reaction in the presence of UvrA1, UvrB and UvrC, but no ATP. Well 13: incision reaction in the presence of ATP, UvrA2, UvrB and UvrC. Well 14: incision reaction in the presence of ATP, UvrA1, UvrA2, UvrB and UvrC. UvrA1 and UvrA2 were added at a concentration of 2 μM, UvrB at 8 μM, UvrC at 4μM, and ATP at 4 mM.

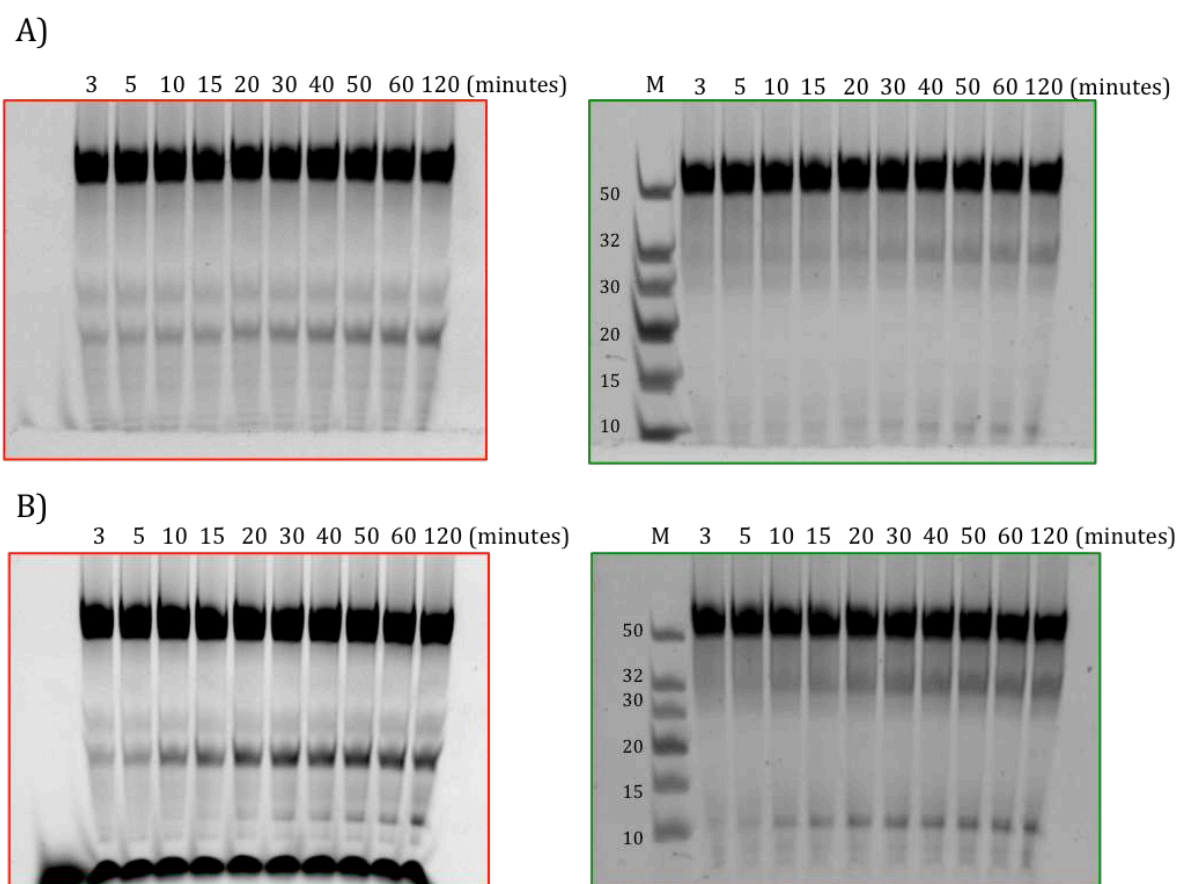


Figure 4.10: Timecourse of the incision reaction incubated either at room temperature (A) or at 37°C (B). The reactions contained the 5' red-50merF26-seq1 DNA substrate, 10x buffer, 4 mM ATP, 2 μ M UvrA1, 8 μ M UvrB and 4 μ M UvrC.

3.2. Optimization of UvrB and UvrC concentrations

We worked on the concentration of UvrB and UvrC to minimize the non-specific incision that could occur (Figure 4.11.A, red arrow).

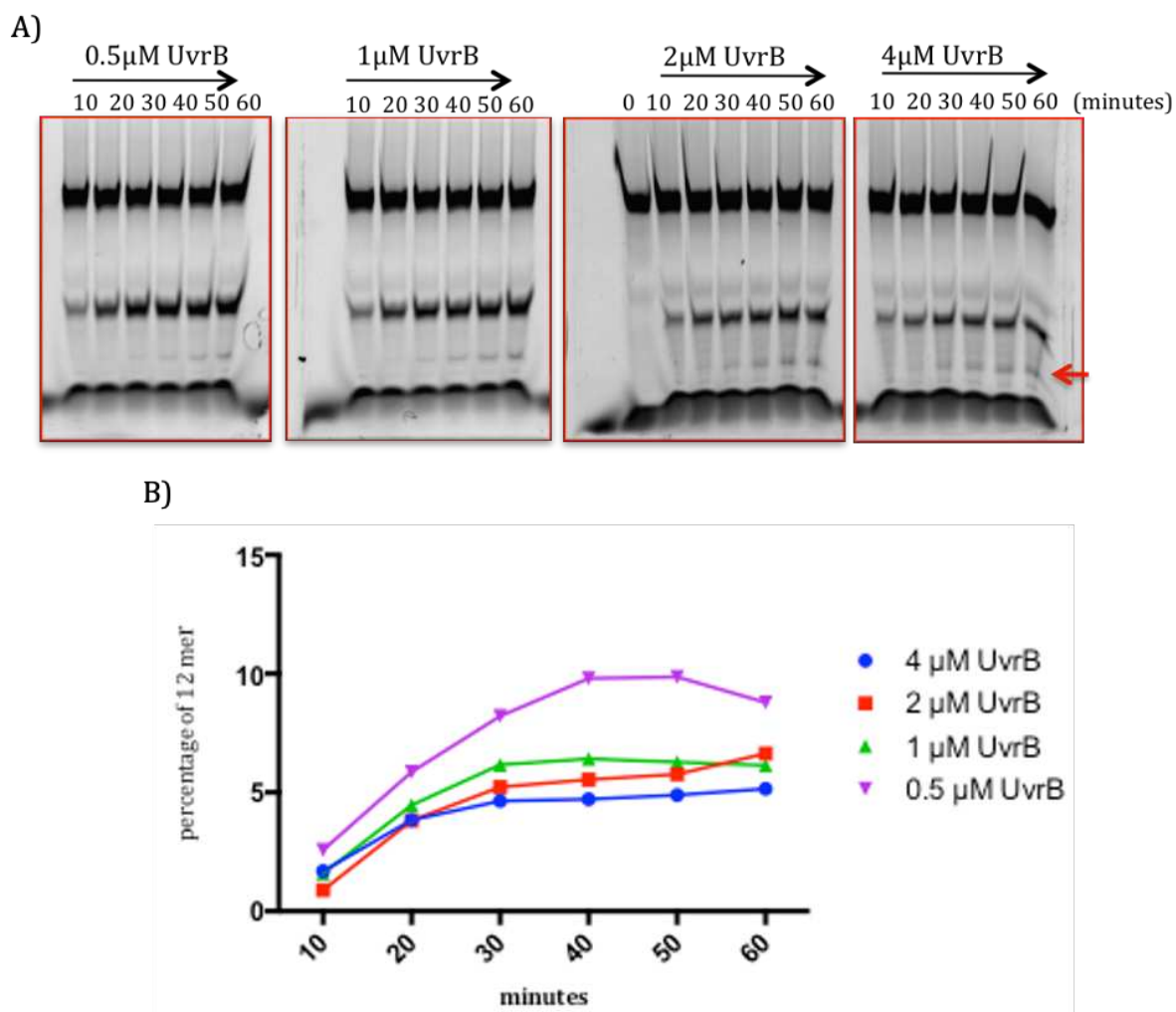


Figure 4.11: Timecourse of the repair of 50nM of 5'red-50merF26-seq1 by 2 μM UvrA1, 2 μM UvrC and a range of UvrB concentrations (0.5 μM- 4 μM). A) The gels were visualised with the Alexa 647 filter. The fragment containing ATTO633 at its 5' end, indicated with the red arrow, resulted from a non-specific incision. B) Quantification of the 12 mer fragment containing the lesion when the incision assay was performed with 2 μM UvrA1, 2 μM UvrC and the different concentrations of UvrB (0.5 μM- 4 μM). Experiments were performed in two replicates.

The quantification of the 12 mer in these different conditions where UvrB was modulated showed that the efficiency of release of the 12 mer fragment containing the lesion is increased when the final concentration of UvrB was lowered to 0.5 μM. The non-specific band was also reduced as shown in the gel (Figure 4.11.A). This concentration of 0.5 μM UvrB was kept for subsequent experiments with a fixed concentration of 2 μM UvrA.

Next, different concentrations of UvrC were tested in order to further increase the repair efficiency of lesions beyond the 10% release (Figure 4.11.B). The concentrations of UvrC used in the incision assays presented in Figure 4.12 were 1 μM, 2 μM, 3 μM and 4 μM that

showed respectively 7, 10, 11 and 14% repair efficiency as measured by the extent of release of the 12 mer after 30 minutes (Figure 4.12.B). The rate of release of the 32 mer fragment was equivalent for 3 μ M and 4 μ M. With more UvrC, there is more final incision to release the lesion (Figure 4.12.C).

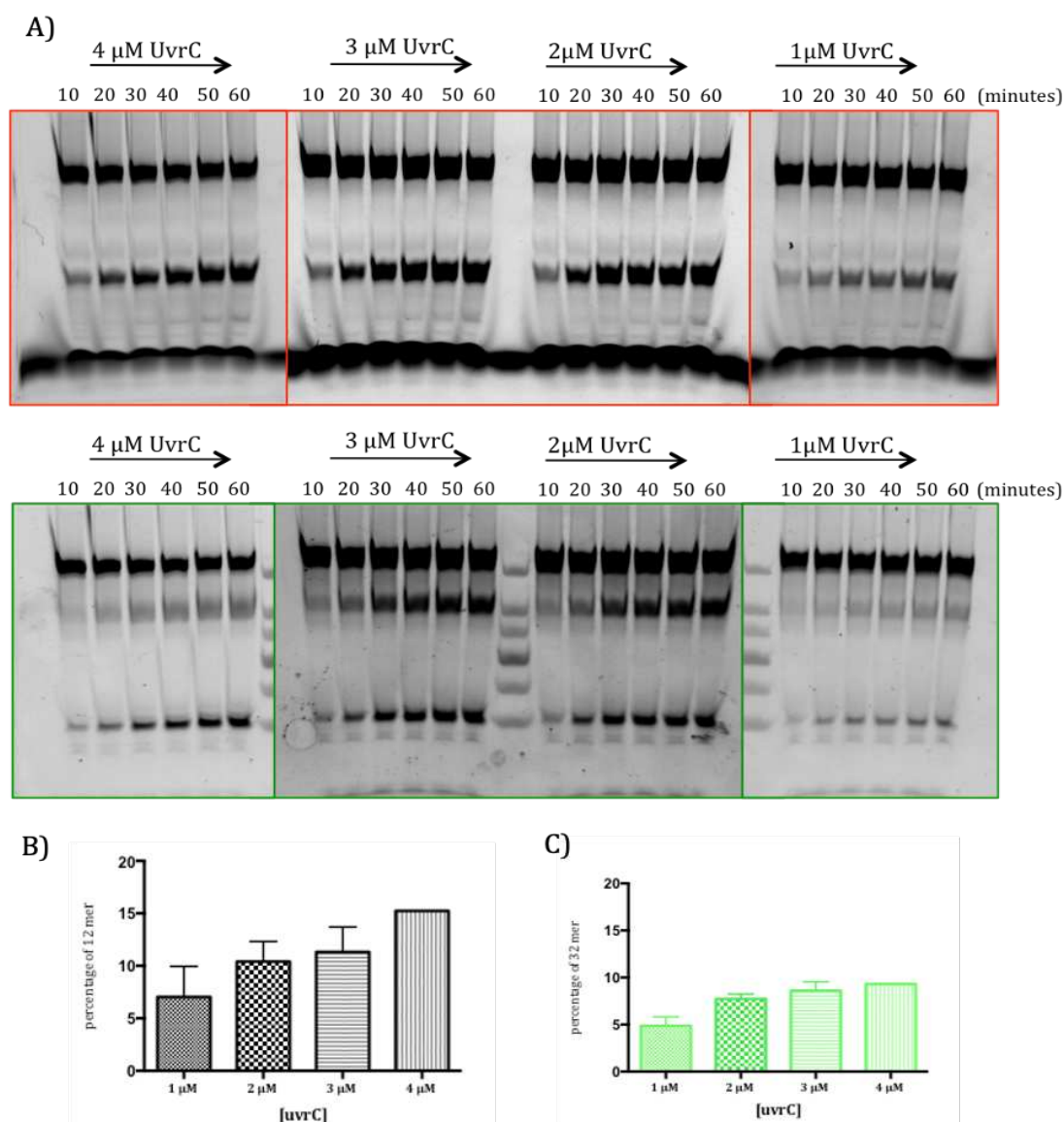


Figure 4.12: Kinetics of the repair of 50nM of 5'red-50merF26-seq1 with 2 μ M UvrA1, 0.5 μ M UvrB and a range of concentration of UvrC (1 μ M- 4 μ M). A) The gels were visualised with the filters Alexa 647 and Fluorescein. B) Quantification of the 12 mer fragment containing the lesion when the incision assay was performed with 2 μ M UvrA1, 0.5 μ M UvrB and the different concentration of UvrC (1 μ M- 4 μ M). C) Quantification of the 32 mer fragment containing the lesion when the incision assay was performed with 2 μ M UvrA1, 0.5 μ M UvrB and the different concentration of UvrC (1 μ M- 4 μ M). The graphs represent the mean and standard deviation of two replicates.

3.3. Optimization of the DNA substrate concentration

We noticed that we could lower the concentration of 5'red-50merF26-seq1 used in the incision assay from 50 nM to 25 nM and still efficiently quantify the DNA bands on the gels. With this lower concentration, the quantification was in fact easier because the fragments of DNA were clearer on the gels. Adjustments were made to the concentration of proteins for this reduced amount of DNA (Figure 4.13.A). The condition 1 corresponds to the same concentrations used previously for 50 nM DNA. With this condition, 11% of the substrate was processed. With the condition 2 in which the amount of proteins was divided by two, we obtained 13% of 12 mer. The conditions 3 and 4 were similar with respectively 12 % and 14 % of 12 mer. The extent of 32 mer production was different however, with 24% for condition 2 as opposed to 9% for condition 4, which suggests that under these conditions the 5' incision reaction is more efficient.

The conditions 5 and 6 were less efficient with an incision efficiency of 9% and 4% respectively. We decided to pursue the experiments with the second condition that produced the best incision efficiency when considering both 3' and 5' cuts (Figure 4.13.B)

A)

| | Control | 1 | 2 | 3 | 4 | 5 | 6 |
|-------|---------|-------------|--------------|--------------|-------------|--------------|-------------|
| UvrA1 | - | 2 μ M | 1 μ M | 1 μ M | 1 μ M | 2 μ M | 2 μ M |
| UvrB | - | 0.5 μ M | 0.25 μ M | 0.25 μ M | 0.5 μ M | 0.25 μ M | 0.1 μ M |
| UvrC | - | 4 μ M | 2 μ M | 4 μ M | 4 μ M | 4 μ M | 4 μ M |

B)

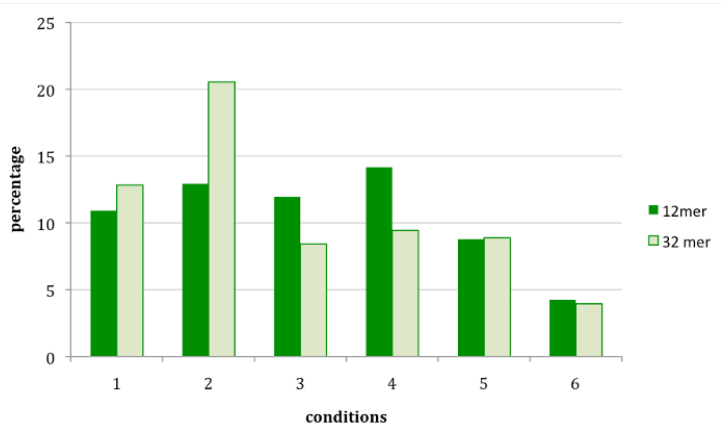


Figure 4.13: Evaluation of the incision efficiency using different ratios of UvrA1, UvrB and UvrC for the repair of 25 nM of 5'red-50merF26-seq1. The incision assay was incubated for 1 hour at 37°C. A) Concentration of proteins used and the gel visualised with the filters Alexa 647 (red) and Fluorescein (green). B) Quantification of the 12 mer (green) and 32 mer (pale green) fragments obtained after the 1h reactions.

3.4. Optimization of the salt concentration and the protein dilution buffer

The concentration of salt in the incision reaction was the next focus to optimize the repair by the NER system. The 10x buffer was prepared without KCl. Different concentration of NaCl and KCl were added to final concentrations of 50 mM, 100 mM, 200 mM and 300 mM. As presented on the graph, after 30 minutes the incision efficiencies of the 12 mer were respectively 39 %, 22 %, 1.6 % and 0.3 % for KCl and 28 %, 10.5 %, 0.2 % and 0.15 % for NaCl. Therefore, the incision assay with 50 mM KCl was more efficient for the activity of the proteins (Figure 4.14)

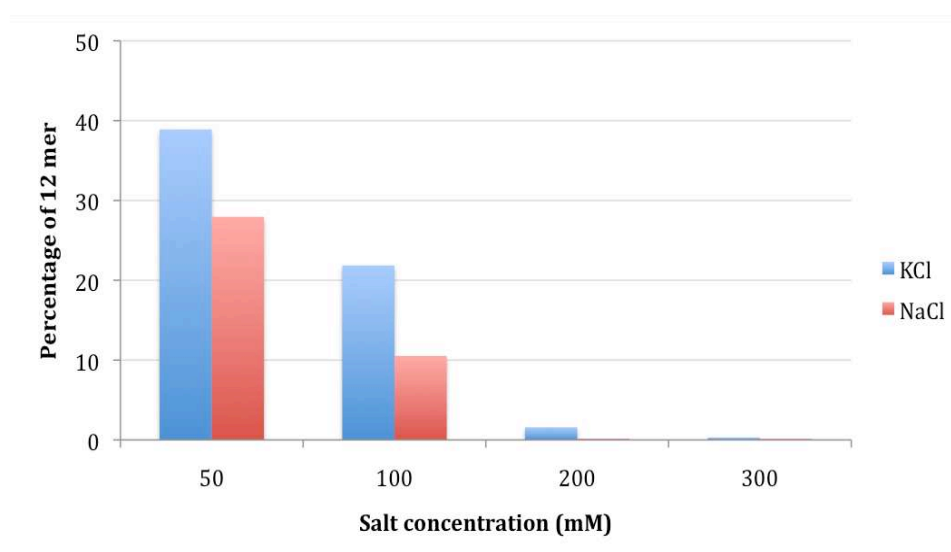


Figure 4.14: Graph illustrating the percentage of 12 mer fragment produced after 30 minutes of incubation of the incision assay using 50 mM, 100 mM, 200 mM and 300 mM of KCl and NaCl. 25 nM 5'red-50merF26-seq1, 1 μ M UvrA1, 0.5 μ M UvrB and 2 μ M UvrC in the presence of 2.5 mM Mg^{2+} and 2.5 mM ATP. The graph represents the mean of two replicates.

The 10x buffer was prepared to add a final concentration of 50 mM KCl to the reaction (500 mM Tris pH 7.5, 500 mM KCl, 50 mM DTT, 20 mM BSA). Variations were also made to the dilution buffer used for adjusting the concentrations of UvrA1, UvrB and UvrC proteins prior to use in the incision assay. Initially 10x concentrated protein stocks of each protein were prepared by diluting the proteins in their respective size-exclusion chromatography buffers. Our aim was therefore to find a single common dilution buffer that could be used for all three proteins. Four common buffers were therefore prepared and tested for the dilution of the Uvr proteins:

- 50mM Tris-HCL pH 8, **250mM NaCl**, 5% glycerol and 2mM BME (Total final concentration of salt: **50 mM KCl + 80.3 mM NaCl**)
- 50mM Tris-HCL pH 8, **250mM KCl**, 5% glycerol and 2mM BME (Total final concentration of salt: **106 mM KCl + 23.8 mM NaCl**)
- 50mM Tris-HCL pH 8, **150mM NaCl**, 5% glycerol and 2mM BME (Total final concentration of salt: **50 mM KCl + 57.7 mM NaCl**)
- 50mM Tris-HCL pH 8, **150mM KCl**, 5% glycerol and 2mM BME (Total final concentration of salt: **83.9 mM KCl + 23.8 mM NaCl**)

It is important to keep in mind that even if the idea is to have only KCl in the reaction, the storage buffers of the proteins will bring some NaCl to the reaction (at least 23.8 mM of NaCl).

As presented in Figure 4.15, this set of reactions showed that changes in the salt concentrations present in the dilution buffer only mildly affected the incision efficiency. The extent of incision of the 12 mer was between 40 and 50% after 2 hours for all four conditions (Figure 4.15.B). With 150 mM NaCl, the amount of 32 mer was higher than for the other conditions, suggesting that the 5' incision reaction is slightly more efficient than the 3' incision in these conditions (Figure 4.15.C). Since the use of a common dilution buffer maintained the incision activity, we decided to use the 150 mM NaCl buffer composed of 50 mM Tris-HCL pH 8, 5% glycerol, 150 mM NaCl and 2 mM BME for the dilution of UvrA1, UvrB and UvrC in subsequent reactions.

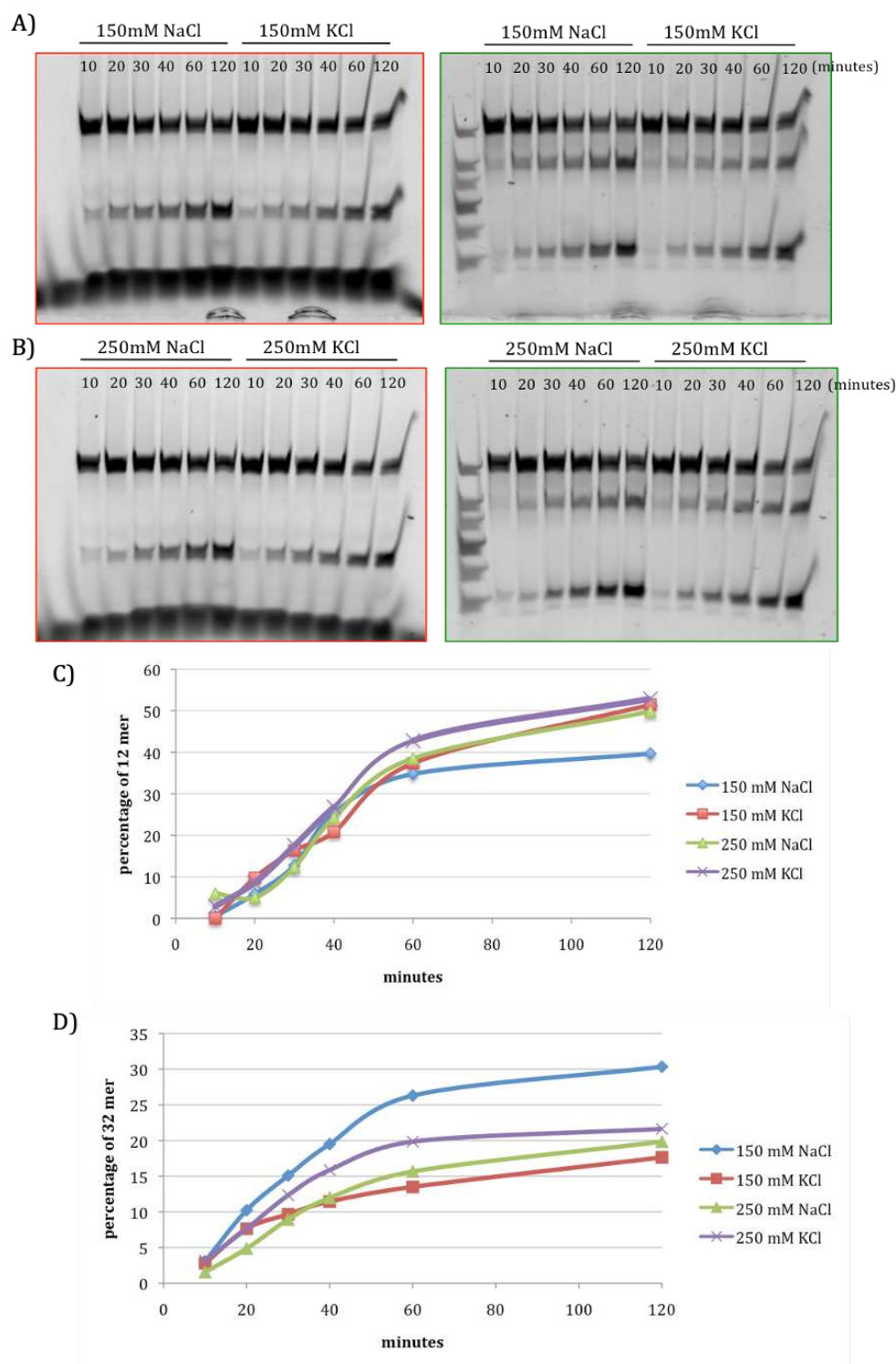


Figure 4.15: Kinetics of repair of 25 nM of 5'red-50merF26-seq1 with 1 μ M UvrA1, 0.5 μ M UvrB and 2 μ M UvrC. The 10x buffer added 50 mM KCl to the reaction and the proteins were diluted in commun buffers containing either 150 mM or 250 mM KCl or NaCl. The urea polyacrylamide gels (A, B) and the graphs illustrating the percentage of 12 mer and 32 mer fragments produced during the incision assay using the different dilution buffers for the proteins (C, D). The assay was performed in the presence of 10 mM Mg^{2+} and 4 mM ATP.

3.5. Optimization of the magnesium concentration

All three Uvr proteins are known to use magnesium as a cofactor, so we evaluated the effects of changing the Mg^{2+} concentration in the incision assay on the repair efficiency. Initially, the amount of Mg^{2+} present in the 10x buffer corresponded to a final concentration of 10 mM in the reaction. A new 10x buffer was thus prepared without Mg^{2+} and magnesium chloride was added separately to the reaction at defined concentrations ranging from 0.1 to 10 mM. We then monitored the UvrABC repair kinetics in these different conditions (Figure 4.16).

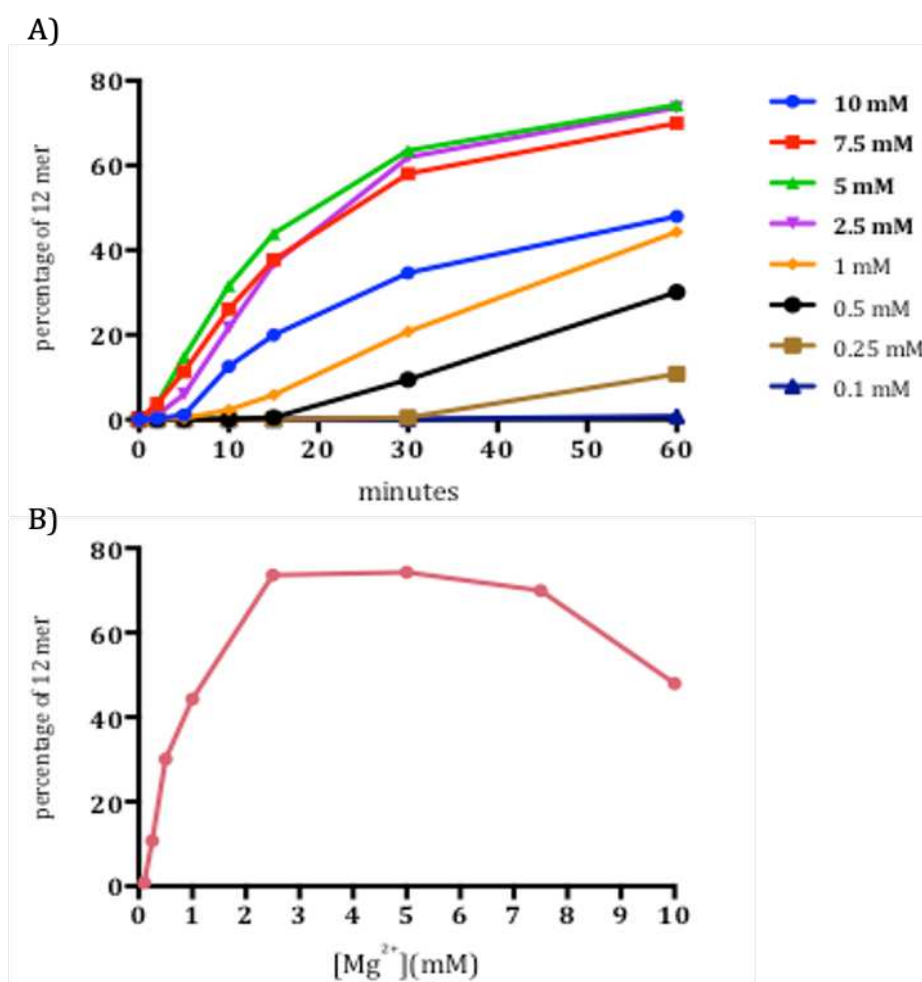


Figure 4.16: Kinetics of repair of 25 nM of 5' red-50merF26-seq1 with 2 μ M UvrA1, 0.5 μ M UvrB and 2 μ M UvrC using a range of Mg^{2+} concentration: 0.1, 0.25, 0.5, 2.5, 7.5 and 10 mM. (A) The graph presents the quantification of the 12 mer fragment produced as a function of time in each of these experiments. (B) The graph presents the percentage of 12 mer produced after 60 minutes of incision assay as a function of Mg^{2+} concentration, showing that the optimum concentration of Mg^{2+} for the incision reaction is between 2.5 mM and 5 mM Mg^{2+} (B). The concentration of ATP used in these assays was 4 mM.

We noticed an increase in the percentage of the 12 mer released when we decreased the concentration to 7.5 mM, 5 mM or 2.5 mM Mg^{2+} . Lower concentrations of Mg^{2+} had a negative effect on the incision of the UvrABC proteins. Furthermore, a closer look at the gels (Figure 4.17) shows a clear difference in the amount of 32 mer fragment accumulating during the reaction when performed at 10 mM Mg^{2+} and 2.5 mM Mg^{2+} : the 32 mer fragment, that is the intermediate product from the first incision on the 5' side of the lesion, represents less than 5% of the product with 2.5 mM Mg^{2+} , whereas there is up to 20% of this fragment with 10 mM Mg^{2+} (Figure 4.17). High concentrations of Mg^{2+} thus appear to impair incision on the 3' side of the lesion. Although the extent of 12 mer production is very similar with 2.5 and 5 mM Mg^{2+} , 2.5 mM Mg^{2+} was chosen for subsequent experiments so as to minimise the accumulation of the 32 mer fragment (Figure 4.17.B). When the two incision reactions on the 5' and 3' sides of the lesion are efficient, they occur almost simultaneously, and very little 32 mer fragment is observed.

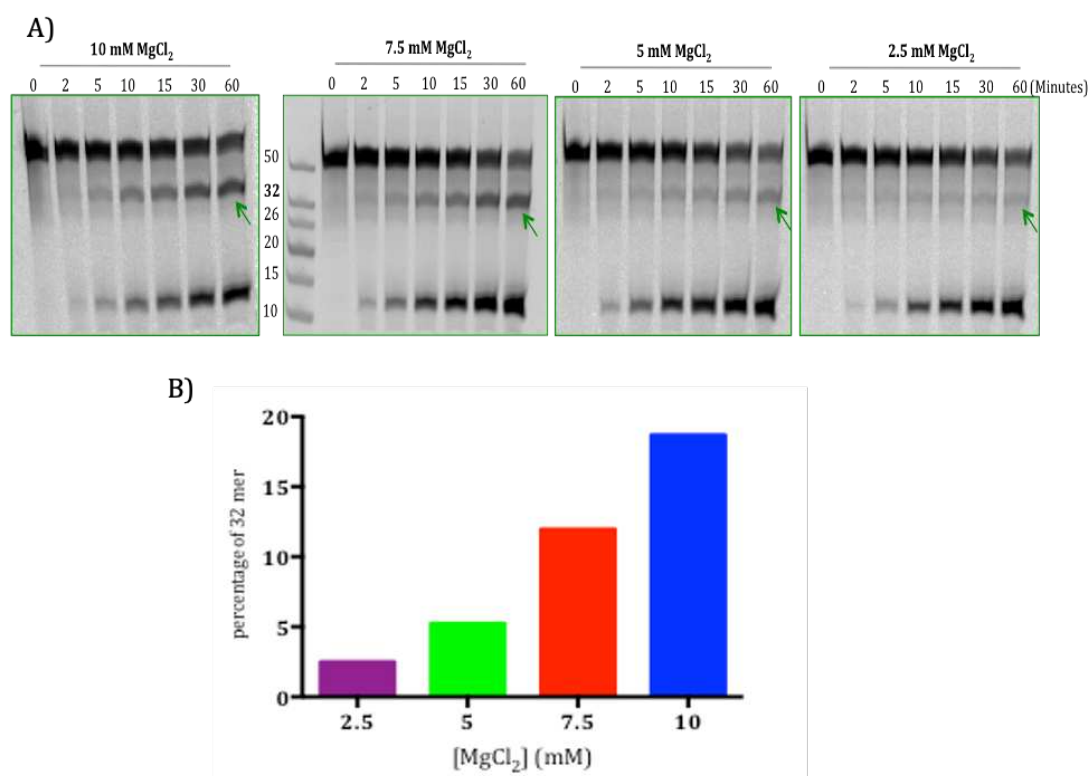


Figure 4.17: Kinetics of repair of 25 nM of 5'red-50merF26-seq1 with 2 μ M UvrA1, 0.5 μ M UvrB and 2 μ M UvrC at 2.5, 5, 7.5 and 10 mM Mg^{2+} concentration. (A) Urea polyacrylamide gel analysis of the repair of 5'red-50merF26-seq1 as a function of time. The 32 mer is indicated with a green arrow in the gels visualised with the green filter. (B) Graph illustrating the percentage of 32 mer fragment produced as a function of Mg^{2+} concentration.

3.6. Optimization of the ATP concentration and Mg^{2+} /ATP ratio

Initial reactions contained 4 mM ATP and 10 mM Mg^{2+} , a well-established co-factor of ATP. Since we observed above that the Mg^{2+} concentration significantly affected the incision activity, we also tested a range of ATP concentrations.

For a fixed concentration of 2.5 mM Mg^{2+} in the assay, the concentration of ATP was varied from 0.1 mM to 10 mM. A peak for the incision of the 12 mer fragment was observed in the condition that combined 2.5 mM ATP and 2.5 mM MgCl_2 (Figure 4.18.A). This same range of ATP concentration was also tested with 5 mM MgCl_2 . The ratio 1:1 was also effective in this condition. Hence, this ratio 1:1 was tested for the full range of Mg^{2+} /ATP concentrations (Figure 4.18.B.). The highest incision rates were observed between 2.5 mM and 5 mM Mg^{2+} /ATP. Subsequent experiments were therefore performed with 2.5 mM Mg^{2+} and ATP.

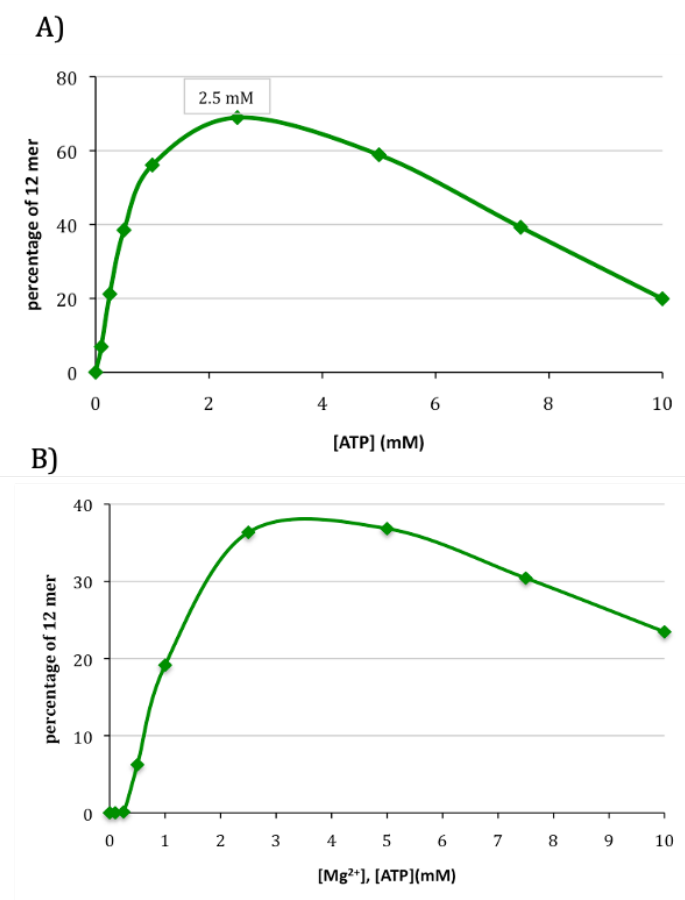


Figure 4.18: Quantification of the 12 mer fragment production by the incision reactions performed with either (A) 2.5 mM Mg^{2+} associated with a range of concentrations of ATP (0.1-10 mM) or (B) a fixed 1:1 ratio of Mg^{2+} and ATP over a range of concentrations (0.1-10 mM).

From these experiments, we concluded that the presence and the concentration of divalent ions along with the nucleotide in the reaction are critical for the activity of the UvrABC system.

3.7. Optimized incision assay conditions

The settings for an efficient repair of the 5'red-50merF26-seq1 substrate are summarized in the following table:

Table 4.1: Optimal conditions for the *D. radiodurans* Uvr incision assay

| <u>Buffer</u> | <u>ATP</u> | <u>Uvr proteins</u> | <u>Substrate:</u> |
|--|-------------------|---|--------------------------|
| 50 mM Tris-HCl pH 7.5 50 mM KCl 5 mM DTT 2.5 mM MgCl ₂ | 2.5 mM | 1 μM UvrA1 0.5 μM UvrB 2 μM UvrC diluted in 50 mM Tris-HCl pH 8, 150 mM NaCl, 5% glycerol and 2 mM freshly added BME | 25 nM DNA |

The order in which the components were added to the reaction and the pre-incubation of the proteins and DNA at 37°C before starting the reaction also turned out to be critical factors contributing to an improved incision assay. In our optimal set-up, we used the following protocol:

For 1 reaction: 10μL

- 1) Add 4.5 μL H₂O
- 2) Add 1 μL 10x buffer containing MgCl₂ and BSA
- 3) Add 0.5 μL 5'red-50merF26-seq1 DNA substrate at 0.5 μM
- 4) Add 1 μL UvrA1 at 10 μM
- 5) Add 1 μL UvrB at 5 μM
- 6) Add 1 μL UvrC at 20 μM
- 7) Incubate the reaction 3 minutes at 37°C
- 8) Add 1 μL ATP 25 mM to start the reaction
- 9) Incubate the tube at 37°C.

The components were added in this order and the reaction was started with the addition of 2.5 mM ATP. Thanks to this pre-incubation at 37°C and also to the addition of fresh BME in the protein dilution buffer, we were able to increase the repair rate. In fact, prior to the optimisation, the initial rate of incision was 1.36 nM/min. Using the set-up described above, the incision rate reached 2.04 nM/min (Figure 4.19) (rates derived from the linear

regions of the graphs between 0 and 30 min). Moreover, the extent of incision reached ~80 % after 1 hour and almost no accumulation of the intermediate 32 mer fragment.

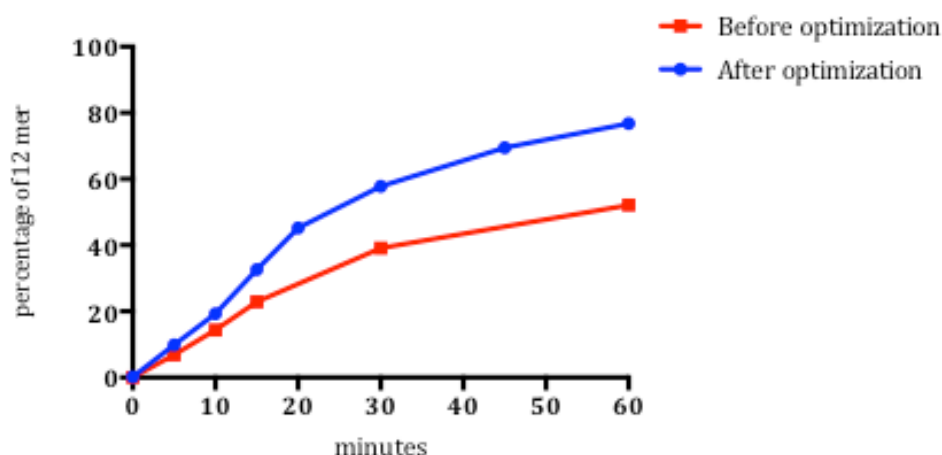


Figure 4.19: Kinetics of repair of 25 nM of 5'-red-50merF26-seq1 with 1 μ M UvrA1, 500 nM UvrB and 2 μ M UvrC before and after performing the reaction in the optimal conditions and applying the specific order of addition of the components.

With these optimal conditions, we also noticed that we no longer observed non-specific cleavage of the DNA. UvrA1, UvrB and UvrC were tested once again, alone or combined, using this optimal setup (Figure 4.20). The fragment resulting from the non-specific incision by UvrB and UvrC was not present anymore and efficient incision was only observed when all three proteins and ATP were present.

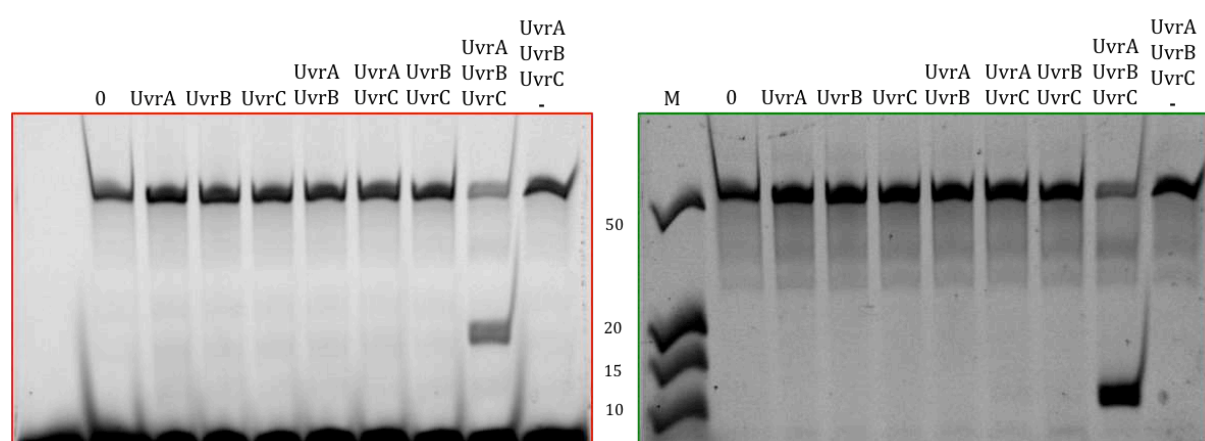


Figure 4.20: Urea polyacrylamide gel visualised with the Alexa 647 and Fluorescein filters showing the incision assay with 25 nM 5'-red-50merF26-seq1, 1 μ M UvrA1, 0.5 μ M UvrB and 2 μ M UvrC alone or combined in the presence of 2.5 mM Mg^{2+} and 2.5 mM ATP. In the last well, the reaction was performed without ATP and the first well (0) corresponds to the DNA substrate alone.

4. Probing the NER activity using the incision assay

4.1. 5' and 3' incision reactions: order and sites of cleavage

The early incision gels (such as those shown in Figure 4.12) suggested that the first cut in the reaction was performed preferentially on the 5' side resulting in the release of the 18 mer fragment detected with the red filter and the 32 mer fragment detected with the green filter. The second cut then occurs on the 3' side of the lesion to release the 12 mer containing the FdT. However, after optimization of the assay, we noticed that the two incision reactions occurred almost simultaneously, and very little 32 mer fragment was observed (Figure 4.19).

In the literature, bacterial NER is proposed to produce a 12 to 13 mer fragment (Truglio et al., 2006a). To determine the precise sites of incision on the 5' and 3' sides of the lesion and the exact size of the fragments resulting from the incisions by the *D. radiodurans* NER system, we used the MALDI-TOF technique to analyze the products of the incision reactions performed on 10 pmoles of 5'red-50merF26-seq1 DNA substrate incubated with the UvrA1, UvrB and UvrC proteins for 1 hour at 37°C. The incision reactions were verified on urea polyacrylamide gels to confirm that the repair was properly achieved before the MALDI-TOF analysis (Figure 4.21).

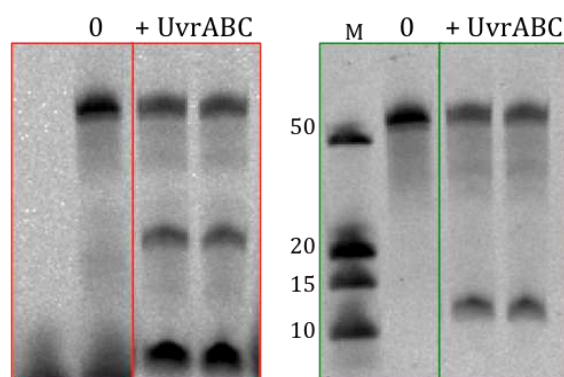


Figure 4.21: Urea polyacrylamide gel visualised with the Alexa 647 and Fluorescein filters showing the incision assay with 25 nM 5'red-50merF26-seq1, 1 μ M UvrA1, 0.5 μ M UvrB and 2 μ M UvrC in the presence of 2.5 mM Mg^{2+} and 2.5 mM ATP. The samples were sent for the MALDI-TOF analysis. The first well (0) corresponds to the DNA substrate alone. Experiments were performed in duplicates

Table 4.2: Sequences and sizes of the major fragments observed by MALDI-TOF analysis of the incision reactions using 5' red-50merF26-seq1 as a substrate.

| Name (length) | Sequence | Expected mass (Da) | Measured mass (Da) |
|-----------------------------|---|--------------------|--------------------|
| 5'-ATTO633-F26-seq1 (50mer) | 5'- X GAC TAC GTA CTG TTA CGG CTC CAT C X C TAC CGC AAT CAG GCC AGA TCT GC -3' | 16465 | 16457.5* |
| Rev-seq1 (50mer) | 5'- GCA GAT CTG GCC TGA TTG CGG TAG AGA TGG AGC CGT AAC AGT ACG TAG TC -3' | 15531 | 15529.7 |
| F26-seq1 (12mer) | 5'- pCTCCATC X CTAC -3' | 4107.4 | 4109.1 |
| 5'-ATTO633-seq1 (18mer) | 5'- X GACTACGTACTGTTACGG -3' | 6226.6 | 6226.5 |
| 3'-seq1 (20mer) | 5'- pCGCAATCAGGCCAGATCTGC -3' | 6167 | 6165.4 |

The analysis of the starting DNA substrate (5' red-50merF26-seq1) is presented in Figure 4.22 and Table 4.2. 5' red-50merF26-seq1 is composed of the oligonucleotides 5'-ATTO633-F26-seq1 and Rev-seq1 with respective theoretical masses of 16465 Da and 15531 Da. We were able to detect the intact oligonucleotides composing the substrate. Two peaks at 16457.5 Da and 15529.7 Da could be seen in the MALDI-TOF spectra (Figure 4.22). After the repair by UvrABC, several DNA fragments were detected on our MALDI spectra. The 18 mer fragment resulting from 5' incision has a theoretical mass of 6226.6 Da and was detected at 6226.5 Da. The fragment containing the lesion was detected at 4109.1 Da and corresponds to a 12 mer oligonucleotide with a phosphate at its 5' end. The sequence is presented in Table 4.2; its theoretical size is 4107.4 Da. A 20 mer fragment carrying a phosphate at its 5' end resulting from 3' incision was detected at 6165.4 Da (theoretical mass: 6167 Da). Although we are not using a quantitative method, we were expecting the peaks of 18 mer (6226.6 Da) and 20 mer (6165.4 Da) to be of the same height (Figure 4.22). Instead, we noticed that the peak corresponding to the 18 mer fragment was systematically lower than the peak of the 20 mer fragment. It could be due either to the difference in ionization or to the further processing of the 18 mer fragment into smaller DNA fragments, which may correspond to the short non-specific fragments observed on some of our urea-TBE gels.

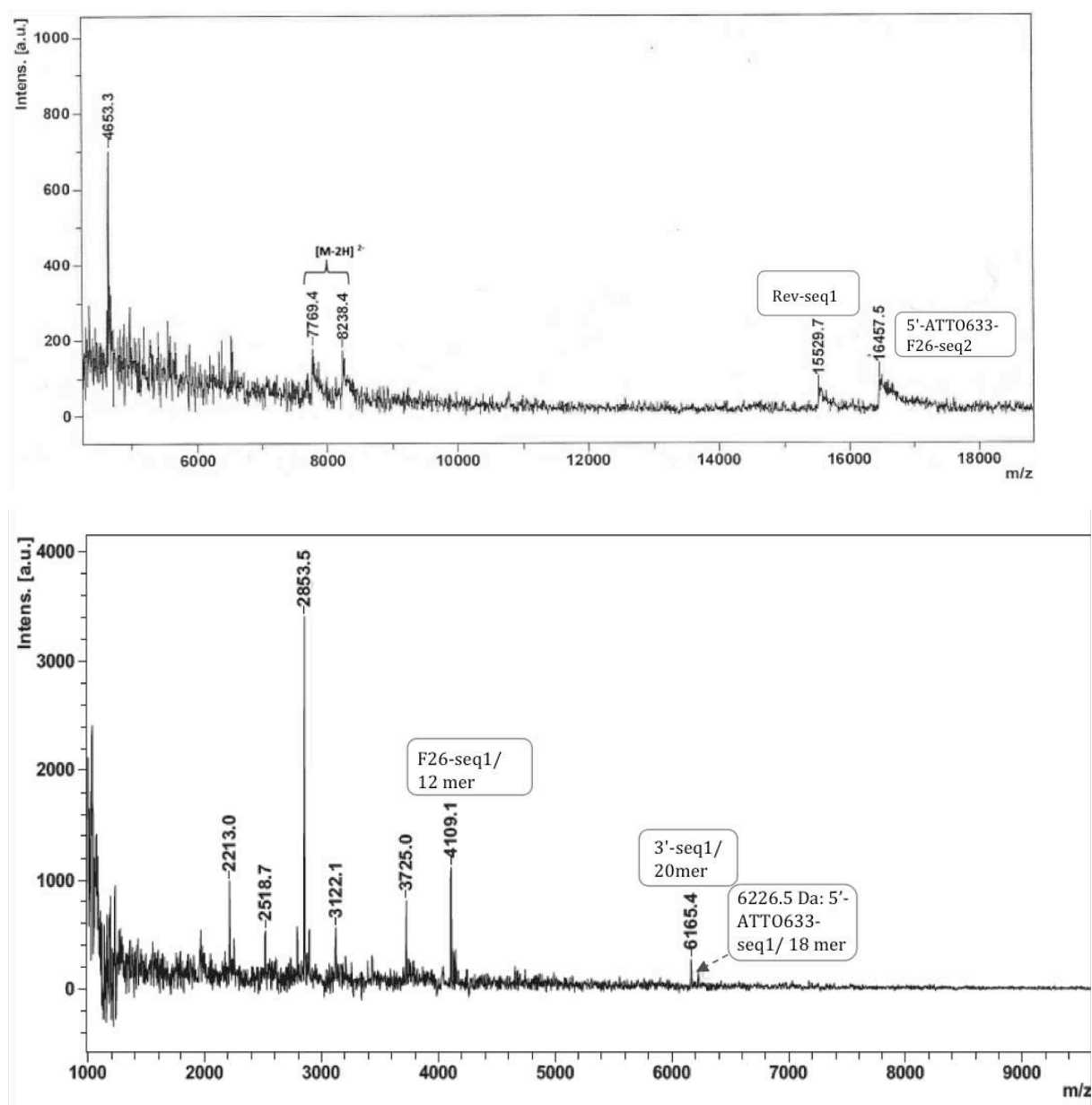


Figure 4.22: MALDI-TOF spectra of the incision reaction substrates (top) and products (bottom). The reactions were performed on 5'-red-50merF26-seq1 DNA with 1 μ M UvrA1, 0.5 μ M UvrB and 2 μ M UvrC. The masses of the different fragments were identified and tagged. Other unknown peaks were also detected.

Based on these analyses, we could unambiguously determine the size of the released fragment and the exact sites of cleavage. The incisions occur 7 nucleotides upstream of the lesion and 4 nucleotides downstream of the lesion, thereby releasing a 12 mer fragment. On the 5' end of the 12 mer fragment, the incision leaves a phosphate, while on the 3' end, cleavage occurs before the phosphate which ends up on the 20 mer fragment.

We did not identify any fragments when the incision assay was performed with UvrB and UvrC proteins only (Figure 4.23)

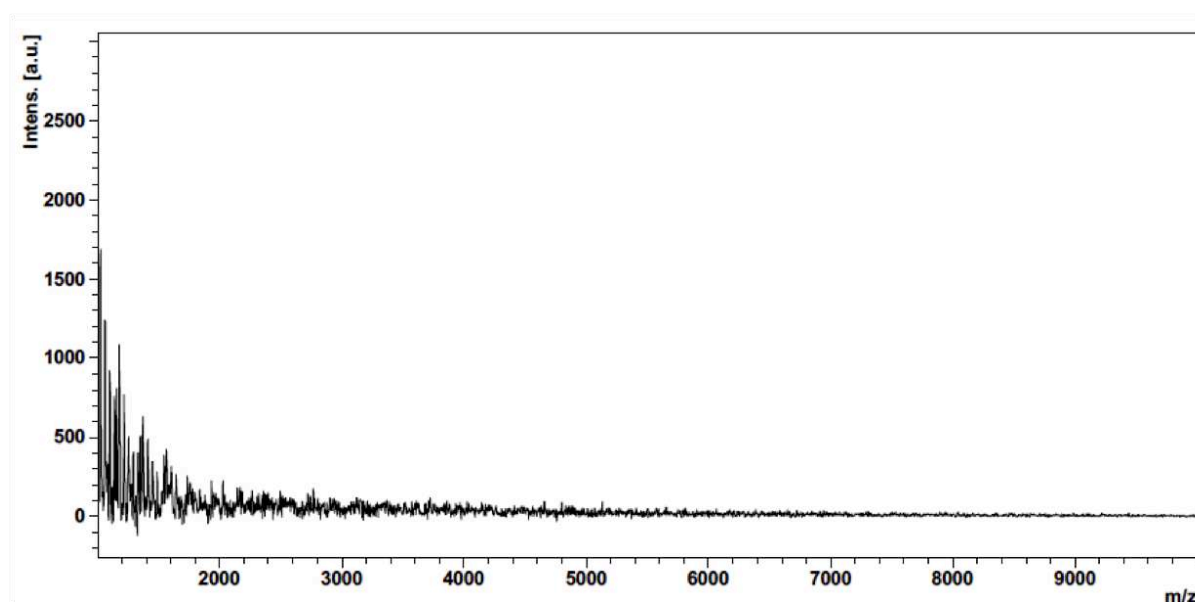


Figure 4.23: MALDI-TOF spectra of the incision reaction performed on 5' red-50merF26-seq1 DNA with 0.5 μ M UvrB and 2 μ M UvrC. No product was detected.

On all the MALDI spectra, several additional low molecular weight peaks were also observed. These may be some degradation products. A large peak at 2850 Da was detected, which could correspond to a short oligonucleotide of 8 or 9 nucleotides, but in fact this fragment was also observed in a sample containing only the UvrA1 protein without any DNA substrate (Figure 4.24).

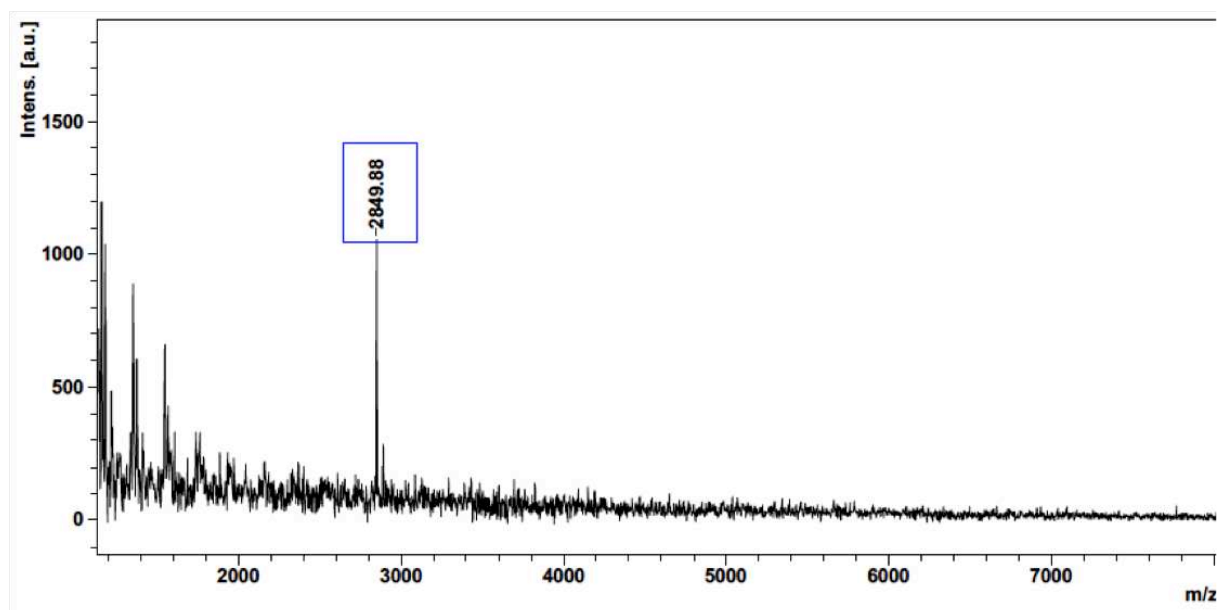


Figure 4.24: Maldi-TOF spectra of the protein UvrA1 alone.

4.2. Kinetics of the incision reaction

In Figure 4.25, we present the kinetics of the incision reaction of 25 nM of 5' red-50merF26-seq1 with 2 μ M UvrA1, 0.5 μ M UvrB and 2 μ M UvrC in presence of 2.5 mM Mg^{2+} and 2.5 mM ATP. We can see the decrease of the substrate, which went from 25 nM to less than 5 nM within the hour of repair. The decrease of the substrate corresponds to the incisions in order to release the intermediate fragment then the fragment containing the lesion. In this kinetic, the amount of 32 mer fragment was low throughout the reaction and the 12 mer fragment reached 20 nM after an hour. The fact that the intermediate fragment was barely detected showed the simultaneity of the incisions on 5' and 3' side of the lesion. This observation was also supported by the rate of incisions of 5' red-50merF26-seq1 presented in Table 4.3: the rates of processing of the 50 mer and the rates of production of the 12 mer are very similar (~ 0.65 nM DNA/min) suggesting that the two incision reactions occur at the same time.

In these conditions, we noticed that there was less 18 mer fragment accumulating than 12 mer fragment (Figure 4.25). Knowing that the formation of the 12 mer fragment is directly coupled to the release of the 18 mer as displayed in Figure 4.1, this difference was surprising. We saw on some gels presented earlier that the 18 mer fragment could be further processed by the UvrABC system into shorter DNA fragments. The processing of

the 18 mer might start early in the reaction as we noticed that its rate accumulation is 0.47 nM/min compared to the rate of 12 mer accumulation which is 0.67 nM/min (Table 4.3).

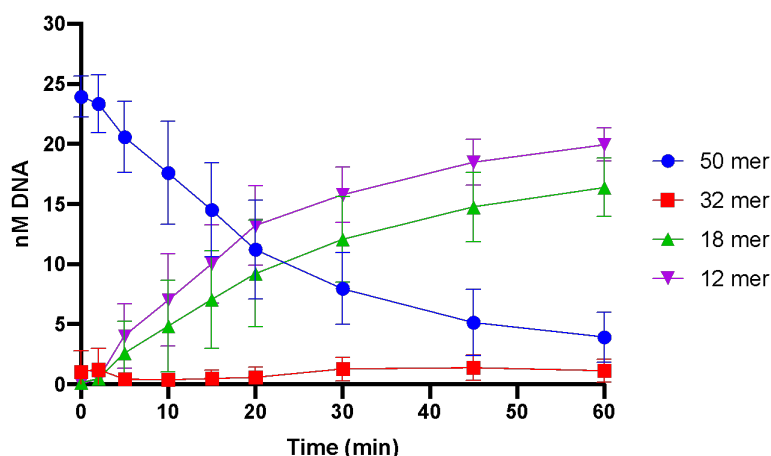


Figure 4.25: Kinetics of repair of 25 nM of 5'-red-50merF26-seq1 by 1 μ M UvrA1, 0.5 μ M UvrB and 2 μ M UvrC in the presence of 2.5 mM Mg^{2+} and 2.5 mM ATP. Reactions were incubated at 37°C for 60 minutes. The graph presents the kinetics of accumulation and disappearance of the various DNA fragments during the course of the reaction: 50 mer, 32 mer, 18 mer and 12 mer. The graph represents the mean and standard deviation of three replicates.

Table 4.3: Rates of incision of 25 nM 5'-red-50merF26-seq1 by 1 μ M UvrA1, 0.5 μ M UvrB and 2 μ M UvrC derived from the linear region (0-20 min) of the graph presented in Figure 4.25.

| Rate of 50 mer decrease | Rate of 18 mer accumulation | Rate of 12 mer accumulation |
|-------------------------|-----------------------------|-----------------------------|
| -0.65 nM/min | 0.47 nM/min | 0.67 nM/min |

Rate of 50 mer decrease => Rate of 5' incision + rate of 3' incision

Rate of 18 mer accumulation => Rate of 5' incision*

Rate of 12 mer accumulation => Rate of the limiting incision (5' or 3'?)

*This is not true if the 18 mer fragment is further processed, which appears to be the case in our experiments.

4.3. Role of ATP in the incision assay

To evaluate the role of ATP binding and hydrolysis during the incision reaction, ATP was replaced by several of its analogues: ADP, the product of ATP hydrolysis, ADP-AlF₄, a transition-state analogue, and AMP-PNP and AMP-PCP, two non-hydrolysable analogues (Figure 4.26.A).

In principle, UvrA1 dimers can bind and hydrolyse 4 ATP molecules, and UvrB also possesses one ATP binding site. Interestingly, we found that none of these analogues could replace ATP in the incision assay. The incision activity was abolished in the presence of these analogues (Figure 4.26.B), which suggests that both binding to ATP and its hydrolysis are needed for the NER activity.

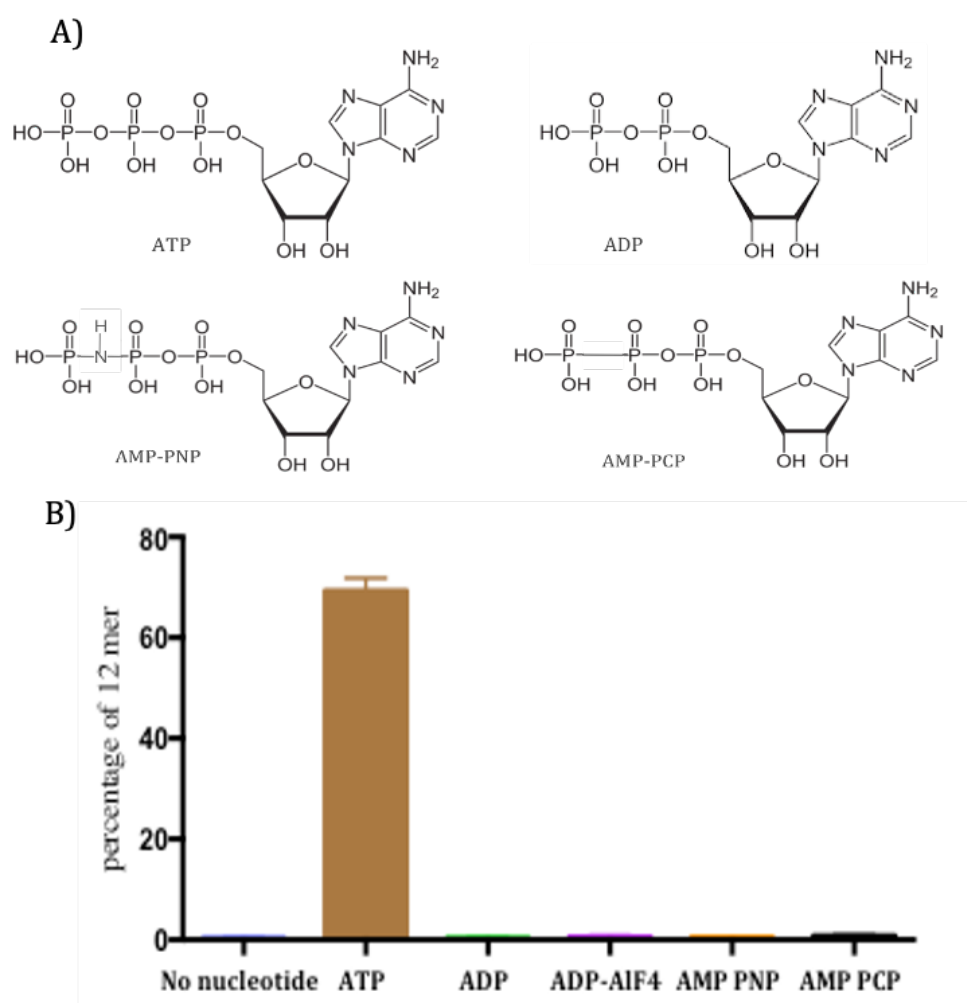


Figure 4.26: Effects of ATP analogues on the incision activity of *D. radiodurans* UvrABC proteins. A) Chemical structure of ATP and its analogues. B) Quantification of the 12 mer production after 45 minutes of incubation of the repair reaction with 25 nM 5' red-50merF26-seq1, 1 μ M UvrA1, 0.5 μ M UvrB and 2 μ M UvrC. The reaction was performed with either no nucleotide or 2.5 mM of ATP, ADP, ADP-AlF₄, AMP-PNP or AMP-PCP. The graph represents the mean and standard deviation of three replicates.

4.4. Role of divalent cations

Manganese is present at high concentrations in *D. radiodurans* cells particularly around the nucleoid (Santos et al., 2019). It is important for the bacterium survival following damaging events like irradiation. Therefore, we tried to incorporate Mn^{2+} in the incision assay. Manganese is predominantly present as a divalent ion instead of a trivalent ion in *D. radiodurans* (Sharma et al., 2013). We determined if it has any enhancing effect in our reconstituted system as manganese could be an efficient co-factor of the Uvr proteins. Different concentrations of Mn^{2+} ranging from 0.1 to 7.5 mM were added to the incision assay in replacement of Mg^{2+} . The highest incision activity was obtained with 1 and 2.5 mM Mn^{2+} , which can efficiently replace Mg^{2+} in this assay (Figure 4.27). The activity of the UvrABC proteins with Mn^{2+} seems very similar to that measured with Mg^{2+} alone.

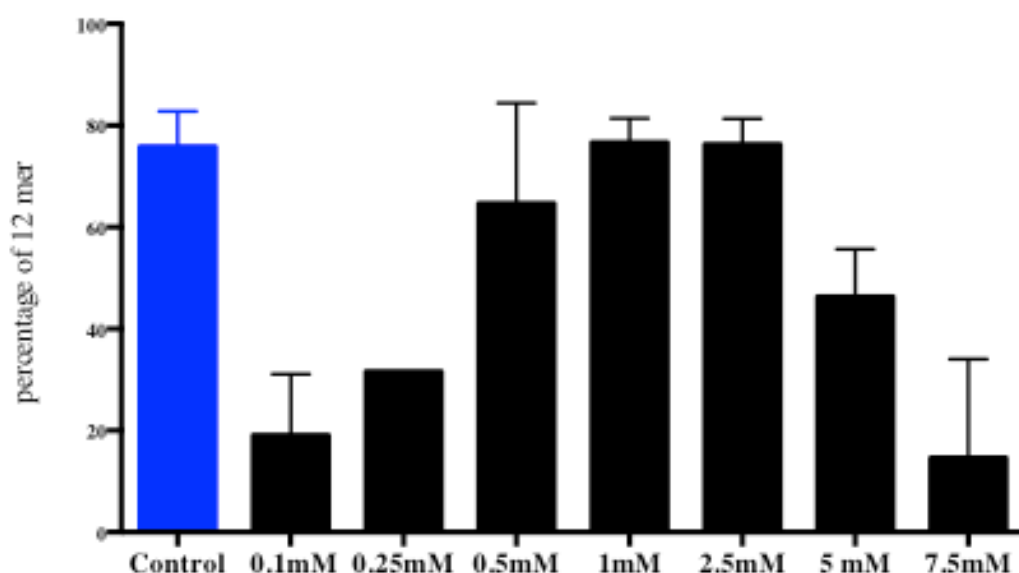


Figure 4.27: Quantification of the 12 mer fragment production in the incision assay with 25 nM 5'red-50merF26-seq1, 1 μ M UvrA1, 0.5 μ M UvrB and 2 μ M UvrC using a range of Mn^{2+} concentration and 2.5 mM ATP. The control reaction (blue) was performed with 2.5 mM Mg^{2+} and 2.5 mM ATP. All reactions were incubated at 37°C for 45 minutes. The graph represents the mean and standard deviation of two replicates.

Next, we performed the incision assay with 2.5 mM Mn^{2+} using UvrA1, UvrB and UvrC proteins either alone or combined (Figure 4.28). In the incision assays with UvrA1, UvrB and UvrC alone, or with UvrA1 combined with either UvrB or UvrC, no activity could be

detected. In the incision reaction containing UvrB and UvrC, a smaller fragment (containing the lesion; visible with the Fluorescein filter) than the usual 12 mer fragment was released during the repair by the NER; such a fragment was not observed in the presence of Mg^{2+} . We also observed a degradation of the DNA substrate in the presence of UvrB and UvrC (Figure 4.28).

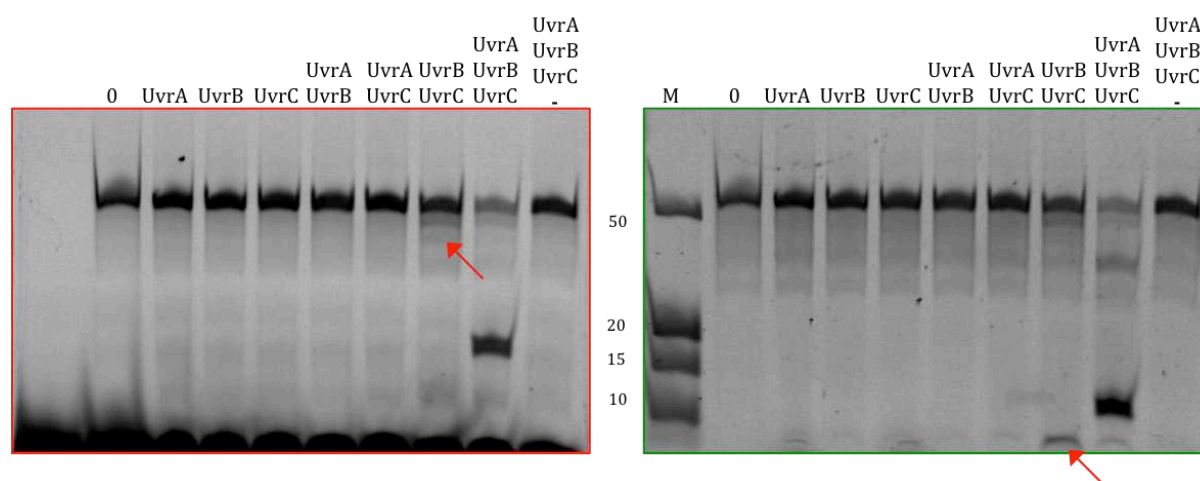


Figure 4.28: Urea polyacrylamide gel visualised with the Alexa 647 and Fluorescein filters showing the incision assay with 25 nM 5'-red-50merF26-seq1, 1 μ M UvrA1, 0.5 μ M UvrB and 2 μ M UvrC alone or combined in the presence of 2.5 mM Mn^{2+} and 2.5 mM ATP. In the last well, the reaction was performed without ATP. The red arrows indicate the extra bands corresponding to a degradation. All reactions were incubated at 37°C for 45 minutes.

We then tried to combine both divalent cations and performed reactions with 2.5 mM Mg^{2+} together with either 0.5 or 2.5 mM Mn^{2+} . The incision efficiency of the 12 mer was a little affected when 0.5 mM Mn^{2+} was added to the incision reaction (Figure 4.29). With 2.5 mM Mg^{2+} -ATP, the incision rate of the 12 mer was around 50% after 60 minutes. With the addition of 0.5 mM Mn^{2+} in this reaction, the rate of 12 mer production was closer to 40% after 60 minutes. The major difference, however, concerned the 32 mer fragment, which starts to accumulate already after five minutes of the reaction in the presence of Mn^{2+} , whereas its accumulation is much slower and reduced when the incision assay is performed with 2.5 mM Mg^{2+} alone (Figure 4.29). These observations indicate that Mn ions may interfere with the 3' incision activity.

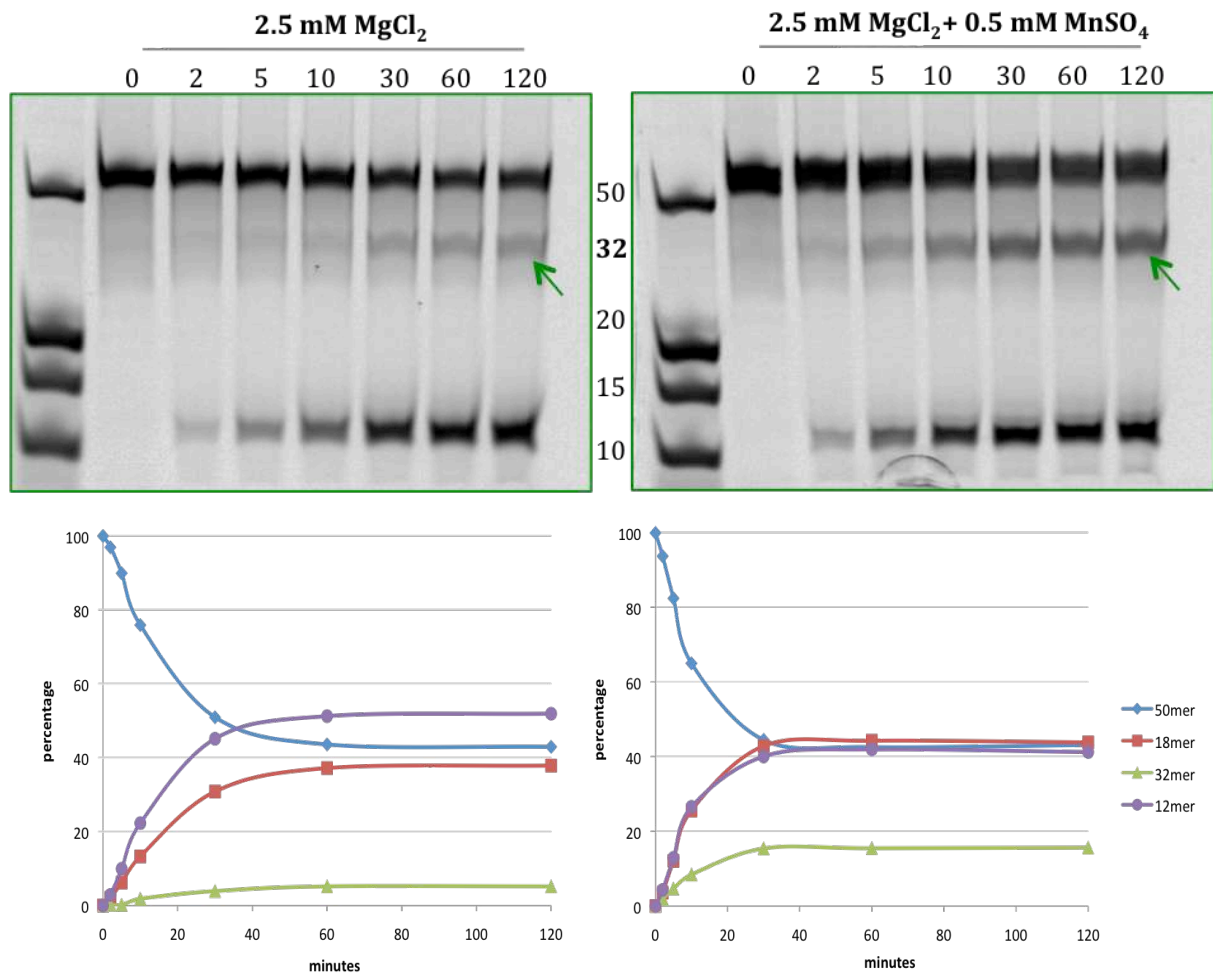


Figure 4.29: Urea polyacrylamide gel visualised with the Fluorescein filter showing the kinetics of the incision reaction with 25 nM 5'red-50merF26-seq1, 1 μ M UvrA1, 0.5 μ M UvrB and 2 μ M UvrC and quantification of the 12 mer fragment in the presence of 2.5 mM Mg²⁺ alone (left) or 2.5 mM Mg²⁺ associated with 0.5 mM Mn²⁺ (right). The accumulation of the 32 mer is indicated with a green arrow.

Interestingly, with 2.5 mM Mn²⁺ and 2.5 mM Mg²⁺ in the reactions, the extent of incision of the 12 mer was higher compared to the incision with 2.5 mM Mg²⁺ alone. The incision was 55 % at 20 minutes and 70% at 45 minutes for Mn²⁺ and Mg²⁺ compared to 30% at 20 minutes and 58% at 45 minutes for Mg²⁺ alone (Figure 4.30).

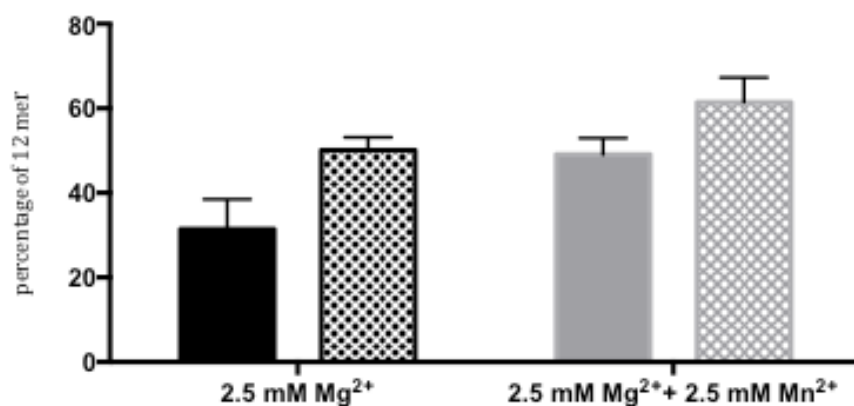


Figure 4.30: Quantification of the 12 mer fragment in the incision assay with 25 nM 5'red-50merF26-seq1, 1 μ M UvrA1, 0.5 μ M UvrB and 2 μ M UvrC in the presence of 2.5 mM Mg²⁺ alone or 2.5 mM Mg²⁺ associated with 2.5 mM Mn²⁺ after 20 minutes (solid colour) and 45 minutes (patterned). The graph represents the mean and standard deviation of three replicates.

However, when the incision reaction was performed with 2.5 mM Mg²⁺ and 2.5 mM Mn²⁺ using UvrA1, UvrB and UvrC proteins either alone or combined (Figure 4.31), the additional smaller fragment containing the lesion was observed below the 12 mer fragment and the non-specific incision activity of UvrB and UvrC was accentuated. There also seems to be some degradation of the substrate as observed previously in the presence of Mn²⁺ alone (Figure 4.28). So, although Mn²⁺ ions can largely replace Mg²⁺ in the incision assay, the specificity of the NER system appears to be affected by this alternative divalent ion.

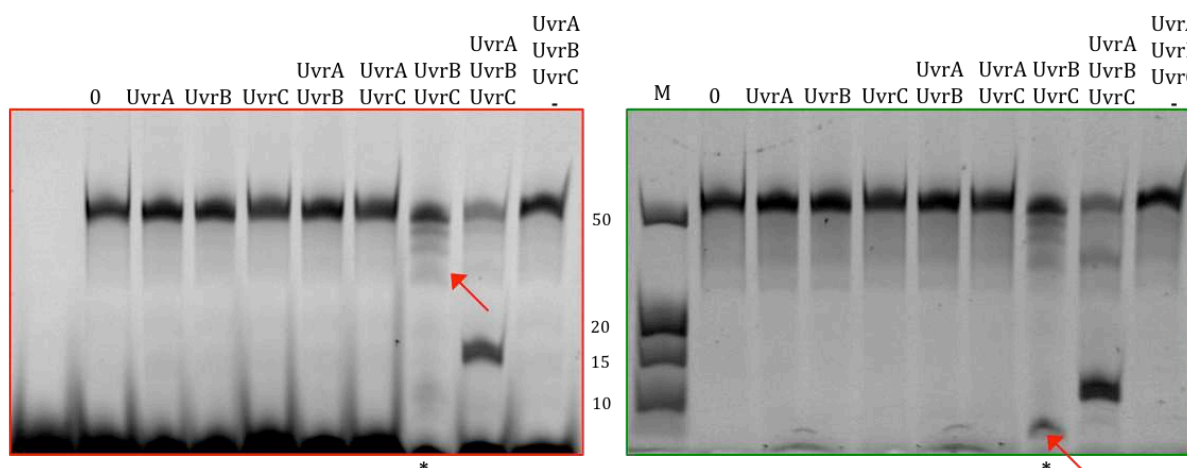


Figure 4.31: Urea polyacrylamide gel visualised with the Alexa 647 and Fluorescein filters showing the incision assay with 25 nM 5'red-50merF26-seq1, 1 μ M UvrA1, 0.5 μ M UvrB and 2 μ M UvrC alone or combined in presence of 2.5 mM Mn²⁺, 2.5 mM of Mg²⁺ and 2.5 mM ATP. In the last well, the reaction was performed without ATP. Incubation conditions: 37°C for 45 minutes

4.5. Role of iron and other divalent ions

After testing the effect of manganese in the incision assay, we decided to evaluate the impact of iron on the NER system, in particular since we had observed that the UvrC protein solution is slightly brown, which could be due to bound iron. In *Deinococcus*, the high Mn/Fe ratio is known to be essential for protecting the bacteria from stress (Daly et al., 2004). The 10x buffer without any divalent cation was prepared for the incision assay. To avoid any further oxidation of the ion, Fe^{3+} was used instead of Fe^{2+} . First of all, Fe^{3+} was added alone (in the absence of Mg^{2+}) to the reaction at final concentrations ranging from 0.1 to 5 mM (Figure 4.32). The concentration of ATP was maintained at 2.5 mM. The activity of the proteins in the presence of Fe^{3+} was compared to that of the control with 2.5 mM Mg^{2+} .

After an incubation of 45 minutes at 37°C, the incision efficiency of the 12 mer fragment was around 80% for the control whilst there was no incision at all for reactions containing 1, 2.5 and 5 mM Fe^{3+} . Below 1 mM Fe^{3+} , we observed between 3% and 10% of incision of the 12 mer. These results suggest that iron cannot efficiently replace Mg^{2+} in this assay, and may in fact inhibit the reaction at higher concentrations.

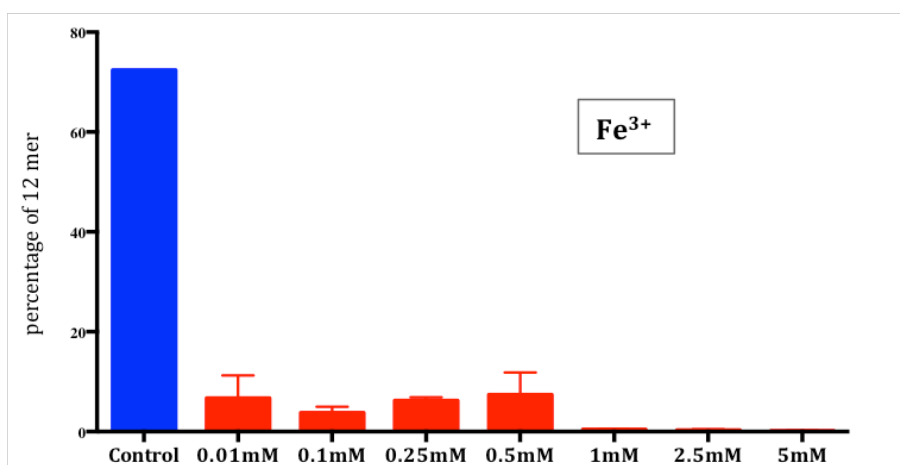
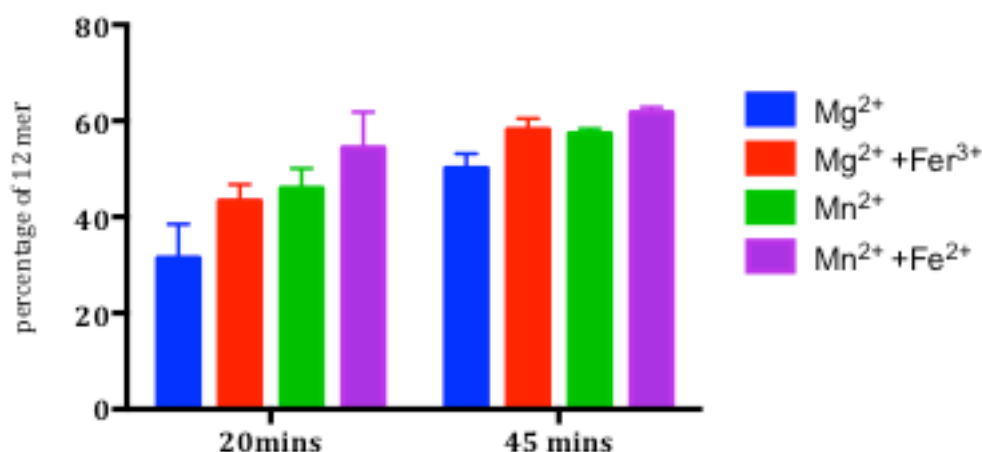


Figure 4.32: Quantification of the 12 mer fragment in the incision assay with 25 nM 5'red-50merF26-seq1, 1 μM UvrA1, 0.5 μM UvrB and 2 μM UvrC using a range of Fe^{3+} concentrations and 2.5 mM ATP. The control is the incision assay performed with 2.5 mM Mg^{2+} and 2.5 mM ATP. Incubation conditions: 37°C for 45 minutes. The graph represents the mean and standard deviation of two replicates.

Next, we tried to combine two cations (either Mn^{2+} and Fe^{3+} or Mg^{2+} and Fe^{3+}) in the incision assay to assess the effect on the repair system. The activity was assessed at 20 minutes and 45 minutes to observe the evolution of the repair with 0.25 mM of Fe^{3+} plus 2.5 mM of Mn^{2+} or Mg^{2+} (Figure 4.33).



| Sidak's multiple comparisons test | Significant? | Summary |
|--|--------------|-----------------|
| %12 mer at 20 minutes | | |
| Mg^{2+} vs. $\text{Mg}^{2+} + \text{Fe}^{3+}$ | Yes | * |
| Mg^{2+} vs. Mn^{2+} | Yes | ** |
| $\text{Mg}^{2+} + \text{Fe}^{3+}$ vs. $\text{Mn}^{2+} + \text{Fe}^{3+}$ | Yes | * |
| Mn^{2+} vs. $\text{Mn}^{2+} + \text{Fe}^{3+}$ | No | Non-significant |
| % 12 mer at 45 minutes | | |
| Mg^{2+} vs. $\text{Mg}^{2+} + \text{Fe}^{3+}$ | No | Non-significant |
| Mg^{2+} vs. Mn^{2+} | No | Non-significant |
| $\text{Mg}^{2+} + \text{Fe}^{3+}$ vs. $\text{Mn}^{2+} + \text{Fe}^{3+}$ | No | Non-significant |
| Mn^{2+} vs. $\text{Mn}^{2+} + \text{Fe}^{3+}$ | No | Non-significant |

Figure 4.33: Quantification of the 12 mer fragment after 20 minutes and 45 minutes of incubation. The incision assays were performed with 25 nM 5'-red-50merF26-seq1, 1 μM UvrA1, 0.5 μM UvrB 2 μM UvrC and 2.5 mM ATP, in presence of 2.5 mM Mg^{2+} , 2.5 mM Mn^{2+} alone or associated with 0.25 mM Fe^{3+} . The two-way analysis of variance performed on the data collected at 20 minutes and at 45 minutes is presented in the table. The graph represents the mean and standard deviation of three replicates.

No significant differences were observed at 45 minutes, probably because the reactions were close to complete and had reached a plateau. However, some differences could be

seen at 20 minutes. In particular, the combination of 2.5 mM Mg^{2+} and 0.25 mM Fe^{3+} appears to significantly enhance the incision activity of UvrABC, with 45% of 12 mer fragment with the two ions compared to 32% with only Mg^{2+} ions. A similar trend is seen with Mn^{2+} ions, although the effect of the Fe^{3+} on the incision activity is not significant in that case.

When performing the assay with UvrA1, UvrB and UvrC alone or combined in the presence of 2.5 mM Mn^{2+} and 0.25 mM Fe^{3+} , the substrate degradation caused by UvrB and UvrC in the presence of 2.5 mM Mn^{2+} alone (Figure 4.28) was not observed, suggesting that Fe^{3+} may block the non-specific activity of UvrB/UvrC (Figure 4.34).

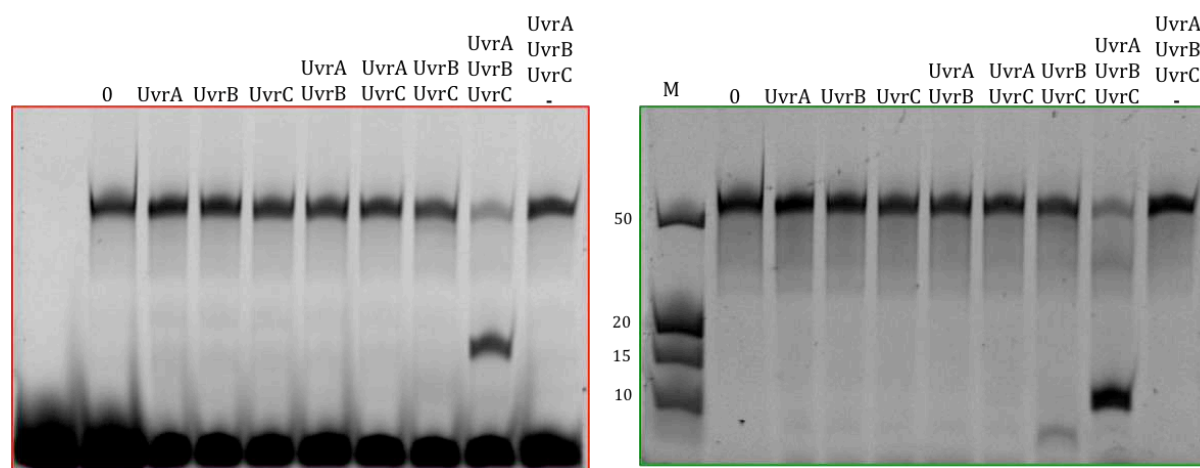


Figure 4.34: Urea polyacrylamide gel visualised with the Alexa 647 and Fluorescein filters showing the incision assay with 25 nM 5'-red-50merF26-seq1, 1 μ M UvrA1, 0.5 μ M UvrB and 2 μ M UvrC alone or combined in presence of 2.5 mM Mn^{2+} and 0.25 mM of Fe^{3+} and 2.5 mM ATP. In the last well, the reaction was performed without ATP. Incubation conditions: 37°C for 45 minutes.

Having seen that Fe^{3+} modulates the NER activity, we decided to explore the effects of other divalent ions, including zinc (Zn^{2+}), a known co-factor of UvrA1, which has 3 zinc-binding sites, cobalt (Co^{2+}), nickel (Ni^{2+}) and copper (Cu^{2+}). First, we examined the incision activity of the UvrABC system in the absence of Mg^{2+} to determine whether any of these ions can replace Mg^{2+} (Figure 4.35). A control reaction containing 2.5 mM Mg^{2+} was performed in parallel. On the graphs monitoring the incision of the 12 mer fragment after 45 minutes of incubation at 37°C, the ions Zn^{2+} and Co^{2+} in the incision assay did not allow any release of fragment. When the Cu^{2+} ion was used, 1% to 5% were released but only at low concentrations (below 1 mM). In the assays performed with 0.1 mM to 1mM

Ni^{2+} , an average of 10% of lesions were released compared to 80% with 2.5 mM Mg^{2+} . None of these ions can thus efficiently replace Mg^{2+} .

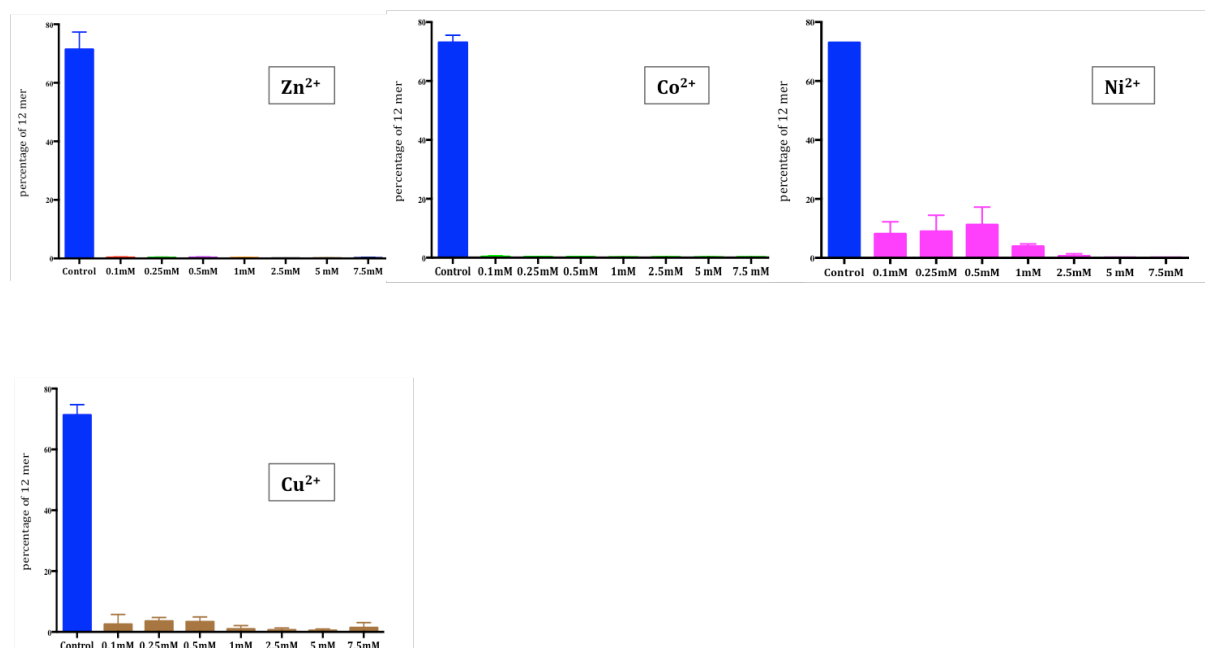
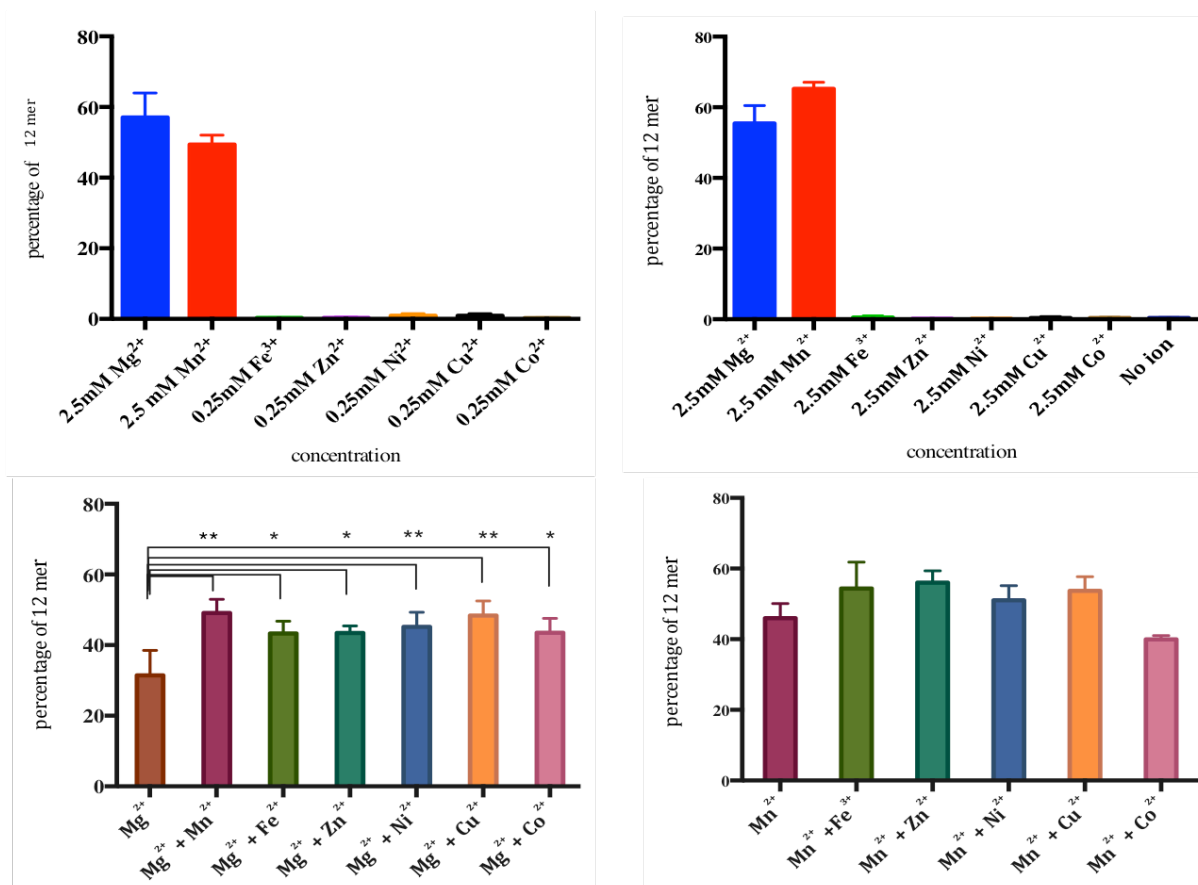


Figure 4.35: Quantification of the 12 mer fragment in the incision assay with 25 nM 5'red-50merF26-seq1, 1 μM UvrA1, 0.5 μM UvrB and 2 μM UvrC using a range of Zn^{2+} , Co^{2+} , Ni^{2+} and Cu^{2+} and 2.5 mM ATP. The control is the incision assay performed with 2.5 mM Mg^{2+} and 2.5 mM ATP. Incubation conditions: 37°C for 45 minutes. The graphs represent the mean and standard deviation of two replicates.

Since the incision assays with 0.25 mM Cu^{2+} and Ni^{2+} showed some activity, we combined this concentration of ions with 2.5 mM Mg^{2+} and also 2.5 mM Mn^{2+} (Figure 4.36). For Mg^{2+} , the incision efficiencies with the combined ions were a little enhanced compared to the condition with Mg^{2+} alone at 20 minutes. For Mn^{2+} , the incision activities were largely unaffected (Figure 4.36). In conclusion, addition of Cu^{2+} , Co^{2+} or Ni^{2+} to the assay did not lead to any significant change in the NER activity in the presence of an excess of Mg^{2+} , and only Ni^{2+} and to a lesser extent Cu^{2+} , could partially replace Mg^{2+} .



Quantification of the 12 mer fragment in the incision assay with 25 nM 5'red-50merF26-seq1, 1 μ M UvrA1, 0.5 μ M UvrB and 2 μ M UvrC using either 2.5 mM Mg²⁺ (left) or Mn²⁺ (right) combined with 0.25 mM of Cu²⁺, Co²⁺, Zn²⁺ or Ni²⁺. Incubation conditions: 37°C for 20 minutes. With a one-way analysis of variance, the significant differences are illustrated for Mg²⁺ associated with the other metal ions. The statistical test performed for Mn²⁺ associated with the other metal ions did not show any significant difference between the conditions. The graphs represent the mean and standard deviation of three replicates.

5. Substrate specificity

Using the optimized NER incision assay, we evaluated the activity of the *D. radiodurans* UvrABC system on two additional DNA substrates containing a fluorescein or a biotin (Figure 4.37):

- 5'red-50merF26-seq2: this substrate is similar in design to the previously used 5'red-50merF26-seq1 substrate, but differs in its sequence (see Materials and Methods). It is doubly labelled on one strand with the fluorophore ATTO633 on the 5' end and the thymine in position 26 is conjugated to fluorescein.

- 5'FAM-50merB26-seq1: this substrate shares the same sequence as 5'red-50merF26-seq1, but the thymine in position 26 is conjugated to biotin instead of fluorescein and the fluorophore on its 5' end is a Fluorescein FAM.

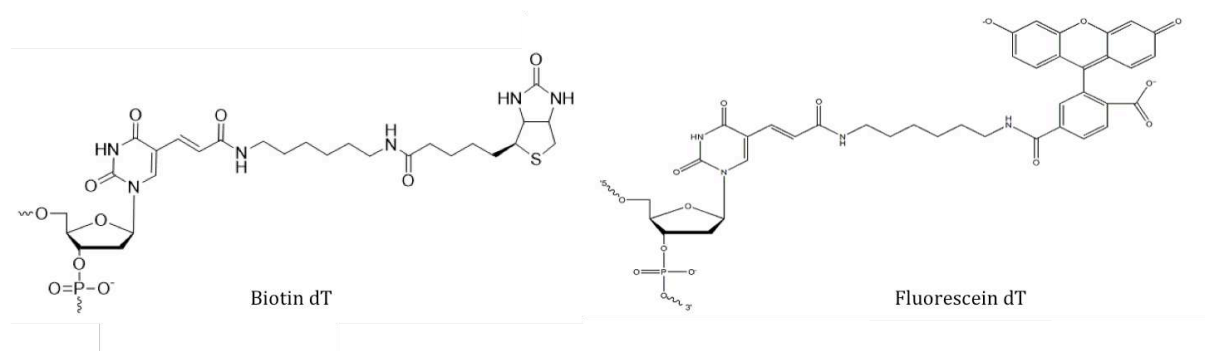


Figure 4.37: Schematic representations of biotin (left) and Fluorescein (right) conjugated to thymine

For the incision of 5'FAM-50merB26-seq1 by the NER, we could only monitor the fragments containing the FAM fluorophore at the 5' end, *i.e.* the 50 mer and the 18 mer resulting from the incision on the 5' side of the lesion, since the biotin is not labelled (Figure 4.38).

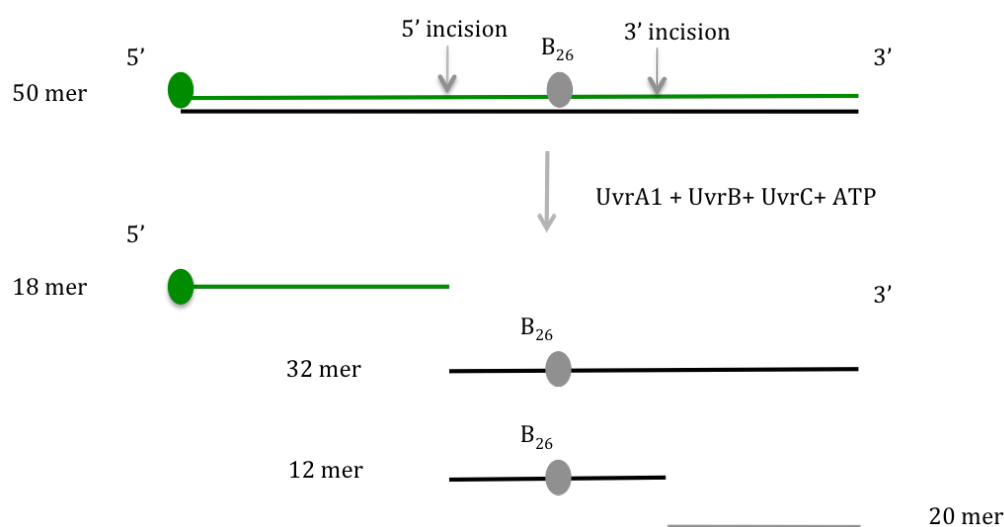


Figure 4.38: Schemes of repair of the 50 mer dsDNA substrate, 5'FAM-50merB26-seq1, analysed on a urea polyacrylamide gel. Unlike 5'red-50merF26-seq1 and 5'red-50merF26-seq2, we could only monitor the production of the 18 mer fragment.

These new substrates were first tested in the incision assay and compared to our classical substrate, 5'FAM-50merF26-seq1, using the conditions presented in Table 4.1: 25 nM DNA substrate, 1 μ M UvrA1, 0.5 μ M UvrB and 2 μ M UvrC, 2.5 mM Mg^{2+} and ATP.

Because of the non-specific fragment that could result from an incision on the 18 mer fragment and the fact that its presence is accentuated during the repair of the FdT-containing substrates, the quantifications presented on the graphs took into account the 12 mer for these substrates for a more accurate quantification of the repair by UvrABC. For 5'FAM-50merB26-seq1, we presented the 18 mer that could be monitored (Figure 4.39)

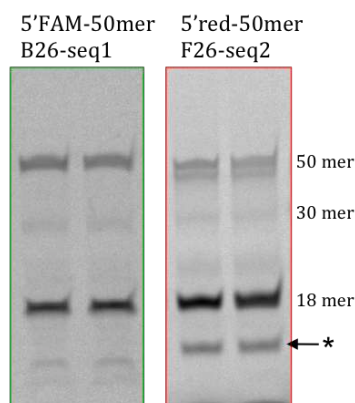


Figure 4.39: Urea polyacrylamide gels visualised with the Alexa 647 filter (5'red-50merF26-seq2) and Fluorescein filter (5'FAM-50merB26-seq1) showing the incision assay with 25 nM of substrates, 1 μ M UvrA1, 0.5 μ M UvrB and 2 μ M UvrC in presence of 2.5 mM of Mg^{2+} and 2.5 mM ATP. The smaller fragment indicated with * is accentuated with 5'red-50merF26-seq2, therefore, the 18 mer quantification can be biased. Incubation conditions: 37°C for 45 minutes.

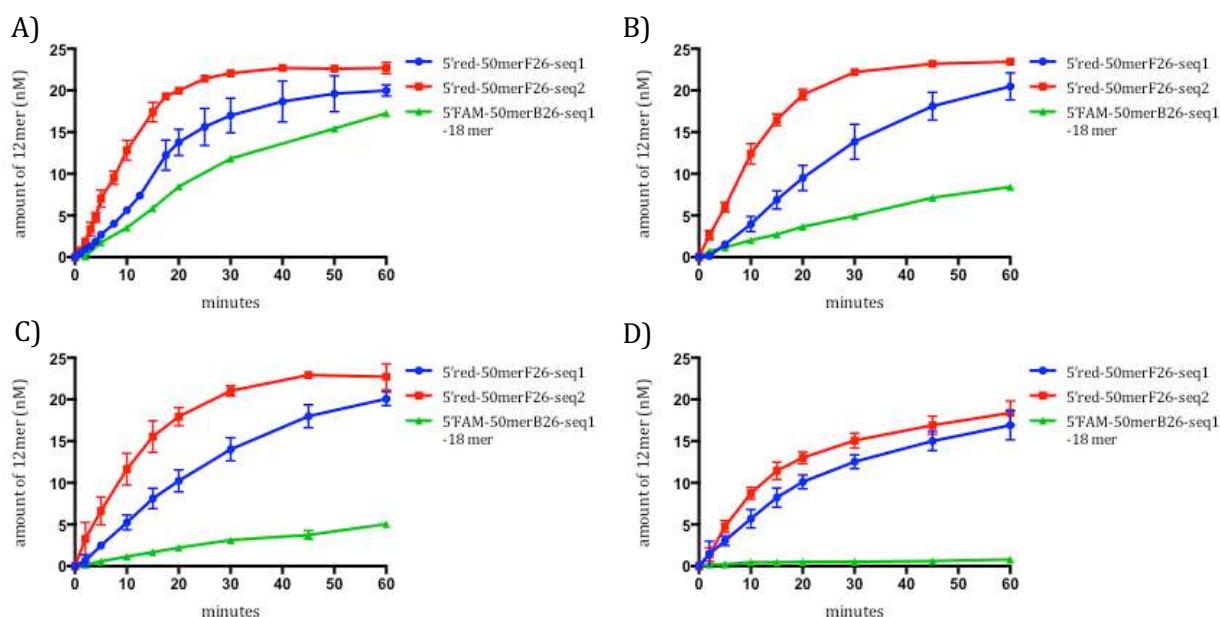


Figure 4.40: Quantification of the kinetics of production of the 12 mer fragment of 5'red-50merF26-seq1 and 5'red-50merF26-seq2 and the 18 mer fragment of 5'FAM-50merB26-seq1 by (A) 1 μ M UvrA1, 0.5 μ M UvrB and 2 μ M UvrC, (B) 0.5 μ M UvrA1, 0.25 μ M UvrB and 1 μ M UvrC, (C) 250 nM UvrA1, 125 nM UvrB and 500 nM UvrC and (D) 100 nM UvrA1, 50 nM UvrB and 200 nM UvrC (D). The concentration of DNA substrate was 25 nM and the Mg^{2+} and ATP were set to 2.5 mM. Experiments performed in four replicates.

Urea polyacrylamide gel analysis of these assays already showed a clear difference in the speed of repair of these substrates by *D. radiodurans* NER. The substrate disappeared rapidly for 5'red-50merF26-seq2 compared to 5'red-50merF26-seq1 and 5'FAM-50merB26-seq1, as was confirmed by the quantification of the bands (Figure 4.40). At all Uvr concentrations, we can see that the two FdT-containing substrates were processed more rapidly by the Uvr proteins than the biotinylated substrate, 5'FAM-50merB26-seq1. During the repair of 5'red-50merF26-seq2, some non-specific incisions at the 5' end of the labelled oligonucleotide were observed after 10 minutes of reaction. These small fragments correspond to the ones observed when the incision assay was performed with UvrB and UvrC only, without the damage sensing protein UvrA1.

The kinetics of repair of the three substrates was also monitored and compared. The rates of incision of these three substrates derived from the linear regions of the graphs

(between 0 and 20 min) are shown in Table 4.4 and Table 4.5. In the second table, the rates have been corrected for the amount of enzyme present and are thus given in nM DNA released per minute per micromolar UvrA1.

Table 4.4: Rates of release of the 12 mer fragment (in nM/min) by different concentrations of the UvrABC system.

| | 5'red-50merF26-seq1 | 5'red-50merF26-seq2 | 5'FAM-50merB26-seq1 |
|--|---------------------|---------------------|---------------------|
| 1 μ M UvrA1; 0.5 μ M UvrB; 2 μ M UvrC | 0.56 nM/min | 1.21 nM/min | 0.37 nM/min |
| 0.5 μ M UvrA1; 0.25 μ M UvrB; 1 μ M UvrC | 0.43 nM/min | 1.15 nM/min | 0.19 nM/min |
| 0.25 μ M UvrA1; 0.125 μ M UvrB; 0.5 μ M UvrC | 0.53 nM/min | 1.10 nM/min | 0.11 nM/min |
| 0.1 μ M M UvrA1; 0.05 μ M UvrB; 0.2 μ M UvrC | 0.56 nM/min | 0.81 nM/min | 0.04 nM/min |

Table 4.5: Rates of release of the 12 mer fragment (in nM/min/ μ M UvrA1) by different concentrations of the UvrABC system.

| | 5'red-50merF26-seq1 | 5'red-50merF26-seq2 | 5'FAM-50merB26-seq1 |
|--|----------------------|----------------------|----------------------|
| 1 μ M UvrA1; 0.5 μ M UvrB; 2 μ M UvrC | 0.56 nM/min/ μ M | 1.21 nM/min/ μ M | 0.37 nM/min/ μ M |
| 0.5 μ M UvrA1; 0.25 μ M UvrB; 1 μ M UvrC | 0.86 nM/min/ μ M | 2.30 nM/min/ μ M | 0.38 nM/min/ μ M |
| 0.25 μ M UvrA1; 0.125 μ M UvrB; 0.5 μ M UvrC | 2.12 nM/min/ μ M | 4.40 nM/min/ μ M | 0.44 nM/min/ μ M |
| 0.1 μ M M UvrA1; 0.05 μ M UvrB; 0.2 μ M UvrC | 5.60 nM/min/ μ M | 8.10 nM/min/ μ M | 0.40 nM/min/ μ M |

For the FdT containing substrates, changing the concentration of UvrABC did not significantly affect the overall rate of incision (Table 4.4), which suggests that the lower the protein concentration, the faster the enzymatic turnover rate (Table 4.5). In contrast, for the biotinylated substrate, the turnover rate is constant regardless of the UvrABC concentration and 10 to 20 times slower than for the FdT substrates at the lowest UvrABC concentration (Table 4.5). We can thus conclude that FdT is a better substrate than biotin perhaps as a result of a higher affinity for the substrate.

For the FdT containing substrates, we nonetheless observed a significant difference in the rate with which they were processed. The 5'red-50merF26-seq2 substrate was indeed processed at almost twice the rate at which the classical 5'red-50merF26-seq1 substrate was incised. This suggests that the sequence of the oligonucleotide also affects tremendously the repair rate by UvrABC.

To verify whether the cleavage sites were the same regardless of the DNA substrate, we performed MALDI-TOF analyses on the 5' red-50merF26-seq2 and 5' FAM-50merB26-seq1 DNA substrates processed with the UvrABC (Figures 4.41 and Figure 4.42). The results were similar to those obtained with 5' red-50merF26-seq1 (Figure 4.22) and the size of the fragments were the same (Tables 4.6 and 4.7). In both cases, 5' incision occurred 7 nucleotides upstream of the conjugated thymine and the 3' incision occurred 4 nucleotides downstream of the modified thymine. Also, as for 5' red-50merF26-seq1, a 5' phosphate was found on the released 12 mer fragment. These findings indicate that the incision sites are the same for all three tested DNA substrates and are thus independent of the type of lesion and of the local sequence surrounding the modified nucleotide.

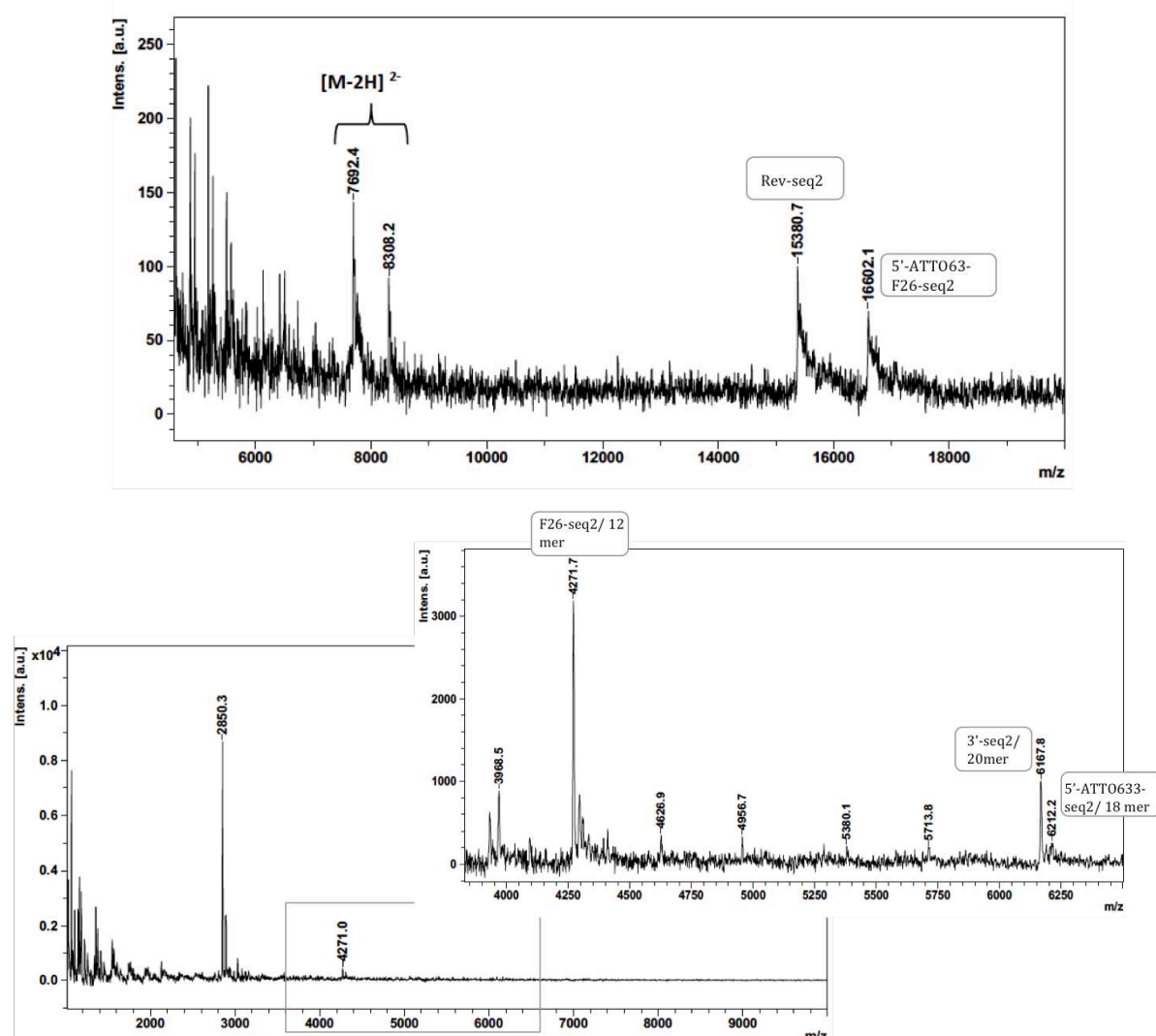


Figure 4.41: MALDI-TOF spectra of the incision reaction substrates (top) and products (bottom). The reactions were performed on 5' red-50merF26-seq2 DNA with 1 μ M UvrA1, 0.5 μ M UvrB and 2 μ M UvrC. The masses of the different fragments were identified and tagged. Other unknown peaks were also detected.

Table 4.6: Sequences and sizes of the major fragments observed by MALDI-TOF analysis of the incision reactions using 5'red-50merF26-seq2 as a substrate.

| Name/Size | Sequence | Expected mass (Da) | Measured mass (Da) |
|-----------------------------|--|--------------------|--------------------|
| 5'-ATTO633-F26-seq2 (50mer) | 5'- X GTT AGC GAA CGA TAC CTT CAG TAG A C AAG TCC TAG CTG ACC GGT TCG GC -3' | 16609 | 16602.1 |
| Rev-seq2 (50mer) | 5'- GCC GAA CCG GTC AGC TAG GAC TTG A T CTA CTG AAG GTA TCG TTC GCT AAC -3' | 15386 | 15380.7 |
| F26-seq2 (12mer) | 5'- pCAGTAGA C CAAG -3' | 4269.4 | 4271.8 |
| 5'-ATTO633-seq2 (18mer) | 5'- X GTTAGCGAACGATACCTT -3' | 6210.6 | 6212.2 |
| 3'-seq2 (20mer) | 5'- pTCCTAGCTGACCGGTTTCGGC -3' | 6165 | 6166.4 |

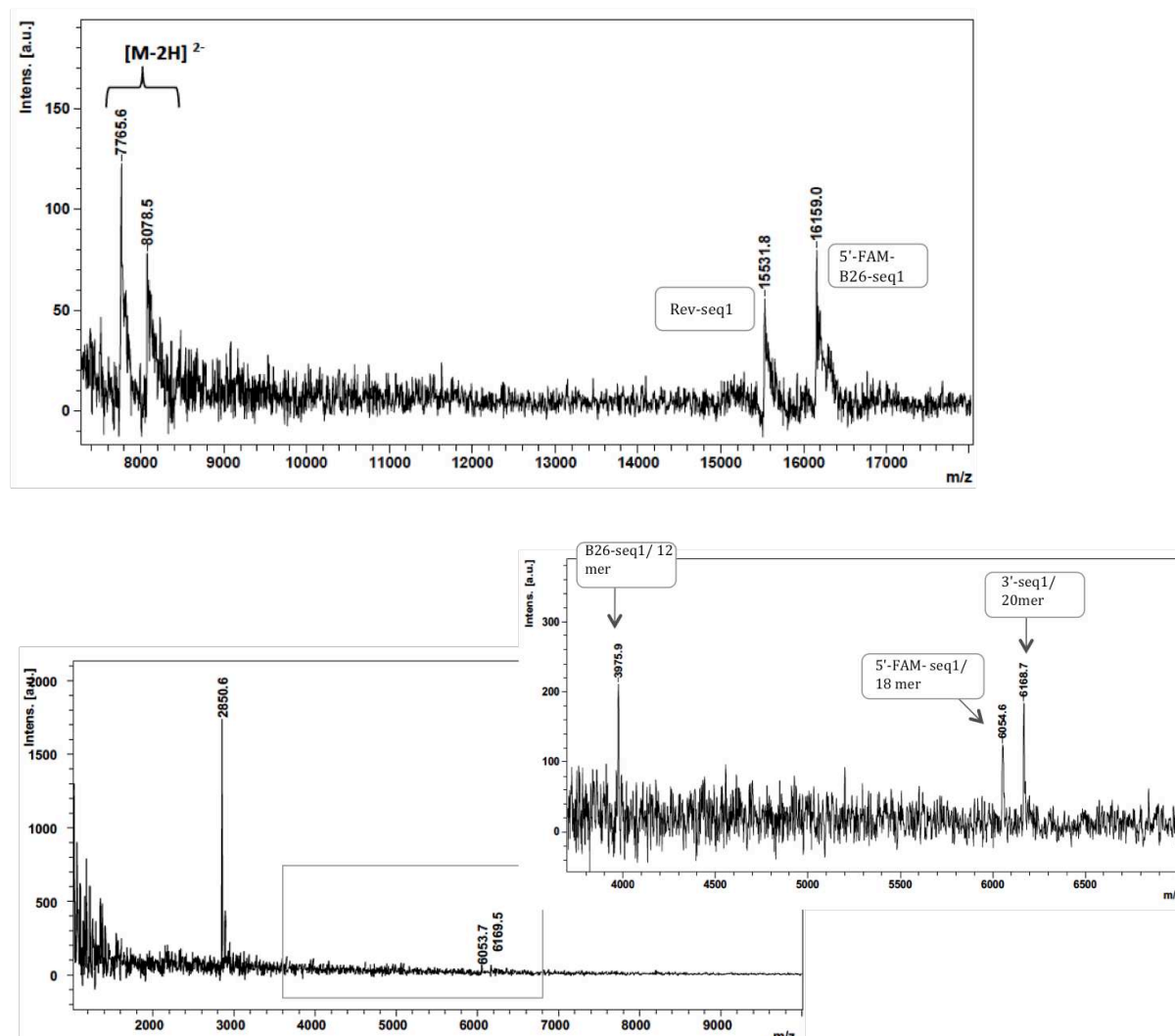
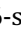

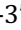



Figure 4.42: MALDI-TOF spectra of the incision reaction substrates (top) and products (bottom). The reactions were performed on 5'red-50merB26-seq1 DNA with 1 μ M UvrA1, 0.5 μ M UvrB and 2 μ M UvrC. The masses of the different fragments were identified and tagged. Other unknown peaks were also detected.

Table 4.7: Sequences and sizes of the major fragments observed by MALDI-TOF analysis of the incision reactions using 5' red-50merB26-seq1 as a substrate.

| Name/Size | Sequence | Expected mass (Da) | Measured mass (Da) |
|-------------------------|---|--------------------|--------------------|
| 5'-FAM-B26-seq1 (50mer) | 5'-  GAC TAC GTA CTG TTA CGG CTC CAT  C TAC CGC AAT CAG GCC AGA TCT GC -3' | 16160 | 16159.0 |
| Rev-seq1 (50mer) | 5'- GCA GAT CTG GCC TGA TTG CGG TAG AGA TGG AGC CGT AAC AGT ACG TAG TC -3' | 15531 | 15531.8 |
| B26-seq1 (12 mer) | 5'- pCTCCATC  CTAC -3' | 3976.4 | 3975.6 |
| 5'-FAM- seq1 (18 mer) | 5'-  GACTACGTACTGTTACGG -3' | 6052.6 | 6054.7 |
| 3'-seq1 (20mer) | 5'- pCGCAATCAGGCCAGATCTGC -3' | 6167 | 6168.0 |

The same difference in height for the 20 mer and 18 mer peaks was observed for 5' red-50merF26-seq1 and 5' red-50merF26-seq2 DNA (Figure 4.22, Figure 4.41). This event was not the case however for 5' red-50merB26-seq1 DNA (Figure 4.42).

Since the three DNA substrates tested so far contained relatively small conjugates, with biotin being smaller than fluorescein, we decided to evaluate the incision activity on a fourth DNA substrate containing a bulkier lesion: 5' FAM-50merB26-strep-seq1. To prepare this substrate, the 5' FAM-50merB26-seq1 DNA was incubated with a 10-fold excess of streptavidin to couple streptavidin to the biotinylated DNA (Figure 4.43.A). A tetramer of streptavidin can trap up to four biotinylated DNA molecules. On native electrophoresis gels (Figure 4.43.B), we could visualize two states of the complex, with one state being favoured at the high streptavidin to biotin ratio which was used in our case. This state most likely corresponds to one tetramer bound to each DNA molecule. The evolution of the coupling is presented in Figure 4.43.A.

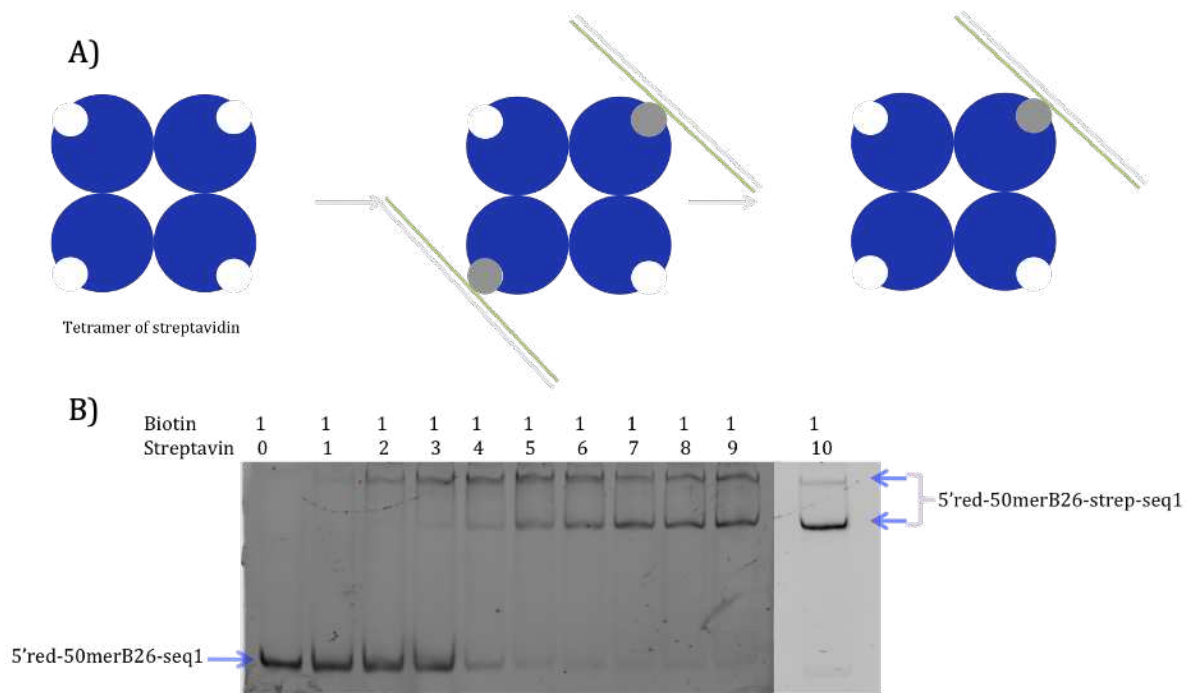


Figure 4.43: (A) Schematic representation of the possible conformations of 5'FAM-50merB26-strep-seq1. At low concentrations of streptavidin, several DNA molecules may bind to a single streptavidin tetramer, while at high streptavidin concentrations as used for the preparation of 50merB26-strep-seq1, complexes composed of a tetramer of streptavidin bound to one DNA molecule should be favoured (lower band in last well). TBE native polyacrylamide gel of the binding of increasing amounts of streptavidin (from 0:1 to 10:1 ratio) to 5'FAM-50merB26-seq1. Free 5'FAM-50merB26-seq1 DNA substrate is seen in the first well.

After the incision assay, we had trouble visualizing the 5'FAM-50merB26-strep-seq1 substrate on gel when using 25 nM of 5'FAM-50merB26-strep-seq1, so we had to use 50 nM of DNA for this substrate. The amount of Uvr proteins used in the reaction was not doubled however. 5'FAM-50merB26-strep-seq1 showed similar release kinetics for the 18 mer fragment as for 5'FAM-50merB26-seq1, indicating that the binding of streptavidin to the biotin moiety does not affect the NER repair efficiency (Figure 4.44).

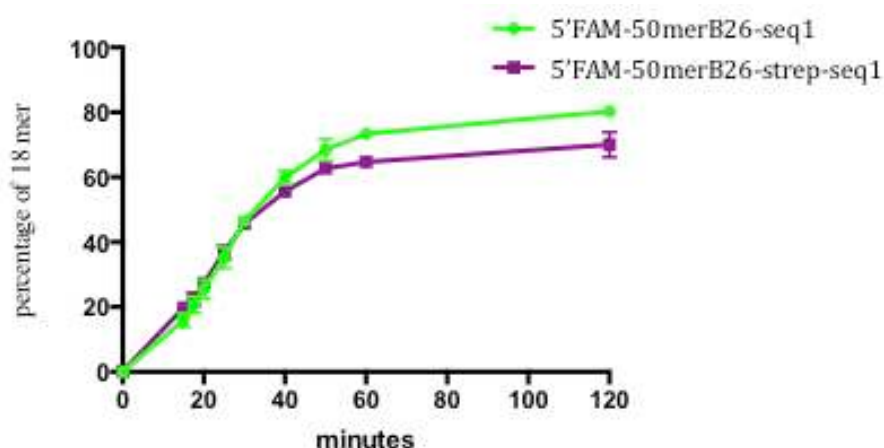


Figure 4.44: Quantification of the release of the 18 mer fragment from either 5'FAM-50merB26-seq1 and 5'FAM-50merB26-strep-seq1 processed with 1 μ M UvrA1, 0.5 μ M UvrB and 2 μ M UvrC. Experiments performed in three replicates.

6. Deciphering the role of UvrC and its domains in the incision reaction

6.1. Characterisation of different UvrC constructs

6.1.1. Preparation of the different constructs

The UvrC protein carries two endonuclease domains that are responsible for the incisions of the lesion. The N-terminus of UvrC, corresponding to the GIY-YIG endonuclease domain, cuts on the 3' side of the lesion and, the C-terminal RNase H endonuclease domain cuts on the 5' side of the lesion (Figure 4.45).

As shown in Figure 4.45, four constructs of UvrC were cloned, expressed and purified in addition to the full length UvrC (denoted UvrC-FL in the following figures) in order to determine the role of each domain in the incision reaction:

- UvrC- Δ HhH: contains both endonuclease domains, but is missing the double helix-hairpin-helix (HhH₂) region at the C-terminus.
- UvrC-N: corresponds to the N-terminal half of UvrC, containing the GIY-YIG endonuclease domain, the cysteine-rich region and the UvrB interaction domain.
- UvrC-C: corresponds to the C-terminal half of UvrC, containing the RNase H endonuclease domain and the HhH₂ region.
- UvrC-NEndo: contains only the N-terminal GIY-YIG endonuclease domain.

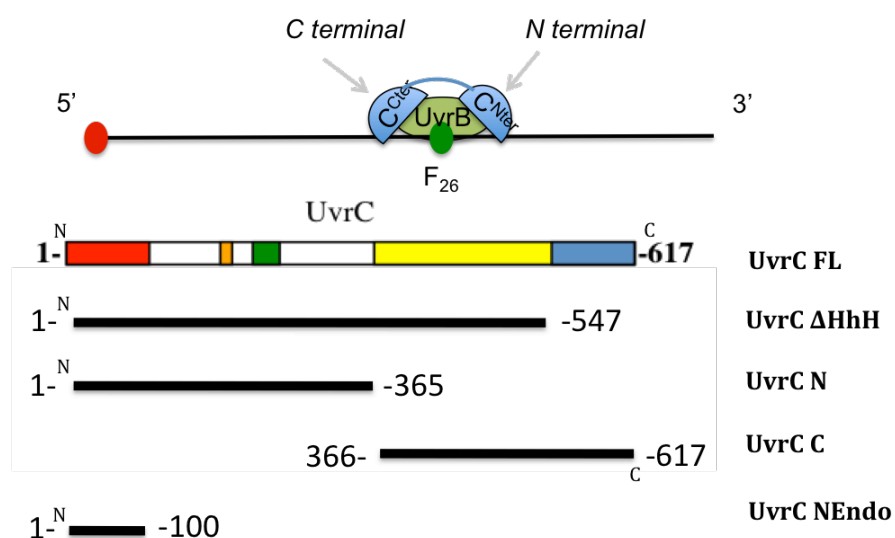


Figure 4.45: Schematic representation of the constructs of UvrC and the domains of UvrC responsible for the dual incision.

The UvrC-ΔHhH, UvrC-N and UvrC-C constructs of UvrC were available in the laboratory at the start of my PhD, while the UvrC-NEndo construct was cloned more recently. All four of these constructs were expressed in *E. coli* and purified with the help of Salvatore De Bonis, the laboratory technician. An SDS-PAGE gel of the purified UvrC fragments is presented in Figure 4.46.

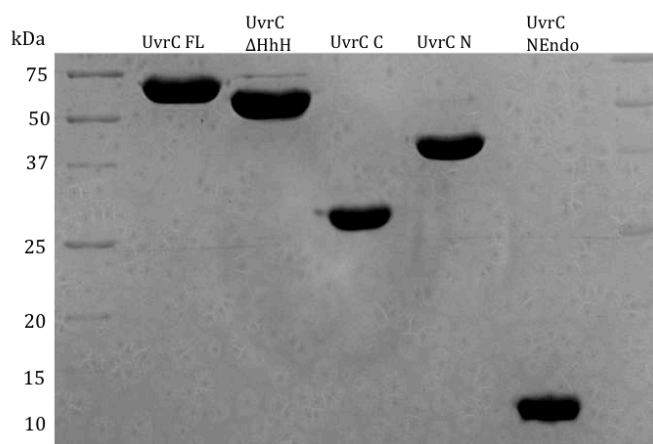


Figure 4.46: SDS-PAGE gel of the constructs of UvrC: UvrC-FL, UvrC-ΔHhH, UvrC-C, UvrC-N and UvrC-NEndo.

6.1.2. Activity of UvrC constructs and domains in the incision assay

The different UvrC constructs were used in the incision assay, alone and combined, along with UvrA1 and UvrB. Different combinations were tested: (i) the two complementary fragments, UvrC-N and UvrC-C, (ii) UvrC-NEndo and UvrC-C and (iii) UvrC-C and UvrC- Δ HhH. The 5'-red-50merF26-seq1 DNA substrate was used for these assays (Figure 4.47 and Figure 4.48). We first compared the activity of these constructs at a given timepoint (Figure 4.47), before monitoring the kinetics of repair by these different UvrC constructs to follow the repair efficiency, the order of the incisions and the accumulation of intermediate fragments (Figure 4.48).

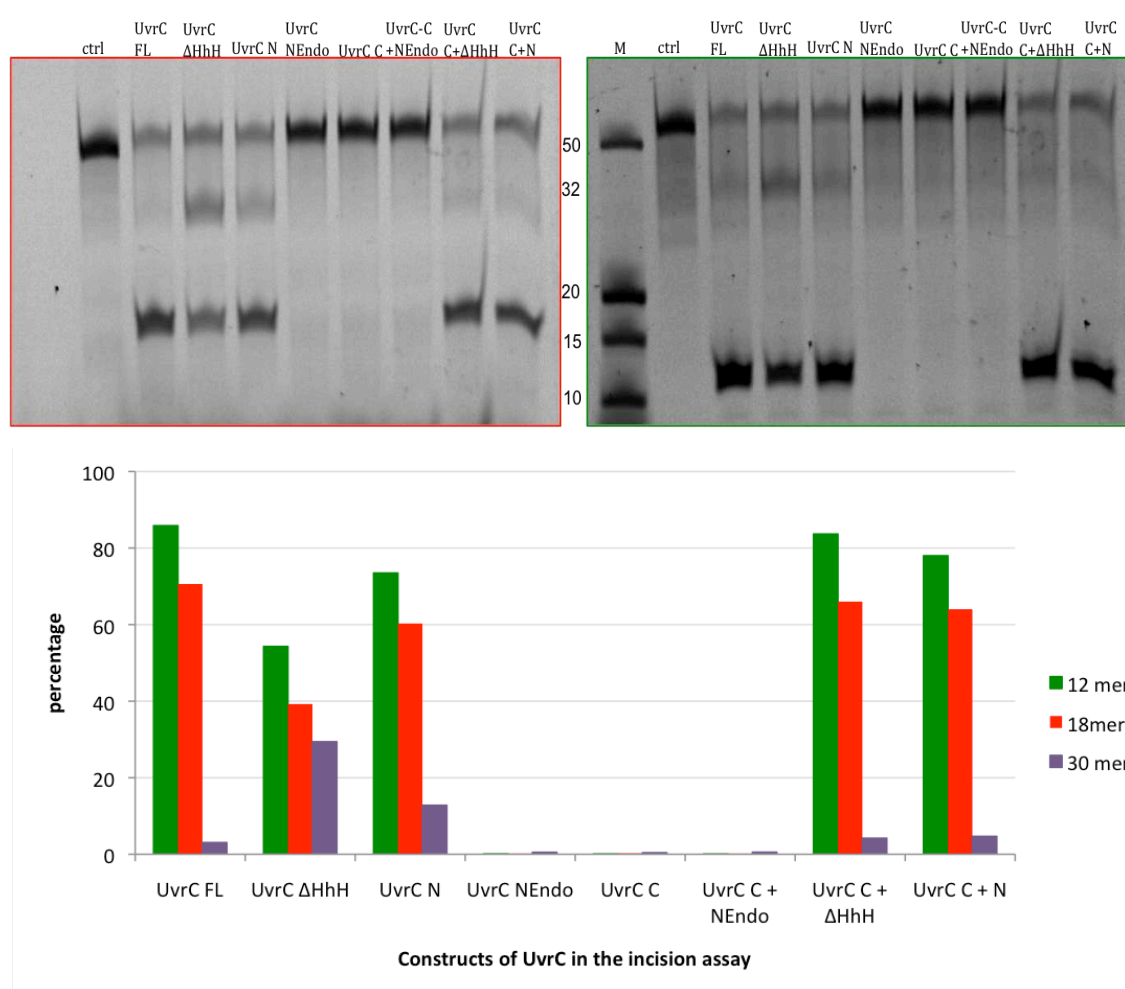
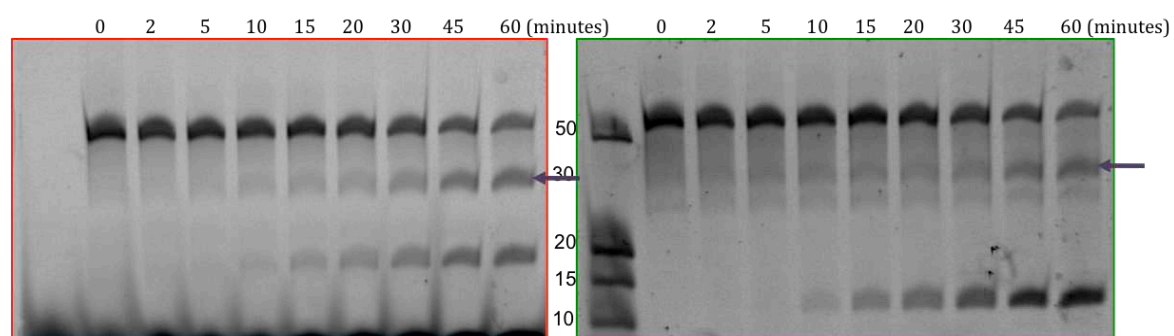


Figure 4.47: Urea polyacrylamide gel (top) visualised with the Alexa 647 and Fluorescein filters showing the incision assay with 25 nM 5'-red-50merF26-seq1, 1 μ M UvrA1, 0.5 μ M UvrB and 2 μ M of the constructs UvrC-FL, UvrC- Δ HhH, UvrC-N, UvrC-NEndo or UvrC-C alone and combined, and 2.5 mM Mg^{2+} and ATP. Incubation conditions: 37°C for 60 minutes. The graph (bottom) presents the percentage of 12 mer, 18 mer and 30 mer fragments released for each condition. The graph represents the mean of three replicates.

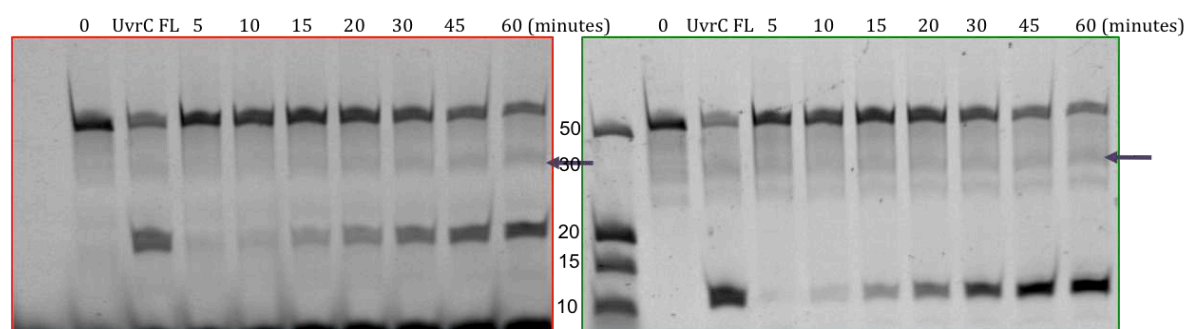
The incision assay with UvrC-FL showed a dual incision efficiency around 85% after 1 hour (Figure 4.47). When UvrC- Δ HhH was used on the same substrate, the incision efficiency dropped to 55% and an extra band of \pm 30 mer was produced that was visible with both Alexa 647 and fluorescein filters, indicating that this fragment carries both the ATTO633 and the fluorescein. This fragment corresponds to a 30 mer fragment from the 5' half of the oligonucleotide resulting from incision on the 3' side of the lesion as illustrated in Figure 4.1.B, and its level starts accumulating after 10 minutes to reach nearly 30% after 1 hour (Figure 4.47). This suggests that without its HhH₂ motif UvrC preferentially cuts the substrate on the 3' side of the lesion. The C-terminal RNase H domain thus appears to be less efficient in the absence of the HhH₂, which is believed to anchor UvrC to the DNA duplex. As a result, with UvrC- Δ HhH, incision on the 3' side is more efficient than on the 5' side of the lesion, which is inverted compared to what was observed in our sub-optimal UvrC-FL assay in which 5' incision was more efficient than 3' incision, leading to the accumulation of the 32 mer fragment (Figure 4.19.A) or optimal UvrC-FL assay in which the two incisions were almost simultaneous (Figure 4.19.B).

The isolated UvrC-NEndo and UvrC-C constructs showed no incision activity, and not surprisingly, when combined the incision activity was not restored (Figure 4.47). These isolated domains may be enzymatically inactive or may not be efficiently recruited to the pre-incision complex by UvrB. Protein-protein interaction studies performed by Salvatore De Bonis in the laboratory do indeed show that UvrC-NEndo and UvrC-C do not form a stable complex with UvrB, unlike UvrC-FL and UvrC- Δ HhH. Moreover, when UvrC- Δ HhH and UvrC-C were used together in the assay, the dual incision efficiency was increased to 83% and the amount of 30 mer was reduced (Figure 4.47, Figure 4.48.A, Figure 4.48.B). This suggests that when combined with UvrC- Δ HhH, UvrC-C is enzymatically active and helps to cut on the 5' side of the lesion to compensate for the reduced 5' incision activity of UvrC- Δ HhH. But these data should be treated with caution, because the RNase H endonuclease domain was present in both constructs and thus at higher molar concentration than in the assays containing either UvrC- Δ HhH or UvrC-C alone (Figure 4.48.A, Figure 4.48.B).

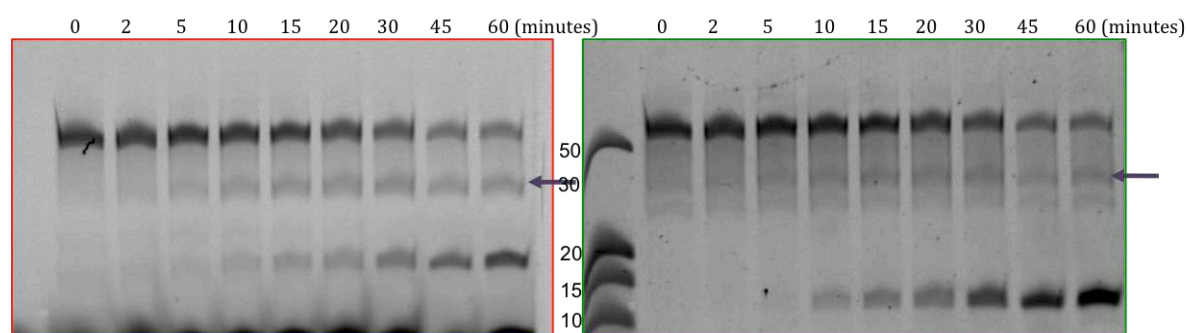
A) With UvrC- Δ HhH



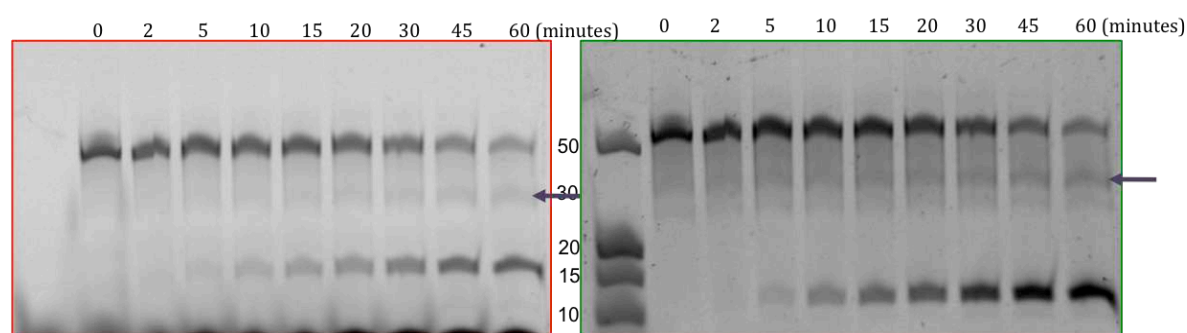
B) With UvrC- Δ HhH plus UvrC-C



C) With UvrC-N



D) With UvrC-N plus UvrC-C



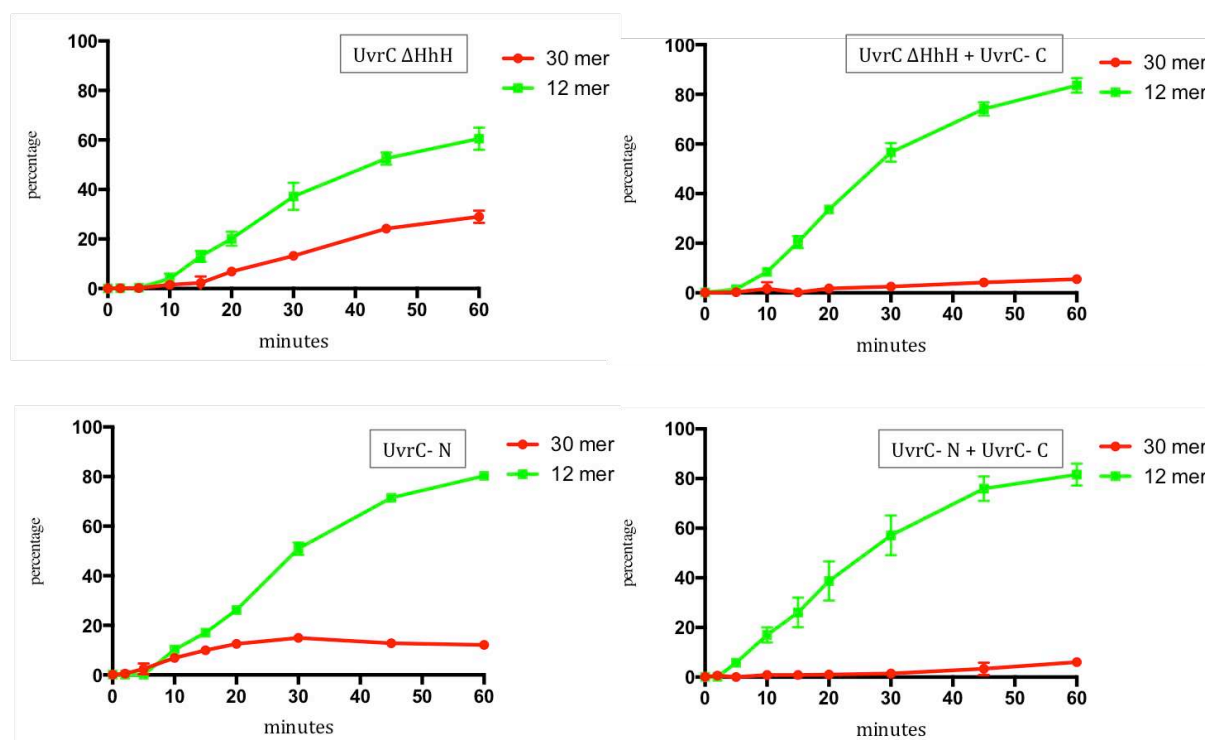


Figure 4.48: Kinetics of the incision assay with 25 nM 5' red-50merF26-seq1, 1 μ M UvrA1, 0.5 μ M UvrB and 2 μ M UvrC- Δ HhH (A), 2 μ M UvrC- Δ HhH plus 2 μ M UvrC-C (B), 2 μ M UvrC-N (C) and 2 μ M UvrC-N plus 2 μ M UvrC-C (D). The quantification of the 12 mer and the 30 mer are presented. The graphs represent the mean and standard deviation of three replicates.

In the incision assay with UvrC-N, the dual incision efficiency was close to 75% after 1 hour and the product corresponds to the same 12 mer fragment obtained with UvrC-FL, as confirmed by MALDI-TOF analysis (Figure 4.49). This result is surprising knowing that only one endonuclease domain is present, the N-terminal GIY-YIG domain. Accumulation of the 30 mer fragment was also observed, although this was to a lesser extent than with UvrC- Δ HhH (13% instead of 30%). The N-terminal endonuclease domain is thus able to cut on both the 3' and 5' sides of the lesion, but with a preference for the 3' incision reaction. When combining the two halves of UvrC, UvrC-C and UvrC-N, the amount of 30 mer fragment was significantly reduced and the production of the 12 mer fragment was around 80%, which is very close to the levels obtained with UvrC-FL (Figure 4.47). In fact, the timecourse experiments showed that the repair kinetics were very similar to those of UvrC-FL (Figure 4.48). The addition of UvrC-C thus minimised the appearance of the intermediate 30 mer fragment by contributing to 5' incision of the substrate (Figure 4.48.C, Figure 4.48.D).

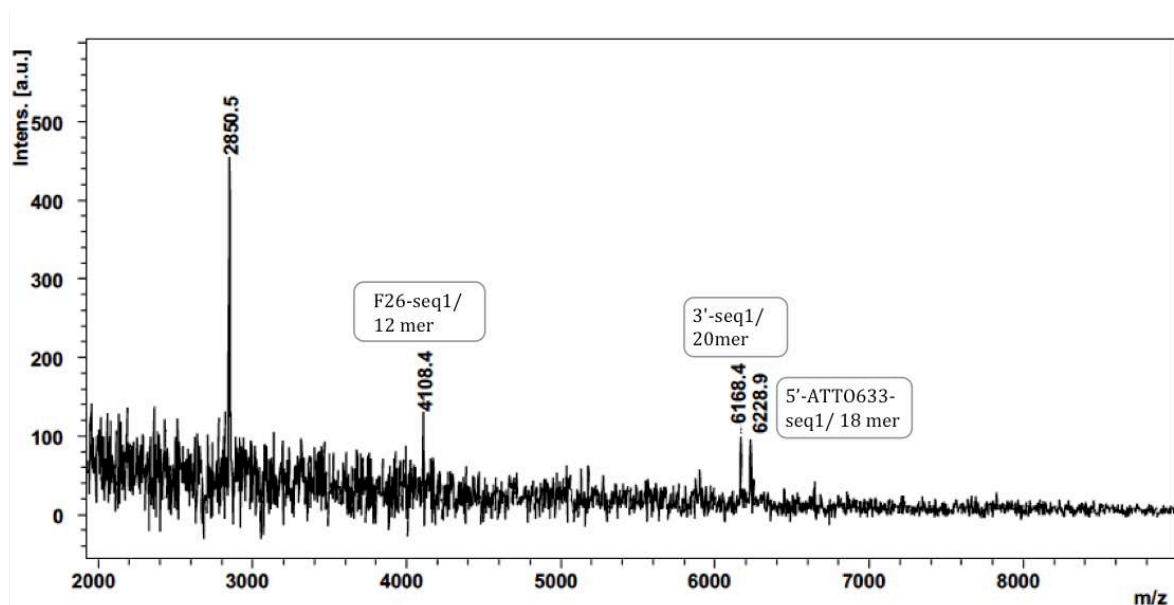


Figure 4.49: MALDI-TOF spectra of the incision reaction products. The reactions were performed on 5'-red-50merF26-seq1 DNA with 1 μ M UvrA1, 0.5 μ M UvrB and 2 μ M UvrC-N. The masses of the different fragments were identified and tagged.

6.2. Characterisation of UvrC mutants

6.2.1. Preparation of UvrC mutants

To better understand the exact role of each endonuclease domain of UvrC individually, we designed and prepared the following mutants to disrupt the catalytic activities of UvrC based on studies of UvrC homologues (Lin and Sancar, 1992; Truglio et al., 2005).

- UvrC-FL^{E72A} to inactivate the N-terminal GIY-YIG endonuclease domain in the full-length construct.
- UvrC-FL^{D391A} to inactivate the C-terminal RNase H endonuclease domain in the full-length construct.
- UvrC-N^{E72A} to inactivate the N-terminal GIY-YIG endonuclease domain in the construct corresponding to the N-terminal half of UvrC.
- UvrC-C^{D391A} to inactivate the C-terminal RNase H endonuclease domain in the construct corresponding to the C-terminal half of UvrC.

The mutants of UvrC were purified following the same protocols as for their wild-type counterparts and showed similar chromatographic profiles indicating that the mutations did not affect the integrity of the proteins (Figure 4.50).

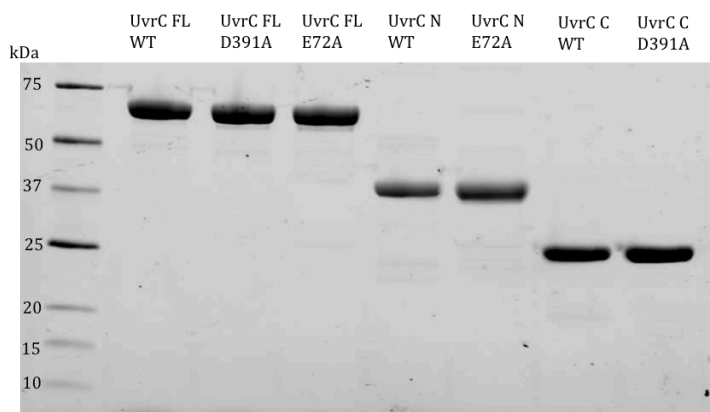


Figure 4.50: SDS-PAGE gel of the purified wild-type and mutant UvrC constructs.

6.2.2. Incision activity of UvrC mutants

The activity of these mutants was tested in the incision assay with 5' red-50merF26-seq1 as a substrate. UvrC-FL^{D391A} did not show any detectable activity after 1 hour, while for UvrC-FL^{E72A}, a very low amount of the 18 mer fragment (5%), resulting from incision on the 5' side of the lesion, was observed (Figure 4.51.A). This indicates that the C-terminal RNase H domain of UvrC-FL^{E72A} still displays some residual activity. We also tested UvrC-FL^{E72A} and UvrC-FL^{D391A} in the incision assay with 5' red-50merF26-seq2, and in that case no incision was observed (Figure 4.51.B), suggesting that the residual activity of the RNase H domain of UvrC-FL^{E72A} may be substrate dependent. Disrupting the catalytic activity of one or the other of the two endonuclease domains of UvrC is thus sufficient to abolish almost entirely the dual incision activity, which suggests that there is a tight coupling between the two activities.

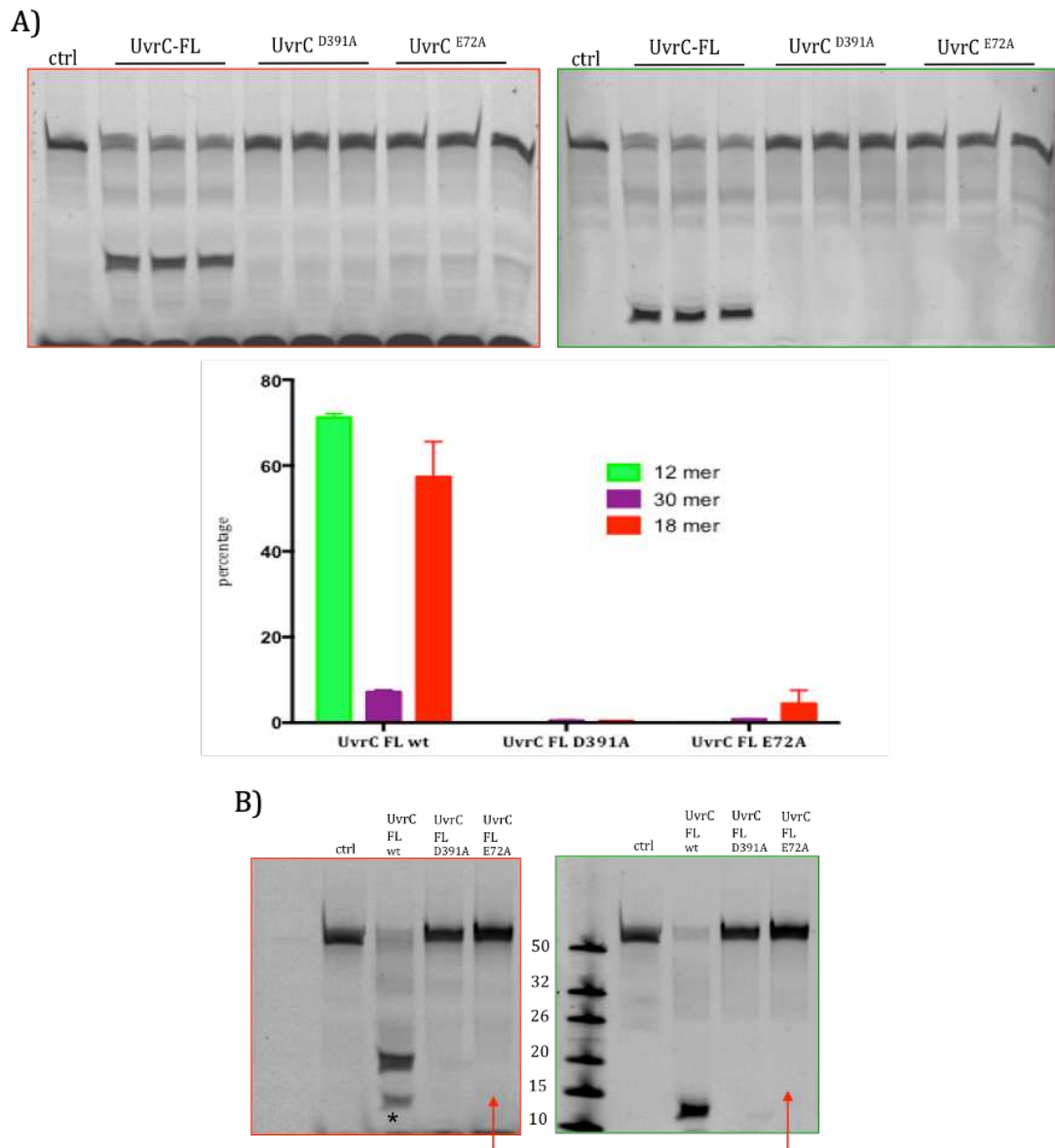


Figure 4.51: Incision assay with the FdT containing substrates, 1 μ M UvrA1, 0.5 μ M UvrB and 2 μ M of the constructs of UvrC and their mutants: 25 nM 5'-red-50merF26-seq1 (A) and 25 nM 5'-red-50merF26-seq2 (B). (A) The activity of the wild type and the mutants were compared via the amount of 12 mer, 18 mer and 30 mer fragments released during the repair. The graph represents the mean and standard deviation of three replicates. (B) The 18 mer fragment was not observed in the incision assay with UvrC-FL^{E72A} and 25 nM 5'-red-50merF26-seq2. (*) indicates the non-specific fragment observed during the incision assay with UvrC-FL and 25 nM 5'-red-50merF26-seq2. Incubation conditions: 37°C for 1h.

As with the wild-type UvrC-C, UvrC-C^{D391A} mutant alone did not perform any incision of the substrate. UvrC-N^{E72A} alone was also completely inactive with both 5' and 3' incisions being impaired (Figure 4.52). When combining UvrC-N^{E72A} with either the wild-type or

mutant UvrC- C^{D391A} , the incision activities were not restored and when combining wild-type UvrC-N with the UvrC- C^{D391A} mutant, the resulting activity was very similar to that obtained with wild-type UvrC-N alone (Figure 4.52). This confirms that the wild-type like activity of the combined UvrC-N and UvrC-C domains results from the catalytic activities of both constructs and not solely from UvrC-N activity.

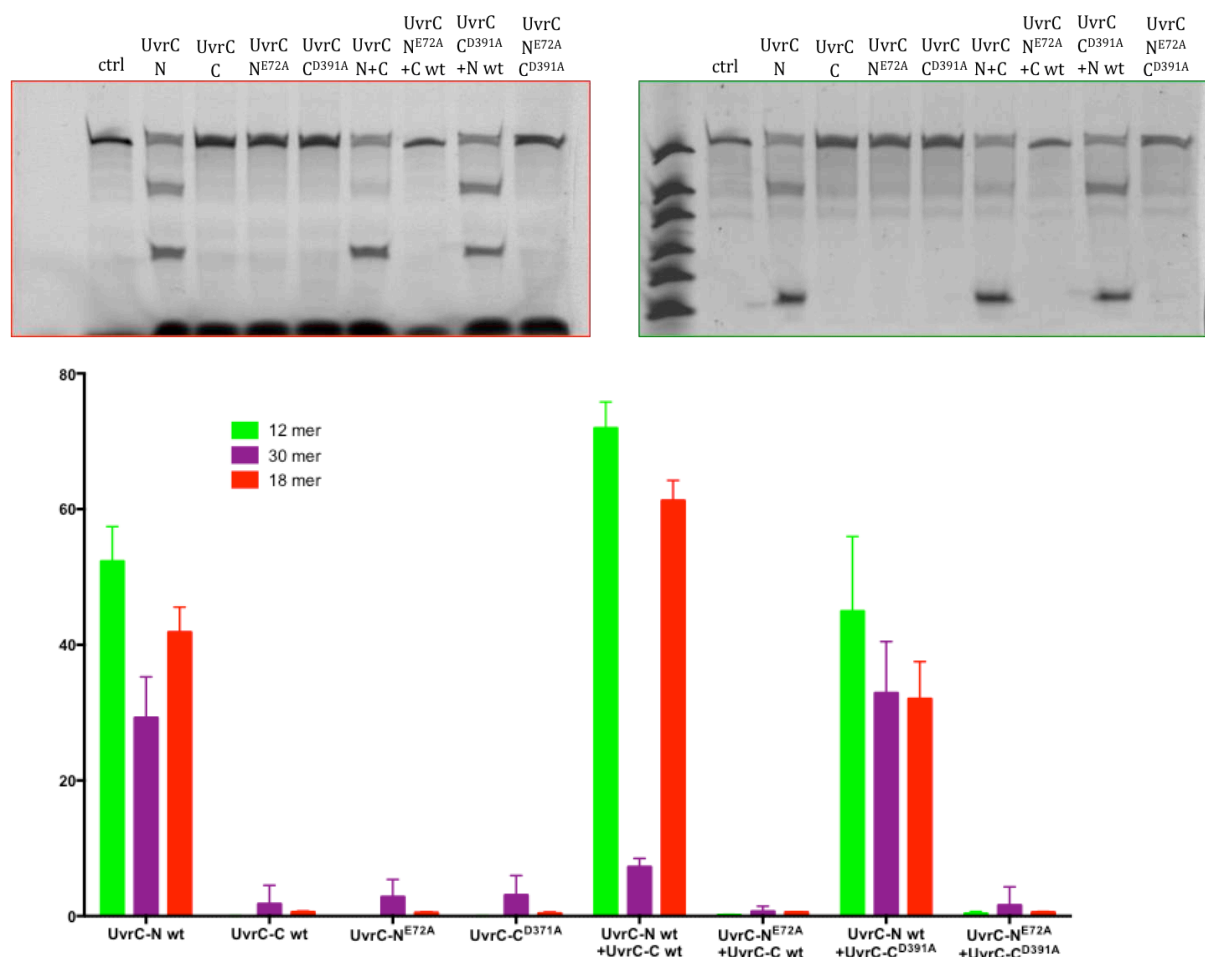


Figure 4.51: Incision assay with 25 nM 5'-red-50merF26-seq1, 1 μ M UvrA1, 0.5 μ M UvrB and 2 μ M of the constructs of UvrC fragments and their mutants. The activity of the wild type and the mutants are compared via the amount of 12 mer, 18 mer and 30 mer fragments released during the repair. The amount of 30 mer fragment detected for UvrC-C wt, UvrC-N^{E72A}, UvrC-C^{D391A}, UvrC-N^{E72A} + UvrC-C wt and UvrC-N^{E72A} + UvrC-C^{D391A} is assimilated to the background. Incubation conditions: 37°C for 1h. The graph represents the mean and standard deviation of three replicates.

Chapter II: Substrate specificity studies on plasmid DNA

The reconstitution of the nucleotide excision repair with the plasmid DNA was performed in parallel with the optimisation of the incision assay with the oligonucleotides. Hence, the set up described in the section “Optimized incision assay conditions” above was not applied from the start of this part. Also, the work involving HPLC MS/MS analyses of the repair activity of the UvrABC system on the various NER substrates is still ongoing. The advantage of using plasmid DNA is that different treatment could be applied in order to introduce different DNA lesions and thus study and compare their repair efficacy by NER. In addition, oligonucleotides containing these lesions are most of the time not commercially available.

1. Preparation of the various DNA substrates

1.1. Separation of the different states of the purified pUC19 plasmid

The plasmid pUC19 was purified from *E. coli* in its mostly negatively supercoiled state. The different states of the purified plasmid, supercoiled, nicked (or circular) and linear are shown in Figure 4.53. The supercoiled DNA migrates faster on the gel. Release of the tension in the strands caused by an incision on one strand for instance, as in the case of the repair by UvrABC, produces nicked plasmid that migrates as the slowest band on the gel. The linear form of the plasmid can be obtained when UvrABC repairs two DNA lesions in close vicinity to each other, but located on opposite strands, leading to double incision of the DNA duplex and the formation of double-strand breaks. The linear pUC19 migrates between the supercoiled band and the nicked band. On some gels, we found bands that migrate slower than the nicked pUC19. These most likely correspond to different relaxed topoisomers or higher molecular weight concatemers.

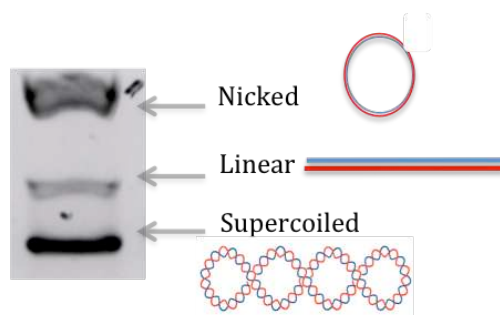


Figure 4.53: Different states of the plasmids observed by electrophoresis of plasmid DNA on a 1% TBE agarose gel.

The advantage of keeping pUC19 in a supercoiled state, before and after treatments, is that we can monitor the repair by UvrABC through the quantification of the different states of the plasmids by gel electrophoresis.

1.2. Plasmid treatments

Supercoiled pUC19 plasmid was treated with UV-C light, BPDE, cisplatin, KMnO_4 or riboflavin and sodium citrate-KCl to generate diverse lesions, including classical NER substrates such as UV-induced pyrimidine dimers, but also oxidized bases, which are usually repaired by the base excision repair pathway.

1.2.1. UV-C treatment

The irradiation with UV-C light was performed using three doses: 0.03 J/cm^2 , 0.15 J/cm^2 , and 0.3 J/cm^2 (Figure 3.47). UV-C light generates CPDs and 6-4PPs. While the first experiments were performed with UVC-pUC19 irradiated with 0.3 J/cm^2 , two lower doses were also used, because HPLC-MS/MS analysis showed the presence of Dewar lesions that are products of further irradiation of 6-4PPs in the DNA irradiated at 0.3 J/cm^2 . The plan was to generate sufficient lesions to visualize repair by agarose gel electrophoresis and by HPLC-MS/MS analysis, but not to over-expose the DNA to avoid the formation of adducts such as Dewar products.

Increasing the UV-C dose leads to the accumulation of increasing amounts of pyrimidine dimers (including both CPDs and 6-4PP) in pUC19 as measured by HPLC-MS/MS analysis. The quantification of the amount of lesions (in fmoles) and the amount of normal nucleotides (in fmoles), dG in this case, enable the determination of the number of lesions present in the plasmid. It showed that the 0.15 J/cm^2 dose of UV-C light generates ~ 40 thymine dimers per pUC19 (2689 bp) plasmid molecule. The plasmid remained in mostly a supercoiled state following the irradiations, although slower migrating bands most likely corresponding to nicked DNA appeared at 0.15 and 0.3 J/cm^2 (Figure 4.54).

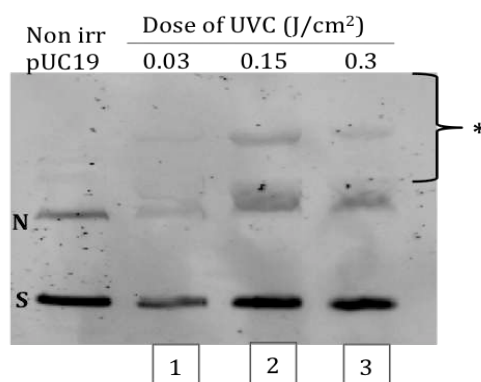


Figure 4.54: Agarose gel presenting the plasmid pUC19 following the irradiation with three doses of UV-C light 0.03 J/cm² (1), 0.15 J/cm² (2), and 0.3 J/cm² (3). S: Supercoiled, N: Nicked. (*: relaxed forms, or concatemers of pUC19).

These bands were observed in the irradiated pUC19 immediately after the treatment, but their intensity increased after storage of the DNA at 4°C (Figure 4.55). These samples containing these relaxed forms of pUC19 were used for the incision assays presented below. To minimise these bands, we tried to limit the presence of the relaxed form of pUC19 in the non-irradiated plasmid used for irradiation. For this, the purified plasmids were loaded on a 0.8% agarose gel and the supercoiled plasmid was isolated by extracting the band from the gel.

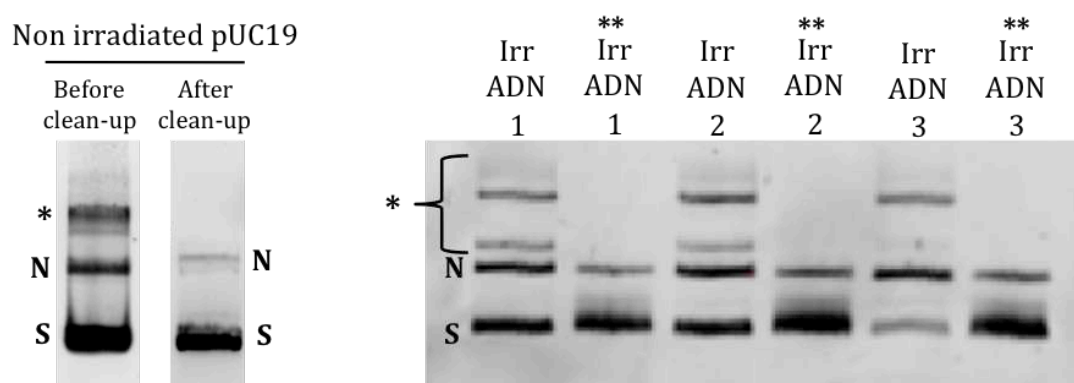


Figure 4.55 : Agarose gels presenting the plasmid pUC19 following its purification by maxiprep. Non-irradiated pUC19 (left), before and after the extraction and the purification of the supercoiled band. Right: The plasmid pUC19 is shown after irradiation with three doses of UV-C light 0.03 J/cm² (1), 0.15 J/cm² (2), and 0.3 J/cm² (3) before and after clean-up (**). S: Supercoiled, N: Nicked. (*: relaxed forms of pUC19, concatemers).

The supercoiled plasmid was then purified from the agarose gel and treated with the three doses of UV-C light. As shown on the gel, the irradiated plasmids resulting from this procedure did not present any of the bands after storage (Figure 4.55). After this, the plasmids were stored at -20°C in small aliquots.

1.2.2. BPDE treatment

The plasmid was treated with 150 μ M of BPDE, which introduced \sim 80 dGuo-BPDE lesions per pUC19 plasmid molecule as measured by HPLC-MS/MS analysis. The plasmid remained in a supercoiled state following the treatment as shown on Figure 4.56. We could notice the presence of the concatemers on this gel that were accentuated over time.

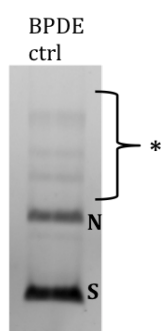


Figure 4.56: Agarose gel presenting the plasmid pUC19 following the treatment with 150 μ M BPDE. S: Supercoiled, N: Nicked. (*: relaxed forms of pUC19, concatemers).

1.2.3. Cisplatin treatment

The plasmid was incubated with 15 μ g of cisplatin. This treatment introduced \sim 70 CisPt GG adducts (covalent bonds with two guanines) per pUC19 plasmid molecule as measured by HPLC-MS/MS analysis. The treated plasmid remained in a supercoiled state as shown on Figure 4.57. Some more relaxed forms of pUC19 were also observed.

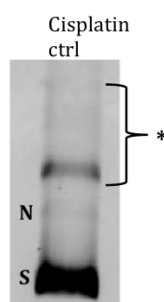


Figure 4.57: Agarose gel presenting the plasmid pUC19 following the treatment with 15 μ g of cisplatin. S: Supercoiled, N: Nicked. (*: relaxed forms of pUC19, concatemers)

1.2.4. KMnO_4 treatment

To introduce thymine glycols into plasmid DNA, we used KMnO_4 . With the initial protocol, the concentration used for the treatment was 0.4 M KMnO_4 , however, with such a concentration all the plasmid was relaxed when we analysed it by agarose gel electrophoresis (Figure 4.58). Therefore, we reduced the KMnO_4 to 0.08 M and 0.2 M to preserve the supercoiled state. These amounts of KMnO_4 did not relax the plasmid to the same extent. With 0.2 M KMnO_4 , ~130 lesions ThyGly were generated per plasmid molecule.

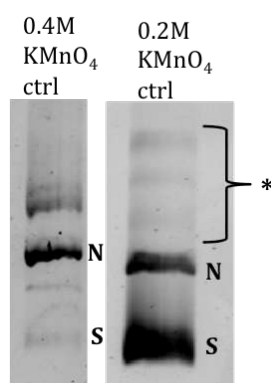


Figure 4.58: Agarose gel presenting the plasmid pUC19 following the treatment with 0.4 M and 0.2 M KMnO_4 . S: Supercoiled, N: Nicked. (*: relaxed forms of pUC19, concatemers).

1.2.5. Riboflavin treatment

The photosensitization of pUC19 with riboflavin created ~ 40 lesions 8-oxo-dG lesions. Following this treatment, we observed that 8-oxodG-containing pUC19 remained in a supercoiled state as shown on Figure 4.59. Some more relaxed forms of pUC19 were also observed.

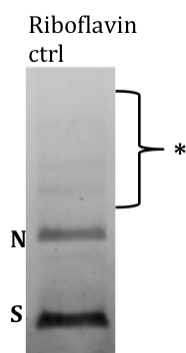


Figure 4.59: Agarose gel presenting the plasmid pUC19 following the treatment with Riboflavin. S: Supercoiled, N: Nicked. (*: relaxed forms of pUC19, concatemers).

1.2.6. Sodium citrate treatment

Sodium citrate treatment was used to introduce abasic sites into pUC19. According to the protocol, the generation of abasic sites requires 4 hours of incubation at 70°C. After 4 hours of incubation, however, we observed that the treated plasmids were almost completely relaxed (Figure 4.60). This is most likely caused by a high number of abasic sites introduced into the plasmid. Thus, we decided to reduce the incubation time and tested 1, 2, 3 and 4 hours of treatment. During this second trial, the plasmid remained supercoiled.

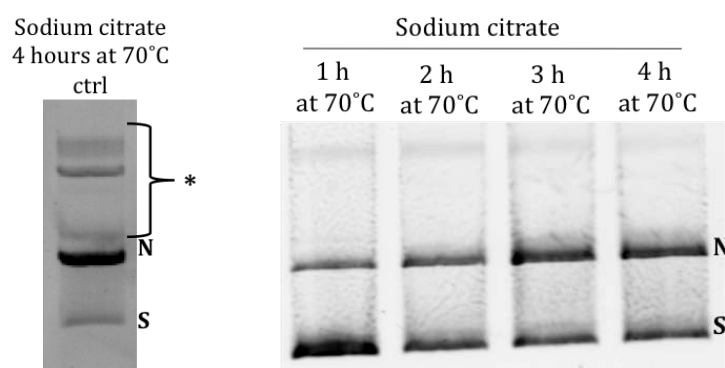


Figure 4.60: Agarose gel presenting the plasmid pUC19 following the treatment with 0.5 M sodium citrate for 4 hours at 70°C. The treatments were performed twice (first treatment on the left and second treatment on the right). During the second treatment, the pH of the sodium citrate and KCl were cautiously measured and maintained at 4.8 and 7.9 respectively. S: Supercoiled, N: Nicked. (*: relaxed forms of pUC19, concatemers).

2. Optimization of the incision assay using UV-C-irradiated plasmid DNA

2.1. Optimization of the experimental set-up using agarose gel electrophoresis

In the first experiments to adapt the UvrABC assay to plasmid DNA as a substrate, we performed the incision assay on the UV-C-treated pUC19 that was irradiated with 0.3 J/cm² of UV-C light and also with the non-treated pUC19 as a control. The aim was to make sure that the concentration of proteins used was not making any non-specific incisions on the control plasmid. Rare non-specific incisions of the plasmid by the UvrABC system may occur and relax the DNA, and untreated plasmid may also contain the occasional damaged base that could be processed by the Uvr proteins. It is important to note that the analysis

on agarose gel was a preliminary method to evaluate the UvrABC activity on pUC19 before performing a more in-depth analysis by HPLC-MS/MS.

When 40 ng of pUC19 were loaded on the agarose gel, we could clearly distinguish the bands for further analysis. This quantity corresponded to 24 nM of plasmid. We started by performing the incision assay using 2 μ M UvrA1, 0.5 μ M UvrB and 4 μ M UvrC, which produced both nicked and linear pUC19 and a marked reduction in the amount of supercoiled DNA after 1h as shown in Figure 4.61. For the control using the non-irradiated DNA, we also observed an increase of the amount of nicked plasmid and some linear pUC19 as well. The non-irradiated plasmid was thus clearly affected by these concentrations of protein.

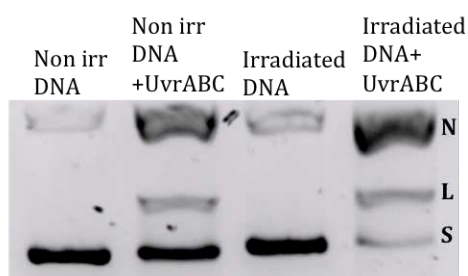


Figure 4.61: Agarose gels presenting the non-irradiated pUC19 and the UV-C (0.3 J/cm²) irradiated pUC19 (40 ng) alone and after the incubation with 2 μ M UvrA1, 0.5 μ M UvrB and 4 μ M UvrC for 1 hour at 37°C in buffer containing 10 mM Mg²⁺. The reaction was started with 4 mM ATP. The plasmid is mostly in a supercoiled state before and after irradiation. The first incision with UvrABC generates nicked DNA, then the repair of additional lesions results in linear plasmid. S: Supercoiled, L: Linear, N: Nicked.

We then tested lower amounts of the proteins, 1 μ M UvrA1, 0.1 μ M UvrB and 2 μ M UvrC, in the incision assay, alone or combined on 40 ng non-irradiated pUC19 and UV-C-irradiated pUC19 (Figure 4.62). From this gel, we observed that on non-irradiated pUC19, UvrA1 and UvrB did not have any affect, while 2 μ M UvrC alone could cause a partial relaxation of the plasmid. UvrA1 and UvrB together did not have any effect either, but when combined with UvrC they produced a little more relaxed DNA. However, we could clearly see a difference in the repair efficiency of the lesion-containing plasmid compared to the non-irradiated pUC19 when we used UvrA, UvrB and UvrC together during the assay. There was no supercoiled DNA left at the end of the reaction when all three Uvr

proteins were incubated with irradiated DNA. The nicked plasmids in the control may be due to the presence of some lesions in the plasmid prior to the treatment, which is normal.

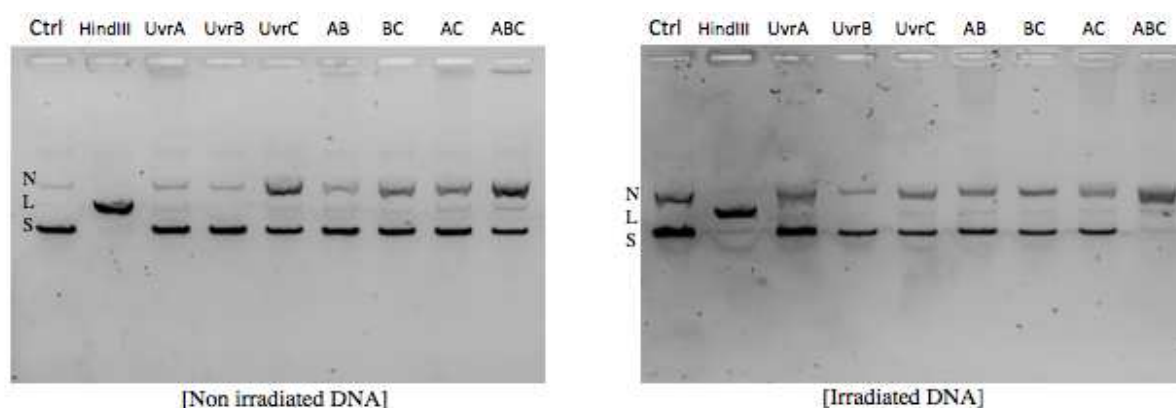


Figure 4.62: Different states of non-irradiated (left) and UV-C-irradiated (0.3 J/cm^2) (right) plasmids after the reaction with $1 \mu\text{M}$ UvrA1, $0.1 \mu\text{M}$ UvrB and/or $2 \mu\text{M}$ UvrC. In the incision assays, UvrA and UvrB alone do not seem to affect the plasmid. UvrC alone or combined with UvrA or UvrB seemed to have an effect on pUC19. Only UvrABC is able to perform a significant repair of the irradiated supercoiled plasmid. The buffer used contained 10 mM Mg^{2+} and the reaction was started with 4 mM ATP . The enzyme HindIII is used to digest the plasmid in order to linearise the DNA and have a control during the migration. The reaction was incubated for 30 minutes at 37°C . S: Supercoiled, L: Linear, N: Nicked.

Next, we tested five different amounts and ratios of the three Uvr proteins on control and UV-C-irradiated plasmid (Figure 4.63). In conditions 1 to 4, the non-irradiated DNA appeared to be affected. In condition 5 in which $0.1 \mu\text{M}$ UvrA1, $0.1 \mu\text{M}$ UvrB and $0.1 \mu\text{M}$ UvrC were incubated with 40 ng plasmid, the non-irradiated pUC19 was largely supercoiled with only a minimal amount of nicked DNA. For the irradiated plasmid, the DNA was completely relaxed in conditions 1 to 4 after 30 minutes. The condition 5 was not as efficient. For an incision of the entire supercoiled DNA, we had to incubate the reaction longer.

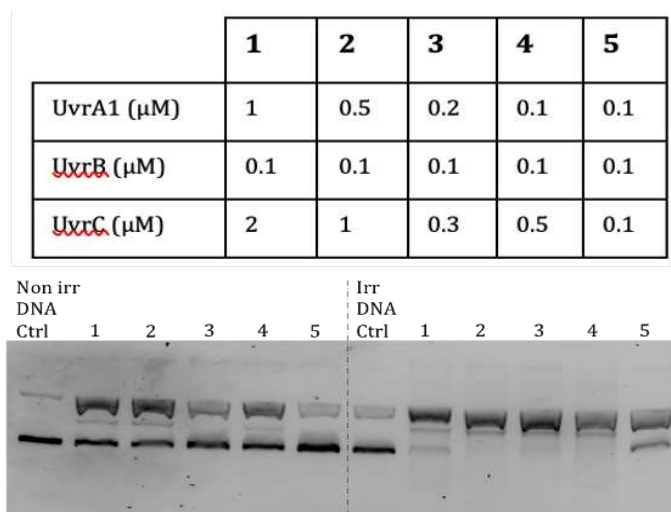


Figure 4.63: Different conditions were tested to assess their effect on the incision of non-irradiated and UV-C-irradiated (0.3 J/cm^2) pUC19 (40 ng). The buffer used contained 10 mM Mg^{2+} and the reactions were started with 4 mM ATP and incubated for 30 minutes at 37°C .

The difference between the conditions 4 and 5 was the concentration of UvrC; in both cases UvrA and UvrB were maintained at $0.1 \mu\text{M}$. So, next we performed the incision assay with $0.1 \mu\text{M}$ UvrA and UvrB and we tested the following concentrations of UvrC: $0.1 \mu\text{M}$, $0.3 \mu\text{M}$ and $0.5 \mu\text{M}$. The incision was performed with and without ATP and the activity of each concentration of UvrC was also assessed alone in the assay (Figure 4.64).

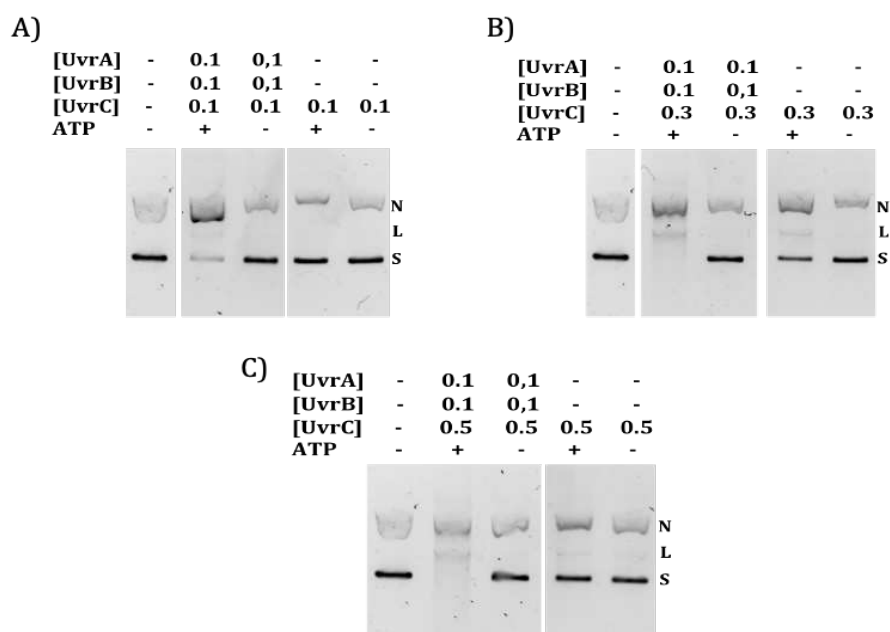


Figure 4.64: Incision assays performed with UV-C-irradiated (0.3 J/cm^2) pUC19 using $0.1 \mu\text{M}$ UvrA and $0.1 \mu\text{M}$ UvrB together with $0.1 \mu\text{M}$, $0.3 \mu\text{M}$ or $0.5 \mu\text{M}$ UvrC. The reaction was performed with or without 4 mM ATP. The concentrations of UvrC were also tested alone. The buffer used contained 10 mM Mg^{2+} . The reactions were incubated for 30 minutes at 37°C .

As expected, no repair was observed by UvrABC without ATP. In the incision assays using 0.3 and 0.5 μM UvrC, we noticed a more efficient repair and even some degradation of the DNA corresponding to the smearing in the wells. With 0.1 μM UvrC, we observed a relaxation of most of the supercoiled UV-C irradiated pUC19. This concentration of UvrC alone did not have any effect on the plasmid, whereas with 0.3 and 0.5 μM UvrC alone the amount of nicked DNA is increased and some linear DNA is also visible on the gel, suggesting that UvrC is cutting the DNA by itself. We used this concentration of 0.1 μM of UvrABC to monitor the kinetics of the repair.

2.2. Kinetics of repair of UV-C treated plasmid DNA

We observed during a timecourse experiment with 40 ng of control and UV-C-irradiated pUC19 and 0.1 μM UvrABC that this concentration of protein did not affect the non-irradiated DNA when the assay was performed at room temperature or 37°C (Figure 4.65). In this experiment, we could see the progressive decrease of the supercoiled band and appearance of nicked DNA resulting from the repair activity of UvrABC, and the accumulation of linear DNA with time. At room temperature, the reaction was slower, but after 3 hours only traces of supercoiled DNA were remaining. The reaction appears to continue throughout the three-hour incubation, suggesting that the proteins were stable for this long period.

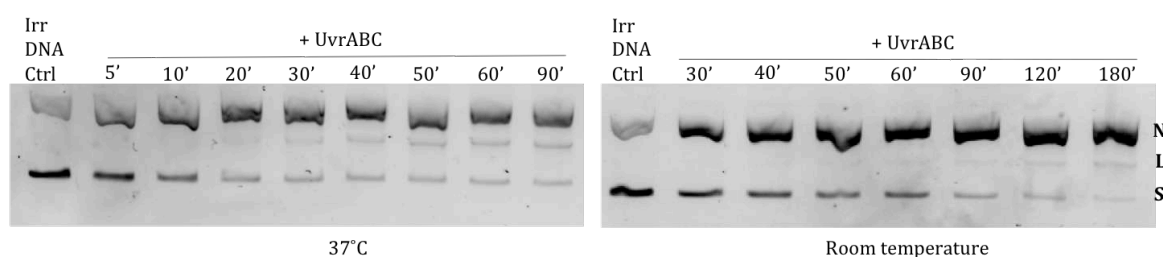


Figure 4.65: Kinetics of the incision assay with non-irradiated and UV-C-irradiated (0.3 J/cm²) pUC19. The concentration of UvrA, UvrB and UvrC was set to 0.1 μM . The buffer used contained 10 mM Mg²⁺. The reaction was started with 4 mM ATP and incubated at either 37°C (left) and at room temperature (right).

We then compared the repair kinetics of plasmid DNA irradiated with 0.03 J/cm² (1), 0.15 J/cm² (2) and 0.3 J/cm² (3) doses of UV-C light (Figure 4.66). The concentration of UvrA,

UvrB and UvrC were all maintained to 0.1 μM in these assays. On this gel, we noticed that the DNA substrate exhibited two extra bands, one above the nicked pUC19 possibly corresponding to concatemers and another below the supercoiled band, possibly corresponding to degraded DNA. Nonetheless, the activity of the UvrABC system could still be observed and assessed by evaluating the abundance of supercoiled, nicked and linear DNA. The two additional bands did not seem to be affected by the addition of UvrABC. With 0.03 J/cm² UV-C irradiation, there was some supercoiled plasmid left after 3 hours of repair by UvrABC at 37°C, while the plasmids irradiated with 0.15 J/cm² or 0.3 J/cm² were completely relaxed after 3 hours, and a significant fraction of linear DNA and some smearing were also observed after 90 min. With the increasing UV-C doses, there are more lesions to repair by the UvrABC in each plasmid molecule. Perhaps, a fraction of the plasmid irradiated with 0.03 J/cm² UV-C did not contain enough lesions and was therefore not processed, and in contrast in plasmids irradiated with 0.15 J/cm² or 0.3 J/cm² numerous lesions located in both strands of the DNA may have been repaired leading to linearization and then fragmentation of the plasmid DNA (corresponding to the smears).

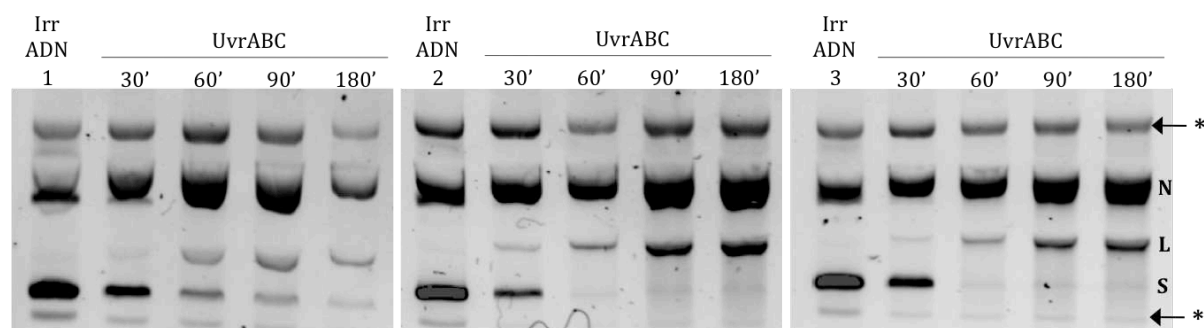


Figure 4.66: Kinetics of the incision assay with the pUC19 irradiated with 0.03 J/cm² (Irr DNA 1), 0.15 J/cm² (Irr DNA 2) and 0.3 J/cm² (Irr DNA 3). The concentration of proteins was 0.1 μM for UvrA, UvrB and UvrC. The buffer used contained 10 mM Mg²⁺ and the reaction was started with 4 mM ATP. Two extra bands indicated with stars were observed in these samples already in the starting substrate DNA. S: Supercoiled, L: Linear, N: Nicked. (*: relaxed forms of pUC19, concatemers or unknown bands).

At this point, we started to work with a new batch of proteins and as seen in the incision assay with the oligonucleotide described earlier (Figure 4.8 for example), the use of freshly purified proteins in the reaction affects the incision efficiency. Therefore, we tried

to use lower concentrations of Uvr proteins to minimise the smearing pattern seen on our gels. Timecourse experiments were performed using the plasmid irradiated with 0.15 J/cm² UV-C. These assays showed that the combinations 25 nM UvrA/UvrB/UvrC or 25 nM UvrA/UvrB with 50 nM UvrC led to efficient repair of pUC19 (Figure 4.67). In both cases, we observed that the supercoiled DNA had largely disappeared after 2 min of reaction.

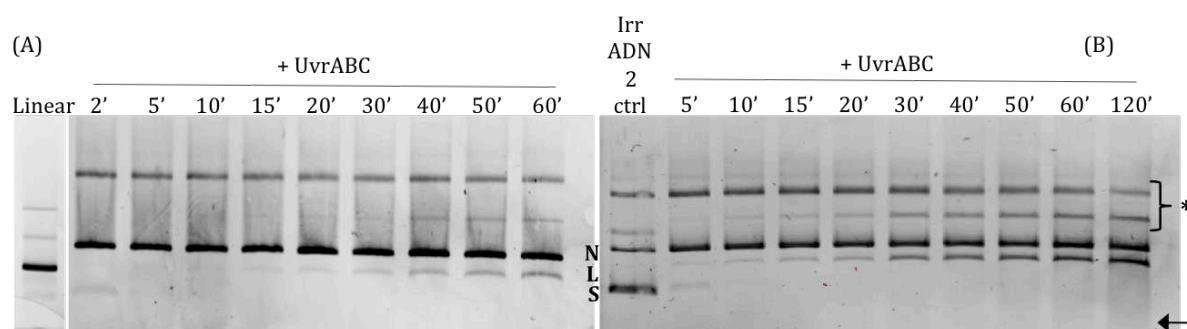


Figure 4.67: Kinetics of the incision assay with the pUC19 irradiated with 0.15 J/cm². The concentrations of proteins were 25 nM UvrA, 25 nM UvrB and 25 nM UvrC (A) and 25 nM UvrA, 25 nM UvrB and 50 nM UvrC (B). The buffer used contained 10 mM Mg²⁺ and the reaction was started with 4 mM ATP. The concatemers were observed on these samples. S: Supercoiled, L: Linear, N: Nicked. (*: relaxed forms of pUC19, concatemers).

3. Quantitative analysis of the repair efficiency by HPLC-MS/MS

Even though the analysis on agarose gel showed the repair of the lesions by the NER system, it was only a qualitative assessment and not a quantitative evaluation, since a single repair event was sufficient to relax the plasmid. Also, analysis on gels does not give any information about the nature of the lesion repaired by the system and whether the double incision to release the 12mer is complete.

The next step was therefore to determine the nature and abundance of the lesions introduced into the plasmid and repaired by the UvrABC system. Prior to the enzymatic digestion of the UvrABC treated DNA for HPLC MS/MS analysis, we introduced a step to separate the 12mer fragment containing the lesion released by the UvrABC system from the rest of the plasmid. For this purpose, a VectaSpin micro centrifuge tube filter with a 30K cut-off (Whatman) was tested using a 15mer oligonucleotide labelled with a fluorescein that we were able to monitor during the centrifugation. Thanks to its fluorescence, the separation was confirmed and this method was used to separate the

different fragments from the repair reaction (Figure 4.68). After the first experiments, the filters were replaced with Nanosep - 30k Omega filters (Pall-vwr) that were as effective.

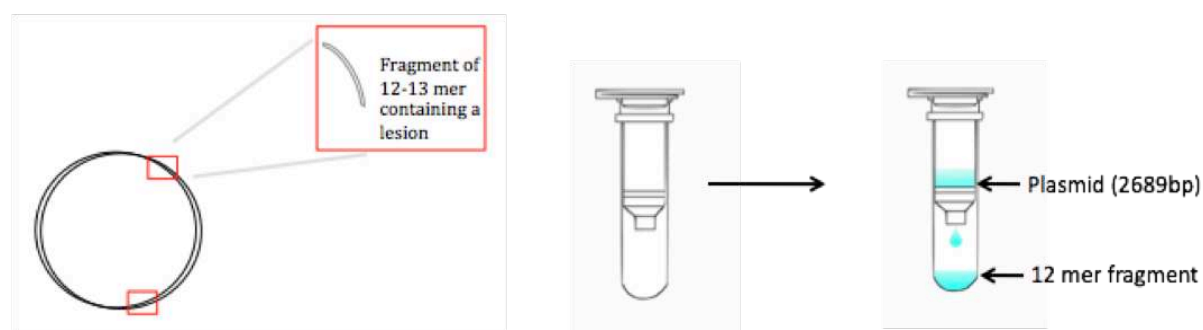


Figure 4.68: Scheme of the fragment resulting from the repair of the plasmid by UvrABC: After the incision reaction, two treatments can be applied prior to the separation on the filter: 1) The DNA can be precipitated with NaCl/EtOH then resuspended in water; 2) the samples can be diluted 10 times in water and heated at 95°C. The heating step denaturates the plasmid. The plasmid is separated from the 12 mer fragment containing the lesion using a membrane filter with a 30-kDa cut-off.

The first assays were performed using 120 ng pUC19 irradiated with 0.03 J/cm², 0.15 J/cm², or 0.3 J/cm² UV-C light incubated with 25 nM UvrA, 25 nM UvrB and 50 nM UvrC. After 2 hours of incubation at 37°C, the reactions were stopped and samples were analysed on agarose gel prior to HPLC-MS/MS analysis (Figure 4.69).

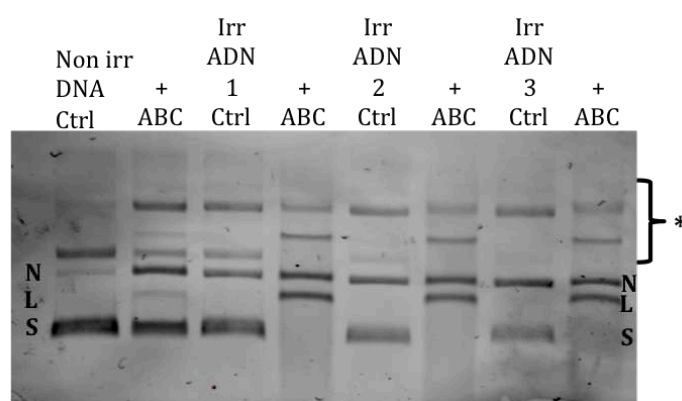


Figure 4.69: Analysis on gel of the reactions with pUC19 irradiated with 0.03 J/cm² (Irr DNA 1), 0.15 J/cm² (Irr DNA 2) and 0.3 J/cm² (Irr DNA 3) of UV-C light using 25 nM UvrA, 25 nM UvrB and 50 nM UvrC after 2 hours at 37°C. The buffer used contained 10 mM Mg²⁺ and the reaction was started with 4 mM ATP. S: Supercoiled, L: Linear, N: Nicked. (*: relaxed forms of pUC19, concatemers).

The non-irradiated plasmid in the presence of 25 nM UvrA, 25 nM UvrB and 50 nM UvrC showed a slight increase of the nicked plasmid and some linear plasmid. After 2 hours, the

plasmid irradiated with 0.03 J/cm² (Irr DNA 1), 0.15 J/cm² (Irr DNA 2) and 0.3 J/cm² (Irr DNA 3) were repaired by the UvrABC and some smearing was seen on the gel.

For HPLC-MS/MS analysis, we precipitated the plasmid DNA treated with UvrABC with NaCl/ethanol and we resuspended it in water before separating the released 12 mer fragment from the plasmid DNA. After the separation step, each fraction was digested into nucleosides as described in “Materials and Methods” prior to the analysis HPLC-MS/MS.

We can see in Figure 4.70 that pyrimidine dimers (CPDs and 6-4PP) are detected in the non-irradiated plasmid at very low levels. This can be due to the exposure of the plasmids to daylight during the experiments. As already mentioned, we noticed that the amounts of lesions in the plasmid used for the reactions increased with the UV-C dose. We can also see that UV-C irradiation generated approximately 4-5 times more CPD lesions than 6-4PPs, but the NER repaired preferentially the 6-4PP lesions, as seen by the extent of CPDs and 6-4PPs found in the 12 mer fractions. If the total amount of lesions in the plasmid following irradiation with UV-C light corresponds to the sum of the number of lesions detected in the plasmid and in the 12 mer fractions, the data presented in Figure 4.70 suggests that the UvrABC system repaired on average 18% Thymine-Thymine CPDs and 55% Thymine- Thymine-64PP. In this condition of repair, therefore, a majority of the lesions (82% TT-CPDs and 45% TT-64PP) are still in the plasmid. The concentration of UvrABC used might not have been sufficient to achieve complete repair. Unfortunately, a more in-depth analysis of this data could not be performed because several controls were missing, in particular the analysis of the plasmids prior to the repair by the UvrABC proteins.

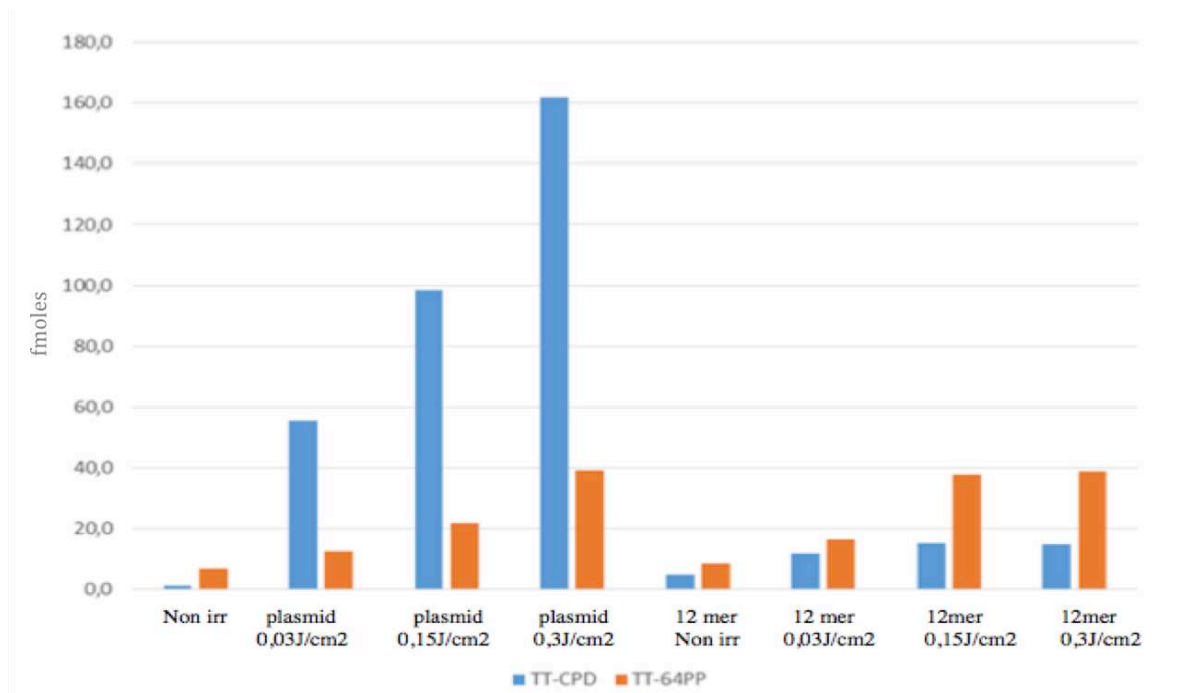


Figure 4.70: Quantification of UV-induced DNA lesions by HPLC MS/MS. The histogram presents the amount of TT-CPD (blue) and TT-64PP (orange) lesions present in the samples after the repair by UvrABC. The plasmids were irradiated with three doses of UV-C light 0.03 J/cm², 0.15 J/cm², and 0.3 J/cm². The reactions were performed with 120 ng of plasmid, 25 nM UvrA, 25 nM UvrB and 50 nM UvrC, incubated 2 hours at 37°C. The samples were then separated on a filter to separate the 12 mer fragment from the plasmid resulting from the repair. The label “plasmid” corresponds to the plasmid fraction separated on a filter from the fragment 12 mer following the repair.

We increased the concentration of proteins to 600 nM UvrA, 600 nM UvrB and 1200 nM UvrC and treated UV-C-irradiated plasmid. For the two doses of irradiation tested, we could see a decrease in the level of lesions present in the plasmid fraction after repair by UvrABC, but we could not detect any lesions in the 12 mer fraction, indicating that the 12 mer fragments may have been lost at some point (Figure 4.71). Unexpectedly, their detection was below the threshold of detection by the HPLC MS/MS. Since we had confirmed that we were able to separate and collect short DNA fragments with the membrane separation step, the loss of the 12 mer fragment here could be linked to the method used to stop the repair reaction.

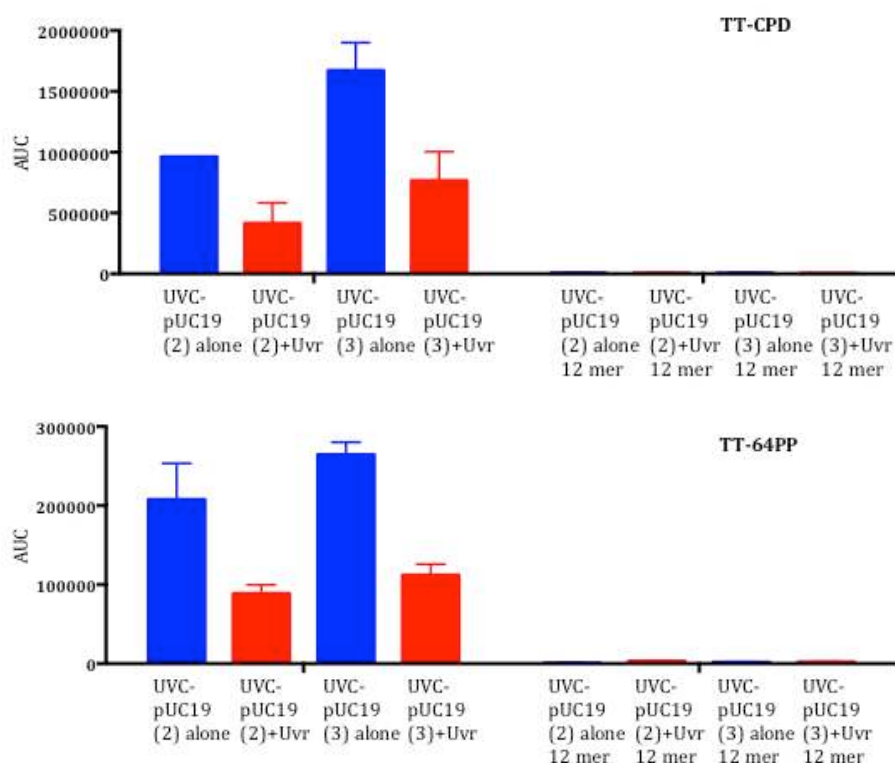


Figure 4.71: Quantification of UV-C induced lesions by HPLC MS/MS. The histogram presents the amounts of lesions, TT-CPD (above) and TT-64PP (below), present in the samples before (blue) and after (red) the repair by UvrABC. The plasmids were irradiated with two doses of UVC light 0.15 J/cm² (condition 2) and 0.3 J/cm² (condition 3). The reactions were performed with 120 ng of plasmid 600 nM UvrA, 600 nM UvrB and 1200 nM UvrC, incubated for 2 hours at 37°C. The buffer used contained 10 mM Mg²⁺ and the reactions were started with 4 mM ATP. The plasmids incubated with the Uvr proteins had been separated from the 12 mer fragments resulting from the repair on a filter prior to HPLC-MS/MS analysis. All reactions were performed in triplicates. Due to the absence of the standards during the analysis, presented data are the areas under the curves (AUC) and correspond to the mean with error bars corresponding to the standard deviation.

In an attempt to improve the amount of repaired lesion detected during the HPLC MS/MS analysis, we modified the processing step after repair by the UvrABC system and before the separation of the plasmid and the 12 mer fragment on filter. Instead of precipitating the DNA at the end of the incision reactions, we simply stopped the reactions by placing the samples on ice. Prior to the separation step, we diluted the sample 10 times with water and denatured the samples by heating them at 95°C. We hoped that by removing the precipitation step, we could recover a maximal amount of the 12 mer fragments. However, this was not the case. We noticed a decrease of the level of lesions present in the plasmid

fraction after repair by UvrABC. The repair seemed to be better with the increased concentration of UvrABC proteins. Unfortunately, we could not detect the 12 mer fragment. Also, the amounts of lesions detected for this experiment were surprisingly low compared to the data collected previously (Figure 4.72).

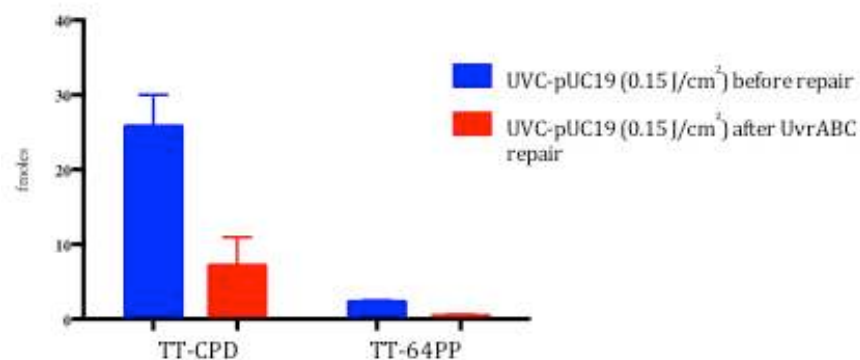


Figure 4.72: Quantification of UV-C-induced lesions by with HPLC MS/MS. Histograms illustrate the amount of lesions, TT-CPD (right) and TT-64PP (left), present in the plasmid fractions before (blue) and after (red) repair by UvrABC. The plasmids were irradiated with 0.15 J/cm² UVC light. The reactions were performed with 120 ng of plasmid 1 μ M UvrA1, 0.5 μ M UvrB and 2 μ M UvrC, incubated for 2 hours at 37°C. The buffer used contained 2.5 mM Mg²⁺ and the reaction was started with 4 mM ATP. The plasmids incubated with the Uvr proteins had been separated from the 12 mer fragments resulting from the repair on a filter prior to HPLC MS/MS analysis. All reactions were performed in triplicates and presented data correspond to the mean with error bars corresponding to the standard deviation.

In addition, we noticed that in some experiments, the abundance of lesions was below the threshold of detection. So, instead of using 120 ng, we increased the amount of substrate DNA to 360 ng UV-C-pUC19. We kept the concentrations of proteins to 1 μ M UvrA1, 0.5 μ M UvrB and 2 μ M UvrC. With these concentrations of proteins, we were sure that the repair of the different substrates would be performed effectively (Figure 4.72).

In the same conditions of repair, we also analysed the repair of calf thymus genomic DNA, instead of supercoiled pUC19 plasmid DNA, irradiated with 0.15 J/cm² of UV-C light and we could also visualise the repair of TT-CPD and TT-64PP lesions in this type of DNA sample (Figure 4.73). The efficiency of repair was good, with almost 75% of CPD lesions being removed from the plasmid. However, once again, the 12 mer fragments were not recovered and no lesions were detected in these fractions.

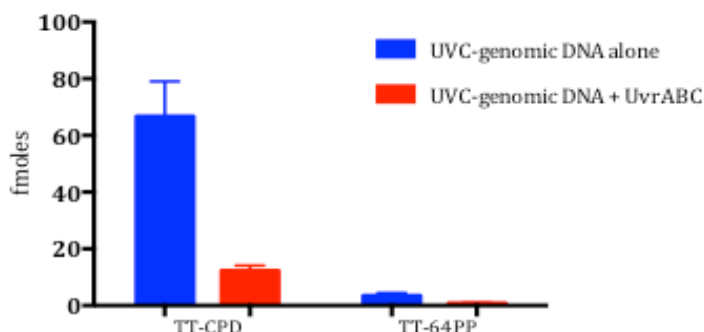


Figure 4.73: Quantification of UV-C-induced lesions by HPLC MS/MS. Histograms illustrate the amount of TT-CPD (right) and TT-64PP (left) lesions present in the samples before (blue) and after (red) repair by UvrABC. The calf thymus DNA was irradiated 0.15 J/cm² UVC light. The reactions were performed with 1 μ M UvrA1, 0.5 μ M UvrB and 2 μ M UvrC and incubated for 2 hours at 37°C. The buffer used contained 2.5 mM Mg²⁺ and the reactions were started with 4 mM ATP. All reactions were performed in triplicates and presented data correspond to the mean with error bars corresponding to the standard deviation.

4. Analysis of the substrate specificity of *D. radiodurans* NER

4.1. Repair of BPDE-conjugated DNA

Different concentrations of UvrABC were tested on the plasmid treated with BPDE (Figure 4.74). With the conditions 1-5, most of the supercoiled plasmid was incised into nicked DNA. After 30 minutes, the condition 2 with 100 nM UvrA, 100 nM UvrB and 500 nM UvrC was the most effective for the repair. The other conditions were less effective: we could only notice an increased amount of relaxed plasmid compared to the control well but the supercoiled plasmid was not completely processed and there was no linearization of the plasmid. In conditions 7-10, containing 25 or 50 nM UvrABC, that repaired the UV-C irradiated plasmid efficiently (Fig. 4. 67), only a small fraction of the DNA appeared to be processed. The amount of nicked BPDE-pUC19 was slightly increased compared to that of the control plasmid, but most of the supercoiled BPDE-pUC19 was still remaining. The kinetics of the reaction with 100 nM UvrA, 100 nM UvrB and 500 nM UvrC was analysed. We could see the rapid conversion of supercoiled BPDE-pUC19 into nicked plasmid starting already at the 2 min time point and we also observed the accumulation of linear

plasmid at 10, 15 and 30 minutes. BPDE adducts are thus efficiently repaired by the UvrABC system.

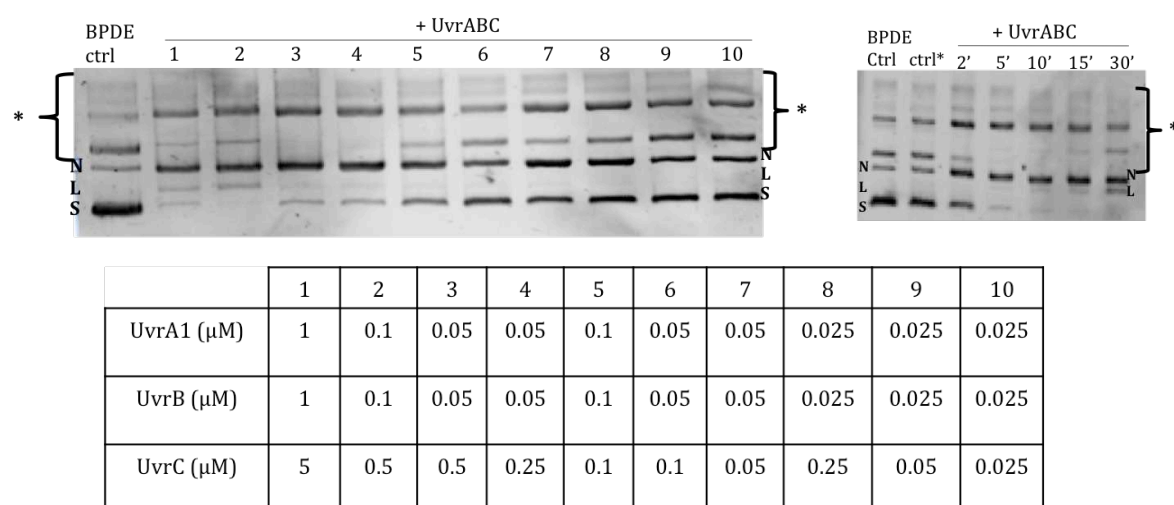


Figure 4.74: Left: Agarose gel electrophoresis analysis of incision assays performed with pUC19 treated with BPDE using different combinations of UvrABC (table below the gels). The incubation time was 30 minutes at 37°C. Right: The condition 2 was used to perform a time course of the reaction. The buffer used contained 10 mM Mg^{2+} and the reaction was started with 4 mM ATP. S: Supercoiled, L: Linear, N: Nicked. (*: relaxed forms of pUC19, concatemers).

HPLC MS/MS data have not yet been collected with this BPDE substrate.

4.2. Repair of cisplatin-treated plasmid DNA

For the cisplatin-treated plasmid DNA, four conditions with different concentrations of UvrABC were tested. It is important to note that during this experiment, 2.5 mM Mg^{2+} were used in the reaction buffer instead of the 10 mM Mg^{2+} used so far in the plasmid-based assays. With the oligonucleotide, using 2.5 instead of 10 mM Mg^{2+} increased the amount of 12 mer repaired in the 5'red-50merF26-seq1 (Figure 4.16.A). In the unprocessed plasmid treated with cisplatin, we observed that there were already some nicked and linear forms of the plasmid.

We noticed that with 25 nM UvrA, 25 nM UvrB and 50 nM UvrC (Condition 4) the repair of cisplatin-treated plasmid was not effective (Figure 4.75). The condition 3 showed some repair; the amount of linear plasmid increased. The condition 1 was the concentration of UvrABC used for the oligonucleotides. As for the condition 2, we observed a complete

linearization of the supercoiled and nicked plasmid. The condition 1 was thus chosen for further analysis by HPLC MS/ MS analysis.

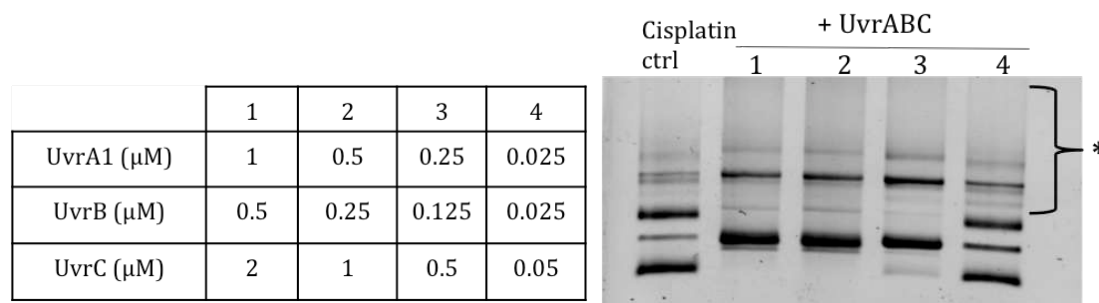


Figure 4.75: Right: Agarose gel electrophoresis analysis of incision assays performed with pUC19 treated with cisplatin using different combinations of UvrABC (table on left). The incubation time was 30 minutes at 37°C. The buffer used contained 2.5 mM Mg^{2+} and the reactions were started with 4 mM ATP. S: Supercoiled, L: Linear, N: Nicked. (*: relaxed forms of pUC19, concatemers).

From the HPLC MS/MS analysis (Figure 4.76), we can see that after the repair by UvrABC, the plasmid fraction contains only 100 of the 600 fmoles of CisPt-GG lesions detected in the starting substrate, suggesting that 85% of the CisPt-GG adducts have been processed by the UvrABC system. However, only a small proportion of the released 12 mer fragments containing the lesion were recovered.

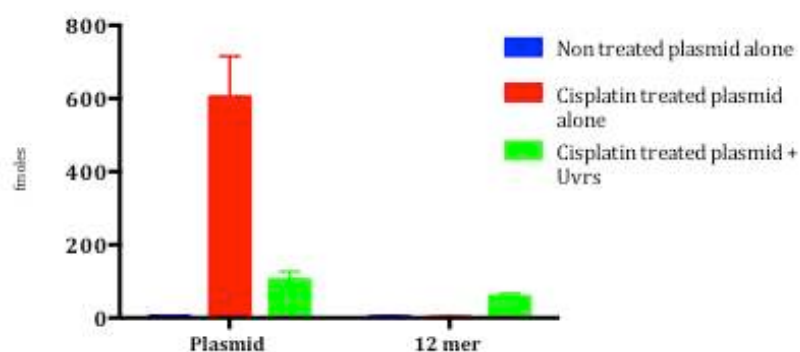


Figure 4.76: Quantification of cisplatin-induced lesions by HPLC MS/MS. Histograms illustrate the amount of CisPt-GG adducts present in the samples before (red) and after (green) repair by UvrABC. The reactions were performed with 120 ng of plasmid 1 μM UvrA1, 0.5 μM UvrB and 2 μM UvrC, incubated for 2 hours at 37°C. The buffer used contained 2.5 mM Mg^{2+} and the reactions were started with 4 mM ATP. The plasmids incubated with the Uvr proteins had been separated from the 12 mer fragments resulting from the repair on a filter. The data corresponding to the plasmid fraction is shown on the left, while the 12 mer fraction is shown on the right. All reactions were performed in triplicates and presented data correspond to the mean with error bars corresponding to the standard deviation.

4.3. Repair of plasmid DNA containing BER substrates (oxidized bases or abasic sites)

4.3.1. Thymine Glycols

Figure 4.77 shows the processing of thymine-glycol (TG) containing plasmid by four concentrations of the UvrABC system. With 25 nM UvrA, 25 nM UvrB and 50 nM UvrC (Condition 4), repair of TG was not effective. With the conditions 1, 2 and 3, there was no supercoiled plasmid remaining, and we noticed the presence of nicked and linear plasmid on the gels.

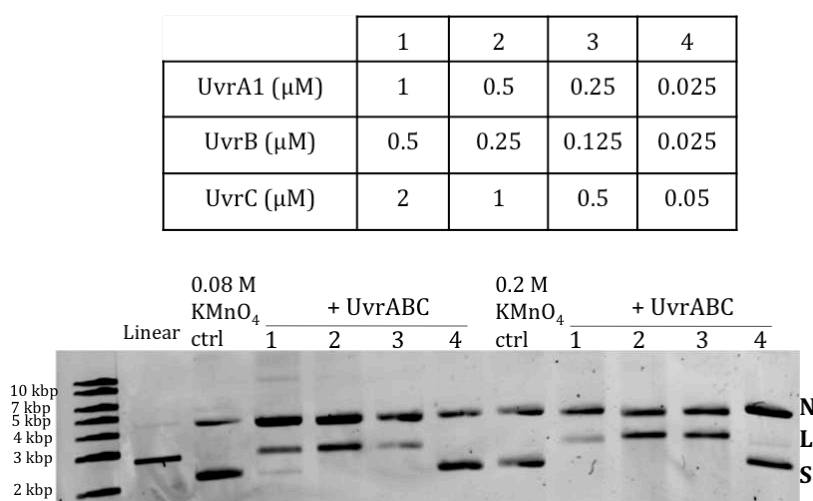


Figure 4.77: Agarose gel electrophoresis analysis of incision assays performed with TG-containing pUC19 using different combinations of UvrABC (presented in the table). The plasmids were treated with either 0.08 M or 0.2 M KMnO_4 . The incision reactions were performed with 120 ng incubated for 2 hours at 37°C with different amounts of UvrABC. The buffer used contained 2.5 mM Mg^{2+} and the reactions were started with 4 mM ATP. S: Supercoiled, L: Linear, N: Nicked.

Condition 1 containing 1 μ M UvrA1, 0.5 μ M UvrB and 2 μ M UvrC was used for further HPLC MS/MS analysis (Figure 4.78).

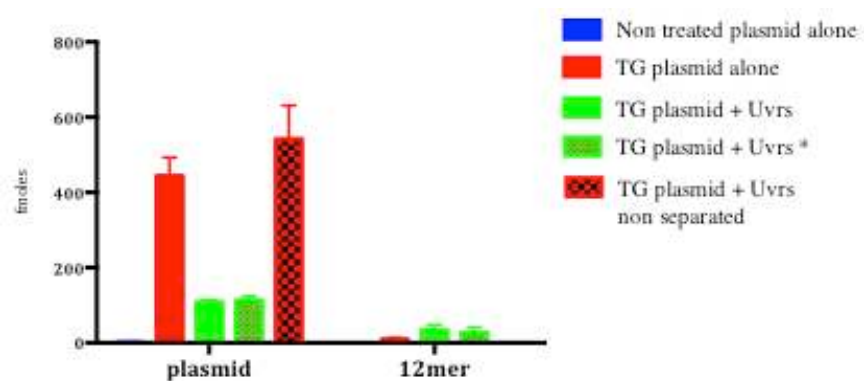


Figure 4.78: Quantification of TG lesions by HPLC MS/MS. Histograms illustrate the amount of TGs present in the samples before (red- solid color) and after the repair by UvrABC. The reactions were performed with 120 ng of plasmid 1 μ M UvrA1, 0.5 μ M UvrB and 2 μ M UvrC, incubated for 2 hours at 37°C. The buffer used contained 2.5 mM Mg^{2+} and the reaction was started with 4 mM ATP. For “TG plasmid + Uvrs” (green-solid colour), the reaction was stopped by putting the tube on ice, and for “TG plasmid + Uvrs*” (green- with pattern), the reaction was stopped by precipitating the DNA. These two plasmid samples were then separated from the 12 mer fragments on a filter, whereas the “TG plasmid + Uvrs non separated” sample (red- with pattern) was not separated on the filter. The data corresponding to the plasmid fraction is shown on the left, while the 12 mer fraction is shown on the right. All reactions were performed in triplicates and presented data correspond to the mean with error bars corresponding to the standard deviation.

The samples “TG plasmid + Uvrs” (green-solid colour) and “TG plasmid + Uvrs*” (green-with pattern) were analysed to compare the methods used to stop the incision reactions and see if they affect the collection of the 12 mer. We can see that both methods gave the same results, indicating that this step does not affect the recovery of the 12 mer fragments. In both cases, we observe efficient processing of TG lesions by the UvrABC system, even though as before, we do not manage to fully recover the released lesions in the 12 mer fraction. In this experiment, we additionally prepared a sample that was processed with the UvrABC system, but was not separated on the filter (red- with pattern). In this sample, we see that the total amount of TG lesions is very similar to that found in the starting substrate, as expected. This indicates that the separation method on filter is functional, but that the 12 mer fragments must be lost at a subsequent step.

4.3.2. Abasic sites

Abasic sites were generated in pUC19 plasmid by either 2-, 3- or 4-hour treatments with sodium citrate. These different substrates were then processed by four different concentrations of UvrABC. Most, but not all, of the supercoiled abasic-site containing plasmid was processed using conditions 1, 2 and 3, while condition 4 was not effective for repair (Figure 4.79). After 4 hours of treatment with sodium citrate, the supercoiled plasmid was completely nicked or linearized. Abasic sites thus appear to be efficiently repaired by the UvrABC system.

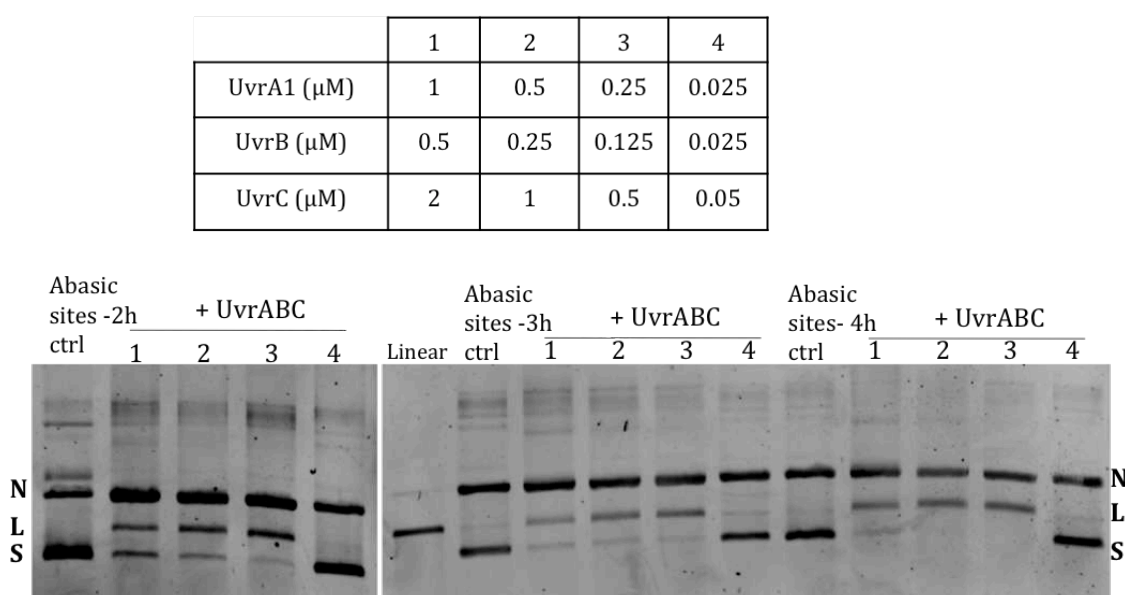


Figure 4.79: Agarose gel electrophoresis analysis of incision assays performed with abasic site-containing pUC19 using four combinations of UvrABC (presented in the table). Incision assays were performed with pUC19 treated with sodium citrate for 2 (left), 3 (middle) or 4h (right). The incubation time was 30 minutes at 37°C. The buffer used contained 2.5 mM Mg²⁺ and the reactions were started with 4 mM ATP. S: Supercoiled, L: Linear, N: Nicked.

HPLC MS/MS data have so far not been collected on this substrate since it is very difficult to measure an abasic site by HPLC-MS/MS (detection of a missing base).

4.3.3. 8-oxodG

Next, we tested the UvrABC repair activity on 8oxodGuo containing pUC19 plasmid. As above, four concentrations of UvrABC were evaluated (Figure 4.80). The condition 4 was not effective for the repair of 8-oxodG lesions, while with conditions 1, 2 and 3, most of the supercoiled plasmid was processed, and the abundance of nicked and linear plasmid were enhanced. The UvrABC's repair efficiency on this substrate thus seems to be lower than with previously tested substrates.

| | 1 | 2 | 3 | 4 |
|-------------------------|-----|------|-------|-------|
| UvrA1 (μM) | 1 | 0.5 | 0.25 | 0.025 |
| UvrB (μM) | 0.5 | 0.25 | 0.125 | 0.025 |
| UvrC (μM) | 2 | 1 | 0.5 | 0.05 |

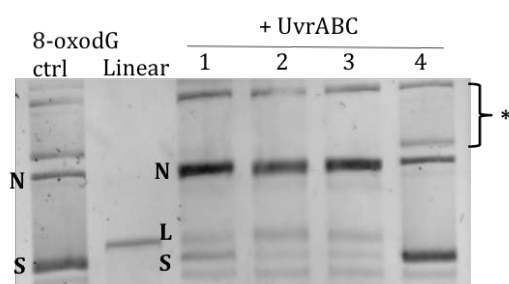


Figure 4.80: Agarose gel electrophoresis analysis of incision assays performed with 8-oxo-dG-containing pUC19 using four combinations of UvrABC (presented in the table). Incision assays performed with pUC19 treated with riboflavin were incubated 30 minutes at 37°C. The buffer used contained 2.5 mM Mg^{2+} and the reactions were started with 4 mM ATP. S: Supercoiled, L: Linear, N: Nicked.

HPLC MS/MS analysis of the repair of 8-oxo-dGuo containing plasmid was then performed using 1 μM UvrA1, 0.5 μM UvrB and 2 μM UvrC (Condition 1) (Figure 4.81). We see that 8-oxodG, is also repaired by the UvrABC, with approximately 50% of the 8-oxo-dG being removed by treatment with the UvrABC system after 2 hours. As for the other pUC19 substrates presented above, we could not recover the 12 mer resulting from the repair (Figure 4.81).

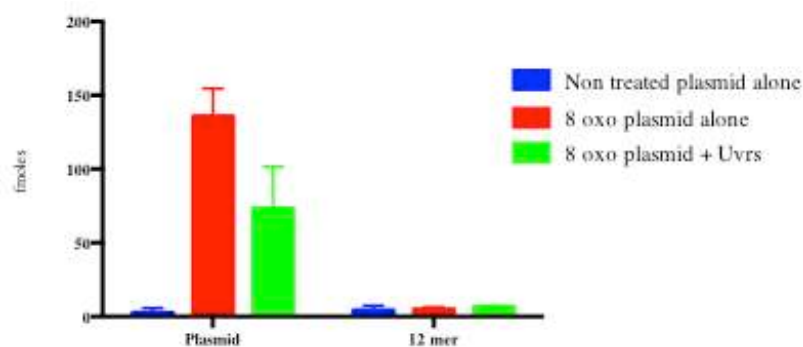


Figure 4.81: Quantification of 8-oxo-dG by HPLC MS/MS. Histograms illustrate the amount of lesions present in the plasmid before (red) and after (green) repair by UvrABC. The reactions were performed with 120 ng of plasmid 1 μ M UvrA1, 0.5 μ M UvrB and 2 μ M UvrC, incubated for 2 hours at 37°C. The buffer used contained 2.5 mM Mg^{2+} and the reaction was started with 4 mM ATP. The plasmids incubated with the Uvr proteins had been separated from the 12 mer fragments resulting from the repair on a filter. The data corresponding to the plasmid fraction is shown on the left, while the 12 mer fraction is shown on the right. All reactions were performed in triplicates and presented data correspond to the mean with error bars corresponding to the standard deviation.

In addition to the analysis of the repair of these single oxidised bases, we also evaluated the repair of tandem lesions by the UvrABC system using HPLC MS/MS (Figure 4.82). These lesions were introduced into the plasmid pUC19 by treating the DNA with ionizing irradiation at a dose of 50 Gy. Following the irradiation, the plasmids were mostly nicked and some linear plasmids were also detected on the gel (Figure 4.82). The irradiation generates both 8-oxodG M and also tandem lesions 8-oxodG M+2. 8-oxodG M are simple lesions and 8-oxodG M+2 are two 8-oxoguanine lesions, located two nucleotides apart on the same DNA strand. There were approximately 7 times more simple lesions introduced into the plasmid compared to tandem lesions, but we nonetheless could clearly see a reduction in the abundance of the lesions in the plasmid after the repair by UvrABC. Almost 80% of the simple 8-oxodG lesions were repaired in this case, and 60% of the tandem lesions. The UvrABC system can thus process both simple and tandem lesions.

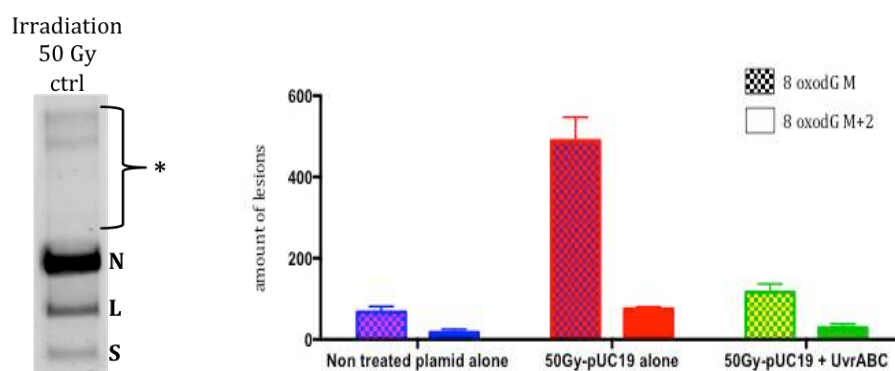


Figure 4.82: Agarose gel presenting the plasmid pUC19 following the treatment with ionizing radiation (left) and Quantification of simple (left bar, checked pattern) and tandem (right bar) 8-oxodG by HPLC MS/MS (right). Histograms illustrate the amounts of lesions present in the plasmid fraction of untreated plasmid (blue), and of the irradiated plasmid before (red) and after (green) repair by UvrABC. The plasmids were irradiated with 50 Gray. The reactions were performed with 1 μ M UvrA1, 0.5 μ M UvrB and 2 μ M UvrC. All samples were incubated for 2 hours at 37°C, and were separated from the 12 mer fragments resulting from the repair on a filter. All reactions were performed in triplicates and presented data correspond to the mean with error bars corresponding to the standard deviation.

5. Repair efficiency of the substrates by the *D. radiodurans* NER

To compare the repair efficiency of the UvrABC system on these different substrates, we normalized the different datasets by setting the number of lesions introduced into the plasmid to 100% and could thus compare the extent of repair of each of these substrates by bacterial NER (Figure 4.83 and Table 4.8).

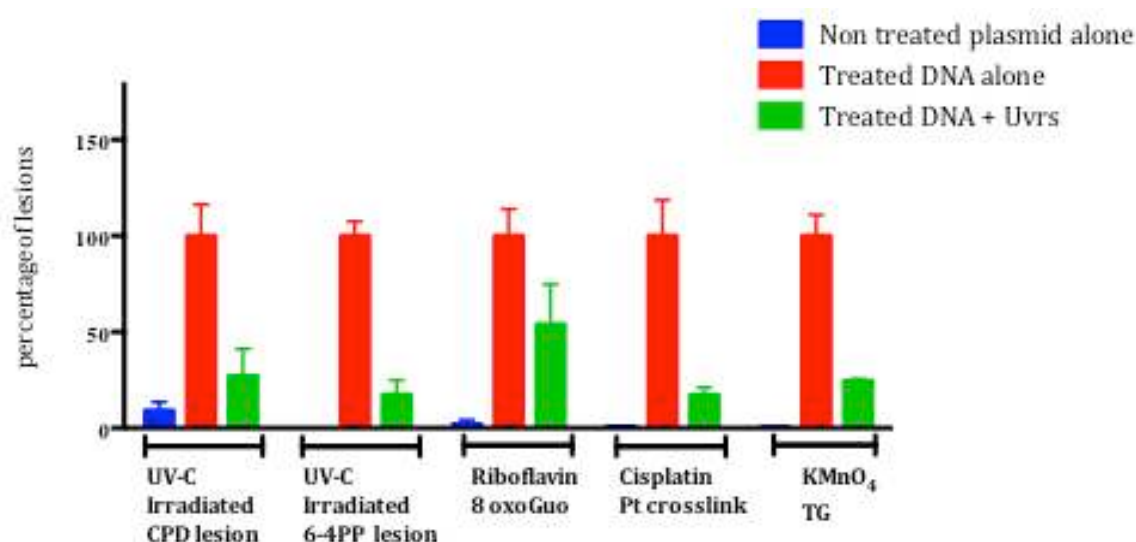


Figure 4.83: Comparison of the extent of repair of UV-induced CPDs, 6-4PPs, 8-oxodGuo, cisplatin GG cross-links and TGs by the UvrABC system analysed by HPLC MS/MS. Histograms illustrate the percentage of lesions present in the plasmid fraction of untreated plasmid (blue), and of the irradiated plasmid before (red) and after (green) repair by UvrABC. All reactions were performed with 1 μ M UvrA1, 0.5 μ M UvrB and 2 μ M UvrC, were incubated for 2 hours at 37°C, and were separated from the 12 mer fragments resulting from the repair on a filter. All reactions were performed in triplicates and presented data correspond to the mean with error bars corresponding to the standard deviation.

Table 4.8: NER repair efficiency on various DNA substrates

| Nature of the lesions | Fmoles of lesions present | Fmoles of lesions repaired | Percentage of lesion repaired |
|-----------------------|---------------------------|----------------------------|-------------------------------|
| CPD | 25.8 | 18.63 | 72.2 |
| 6-4 PP | 2.3 | 0.4 | 82.6 |
| 8oxodG | 135.7 | 62.5 | 46.0 |
| Pt Crosslink | 603.7 | 499.9 | 82.8 |
| Thymine Glycol | 444.6 | 335.7 | 75.5 |

This comparison reveals that 6-4PPs, CPDs, platinum crosslinks and TGs are very efficiently processed, while 8-oxodGuo is a poorer substrate of our bacterial NER system.

6. Kinetic analysis of the repair of lesion containing plasmid by HPLC MS/MS

Having shown that *D. radiodurans* NER can process a broad range of substrates, we next wished to follow the kinetics of the repair of each of these different substrates. For this purpose, we stopped the incision reactions at different timepoints. These analyses, which are still in progress, were performed with a new batch of proteins and more importantly using the 'optimized incision assay conditions' described in the section on the oligonucleotide-based assay. As a result, the repair efficiency under these new conditions was much greater, leading to complete fragmentation or digestion of the plasmids containing >50 lesions per plasmid molecule, which was the case for most of our samples.

When we verified the samples after 2 hours of incision reaction, we observed a lot of smearing on the gel resulting from the degradation of the DNA (Figure 4.84).

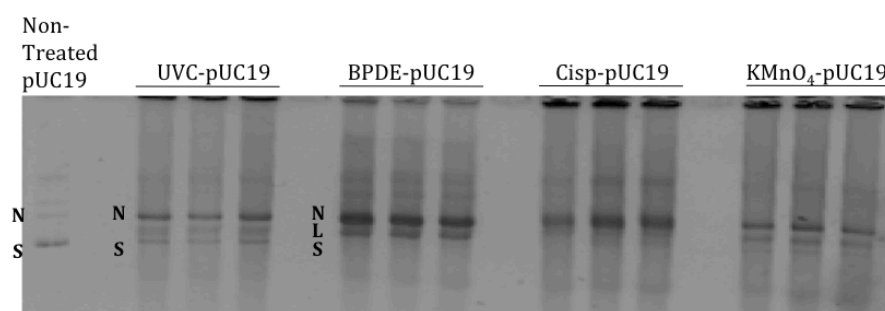


Figure 4.84: Agarose gel electrophoresis of the incision reactions performed in triplicate (side by side) using UV-C, BPDE-, cisplatin- and KMnO_4 -treated pUC19 incubated with 1 μM UvrA1, 0.5 μM UvrB and 2 μM UvrC for 2 hours at 37°C. The buffer used contained 2.5 mM Mg^{2+} and the reactions were started with 2.5 mM ATP. S: Supercoiled, L: Linear, N: Nicked.

This fragmentation of the plasmid created many small DNA fragments that were recovered in the 12 mer fraction after separation on the filter prior to HPLC MS/MS analysis. As a result, the HPLC-MS/MS analysis detected high amounts of normal nucleoside in the 12 mer fraction.

We verified that this problem was not due to an endonuclease contamination by checking each constituent separately (Figure 4.85). First, we verified the plasmids alone at room temperature and at 37°C. We did not detect any degradation on the gel (Figure 4.85.A).

We picked the UV-C irradiated pUC19 for further analysis. The plasmid was incubated at 37°C with each component: reaction buffer, ATP, dilution buffer of the proteins, UvrA, UvrB, UvrC or UvrABC+ATP. Following the reaction, the samples were directly loaded on the agarose gel or heated for 5 mins at 95°C before loading to check if this step changes the migration profile (Figure 4.85.B). After the reactions, we did not observe any degradation with the components taken separately. The additional step of heating the samples at 95°C released a little amount of linear plasmid but no smearing was observed. With UvrA, UvrB and UvrC in the incision assay, the plasmid was completely repaired and we noticed the presence of smearing. Therefore, the degradation of the plasmid was not due to an endonuclease activity. The smears on the gel presented in Figure 4.84 and observed in the last wells of the gel in Figure 4.85 thus result from the specific repair by the NER.

For subsequent HPLC MS/MS analyses, we therefore had to lower the UvrABC concentrations and adjust them for each substrate.

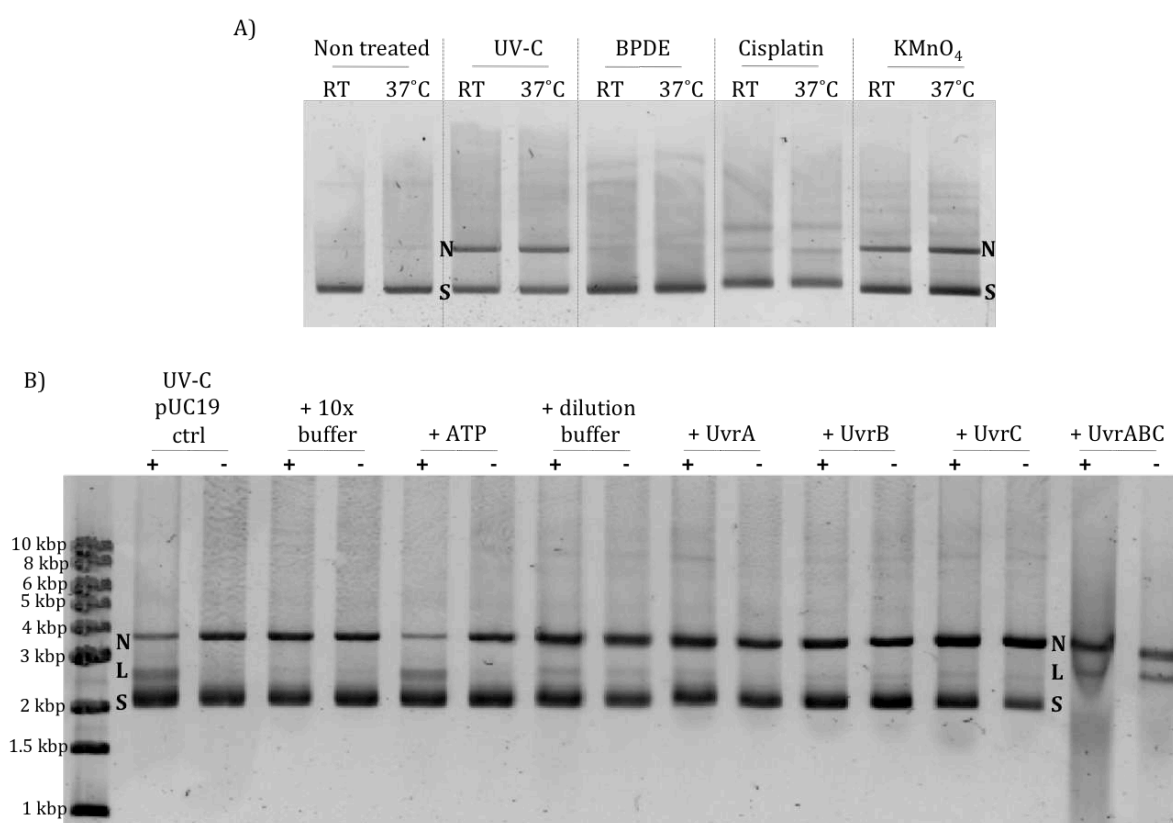


Figure 4.85: Verification of the plasmids on agarose gel: A) the plasmids were incubated at RT and 37°C for 2 h. B) UV-C irradiated pUC19 was incubated with each component of the reaction for 2h at 37°C. The samples were heated at 95°C (+) or loaded directly after the reaction (-) for the analysis on gel.

6.1. New conditions of repair for UV-C-pUC19 by UvrABC

We therefore tried to reduce the concentration of UvrABC. This time, we kept the ratio of UvrA1/UvrB/UvrC constant. The initial concentrations used for the experiment presented in Figure 4.85, 1 μ M UvrA1, 0.5 μ M UvrB and 2 μ M UvrC (Condition 1), were divided by two (Condition 2), by four (Condition 3), by five (condition 4), by ten (condition 5) and by twenty (Condition 6). As shown in Figure 4.86, 15 minutes after the beginning of the reaction, smearing can be seen in all the wells already, except for condition 6. The conditions 1-5 were thus not suitable for HPLC MS/MS analysis. With the condition 6, there was no smearing on the gel, and although not all the supercoiled plasmid was processed, we could visualise the accumulation of linear plasmid. For the HPLC MS/MS analysis of UV-C-pUC19, we thus chose the condition 6.

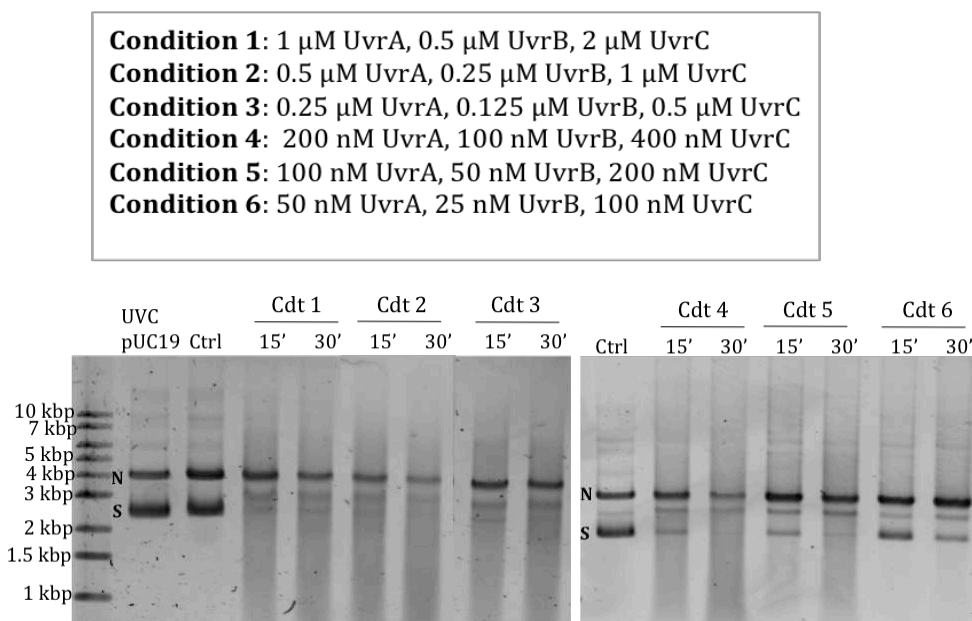


Figure 4.86: Agarose gel electrophoresis of the incision reactions performed on pUC19 treated with 0.15 J/cm² UV-C light using different combinations of UvrABC (see Table above the gel). The reactions were incubated for 15 and 30 minutes at 37°C. The buffer used contained 2.5 mM Mg²⁺ and the reactions were started with 2.5 mM ATP. S: Supercoiled, L: Linear, N: Nicked.

6.2. New conditions of repair for cisplatin-pUC19 by UvrABC

For the plasmids treated with cisplatin, the assays in conditions 1-4 showed smearing on the gel. With the condition 5, there is a repair by the NER system and we can see a decrease of the supercoiled. With the condition 6, there is an increase of the nicked plasmid and some supercoiled plasmid remaining. There was no smearing observed in this condition. For the HPLC-MS/MS analysis, we used the condition 5 to make sure that we could detect enough 12 mer fragments containing the lesions (Figure 4.87).

Condition 1: 1 μ M UvrA, 0.5 μ M UvrB, 2 μ M UvrC
Condition 2: 0.5 μ M UvrA, 0.25 μ M UvrB, 1 μ M UvrC
Condition 3: 0.25 μ M UvrA, 0.125 μ M UvrB, 0.5 μ M UvrC
Condition 4: 200 nM UvrA, 100 nM UvrB, 400 nM UvrC
Condition 5: 100 nM UvrA, 50 nM UvrB, 200 nM UvrC
Condition 6: 50 nM UvrA, 25 nM UvrB, 100 nM UvrC

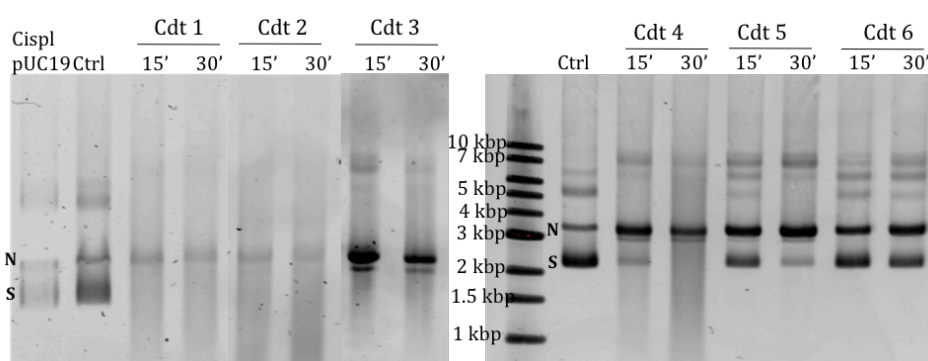


Figure 4.87: Agarose gel electrophoresis of the incision reactions performed on pUC19 treated with 1 mg/mL cisplatin using different combinations of UvrABC (see Table above the gel). The reactions were incubated for 15 and 30 minutes at 37°C. The buffer used contained 2.5 mM Mg²⁺ and the reactions were started with 2.5 mM ATP. S: Supercoiled, N: Nicked. (*: relaxed forms of pUC19, concatemers).

6.3. New conditions of repair for KMnO₄-pUC19 by UvrABC

For the plasmids treated with KMnO₄, the assays in conditions 1-4 showed smearing on the gel. With the condition 5, the smearing was limited and started appearing at 30 minutes. There is some supercoiled plasmid left. With the condition 6, there was no

smearing. For the HPLC MS/MS analysis, we used the condition 5 to make sure that we could detect enough 12 mer fragments containing the lesions (Figure 4.88).

Condition 1: 1 μ M UvrA, 0.5 μ M UvrB, 2 μ M UvrC
Condition 2: 0.5 μ M UvrA, 0.25 μ M UvrB, 1 μ M UvrC
Condition 3: 0.25 μ M UvrA, 0.125 μ M UvrB, 0.5 μ M UvrC
Condition 4: 200 nM UvrA, 100 nM UvrB, 400 nM UvrC
Condition 5: 100 nM UvrA, 50 nM UvrB, 200 nM UvrC
Condition 6: 50 nM UvrA, 25 nM UvrB, 100 nM UvrC

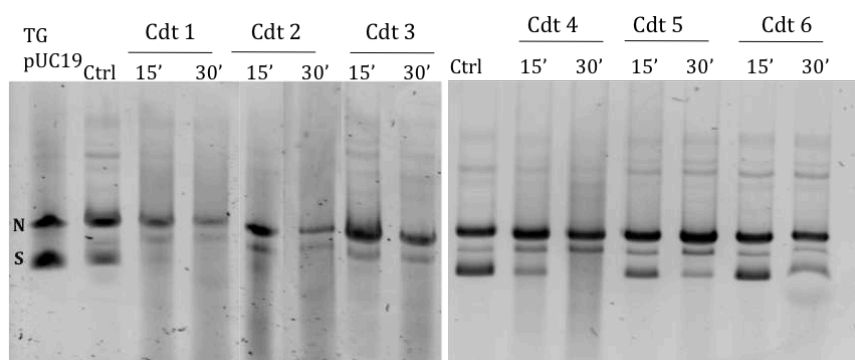


Figure 4.88: Agarose gel electrophoresis of the incision reactions performed on pUC19 treated with 0.2 M KMnO_4 using different combinations of UvrABC (see Table above the gel). The reactions were incubated for 15 and 30 minutes at 37°C. The buffer used contained 2.5 mM Mg^{2+} and the reactions were started with 2.5 mM ATP. S: Supercoiled, N: Nicked.

6.4. New conditions of repair for BPDE-pUC19 by UvrABC

For the plasmids treated with BPDE, the assays in conditions 1-4 showed some smearing (Figure 4.89). With the condition 5, the smearing was significantly reduced and started appearing at 30 minutes, and there is some supercoiled plasmid left. With the condition 6, there was no smearing, but the plasmid does not seem to be processed much.

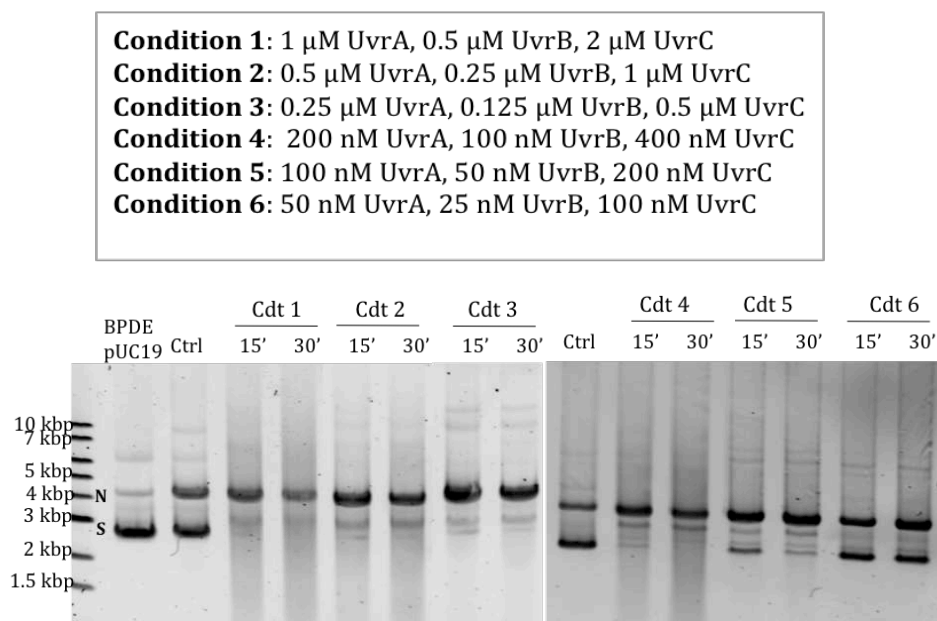


Figure 4.89: Agarose gel electrophoresis of the incision reactions performed on pUC19 treated with 150 μ M BPDE using different combinations of UvrABC (see Table above the gel). The reactions were incubated for 15 and 30 minutes at 37°C. The buffer used contained 2.5 mM Mg^{2+} and the reactions were started with 2.5 mM ATP. S: Supercoiled, N: Nicked.

For the HPLC MS/MS analysis, we thus used the condition 5 to make sure that we could detect enough 12 mer fragments containing the lesions (Figure 4.90). We were able to visualize the repair of the BPDE-dGuo with a marked decrease in the number of lesions present in the plasmid after treatment with UvrABC. However, we could not monitor the kinetics of repair using the plasmid fraction after the filtration step, but could with the 12 mer fraction. This time, we were indeed able to detect a large amount of 12 mer fragment containing the lesion, allowing us to detect the progressive increase in the amount of BPDE dGuo repaired by UvrABC during 1 h of incubation at 37°C. The improved detection of the 12 mer fragment may result from the use of low binding DNA eppendorf tubes in this experiment to recover the filtrate during our filtration step. These tubes are meant to minimize the potential binding of the 12mer fragment containing the lesion to the tube during the separation step (Figure 4.91).

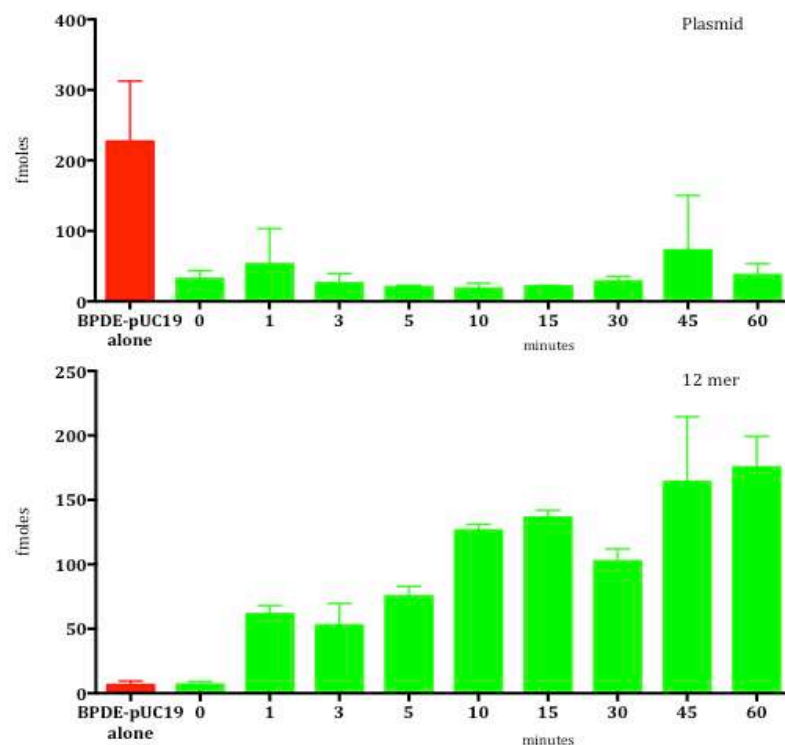


Figure 4.90: Kinetics of the repair monitored by HPLC MS/MS. Histograms illustrate the amount of BPDE-dGuo present in the plasmid before (red) and after (green) repair by UvrABC. The reactions were performed with 360 ng of plasmid 100 nM UvrA1, 50 nM UvrB and 200 nM UvrC, incubated for 60 minutes at 37°C. The buffer used contained 2.5 mM Mg²⁺ and the reaction was started with 2.5 mM ATP. The plasmids incubated with the Uvr proteins had been separated from the 12 mer fragments resulting from the repair on a filter. The data corresponding to the plasmid fraction is shown above, while the 12 mer fraction is shown below. All reactions were performed in triplicates and presented data correspond to the mean with error bars corresponding to the standard deviation.

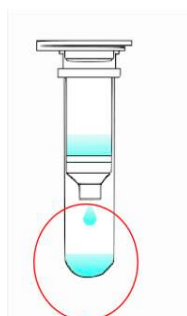


Figure 4.91: Tube that has been changed into low binding DNA Eppendorf tubes to collect the 12 mer fragment resulting from the repair by UvrABC.

The fact that we could not monitor the repair with the plasmid fraction could be linked to the membrane used at the filtration step. In fact, during the analysis of the kinetics of the repair presented on Figure 4.90, we kept a reaction that was stopped after 15 min of incubation at 37°C. This sample was not separated on the filter. We compared it to the sample BPDE-pUC19 alone (red) that was filtered prior to the analysis. We detected a total amount of lesions BPDE dGuo that was almost 10 times higher in the sample that had not been filtered (Figure 4.92). This means that the membrane trapped some of the plasmids. This event may be accentuated in presence of the proteins.

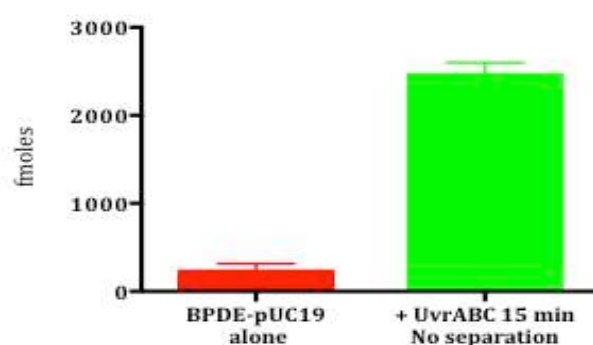


Figure 4.92: Quantification of BPDE-dGuo by HPLC MS/MS. Histograms illustrate the amounts of lesions present in the samples before (red) and after 15 min of repair by UvrABC (green). The repaired plasmid was not separated on the filter. The data corresponds to the plasmid fraction for “BPDE-pUC19 alone”. All reactions were performed in triplicates and presented data correspond to the mean with error bars corresponding to the standard deviation.

Due to the COVID19 crisis, we were not able to finalise these measurements, but new HPLC MS/MS experiments are scheduled for the coming weeks now that we have defined the optimal UvrABC enzyme concentrations to use for efficient repair.

DISCUSSION & PERSPECTIVES

1. Development of a functional NER incision assay

In this work, we have succeeded in establishing a functional NER incision assay with the UvrABC proteins from *D. radiodurans*, which has the advantage of being stable and active at 37°C for at least 2 hours. The first step for the reconstitution of this bacterial NER was the purification of the proteins. The use of fresh proteins clearly had a positive impact on the incision reaction. We saw that the release of the 12 mer fragment was more efficient when a fresh batch of proteins was used for the incision of the oligonucleotide (Figure 4.8), but also for the incision of the plasmid (Figure 4.67). With drUvrA1, we could see that a proper folding of the protein without any aggregation was also crucial: the chromatogram from the gel filtration column showed two peaks of UvrA1 at the last step of the purification that had different effectiveness in the assay (Figure 4.2). During the purification, the efficiency of the steps to reduce DNA contamination, which can affect the binding and activity of the proteins under study, or to eliminate the His-tag and the choice of columns to use were important. For instance, during the affinity chromatography of UvrC, the choice of the Nickel affinity resin was determinant for the final protein activity. The necessity of a properly folded protein is also explained by the fact that the NER system repairs in a sequential manner, and the flexibility and the interaction of the proteins are essential for damage sensing, damage verification, formation of protein complexes and the dual incision of the DNA.

We started the optimization of our incision assay using settings available for the reconstitution of other bacterial NER systems like the ones presented in Table 1.4. We then optimized the assay step by step to adapt to the specificities of the UvrABC proteins from *D. radiodurans*.

2. Influence of salt on the incision assay

At the end of their purification, each Uvr protein was stored in a buffer containing between 100 and 500 mM NaCl so as to stabilise the individual proteins. When used in the incision assay, the final NaCl concentration in the reaction was close to 25 mM. The effect of changing the KCl and NaCl concentrations in the assay was evaluated. 50 mM KCl showed the highest dual incision rate. The concentration of salt has been reported to

impact the strength of damage-specific binding and the discrimination between damaged and undamaged sites by *E. coli* Uvr proteins (Mazur and Grossman, 1991). Predictions on the effects of salts on the interaction of UvrA with DNA postulate that Na⁺ and K⁺ should have an equivalent effect on the binding (Zou et al., 1998a). Mazur et al showed that at 50 mM KCl, *E. coli* UvrA efficiently binds the DNA and discriminates between damaged and undamaged DNA in the presence of ATP. They also showed that at 200 mM KCl, the binding of UV-irradiated DNA was weaker in both the presence and absence of ATP (Mazur and Grossman, 1991). In our experiment, when we increased the salt concentration to 200 and 300 mM, the incision activity was reduced and we observed some degradation of the oligonucleotide. This might be caused by the incapacity of UvrA to bind the substrate at such salt concentrations and engage the subsequent UvrB and UvrC proteins in a proper repair cascade.

3. Roles of UvrA1, UvrA2 and UvrB in the incision assay

As mentioned previously, *D. radiodurans*' genome encodes for two UvrAs, a class I UvrA1 and a class II UvrA2. The role of UvrA2 in NER was questionable based on the study of *uvrA* deletion mutants and survival experiments following irradiation (Tanaka et al., 2005). With the determination of the minimal composition of the NER, we saw that UvrA2 does not participate in the NER pathway and cannot replace UvrA1, most likely as a result of the missing domain required for a stable interaction with UvrB and its recruitment to the DNA. The ability of UvrA2 to bind damaged DNA could explain why the non-specific incisions of the oligonucleotide caused by UvrB and UvrC in the absence of UvrA1 were reduced in the presence of UvrA2, which may limit the access to the DNA for non-specific processing by UvrB/UvrC (Timmins et al., 2009).

In our system, the UvrA1 concentration was double that of UvrB. This setting does not respect physiological conditions in which UvrB is more abundant than UvrA. In *E. coli*, after induction of the SOS response, UvrB expression levels reach around 1000 copies, which is 10-fold higher than UvrA1 and 20-fold higher than UvrC levels. UvrA1 does not remain on the lesion; it promotes the formation of the preincision complex UvrB:DNA and then leaves the DNA. One UvrA1 dimer can therefore load multiple UvrB proteins onto different damaged sites. However, a 1:1:1 ratio of purified UvrABC was efficient for the

incision in the first assays (Sancar and Rupp, 1983; Yeung et al., 1983). More recent studies used the following ratios of UvrA- UvrB- UvrC: 1:2:1, 1:5:2, 1:4:1, 1:17:3 or 1:100:10, with the UvrB protein being always in excess of the other two factors (Croteau et al., 2006; Jaciuk et al., 2020; Jiang et al., 2006; Verhoeven et al., 2002; Zou et al., 2004). High concentrations of UvrA1 *in vitro* have been shown to inhibit the incision reaction (Zou et al., 1998b). This may be due to the fact that UvrA may not dissociate from the UvrA₂:UvrB₂ complex under such conditions to allow the formation of the preincision complex and the subsequent binding and cleavage by UvrC. In our optimal setting, we used a 1:0.5:2 ratio of UvrABC and unlike these earlier studies, we found that increasing the UvrB concentration led to reduced incision activity, similar to what has been reported for UvrA. These differences could be explained by the enhanced stability and/or activity of our proteins, the affinities of the transient interactions between the UvrA, UvrB and UvrC proteins occurring during the assay, and the different protein concentrations used in the assays. In our laboratory, for example, we have shown that UvrA and UvrB from *D. radiodurans* do not form a stable complex, whereas UvrB and UvrC proteins do. This is different from what has been reported for *E. coli* or *B. caldovenax* Uvr proteins (Kad et al., 2010; Kisker et al., 2013; Truglio et al., 2006a, 2004)

During the incision assay with the plasmid, higher concentrations of UvrC led to increased incision of the supercoiled plasmid and formation of nicked DNA. This could be due to the observation above: UvrB does not bind DNA alone without UvrA, but since we have a higher concentration of UvrA compared to UvrB, there might not be enough UvrB in our reconstituted system to ensure efficient pre-incision complex UvrB:DNA formation to recruit UvrC.

4. Roles of divalent ions in the incision assay

In our initial assay, we observed a big difference compared to the NER systems studied so far. In *D. radiodurans*, the first incision appeared to occur on the 5' side of the lesion followed by the second incision on the 3' side of the lesion, while it has been reported to occur in the opposite order with other bacterial NER systems (Sancar and Rupp, 1983; Verhoeven et al., 2000).

The presence of divalent ions is essential for the endonuclease activity of UvrC. Residues in the N-terminal GIY-YIG domain of UvrC have been shown to bind an ion, which activates a water molecule for nucleophilic attack on the phosphodiester bond.

We used 10 mM Mg^{2+} in the beginning of our work. This concentration was used in the reconstituted NER cited in Table 1.4. However, the incision efficiency was significantly improved when we decreased the Mg^{2+} concentration from 10 mM to 2.5 mM. The concentration of the ion modulated the endonuclease activities of UvrC: with 10 mM Mg^{2+} , the C-terminal RNase H endonuclease activity (5' cleavage) was more efficient than the N-terminal GIY-YIG activity (3' cleavage), leading to the accumulation of the 32 mer intermediate fragment (Figure 4.1). With 2.5 mM Mg^{2+} , the dual incision reactions were almost simultaneous and no (or very little) intermediate fragment was observed. With 1 mM Mg^{2+} , the order of incision was then inverted, with the GIY-YIG activity becoming more active than the RNaseH domain (Figure 5.1).

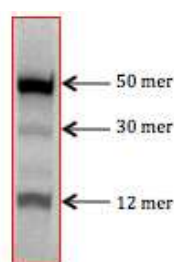


Figure 5.1: Accumulation of 30 mer after the repair of 5' red-50merF26-seq1 by UvrABC in the presence of 1 mM Mg^{2+} .

Interestingly, in these conditions where the 5' incision reaction is less efficient than the 3' cleavage, we observed the appearance of a 30 mer fragment, which suggests that the dual incision can occur in either order (3' then 5' or 5' then 3') and that unlike in *E. coli* NER, 3' cleavage is not a prerequisite for 5' cleavage (Lin and Sancar, 1992).

We also tested the influence of other divalent cations on the incision efficiency. The most effective one was Mn^{2+} . This could be explained by the presence of high levels of manganese under physiological conditions in *D. radiodurans* following irradiation (Sharma et al., 2013). Mn^{2+} and Mg^{2+} were used at the same concentration. With 2.5 mM Mg^{2+} , we did not observe the non-specific activity of the incision complex UvrB:UvrC:DNA in the absence of UvrA. This activity that was present when we used 10 mM Mg^{2+} was

accentuated during the incision assay using 2.5 mM Mn^{2+} (Figure 4.31), UvrB and UvrC. The non-specific incision of the fragment turned into a degradation of the substrate when magnesium and manganese were combined. The addition of 0.25 mM Fe^{3+} seemed to have a stabilizing effect on the proteins. This can be linked to the fact that in *D. radiodurans*, the proteins are protected from degradation in a cellular environment containing high Mn/Fe ratio (Daly, 2009; Daly et al., 2004).

Other divalent ions did not show any marked effects on the reconstituted NER, but could not replace magnesium.

5. Role of ATP binding and hydrolysis in the incision assay

In the NER system, the DNA scanning is based on a dynamic ATPase activity of the UvrA protein. Without ATP, we observed no repair, and thus ATP was used to initiate the incision reaction. ATP is also required for the 3' and 5' incisions by the incision complex UvrB:UvrC:DNA in *E. coli* (Verhoeven et al., 2000).

The UvrA dimer carries four ATP binding sites and UvrB contains one ATP binding site. Case et al explained the complex mechanism in which UvrA proximal and distal sites bind and hydrolyse ATP in a asymmetric way and how this activity triggered by the presence of both damage or non-damaged DNA explains the formation of stable complexes with UvrB on damaged DNA compared with weaker, more dynamic complexes on non-damaged DNA (Case et al., 2019).

The assay with ATP analogs, ADP, ADP- AlF_4 , AMP-PNP and AMP-PCP confirmed that both ATP binding and ATP hydrolysis are needed for the NER activity. The complex of ATP with proteins also requires the presence of Mg^{2+} . When we tested a range of concentrations of both divalent ion and ATP, the best condition was the one using the 1:1 Mg^{2+} -ATP ratio.

6. Characterization of the UvrC protein

In this work, we made a particular focus on UvrC. We studied different domains of the protein to assess their respective roles in the dual incision activity. Table 5.1 below

provides a summary of our major findings. With UvrC-ΔHhH, the missing helix-hairpin-helix (HhH₂) region lowered the activity of UvrC. The efficiency of the incision on the 5' side of the lesion was reduced. This observation is similar to the results obtained with *E. coli* UvrC: the 3' incision is performed normally but the incision 5' is reduced. The (HhH)₂ motif is known to bind the ssDNA in the repair bubble, thus, when absent, UvrC is not able to stabilize the binding of the C-terminal RNase H endonuclease domain on the DNA substrate (Moolenaar et al., 1998b).

The C-terminal half of UvrC, UvrC-C, contains the RNase H endonuclease and the (HhH)₂ motif. This region did not show any activity by itself. This could be due to the absence of a UvrB interacting domain to recruit it to the pre-incision complex.

The combination of UvrC-C and UvrC-ΔHhH in the incision assay restored the proper incision on the 5' side of the lesion, indicating that the RNase H endonuclease domain of UvrC-C was functional but needed to be recruited to the DNA either through direct interaction with UvrB or through interaction with UvrC. However, the endonucleases GIY-YIG and RNase H were present in a 1:2 ratio in this reaction, which could influence the relative cleavage by each of the domains.

The UvrC-N construct contains the GIY-YIG endonuclease domain, the cysteine-rich region and the UvrB interaction domain. Surprisingly, UvrC-N is able to cut the DNA more efficiently than UvrC-ΔHhH that contains both endonuclease domains. Also, to our surprise, UvrC-N is able to cut on both the 3' and 5' sides of the lesion although it is missing the C-terminal RNase H domain that is normally responsible for the 5' cleavage reaction. Although UvrC-N is able to cut on the 5' side of the lesion, its cleavage on the 3' side of the lesion is more efficient as we could see an accumulation of the 30 mer fragment.

The incision assay with UvrC-N_{Endo} that carries only the GIY-YIG endonuclease domain illustrates the importance of the cysteine-rich region and the UvrB interaction domain for the incision activity. Without these two regions, no incision was observed. These domains may participate in the recruitment by UvrB. The UvrC homologue, Cho in *E. coli*, binds UvrB differently than UvrC; the presence of the cysteine-rich region and the UvrB

interaction domain is necessary for the activity of Cho (Moolenaar et al., 2002). Unlike Cho, UvrC-N is able to cut on the 3' but also on the 5' side of the lesion.

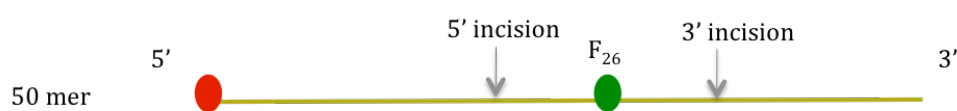
The combination of the UvrC-C and UvrC-N constructs in order to reconstitute the full-length protein in the incision assay fully restored the activity of intact UvrC without any accumulation of intermediate fragments. The incisions were simultaneous once more. This suggests that the two halves of UvrC may interact with each other to allow the recruitment of both parts to the pre-incision complex despite only one half contains a UvrB domain. This interaction makes a direct link between the two halves dispensable for a fully functional protein. Verhoeven et al showed that the UvrC-C construct in *E. coli* was able to perform an incision on the 5' side of the lesion, when the substrate was nicked on the 3' side of the lesion. Without this first incision, UvrC-C did not show any activity. This assay was not performed for *D. radiodurans* UvrC-C, but in the presence of UvrC-N, that performed the nick on 3', the same activity was observed (Verhoeven et al., 2000).

To properly isolate the UvrC endonuclease domains of UvrC-FL, we then mutated residues in each active site. The mutant UvrC-FL^{D391A} in the C-terminal RNase H domain did not show any activity. In *E. coli*, the equivalent mutant, Asp399Ala, was still active for the 3' incision (Moolenaar et al., 1995; Verhoeven et al., 2000). In the N-terminal GIY-YIG domain, the residue E72 is involved in metal binding. The mutant UvrC-FL^{E72A} showed a very reduced activity with the substrate 5'-red-50merF26-seq1: the C-terminal domain in UvrC-FL^{E72A} performed less than 5% of the incision on the 5' side of the lesion. With the second substrate 5'-red-50merF26-seq2, no incision was detected at all. In *E. coli*, this mutant also showed no activity, but this is because the order of the incisions (3' then 5') did not allow the second cut on the 5' side of the lesion by the remaining active C-terminal domain (Truglio et al., 2005). In *D. radiodurans* UvrC, we observe that a single point mutant in one of the two endonucleases domains abolishes both incision reactions, which strongly suggests that the cleavage reactions are somehow coupled.

The UvrC-N^{E72A} mutant also did not show any activity, even when combined with UvrC-C. If the *D. radiodurans* UvrC-C behaves the same as *E. coli* UvrC-C, a nick on the 3' side might be necessary to detect any activity. Not surprisingly, the UvrC-C^{D391A} alone did not show any activity, but when combined with UvrC-N, incision activity was detected, which was

slightly different from the activity observed with UvrC-N alone. We detected more 30 mer fragment. Our hypothesis is that UvrC-C^{D391A} is still able to bind on the 5' side of the lesion despite the mutation and that this binding hinders the incision on the 5' side by UvrC-N. 3' cleavage is unaffected in this case.

Table 5.1: Overview of the incision reactions performed by the different UvrC constructs in the presence of UvrA and UvrB.



| | 5' incision | 3' incision | Order- Specificity |
|--|-------------|-------------|--|
| UvrC-FL | ++ | +++ | 1 mM Mg ²⁺ : 3' then 5' |
| | +++ | +++ | 2.5 mM Mg ²⁺ : Simultaneous |
| | +++ | ++ | 10 mM Mg ²⁺ : 5' then 3' |
| UvrC-FL ^{E72A} | +/- | - | Substrate dependent |
| UvrC-FL ^{D399A} | - | - | - |
| UvrC-ΔHhH | ++ | +++ | 3' then 5' |
| UvrC-NEndo | - | - | - |
| UvrC-N | ++ | +++ | 3' then 5' |
| UvrC-C | - | - | - |
| UvrC-N + UvrC-C | +++ | +++ | Simultaneous |
| UvrC-N ^{E72A} | - | - | - |
| UvrC-C ^{D391A} | - | - | - |
| UvrC-N ^{E72A} + UvrC-C ^{D391A} | - | - | - |
| UvrC-N + UvrC-C ^{D391A} | + | +++ | 3' then 5' |

7. Sites of incision

Thanks to Maldi-TOF analysis, we were able to precisely determine the sites of incision by UvrC on the 5' and 3' sides of the lesion. For all the substrates tested, two fluorescein containing substrates with different sequences and a biotin containing substrates, the incisions occurred 7 nucleotides on the 5' side of the lesion and 4 nucleotides on 3' side. The cuts resulted in the release of a 12 mer fragment with a 5' phosphate: 5'-Phos-NNNNNNNXNNNN-3' where N is any nucleotide and X is the damaged base recognized by the NER system. *E. coli*, the incision on 3' side could vary depending on the substrates. The incision occurred at the fourth or fifth phosphodiester bond 3' to the lesion, leaving a 3'-OH terminus. The second cut constantly occurred eight phosphodiester bonds 5' to the lesion and produced a 5'-Phos terminus (Sancar and Rupp, 1983).

Moreover, we found that the intact UvrC and the N-terminal half of UvrC produced the same two cuts on our oligonucleotide substrates, which suggests that it is most likely the position of UvrB on the DNA that guides the sites of incision through steric hindrance.

8. Substrate specificity

Fluorescein conjugated thymine or FdT is a well-known substrate of the NER pathway (DellaVecchia et al., 2004). Using the substrate 5'red-50merF26-seq1, we confirmed that FdT is also efficiently processed by *D. radiodurans* UvrABC. A second fluorescein containing substrate 5'red-50merF26-seq2 differing only in terms of sequence (the FdT was in the same position and the lengths of the substrates were identical) showed a difference in the rate of substrate processing. This was a little surprising considering that UvrA does not bind the DNA in a sequence specific manner (Truglio et al., 2006a). The local sequence around the lesion may be determinant for this difference. The presence of several A-T base pairs, which are weaker than G≡C pairs, around the lesion might explain the ease of repair by the NER on this substrate. As a substrate, 5'red-50merF26-seq2 might be easier to melt thus favouring a more efficient repair.

Based on our results, FdT appears to be a better substrate than biotin conjugated thymine. The size of the lesion and extent of distortion of the DNA helix caused by the lesion are

known to influence the repair of the substrate (Truglio et al., 2006a). It would be interesting to understand how these two thymine conjugates affect the DNA helix.

The incision assay performed on plasmid DNA also revealed different repair efficiencies for the various substrates tested. UV-C treatment of the plasmid introduces mostly cyclobutane pyrimidine dimers (CPDs) (80%) and only a smaller amount of pyrimidine-pyrimidone (6-4) photoproducts (6-4PPs) (20%) (Ravanat et al., 2001). However, we observed that the UvrABC system preferentially repairs 6-4PP lesions in agreement with earlier studies (Tanaka et al., 2005). In this case, this preference for 6-4PP lesions could be due to the distortion triggered by the lesions that is known to be accentuated with 6-4PP lesions compared to CPDs (Horikoshi et al., 2016; Osakabe et al., 2015).

When comparing the efficiency of repair of different types of lesions introduced into the plasmid DNA, we could see that the UvrABC does not repair all lesions with the same efficiency. When comparing the fraction of lesions repaired, the lesions were repaired in the following order: CisPT-GG > TGs > TT-CPD > 8-oxodG. However, a more thorough comparison of these efficiencies would require that the same (or similar) number of lesions be introduced into the plasmid for all substrates, which is technically challenging. Our experimental set-up nonetheless clearly showed that the TGs and 8-oxodG lesions, well-known substrates of the base excision repair, were also efficiently repaired by UvrABC. The repair of TGs by bacterial NER has been reported earlier (Kow et al., 1990). For 8oxodG, there are several reports of the UvrABC repairing 8oxodG directly (Czeczot et al., 1991). In addition, UvrABC have been shown to be involved in the repair of 8oxodG oxidation products, guanidinohydantoin (Gh) and spiroiminodihydantoin (Sp) lesions (McKibbin et al., 2013). The repair efficiency of some of these oxidation products by the NER system composed of *B. caldotenax* UvrA, UvrB and *T. maritima* UvrC was found to be significantly lower than the repair of FdT used as a reference substrate (McKibbin et al., 2013). In our system, when we compared the repair of 8oxodG to the more classical NER substrates introduced into the plasmid (e.g. photoproducts or cisplatin crosslinks), the difference was less accentuated. *D. radiodurans* NER thus seems to repair 8oxodG more effectively. The preparation of an oligonucleotide substrate containing 8oxodG would allow us to better assess 8oxodG as a substrate in our system and monitor its repair by *D. radiodurans* NER and by the DNA glycosylase Fpg as a control.

For future analysis, it would also be interesting to incubate our UvrABC system with a mix of plasmids containing different lesions to determine which lesions are preferentially repaired by the UvrABC proteins. But beforehand, some improvements need to be brought to the separation step used during the HPLC MS/MS analysis to enhance our recovery of both the plasmid and 12 mer fractions.

In this work, we have successfully reconstituted a functional *D. radiodurans* NER system allowing us to assess the repair efficiency and substrate specificity of bacterial NER on both oligonucleotide substrates and in treated plasmid DNA. We found that *D. radiodurans* UvrABC efficiently repairs a broad range of lesions including well-known substrates of the BER pathway. This work also allowed us to better understand the dual incision reaction carried out by the UvrC protein by preparing truncation and point mutants of this key enzyme in the NER pathway.

In the future, it would be interesting to study the interactions between the proteins of the NER and the BER pathways and to determine if the NER is a back-up system for the removal of oxidized bases in the absence of BER or in response to high doses of ionizing radiation that cause numerous base damages and strand breaks. These kind of studies aiming to decipher the cross-talk between different repair pathways have already begun for the eukaryotic NER system (Kumar et al., 2020).

BIBLIOGRAPHY

- Abbotts, R., Wilson, D.M., 2017. Coordination of DNA single strand break repair. *Free Radic. Biol. Med.* 107, 228–244. <https://doi.org/10.1016/j.freeradbiomed.2016.11.039>
- Acharya, S., Foster, P.L., Brooks, P., Fishel, R., 2003. The Coordinated Functions of the E. coli MutS and MutL Proteins in Mismatch Repair. *Mol. Cell* 12, 233–246. [https://doi.org/10.1016/S1097-2765\(03\)00219-3](https://doi.org/10.1016/S1097-2765(03)00219-3)
- Agostini, H.J., Carroll, J.D., Minton, K.W., 1996. Identification and characterization of *uvrA*, a DNA repair gene of *Deinococcus radiodurans*. *J Bacteriol* 178, 6759–65.
- Akiyama, M., Maki, H., Sekiguchi, M., Horiuchi, T., 1989. A specific role of MutT protein: to prevent dG.dA mispairing in DNA replication. *Proc. Natl. Acad. Sci. U. S. A.* 86, 3949–3952. <https://doi.org/10.1073/pnas.86.11.3949>
- Alexandrovich, A., Czisch, M., Frenkiel, T.A., Kelly, G.P., Goosen, N., Moolenaar, G.F., Chowdhry, B.Z., Sanderson, M.R., Lane, A.N., 2001. Solution structure, hydrodynamics and thermodynamics of the UvrB C-terminal domain. *J Biomol Struct Dyn* 19, 219–36.
- Alexandrovich, A., Sanderson, M.R., Moolenaar, G.F., Goosen, N., Lane, A.N., 1999. NMR assignments and secondary structure of the UvrC binding domain of UvrB. *FEBS Lett* 451, 181–5.
- Ali, J.A., Maluf, N.K., Lohman, T.M., 1999. An oligomeric form of E. coli UvrD is required for optimal helicase activity. *J Mol Biol* 293, 815–34. <https://doi.org/10.1006/jmbi.1999.3185>
- Aravind, L., Walker, D.R., Koonin, E.V., 1999. Conserved domains in DNA repair proteins and evolution of repair systems. *Nucleic Acids Res* 27, 1223–42.
- Arthur, H.M., Lloyd, R.G., 1980. Hyper-recombination in *uvrD* mutants of *Escherichia coli* K-12. *Mol Gen Genet* 180, 185–91.
- Assenmacher, N., Wenig, K., Lammens, A., Hopfner, K.P., 2006. Structural basis for transcription-coupled repair: the N terminus of Mfd resembles UvrB with degenerate ATPase motifs. *J Mol Biol* 355, 675–83. <https://doi.org/10.1016/j.jmb.2005.10.033>
- Atkinson, J., Guy, C.P., Cadman, C.J., Moolenaar, G.F., Goosen, N., McGlynn, P., 2009. Stimulation of UvrD helicase by UvrAB. *J Biol Chem* 284, 9612–23. <https://doi.org/10.1074/jbc.M808030200>
- Au, K.G., Welsh, K., Modrich, P., 1992. Initiation of methyl-directed mismatch repair. *J. Biol. Chem.* 267, 12142–12148.
- Ayora, S., Carrasco, B., Cardenas, P.P., Cesar, C.E., Canas, C., Yadav, T., Marchisone, C., Alonso, J.C., 2011. Double-strand break repair in bacteria: a view from *Bacillus subtilis*. *FEMS Microbiol Rev* 35, 1055–81. <https://doi.org/10.1111/j.1574-6976.2011.00272.x>
- Banavali, N.K., MacKerell, A.D., 2002. Free energy and structural pathways of base flipping in a DNA GCGC containing sequence. *J. Mol. Biol.* 319, 141–160.

[https://doi.org/10.1016/S0022-2836\(02\)00194-8](https://doi.org/10.1016/S0022-2836(02)00194-8)

- Banerjee, A., Santos, W.L., Verdine, G.L., 2006. Structure of a DNA glycosylase searching for lesions. *Science* 311, 1153–1157. <https://doi.org/10.1126/science.1120288>
- Banerjee, A., Yang, W., Karplus, M., Verdine, G.L., 2005. Structure of a repair enzyme interrogating undamaged DNA elucidates recognition of damaged DNA. *Nature* 434, 612–618. <https://doi.org/10.1038/nature03458>
- Bangalore, D.M., Heil, H.S., Mehrlinger, C.F., Hirsch, L., Hemmen, K., Heinze, K.G., Tessmer, I., 2020. Automated AFM analysis of DNA bending reveals initial lesion sensing strategies of DNA glycosylases. *Sci. Rep.* 10, 15484. <https://doi.org/10.1038/s41598-020-72102-7>
- Battista, J.R., 1997. Against all odds: the survival strategies of *Deinococcus radiodurans*. *Annu Rev Microbiol* 51, 203–24.
- Beck, D.J., Popoff, S., Sancar, A., Rupp, W.D., 1985. Reactions of the UVRABC excision nuclease with DNA damaged by diamminedichloroplatinum(II). *Nucleic Acids Res.* 13, 7395–7412. <https://doi.org/10.1093/nar/13.20.7395>
- Bellamy, S.R.W., Krusong, K., Baldwin, G.S., 2007. A rapid reaction analysis of uracil DNA glycosylase indicates an active mechanism of base flipping. *Nucleic Acids Res.* 35, 1478–1487. <https://doi.org/10.1093/nar/gkm018>
- Bentschikou, E., Servant, P., Coste, G., Sommer, S., 2010. A major role of the RecFOR pathway in DNA double-strand-break repair through ESDSA in *Deinococcus radiodurans*. *PLoS Genet.* 6, e1000774. <https://doi.org/10.1371/journal.pgen.1000774>
- Bertrand, C., Thibessard, A., Bruand, C., Lecointe, F., Leblond, P., 2019. Bacterial NHEJ: a never ending story. *Mol. Microbiol.* 111, 1139–1151. <https://doi.org/10.1111/mmi.14218>
- Bessman, M.J., Frick, D.N., O’Handley, S.F., 1996. The MutT proteins or “Nudix” hydrolases, a family of versatile, widely distributed, “housecleaning” enzymes. *J. Biol. Chem.* 271, 25059–25062. <https://doi.org/10.1074/jbc.271.41.25059>
- Blainey, P.C., van Oijen, A.M., Banerjee, A., Verdine, G.L., Xie, X.S., 2006. A base-excision DNA-repair protein finds intrahelical lesion bases by fast sliding in contact with DNA. *Proc. Natl. Acad. Sci. U. S. A.* 103, 5752–5757. <https://doi.org/10.1073/pnas.0509723103>
- Blanchard, L., Guérin, P., Roche, D., Cruveiller, S., Pignol, D., Vallenet, D., Armengaud, J., de Groot, A., 2017. Conservation and diversity of the IrrE/DdrO-controlled radiation response in radiation-resistant *Deinococcus* bacteria. *MicrobiologyOpen* in press.
- Blasius, M., Sommer, S., Hubscher, U., 2008. *Deinococcus radiodurans*: What belongs to the survival kit? *Crit. Rev. Biochem. Mol. Biol.* 43, 221–238. <https://doi.org/10.1080/10409230802122274>
- Boiteux, S., Gajewski, E., Laval, J., Dizdaroglu, M., 1992. Substrate specificity of the

Escherichia coli Fpg protein (formamidopyrimidine-DNA glycosylase): excision of purine lesions in DNA produced by ionizing radiation or photosensitization. *Biochemistry* 31, 106–110. <https://doi.org/10.1021/bi00116a016>

- Bowater, R., Doherty, A.J., 2006. Making ends meet: repairing breaks in bacterial DNA by non-homologous end-joining. *PLoS Genet* 2, e8. <https://doi.org/10.1371/journal.pgen.0020008>
- Brissett, N.C., Doherty, A.J., 2009. Repairing DNA double-strand breaks by the prokaryotic non-homologous end-joining pathway. *Biochem. Soc. Trans.* 37, 539–545. <https://doi.org/10.1042/BST0370539>
- Brooks, S.C., Adhikary, S., Robinson, E.H., Eichman, B.F., 2013. Recent advances in the structural mechanisms of DNA glycosylases. *Biochim. Biophys. Acta* 1834, 247–271. <https://doi.org/10.1016/j.bbapap.2012.10.005>
- Brown, J., Brown, T., Fox, K.R., 2001. Affinity of mismatch-binding protein MutS for heteroduplexes containing different mismatches. *Biochem. J.* 354, 627–633.
- Bruand, C., Ehrlich, S.D., 2000. UvrD-dependent replication of rolling-circle plasmids in *Escherichia coli*. *Mol Microbiol* 35, 204–10.
- Burdett, V., Baitinger, C., Viswanathan, M., Lovett, S.T., Modrich, P., 2001. In vivo requirement for RecJ, ExoVII, ExoI, and ExoX in methyl-directed mismatch repair. *Proc. Natl. Acad. Sci. U. S. A.* 98, 6765–6770. <https://doi.org/10.1073/pnas.121183298>
- Cao, C., Jiang, Y.L., Stivers, J.T., Song, F., 2004. Dynamic opening of DNA during the enzymatic search for a damaged base. *Nat. Struct. Mol. Biol.* 11, 1230–1236. <https://doi.org/10.1038/nsmb864>
- Caron, P.R., Grossman, L., 1988. Incision of damaged versus nondamaged DNA by the *Escherichia coli* UvrABC proteins. *Nucleic Acids Res.* 16, 7855–7865. <https://doi.org/10.1093/nar/16.16.7855>
- Caron, P.R., Kushner, S.R., Grossman, L., 1985. Involvement of helicase II (uvrD gene product) and DNA polymerase I in excision mediated by the uvrABC protein complex. *Proc Natl Acad Sci U A* 82, 4925–9.
- Case, B.C., Hartley, S., Osuga, M., Jeruzalmi, D., Hingorani, M.M., 2019. The ATPase mechanism of UvrA2 reveals the distinct roles of proximal and distal ATPase sites in nucleotide excision repair. *Nucleic Acids Res.* 47, 4136–4152. <https://doi.org/10.1093/nar/gkz180>
- Chatterjee, N., Walker, G.C., 2017. Mechanisms of DNA damage, repair, and mutagenesis. *Environ. Mol. Mutagen.* 58, 235–263. <https://doi.org/10.1002/em.22087>
- Claassen, L.A., Grossman, L., 1991. Deletion mutagenesis of the *Escherichia coli* UvrA protein localizes domains for DNA binding, damage recognition, and protein-protein

interactions. *J. Biol. Chem.* 266, 11388–11394.

- Cox, M.M., Battista, J.R., 2005. *Deinococcus radiodurans* - the consummate survivor. *Nat Rev Microbiol* 3, 882–92. <https://doi.org/10.1038/nrmicro1264>
- Cox, M.M., Keck, J.L., Battista, J.R., 2010. Rising from the Ashes: DNA Repair in *Deinococcus radiodurans*. *PLoS Genet* 6. <https://doi.org/10.1371/journal.pgen.1000815>
- Croteau, D.L., DellaVecchia, M.J., Perera, L., Van Houten, B., 2008. Cooperative damage recognition by UvrA and UvrB: identification of UvrA residues that mediate DNA binding. *DNA Repair Amst* 7, 392–404. <https://doi.org/10.1016/j.dnarep.2007.11.013>
- Croteau, D.L., DellaVecchia, M.J., Wang, H., Bienstock, R.J., Melton, M.A., Van Houten, B., 2006. The C-terminal zinc finger of UvrA does not bind DNA directly but regulates damage-specific DNA binding. *J Biol Chem* 281, 26370–81. <https://doi.org/10.1074/jbc.M603093200>
- Czczot H., Tudek B., Lambert B., Laval J., Boiteux S., 1991. *Escherichia coli* Fpg protein and UvrABC endonuclease repair DNA damage induced by methylene blue plus visible light in vivo and in vitro. *J Bacteriol* 173, 3419–3424. doi: 10.1128/jb.173.11.3419-3424.1991.
- Dalhus, B., Laerdahl, J.K., Backe, P.H., Bjørås, M., 2009. DNA base repair--recognition and initiation of catalysis. *FEMS Microbiol. Rev.* 33, 1044–1078. <https://doi.org/10.1111/j.1574-6976.2009.00188.x>
- Daly, M.J., 2009. A new perspective on radiation resistance based on *Deinococcus radiodurans*. *Nat. Rev. Microbiol.* 7, 237–245. <https://doi.org/10.1038/nrmicro2073>
- Daly, M.J., Gaidamakova, E.K., Matrosova, V.Y., Kiang, J.G., Fukumoto, R., Lee, D.Y., Wehr, N.B., Viteri, G.A., Berlett, B.S., Levine, R.L., 2010. Small-Molecule Antioxidant Proteome-Shields in *Deinococcus radiodurans*. *PLoS One* 5. <https://doi.org/10.1371/journal.pone.0012570>
- Daly, M.J., Gaidamakova, E.K., Matrosova, V.Y., Vasilenko, A., Zhai, M., Leapman, R.D., Lai, B., Ravel, B., Li, S.M., Kemner, K.M., Fredrickson, J.K., 2007. Protein oxidation implicated as the primary determinant of bacterial radioresistance. *PLoS Biol* 5, e92. <https://doi.org/10.1371/journal.pbio.0050092>
- Daly, M.J., Gaidamakova, E.K., Matrosova, V.Y., Vasilenko, A., Zhai, M., Venkateswaran, A., Hess, M., Omelchenko, M.V., Kostandarithes, H.M., Makarova, K.S., Wackett, L.P., Fredrickson, J.K., Ghosal, D., 2004. Accumulation of Mn(II) in *Deinococcus radiodurans* facilitates gamma-radiation resistance. *Science* 306, 1025–8. <https://doi.org/10.1126/science.1103185>
- Dao, V., Modrich, P., 1998. Mismatch-, MutS-, MutL-, and helicase II-dependent unwinding from the single-strand break of an incised heteroduplex. *J. Biol. Chem.* 273, 9202–9207. <https://doi.org/10.1074/jbc.273.15.9202>

- Davies, M.J., 2005. The oxidative environment and protein damage. *Biochim. Biophys. Acta* 1703, 93–109. <https://doi.org/10.1016/j.bbapap.2004.08.007>
- de la Tour, C.B., Passot, F.M., Toueille, M., Mirabella, B., Guerin, P., Blanchard, L., Servant, P., de Groot, A., Sommer, S., Armengaud, J., 2013. Comparative proteomics reveals key proteins recruited at the nucleoid of *Deinococcus* after irradiation-induced DNA damage. *Proteomics* 13, 3457–69. <https://doi.org/10.1002/pmic.201300249>
- DellaVecchia, M.J., Croteau, D.L., Skorvaga, M., Dezhurov, S.V., Lavrik, O.I., Van Houten, B., 2004. Analyzing the handoff of DNA from UvrA to UvrB utilizing DNA-protein photoaffinity labeling. *J Biol Chem* 279, 45245–56. Epub 2004 Aug 11.
- Denver, D.R., Swenson, S.L., Lynch, M., 2003. An evolutionary analysis of the helix-hairpin-helix superfamily of DNA repair glycosylases. *Mol. Biol. Evol.* 20, 1603–1611. <https://doi.org/10.1093/molbev/msg177>
- Devigne, A., Ithurbide, S., Bouthier de la Tour, C., Passot, F., Mathieu, M., Sommer, S., Servant, P., 2015. DdrO is an essential protein that regulates the radiation desiccation response and the apoptotic-like cell death in the radioresistant *Deinococcus radiodurans* bacterium. *Mol. Microbiol.* 96, 1069–1084. <https://doi.org/10.1111/mmi.12991>
- Dianov, G., Lindahl, T., 1994. Reconstitution of the DNA base excision-repair pathway. *Curr. Biol. CB* 4, 1069–1076. [https://doi.org/10.1016/s0960-9822\(00\)00245-1](https://doi.org/10.1016/s0960-9822(00)00245-1)
- Dillingham, M.S., Kowalczykowski, S.C., 2008. RecBCD enzyme and the repair of double-stranded DNA breaks. *Microbiol Mol Biol Rev* 72, 642–71, Table of Contents. <https://doi.org/10.1128/MMBR.00020-08>
- Dizdaroglu, M., 2005. Base-excision repair of oxidative DNA damage by DNA glycosylases. *Mutat Res* 591, 45–59. <https://doi.org/10.1016/j.mrfmmm.2005.01.033>
- Doetsch, P., Beljanski, V., Song, B., 2005. The Ultraviolet Damage Endonuclease (UVDE) Protein and Alternative Excision Repair: A Highly Diverse System for Damage Recognition and Processing. *DNA Damage Recognit.* 223–238.
- Dohet, C., Wagner, R., Radman, M., 1985. Repair of defined single base-pair mismatches in *Escherichia coli*. *Proc. Natl. Acad. Sci. U. S. A.* 82, 503–505. <https://doi.org/10.1073/pnas.82.2.503>
- Doolittle, R.F., Johnson, M.S., Husain, I., Van Houten, B., Thomas, D.C., Sancar, A., 1986. Domainal evolution of a prokaryotic DNA repair protein and its relationship to active-transport proteins. *Nature.* 323, 451–3.
- Earl, A.M., Mohundro, M.M., Mian, I.S., Battista, J.R., 2002. The IrrE protein of *Deinococcus radiodurans* R1 is a novel regulator of recA expression. *J Bacteriol* 184, 6216–24.
- Eisen, J.A., Wu, M., 2002. Phylogenetic analysis and gene functional predictions: phylogenomics in action. *Theor Popul Biol* 61, 481–7.

- Eltsov, M., Dubochet, J., 2005. Fine structure of the *Deinococcus radiodurans* nucleoid revealed by cryoelectron microscopy of vitreous sections. *J Bacteriol* 187, 8047–8054. <https://doi.org/10.1128/Jb.187.23.8047-8054.2005>
- Eryilmaz, J., Ceschini, S., Ryan, J., Geddes, S., Waters, T.R., Barrett, T.E., 2006. Structural insights into the cryptic DNA-dependent ATPase activity of UvrB. *J Mol Biol* 357, 62-72. Epub 2006 Jan 6.
- Fazakerley, G.V., Quignard, E., Woisard, A., Guschlbauer, W., van der Marel, G.A., van Boom, J.H., Jones, M., Radman, M., 1986. Structures of mismatched base pairs in DNA and their recognition by the *Escherichia coli* mismatch repair system. *EMBO J* 5, 3697–3703.
- Fishel, R., 2015. Mismatch Repair. *J. Biol. Chem.* 290, 26395–26403. <https://doi.org/10.1074/jbc.R115.660142>
- Friedberg, E.C., Walker, G.C., Siede, W., Wood, R.D., Schultz, R.A., Ellenberger, T., 2006. *DNA Repair and Mutagenesis*, 2nd ed. ASM Press.
- Fromme, J.C., Banerjee, A., Huang, S.J., Verdine, G.L., 2004. Structural basis for removal of adenine mispaired with 8-oxoguanine by MutY adenine DNA glycosylase. *Nature* 427, 652–656. <https://doi.org/10.1038/nature02306>
- Fromme, J.C., Verdine, G.L., 2003. Structure of a trapped endonuclease III-DNA covalent intermediate. *EMBO J* 22, 3461–71. <https://doi.org/10.1093/emboj/cdg311>
- Fukui, K., 2010. DNA Mismatch Repair in Eukaryotes and Bacteria. *J. Nucleic Acids* 2010. <https://doi.org/10.4061/2010/260512>
- Ganesan, A., Spivak, G., Hanawalt, P.C., 2012. Transcription-coupled DNA repair in prokaryotes. *Prog. Mol. Biol. Transl. Sci.* 110, 25–40. <https://doi.org/10.1016/B978-0-12-387665-2.00002-X>
- Gao, L., Zhou, Z., Chen, X., Zhang, W., Lin, M., Chen, M., 2020. Comparative Proteomics Analysis Reveals New Features of the Oxidative Stress Response in the Polyextremophilic Bacterium *Deinococcus radiodurans*. *Microorganisms* 8. <https://doi.org/10.3390/microorganisms8030451>
- Gerard, E., Jolivet, E., Prieur, D., Forterre, P., 2001. DNA protection mechanisms are not involved in the radioresistance of the hyperthermophilic archaea *Pyrococcus abyssi* and *P. furiosus*. *Mol Genet Genomics* 266, 72–8.
- Ghosal, D., Omelchenko, M.V., Gaidamakova, E.K., Matrosova, V.Y., Vasilenko, A., Venkateswaran, A., Zhai, M., Kostandarithes, H.M., Brim, H., Makarova, K.S., Wackett, L.P., Fredrickson, J.K., Daly, M.J., 2005. How radiation kills cells: survival of *Deinococcus radiodurans* and *Shewanella oneidensis* under oxidative stress. *FEMS Microbiol Rev* 29, 361–75. <https://doi.org/10.1016/j.femsre.2004.12.007>
- Gillet, L.C.J., Schärer, O.D., 2006. Molecular mechanisms of mammalian global genome

nucleotide excision repair. *Chem. Rev.* 106, 253–276. <https://doi.org/10.1021/cr040483f>

- Glickman, M.S., 2014. Double-Strand DNA Break Repair in Mycobacteria. *Microbiol. Spectr.* 2. <https://doi.org/10.1128/microbiolspec.MGM2-0024-2013>
- Goosen, N., Moolenaar, G.F., 2008. Repair of UV damage in bacteria. *DNA Repair Amst* 7, 353–79. <https://doi.org/10.1016/j.dnarep.2007.09.002>
- Goosen, N., Moolenaar, G.F., 2001. Role of ATP hydrolysis by UvrA and UvrB during nucleotide excision repair. *Res Microbiol* 152, 401–9.
- Gorbalenya, A.E., Koonin, E.V., 1993. Helicases: amino acid sequence comparisons and structure-function relationships. *Curr. Opin. Struct. Biol.* 3, 419–429.
- Gorman, J., Chowdhury, A., Surtees, J.A., Shimada, J., Reichman, D.R., Alani, E., Greene, E.C., 2007. Dynamic basis for one-dimensional DNA scanning by the mismatch repair complex Msh2-Msh6. *Mol. Cell* 28, 359–370. <https://doi.org/10.1016/j.molcel.2007.09.008>
- Grossman, L., Thiagalingam, S., 1993. Nucleotide excision repair, a tracking mechanism in search of damage. *J Biol Chem* 268, 16871–4.
- Guarné, A., Charbonnier, J.-B., 2015. Insights from a decade of biophysical studies on MutL: Roles in strand discrimination and mismatch removal. *Prog. Biophys. Mol. Biol.* 117, 149–156. <https://doi.org/10.1016/j.pbiomolbio.2015.02.002>
- Hamm, M.L., Gill, T.J., Nicolson, S.C., Summers, M.R., 2007. Substrate specificity of Fpg (MutM) and hOGG1, two repair glycosylases. *J. Am. Chem. Soc.* 129, 7724–7725. <https://doi.org/10.1021/ja0716453>
- Hansen, M.T., 1978. Multiplicity of genome equivalents in the radiation-resistant bacterium *Micrococcus radiodurans*. *J Bacteriol* 134, 71–5.
- Harsojo, Kitayama, S., Matsuyama, A., 1981. Genome multiplicity and radiation resistance in *Micrococcus radiodurans*. *J Biochem* 90, 877–80.
- Hawkins, C.L., Davies, M.J., 2001. Generation and propagation of radical reactions on proteins. *Biochim. Biophys. Acta* 1504, 196–219. [https://doi.org/10.1016/s0005-2728\(00\)00252-8](https://doi.org/10.1016/s0005-2728(00)00252-8)
- Hollis, T., Ichikawa, Y., Ellenberger, T., 2000. DNA bending and a flip-out mechanism for base excision by the helix-hairpin-helix DNA glycosylase, *Escherichia coli* AlkA. *EMBO J.* 19, 758–766. <https://doi.org/10.1093/emboj/19.4.758>
- Hopfner, K.P., Tainer, J.A., 2003. Rad50/SMC proteins and ABC transporters: unifying concepts from high-resolution structures. *Curr Opin Struct Biol* 13, 249–55.
- Horikoshi, N., Tachiwana, H., Kagawa, W., Osakabe, A., Matsumoto, S., Iwai, S., Sugasawa, K., Kurumizaka, H., 2016. Crystal structure of the nucleosome containing ultraviolet light-induced cyclobutane pyrimidine dimer. *Biochem. Biophys. Res. Commun.* 471, 117–122. <https://doi.org/10.1016/j.bbrc.2016.01.170>

- Hsu, D.S., Kim, S.T., Sun, Q., Sancar, A., 1995. Structure and function of the UvrB protein. *J Biol Chem* 270, 8319–27.
- Hu, C., Zhao, Y., Sun, H., Yang, Y., 2017. Synergism of Dam, MutH, and MutS in methylation-directed mismatch repair in *Escherichia coli*. *Mutat. Res.* 795, 31–33. <https://doi.org/10.1016/j.mrfmmm.2016.12.002>
- Hughes, C.D., Wang, H., Ghodke, H., Simons, M., Towheed, A., Peng, Y., Van Houten, B., Kad, N.M., 2013. Real-time single-molecule imaging reveals a direct interaction between UvrC and UvrB on DNA tightropes. *Nucleic Acids Res* 41, 4901–12. <https://doi.org/10.1093/nar/gkt177>
- Husain, I., Van Houten, B., Thomas, D.C., Abdel-Monem, M., Sancar, A., 1985. Effect of DNA polymerase I and DNA helicase II on the turnover rate of UvrABC excision nuclease. *Proc Natl Acad Sci U A* 82, 6774–8.
- Ivancic-Bace, I., Peharec, P., Moslavac, S., Skrobot, N., Salaj-Smic, E., Brcic-Kostic, K., 2003. RecFOR Function Is Required for DNA Repair and Recombination in a RecA Loading-Deficient recB Mutant of *Escherichia coli*. *Genetics* 163, 485–94.
- Jaciuk, M., Nowak, E., Skowronek, K., Tanska, A., Nowotny, M., 2011. Structure of UvrA nucleotide excision repair protein in complex with modified DNA. *Nat Struct Mol Biol* 18, 191–7. <https://doi.org/10.1038/nsmb.1973>
- Jaciuk, M., Swuec, P., Gaur, V., Kasprzak, J.M., Renault, L., Dobrychłop, M., Nirwal, S., Bujnicki, J.M., Costa, A., Nowotny, M., 2020. A combined structural and biochemical approach reveals translocation and stalling of UvrB on the DNA lesion as a mechanism of damage verification in bacterial nucleotide excision repair. *DNA Repair* 85, 102746. <https://doi.org/10.1016/j.dnarep.2019.102746>
- Jacobs, A.L., Schar, P., 2012. DNA glycosylases: in DNA repair and beyond. *Chromosoma* 121, 1–20. <https://doi.org/10.1007/s00412-011-0347-4>
- Jiang, G.H., Skovvaga, M., Croteau, D.L., Van Houten, B., States, J.C., 2006. Robust incision of Benzo[a]pyrene-7,8-dihydrodiol-9,10-epoxide-DNA adducts by a recombinant thermoresistant interspecies combination UvrABC endonuclease system. *Biochemistry* 45, 7834–43. <https://doi.org/10.1021/bi052515e>
- Jiang, J., Bai, L., Surtees, J.A., Gemici, Z., Wang, M.D., Alani, E., 2005. Detection of high-affinity and sliding clamp modes for MSH2-MSH6 by single-molecule unzipping force analysis. *Mol. Cell* 20, 771–781. <https://doi.org/10.1016/j.molcel.2005.10.014>
- Johnson, P.E., Joshi, M.D., Tomme, P., Kilburn, D.G., McIntosh, L.P., 1996. Structure of the N-terminal cellulose-binding domain of *Cellulomonas fimi* CenC determined by nuclear magnetic resonance spectroscopy. *Biochemistry* 35, 14381–94.
- Junop, M.S., Obmolova, G., Rausch, K., Hsieh, P., Yang, W., 2001. Composite active site of an

ABC ATPase: MutS uses ATP to verify mismatch recognition and authorize DNA repair. *Mol. Cell* 7, 1–12. [https://doi.org/10.1016/s1097-2765\(01\)00149-6](https://doi.org/10.1016/s1097-2765(01)00149-6)

- Kad, N.M., Van Houten, B., 2012. Dynamics of lesion processing by bacterial nucleotide excision repair proteins. *Prog. Mol. Biol. Transl. Sci.* 110, 1–24. <https://doi.org/10.1016/B978-0-12-387665-2.00001-8>
- Kad, N.M., Wang, H., Kennedy, G.G., Warshaw, D.M., Van Houten, B., 2010. Collaborative dynamic DNA scanning by nucleotide excision repair proteins investigated by single-molecule imaging of quantum-dot-labeled proteins. *Mol Cell* 37, 702–13. <https://doi.org/10.1016/j.molcel.2010.02.003>
- Karakas, E., Truglio, J.J., Croteau, D., Rhau, B., Wang, L., Van Houten, B., Kisker, C., 2007. Structure of the C-terminal half of UvrC reveals an RNase H endonuclease domain with an Argonaute-like catalytic triad. *EMBO J* 26, 613–22. <https://doi.org/10.1038/sj.emboj.7601497>
- Kisker, C., Kuper, J., Van Houten, B., 2013. Prokaryotic nucleotide excision repair. *Cold Spring Harb Perspect Biol* 5, a012591. <https://doi.org/10.1101/cshperspect.a012591>
- Koo, H.S., Claassen, L., Grossman, L., Liu, L.F., 1991. ATP-dependent partitioning of the DNA template into supercoiled domains by *Escherichia coli* UvrAB. *Proc. Natl. Acad. Sci. U. S. A.* 88, 1212–1216. <https://doi.org/10.1073/pnas.88.4.1212>
- Kow, Y.W., 1994. Base excision repair in *E. coli*--an overview. *Ann. N. Y. Acad. Sci.* 726, 178–180. <https://doi.org/10.1111/j.1749-6632.1994.tb52812.x>
- Kow, Y.W., Wallace, S.S., Van Houten, B., 1990. UvrABC nuclease complex repairs thymine glycol, an oxidative DNA base damage. *Mutat. Res.* 235, 147–156. [https://doi.org/10.1016/0921-8777\(90\)90068-g](https://doi.org/10.1016/0921-8777(90)90068-g)
- Kraithong, T., Channgam, K., Itsathitphaisarn, O., Tiensuwan, M., Jeruzalmi, D., Pakotiprapha, D., 2017. Movement of the β -hairpin in the third zinc-binding module of UvrA is required for DNA damage recognition. *DNA Repair* 51, 60–69. <https://doi.org/10.1016/j.dnarep.2017.02.003>
- Kramer, B., Kramer, W., Fritz, H.J., 1984. Different base/base mismatches are corrected with different efficiencies by the methyl-directed DNA mismatch-repair system of *E. coli*. *Cell* 38, 879–887. [https://doi.org/10.1016/0092-8674\(84\)90283-6](https://doi.org/10.1016/0092-8674(84)90283-6)
- Krisko, A., Radman, M., 2013. Biology of extreme radiation resistance: the way of *Deinococcus radiodurans*. *Cold Spring Harb Perspect Biol* 5. <https://doi.org/10.1101/cshperspect.a012765>
- Krokan, H.E., Standal, R., Slupphaug, G., 1997. DNA glycosylases in the base excision repair of DNA. *Biochem. J.* 325 (Pt 1), 1–16. <https://doi.org/10.1042/bj3250001>
- Kumar, N., Raja, S., Van Houten, B., 2020. The involvement of nucleotide excision repair

proteins in the removal of oxidative DNA damage. *Nucleic Acids Res.* 48, 11227–11243.
<https://doi.org/10.1093/nar/gkaa777>

- Kunkel, T.A., Erie, D.A., 2005. DNA mismatch repair. *Annu. Rev. Biochem.* 74, 681–710.
<https://doi.org/10.1146/annurev.biochem.74.082803.133243>
- Kurthkoti, K., Kumar, P., Sang, P.B., Varshney, U., 2020. Base excision repair pathways of bacteria: new promise for an old problem. *Future Med. Chem.*
<https://doi.org/10.4155/fmc-2019-0267>
- Lacks, S.A., Dunn, J.J., Greenberg, B., 1982. Identification of base mismatches recognized by the heteroduplex-DNA-repair system of *Streptococcus pneumoniae*. *Cell* 31, 327–336.
[https://doi.org/10.1016/0092-8674\(82\)90126-x](https://doi.org/10.1016/0092-8674(82)90126-x)
- Lee, H.-W., Brice, A.R., Wright, C.B., Dominy, B.N., Cao, W., 2010. Identification of *Escherichia coli* Mismatch-specific Uracil DNA Glycosylase as a Robust Xanthine DNA Glycosylase. *J. Biol. Chem.* 285, 41483–41490. <https://doi.org/10.1074/jbc.M110.150003>
- Lee, J.Y., Yang, W., 2006. UvrD helicase unwinds DNA one base pair at a time by a two-part power stroke. *Cell* 127, 1349–60. <https://doi.org/10.1016/j.cell.2006.10.049>
- Lee, S.-J., Sung, R.-J., Verdine, G.L., 2019. Mechanism of DNA Lesion Homing and Recognition by the Uvr Nucleotide Excision Repair System [WWW Document]. *Research*. URL <https://spj.sciencemag.org/research/2019/5641746/> (accessed 6.2.20).
- Li, G.-M., 2008. Mechanisms and functions of DNA mismatch repair. *Cell Res.* 18, 85–98.
<https://doi.org/10.1038/cr.2007.115>
- Lieb, M., 1987. Bacterial genes *mutL*, *mutS*, and *dcm* participate in repair of mismatches at 5-methylcytosine sites. *J. Bacteriol.* 169, 5241–5246.
- Lin, J.J., Sancar, A., 1992. Active site of (A)BC excinuclease. I. Evidence for 5' incision by UvrC through a catalytic site involving Asp399, Asp438, Asp466, and His538 residues. *J. Biol. Chem.* 267, 17688–17692.
- Lindahl, T., 1993. Instability and decay of the primary structure of DNA. *Nature* 362, 709–15. <https://doi.org/10.1038/362709a0>
- Lipton, M.S., Paša-Tolić, L., Anderson, G.A., Anderson, D.J., Auberry, D.L., Battista, J.R., Daly, M.J., Fredrickson, J., Hixson, K.K., Kostandarithes, H., Masselon, C., Markillie, L.M., Moore, R.J., Romine, M.F., Shen, Y., Stritmatter, E., Tolić, N., Udseth, H.R., Venkateswaran, A., Wong, K.-K., Zhao, R., Smith, R.D., 2002. Global analysis of the *Deinococcus radiodurans* proteome by using accurate mass tags. *Proc. Natl. Acad. Sci. U. S. A.* 99, 11049–11054.
<https://doi.org/10.1073/pnas.172170199>
- Liu, Y., Zhou, J., Omelchenko, M.V., Beliaev, A.S., Venkateswaran, A., Stair, J., Wu, L., Thompson, D.K., Xu, D., Rogozin, I.B., Gaidamakova, E.K., Zhai, M., Makarova, K.S., Koonin, E.V., Daly, M.J., 2003. Transcriptome dynamics of *Deinococcus radiodurans* recovering

from ionizing radiation. *Proc Natl Acad Sci U A* 100, 4191–6. Epub 2003 Mar 21.

- Locher, K.P., 2004. Structure and mechanism of ABC transporters. *Curr Opin Struct Biol* 14, 426–31. <https://doi.org/10.1016/j.sbi.2004.06.005>
- Lomovskaya, N., Hong, S.K., Kim, S.U., Fonstein, L., Furuya, K., Hutchinson, R.C., 1996. The *Streptomyces peucetius* *drnC* gene encodes a UvrA-like protein involved in daunorubicin resistance and production. *J Bacteriol* 178, 3238–45.
- Lovett, S.T., 2011. The DNA exonucleases of *Escherichia coli*. *EcoSal Plus* 4. <https://doi.org/10.1128/ecosalplus.4.4.7>
- Lovett, S.T., Clark, A.J., 1984. Genetic analysis of the *recJ* gene of *Escherichia coli* K-12. *J. Bacteriol.* 157, 190–196.
- Lovett, S.T., Kolodner, R.D., 1989. Identification and purification of a single-stranded-DNA-specific exonuclease encoded by the *recJ* gene of *Escherichia coli*. *Proc. Natl. Acad. Sci. U. S. A.* 86, 2627–2631. <https://doi.org/10.1073/pnas.86.8.2627>
- Lu, A.L., Li, X., Gu, Y., Wright, P.M., Chang, D.Y., 2001. Repair of oxidative DNA damage: mechanisms and functions. *Cell Biochem. Biophys.* 35, 141–170. <https://doi.org/10.1385/CBB:35:2:141>
- Machius, M., Henry, L., Palnitkar, M., Deisenhofer, J., 1999. Crystal structure of the DNA nucleotide excision repair enzyme UvrB from *Thermus thermophilus*. *Proc Natl Acad Sci U A* 96, 11717–22.
- Madian, A.G., Regnier, F.E., 2010. Proteomic identification of carbonylated proteins and their oxidation sites. *J. Proteome Res.* 9, 3766–3780. <https://doi.org/10.1021/pr1002609>
- Makarova, K.S., Aravind, L., Wolf, Y.I., Tatusov, R.L., Minton, K.W., Koonin, E.V., Daly, M.J., 2001. Genome of the extremely radiation-resistant bacterium *Deinococcus radiodurans* viewed from the perspective of comparative genomics. *Microbiol Mol Biol Rev* 65, 44–79.
- Malta, E., Moolenaar, G.F., Goosen, N., 2007. Dynamics of the UvrABC nucleotide excision repair proteins analyzed by fluorescence resonance energy transfer. *Biochemistry* 46, 9080–8. <https://doi.org/10.1021/bi7002235>
- Maluf, N. K., Ali, J.A., Lohman, T.M., 2003. Kinetic mechanism for formation of the active, dimeric UvrD helicase-DNA complex. *J Biol Chem* 278, 31930–40. <https://doi.org/10.1074/jbc.M304223200>
- Maluf, Nasib K., Fischer, C.J., Lohman, T.M., 2003. A Dimer of *Escherichia coli* UvrD is the active form of the helicase in vitro. *J. Mol. Biol.* 325, 913–935. [https://doi.org/10.1016/s0022-2836\(02\)01277-9](https://doi.org/10.1016/s0022-2836(02)01277-9)
- Manelyte, L., Guy, C.P., Smith, R.M., Dillingham, M.S., McGlynn, P., Savery, N.J., 2009. The unstructured C-terminal extension of UvrD interacts with UvrB, but is dispensable for nucleotide excision repair. *DNA Repair Amst* 8, 1300–10.

<https://doi.org/10.1016/j.dnarep.2009.08.005>

- Manelyte, L., Kim, Y.-I.T., Smith, A.J., Smith, R.M., Savery, N.J., 2010. Regulation and Rate Enhancement during Transcription-Coupled DNA Repair. *Mol. Cell* 40, 714–724. <https://doi.org/10.1016/j.molcel.2010.11.012>
- Manuel, R.C., Hitomi, K., Arvai, A.S., House, P.G., Kurtz, A.J., Dodson, M.L., McCullough, A.K., Tainer, J.A., Lloyd, R.S., 2004. Reaction intermediates in the catalytic mechanism of *Escherichia coli* MutY DNA glycosylase. *J. Biol. Chem.* 279, 46930–46939. <https://doi.org/10.1074/jbc.M403944200>
- Matson, S.W., George, J.W., 1987. DNA helicase II of *Escherichia coli*. Characterization of the single-stranded DNA-dependent NTPase and helicase activities. *J Biol Chem* 262, 2066–76.
- Matson, S.W., Robertson, A.B., 2006. The UvrD helicase and its modulation by the mismatch repair protein MutL. *Nucleic Acids Res* 34, 4089–97. <https://doi.org/10.1093/nar/gkl450>
- Mattimore, V., Battista, J.R., 1996. Radioresistance of *Deinococcus radiodurans*: Functions necessary to survive ionizing radiation are also necessary to survive prolonged desiccation. *J Bacteriol* 178, 633–637.
- Mazloum, N., Stegman, M.A., Croteau, D.L., Van Houten, B., Kwon, N.S., Ling, Y., Dickinson, C., Venugopal, A., Towheed, M.A., Nathan, C., 2011. Identification of a chemical that inhibits the mycobacterial UvrABC complex in nucleotide excision repair. *Biochemistry* 50, 1329–35. <https://doi.org/10.1021/bi101674c>
- Mazur, S.J., Grossman, L., 1991. Dimerization of *Escherichia coli* UvrA and its binding to undamaged and ultraviolet light damaged DNA. *Biochemistry* 30, 4432–43.
- McCann, J.A.B., Berti, P.J., 2008. Transition-state analysis of the DNA repair enzyme MutY. *J. Am. Chem. Soc.* 130, 5789–5797. <https://doi.org/10.1021/ja711363s>
- McCullough, A.K., Dodson, M.L., Lloyd, R.S., 1999. Initiation of base excision repair: glycosylase mechanisms and structures. *Annu. Rev. Biochem.* 68, 255–285. <https://doi.org/10.1146/annurev.biochem.68.1.255>
- McKibbin, P.L., Fleming, A.M., Towheed, M.A., Van Houten, B., Burrows, C.J., David, S.S., 2013. Repair of hydantoin lesions and their amine adducts in DNA by base and nucleotide excision repair. *J Am Chem Soc* 135, 13851–61. <https://doi.org/10.1021/ja4059469>
- Mol, C.D., Parikh, S.S., Putnam, C.D., Lo, T.P., Tainer, J.A., 1999. DNA repair mechanisms for the recognition and removal of damaged DNA bases. *Annu. Rev. Biophys. Biomol. Struct.* 28, 101–128. <https://doi.org/10.1146/annurev.biophys.28.1.101>
- Moolenaar, G.F., Bazuine, M., van Knippenberg, I.C., Visse, R., Goosen, N., 1998a. Characterization of the *Escherichia coli* damage-independent UvrBC endonuclease

activity. *J. Biol. Chem.* 273, 34896–34903. <https://doi.org/10.1074/jbc.273.52.34896>

- Moolenaar, G.F., Franken, K.L., Dijkstra, D.M., Thomas-Oates, J.E., Visse, R., van de Putte, P., Goosen, N., 1995. The C-terminal region of the UvrB protein of *Escherichia coli* contains an important determinant for UvrC binding to the preincision complex but not the catalytic site for 3'-incision. *J Biol Chem* 270, 30508–15.
- Moolenaar, G.F., Franken, K.L., van de Putte, P., Goosen, N., 1997. Function of the homologous regions of the *Escherichia coli* DNA excision repair proteins UvrB and UvrC in stabilization of the UvrBC-DNA complex and in 3'-incision. *Mutat. Res.* 385, 195–203. [https://doi.org/10.1016/s0921-8777\(97\)00042-6](https://doi.org/10.1016/s0921-8777(97)00042-6)
- Moolenaar, G.F., Herron, M.F., Monaco, V., van der Marel, G.A., van Boom, J.H., Visse, R., Goosen, N., 2000a. The role of ATP binding and hydrolysis by UvrB during nucleotide excision repair. *J Biol Chem* 275, 8044–50.
- Moolenaar, G.F., Höglund, L., Goosen, N., 2001. Clue to damage recognition by UvrB: residues in the beta-hairpin structure prevent binding to non-damaged DNA. *EMBO J.* 20, 6140–6149. <https://doi.org/10.1093/emboj/20.21.6140>
- Moolenaar, G.F., Monaco, V., van der Marel, G.A., van Boom, J.H., Visse, R., Goosen, N., 2000b. The effect of the DNA flanking the lesion on formation of the UvrB-DNA preincision complex. Mechanism for the UvrA-mediated loading of UvrB onto a DNA damaged site. *J Biol Chem* 275, 8038–43.
- Moolenaar, G.F., Moorman, C., Goosen, N., 2000c. Role of the *Escherichia coli* nucleotide excision repair proteins in DNA replication. *J. Bacteriol.* 182, 5706–5714. <https://doi.org/10.1128/jb.182.20.5706-5714.2000>
- Moolenaar, G.F., Uiterkamp, R.S., Zwijnenburg, D.A., Goosen, N., 1998b. The C-terminal region of the *Escherichia coli* UvrC protein, which is homologous to the C-terminal region of the human ERCC1 protein, is involved in DNA binding and 5'-incision. *Nucleic Acids Res.* 26, 462–468. <https://doi.org/10.1093/nar/26.2.462>
- Moolenaar, G.F., van Rossum-Fikkert, S., van Kesteren, M., Goosen, N., 2002. Cho, a second endonuclease involved in *Escherichia coli* nucleotide excision repair. *Proc. Natl. Acad. Sci. U. S. A.* 99, 1467–1472. <https://doi.org/10.1073/pnas.032584099>
- Morita, R., Nakane, S., Shimada, A., Inoue, M., Iino, H., Wakamatsu, T., Fukui, K., Nakagawa, N., Masui, R., Kuramitsu, S., 2010. Molecular Mechanisms of the Whole DNA Repair System: A Comparison of Bacterial and Eukaryotic Systems [WWW Document]. *J. Nucleic Acids*. <https://doi.org/10.4061/2010/179594>
- Moseley, B.E., Copland, H.J., 1975. Isolation and properties of a recombination-deficient mutant of *Micrococcus radiodurans*. *J. Bacteriol.* 121, 422–428.
- Munteanu, A.-C., Uivarosi, V., Andries, A., 2015. Recent progress in understanding the

molecular mechanisms of radioresistance in *Deinococcus* bacteria. *Extrem. Life Extreme Cond.* 19, 707–719. <https://doi.org/10.1007/s00792-015-0759-9>

- Myles, G.M., Sancar, A., 1991. Isolation and characterization of functional domains of UvrA. *Biochemistry* 30, 3834–40.
- Nakagawa, N., Masui, R., Kato, R., Kuramitsu, S., 1997. Domain structure of *Thermus thermophilus* UvrB protein. Similarity in domain structure to a helicase. *J Biol Chem* 272, 22703–13.
- Nakagawa, N., Sugahara, M., Masui, R., Kato, R., Fukuyama, K., Kuramitsu, S., 1999. Crystal structure of *Thermus thermophilus* HB8 UvrB protein, a key enzyme of nucleotide excision repair. *J Biochem* 126, 986–90.
- Navaratnam, S., Myles, G.M., Strange, R.W., Sancar, A., 1989. Evidence from extended X-ray absorption fine structure and site-specific mutagenesis for zinc fingers in UvrA protein of *Escherichia coli*. *J Biol Chem* 264, 16067–71.
- Nestmann, E.R., 1977. Antimutagenic effects of spermine and guanosine in continuous cultures of *Escherichia coli* mutator strain mutH. *Mol. Gen. Genet. MGG* 152, 109–110. <https://doi.org/10.1007/bf00264947>
- Nikitaki, Z., Hellweg, C.E., Georgakilas, A.G., Ravanat, J.-L., 2015. Stress-induced DNA damage biomarkers: applications and limitations. *Front. Chem.* 3, 35. <https://doi.org/10.3389/fchem.2015.00035>
- O'Brien, P.J., Ellenberger, T., 2004. The *Escherichia coli* 3-methyladenine DNA glycosylase AlkA has a remarkably versatile active site. *J. Biol. Chem.* 279, 26876–26884. <https://doi.org/10.1074/jbc.M403860200>
- Oh, E.Y., Claassen, L., Thiagalingam, S., Mazur, S., Grossman, L., 1989. ATPase activity of the UvrA and UvrAB protein complexes of the *Escherichia coli* UvrABC endonuclease. *Nucleic Acids Res.* 17, 4145–4159. <https://doi.org/10.1093/nar/17.11.4145>
- Oh, E.Y., Grossman, L., 1987. Helicase properties of the *Escherichia coli* UvrAB protein complex. *Proc. Natl. Acad. Sci. U. S. A.* 84, 3638–3642. <https://doi.org/10.1073/pnas.84.11.3638>
- Orren, D.K., Sancar, A., 1990. Formation and enzymatic properties of the UvrB.DNA complex. *J Biol Chem* 265, 15796–803.
- Orren, D.K., Sancar, A., 1989. The (A)BC excinuclease of *Escherichia coli* has only the UvrB and UvrC subunits in the incision complex. *Proc Natl Acad Sci U A* 86, 5237–41.
- Orren, D.K., Selby, C.P., Hearst, J.E., Sancar, A., 1992. Post-incision steps of nucleotide excision repair in *Escherichia coli*. Disassembly of the UvrBC-DNA complex by helicase II and DNA polymerase I. *J. Biol. Chem.* 267, 780–788.
- Osakabe, A., Tachiwana, H., Kagawa, W., Horikoshi, N., Matsumoto, S., Hasegawa, M.,

- Matsumoto, N., Toga, T., Yamamoto, J., Hanaoka, F., Thomä, N.H., Sugasawa, K., Iwai, S., Kurumizaka, H., 2015. Structural basis of pyrimidine-pyrimidone (6-4) photoproduct recognition by UV-DDB in the nucleosome. *Sci. Rep.* 5, 16330. <https://doi.org/10.1038/srep16330>
- Ott, E., Kawaguchi, Y., Kölbl, D., Chaturvedi, P., Nakagawa, K., Yamagishi, A., Weckwerth, W., Milojevic, T., 2017. Proteometabolomic response of *Deinococcus radiodurans* exposed to UVC and vacuum conditions: Initial studies prior to the Tanpopo space mission. *PLoS ONE* 12. <https://doi.org/10.1371/journal.pone.0189381>
 - Pakotiprapha, D., Inuzuka, Y., Bowman, B.R., Moolenaar, G.F., Goosen, N., Jeruzalmi, D., Verdine, G.L., 2008. Crystal structure of *Bacillus stearothermophilus* UvrA provides insight into ATP-modulated dimerization, UvrB interaction, and DNA binding. *Mol Cell* 29, 122–33. <https://doi.org/10.1016/j.molcel.2007.10.026>
 - Pakotiprapha, D., Jeruzalmi, D., 2013. Small-angle X-ray scattering reveals architecture and A(2)B(2) stoichiometry of the UvrA-UvrB DNA damage sensor. *Proteins* 81, 132–9. <https://doi.org/10.1002/prot.24170>
 - Pakotiprapha, D., Liu, Y., Verdine, G.L., Jeruzalmi, D., 2009. A structural model for the damage-sensing complex in bacterial nucleotide excision repair. *J. Biol. Chem.* 284, 12837–12844. <https://doi.org/10.1074/jbc.M900571200>
 - Pakotiprapha, D., Samuels, M., Shen, K., Hu, J.H., Jeruzalmi, D., 2012. Structure and mechanism of the UvrA-UvrB DNA damage sensor. *Nat. Struct. Mol. Biol.* 19, 291–298. <https://doi.org/10.1038/nsmb.2240>
 - Pang, P.P., Lundberg, A.S., Walker, G.C., 1985. Identification and characterization of the mutL and mutS gene products of *Salmonella typhimurium* LT2. *J. Bacteriol.* 163, 1007–1015.
 - Parikh, S.S., Mol, C.D., Hosfield, D.J., Tainer, J.A., 1999. Envisioning the molecular choreography of DNA base excision repair. *Curr. Opin. Struct. Biol.* 9, 37–47. [https://doi.org/10.1016/s0959-440x\(99\)80006-2](https://doi.org/10.1016/s0959-440x(99)80006-2)
 - Park, H.W., Kim, S.T., Sancar, A., Deisenhofer, J., 1995. Crystal structure of DNA photolyase from *Escherichia coli*. *Science*. 268, 1866–72.
 - Parker, J.B., Bianchet, M.A., Krosky, D.J., Friedman, J.I., Amzel, L.M., Stivers, J.T., 2007. Enzymatic capture of an extrahelical thymine in the search for uracil in DNA. *Nature* 449, 433–437. <https://doi.org/10.1038/nature06131>
 - Paspaleva, K., Thomassen, E., Pannu, N.S., Iwai, S., Moolenaar, G.F., Goosen, N., Abrahams, J.P., 2007. Crystal structure of the DNA repair enzyme ultraviolet damage endonuclease. *Struct. Lond. Engl.* 15, 1316–1324. <https://doi.org/10.1016/j.str.2007.05.010>
 - Pegg, A.E., 2000. Repair of O(6)-alkylguanine by alkyltransferases. *Mutat. Res.* 462, 83–

100. [https://doi.org/10.1016/s1383-5742\(00\)00017-x](https://doi.org/10.1016/s1383-5742(00)00017-x)

- Pitcher, R.S., Brissett, N.C., Doherty, A.J., 2007. Nonhomologous end-joining in bacteria: a microbial perspective. *Annu. Rev. Microbiol.* 61, 259–282. <https://doi.org/10.1146/annurev.micro.61.080706.093354>
- Priyakumar, U.D., MacKerell, A.D., 2006. Computational approaches for investigating base flipping in oligonucleotides. *Chem. Rev.* 106, 489–505. <https://doi.org/10.1021/cr040475z>
- Qi, Y., Spong, M.C., Nam, K., Banerjee, A., Jiralerspong, S., Karplus, M., Verdine, G.L., 2009. Encounter and extrusion of an intrahelical lesion by a DNA repair enzyme. *Nature* 462, 762–766. <https://doi.org/10.1038/nature08561>
- Rastogi, R.P., Richa, null, Kumar, A., Tyagi, M.B., Sinha, R.P., 2010. Molecular mechanisms of ultraviolet radiation-induced DNA damage and repair. *J. Nucleic Acids* 2010, 592980. <https://doi.org/10.4061/2010/592980>
- Ravanat, J.L., Douki, T., Cadet, J., 2001. Direct and indirect effects of UV radiation on DNA and its components. *J. Photochem. Photobiol. B* 63, 88–102. [https://doi.org/10.1016/s1011-1344\(01\)00206-8](https://doi.org/10.1016/s1011-1344(01)00206-8)
- Rill, N., Mukhortava, A., Lorenz, S., Tessmer, I., 2020. Alkyltransferase-like protein clusters scan DNA rapidly over long distances and recruit NER to alkyl-DNA lesions. *Proc. Natl. Acad. Sci.* 117, 9318–9328. <https://doi.org/10.1073/pnas.1916860117>
- Rocha, E.P., Cornet, E., Michel, B., 2005. Comparative and evolutionary analysis of the bacterial homologous recombination systems. *PLoS Genet* 1, e15.
- Rossi, F., Khanduja, J.S., Bortoluzzi, A., Houghton, J., Sander, P., Güthlein, C., Davis, E.O., Springer, B., Böttger, E.C., Relini, A., Penco, A., Muniyappa, K., Rizzi, M., 2011. The biological and structural characterization of *Mycobacterium tuberculosis* UvrA provides novel insights into its mechanism of action. *Nucleic Acids Res.* 39, 7316–7328. <https://doi.org/10.1093/nar/gkr271>
- Rothfuss, H., Lara, J.C., Schmid, A.K., Lidstrom, M.E., 2006. Involvement of the S-layer proteins Hpi and SlpA in the maintenance of cell envelope integrity in *Deinococcus radiodurans* R1. *Microbiology* 152, 2779–87. <https://doi.org/10.1099/mic.0.28971-0>
- Sancar, A., Rupp, W.D., 1983. A novel repair enzyme: UVRABC excision nuclease of *Escherichia coli* cuts a DNA strand on both sides of the damaged region. *Cell.* 33, 249–60.
- Sancar, G.B., Sancar, A., Rupp, W.D., 1984. Sequences of the *E. coli* uvrC gene and protein. *Nucleic Acids Res.* 12, 4593–4608. <https://doi.org/10.1093/nar/12.11.4593>
- Sandler, S.J., Clark, A.J., 1994. RecOR suppression of recF mutant phenotypes in *Escherichia coli* K-12. *J Bacteriol* 176, 3661–72.
- Santos, S.P., Yang, Y., Rosa, M.T.G., Rodrigues, M.A.A., De La Tour, C.B., Sommer, S., Teixeira,

- M., Carrondo, M.A., Cloetens, P., Abreu, I.A., Romão, C.V., 2019. The interplay between Mn and Fe in *Deinococcus radiodurans* triggers cellular protection during paraquat-induced oxidative stress. *Sci. Rep.* 9, 17217. <https://doi.org/10.1038/s41598-019-53140-2>
- Sarre, A., Stelter, M., Rollo, F., De Bonis, S., Seck, A., Hognon, C., Ravanat, J.-L., Monari, A., Dehez, F., Moe, E., Timmins, J., 2019. The three Endonuclease III variants of *Deinococcus radiodurans* possess distinct and complementary DNA repair activities. *DNA Repair* 78, 45–59. <https://doi.org/10.1016/j.dnarep.2019.03.014>
 - Schofield, M.J., Hsieh, P., 2003. DNA mismatch repair: molecular mechanisms and biological function. *Annu. Rev. Microbiol.* 57, 579–608. <https://doi.org/10.1146/annurev.micro.57.030502.090847>
 - Seeley, T.W., Grossman, L., 1990. The role of *Escherichia coli* UvrB in nucleotide excision repair. *J Biol Chem* 265, 7158–65.
 - Seeley, T.W., Grossman, L., 1989. Mutations in the *Escherichia coli* UvrB ATPase motif compromise excision repair capacity. *Proc Natl Acad Sci U A* 86, 6577–81.
 - Selby, C.P., 2017. Mfd Protein and Transcription-Repair Coupling in *Escherichia coli*. *Photochem. Photobiol.* 93, 280–295. <https://doi.org/10.1111/php.12675>
 - Shanabruch, W.G., Behlau, I., Walker, G.C., 1981. Spontaneous mutators of *salmonella typhimurium* LT2 generated by insertion of transposable elements. *J. Bacteriol.* 147, 827–835.
 - Sharma, A., Gaidamakova, E.K., Matrosova, V.Y., Bennett, B., Daly, M.J., Hoffman, B.M., 2013. Responses of Mn²⁺ speciation in *Deinococcus radiodurans* and *Escherichia coli* to γ -radiation by advanced paramagnetic resonance methods. *Proc. Natl. Acad. Sci. U. S. A.* 110, 5945–5950. <https://doi.org/10.1073/pnas.1303376110>
 - Shi, Q., Thresher, R., Sancar, A., Griffith, J., 1992. Electron microscopic study of (A)BC excinuclease. DNA is sharply bent in the UvrB-DNA complex. *J Mol Biol* 226, 425–32.
 - Shuman, S., Glickman, M.S., 2007. Bacterial DNA repair by non-homologous end joining. *Nat Rev Microbiol* 5, 852–61. <https://doi.org/10.1038/nrmicro1768>
 - Sibghat-Ullah, null, Sancar, A., Hearst, J.E., 1990. The repair patch of *E. coli* (A)BC excinuclease. *Nucleic Acids Res.* 18, 5051–5053. <https://doi.org/10.1093/nar/18.17.5051>
 - Simmons, L.A., Davies, B.W., Grossman, A.D., Walker, G.C., 2008. Beta clamp directs localization of mismatch repair in *Bacillus subtilis*. *Mol. Cell* 29, 291–301. <https://doi.org/10.1016/j.molcel.2007.10.036>
 - Singh, S., Folkers, G.E., Bonvin, A.M.J.J., Boelens, R., Wechselberger, R., Niztayev, A., Kaptein, R., 2002. Solution structure and DNA-binding properties of the C-terminal domain of UvrC from *E.coli*. *EMBO J.* 21, 6257–6266. <https://doi.org/10.1093/emboj/cdf627>

- Singleton, M.R., Dillingham, M.S., Wigley, D.B., 2007. Structure and mechanism of helicases and nucleic acid translocases. *Annu Rev Biochem* 76, 23–50. <https://doi.org/10.1146/annurev.biochem.76.052305.115300>
- Skorvaga, M., DellaVecchia, M.J., Croteau, D.L., Theis, K., Truglio, J.J., Mandavilli, B.S., Kisker, C., Van Houten, B., 2004. Identification of residues within UvrB that are important for efficient DNA binding and damage processing. *J Biol Chem* 279, 51574–80. <https://doi.org/10.1074/jbc.M409266200>
- Skorvaga, M., Theis, K., Mandavilli, B.S., Kisker, C., Van Houten, B., 2002. The beta -hairpin motif of UvrB is essential for DNA binding, damage processing, and UvrC-mediated incisions. *J Biol Chem* 277, 1553–9. <https://doi.org/10.1074/jbc.M108847200>
- Slade, D., Radman, M., 2011. Oxidative stress resistance in *Deinococcus radiodurans*. *Microbiol Mol Biol Rev* 75, 133–91. <https://doi.org/10.1128/MMBR.00015-10>
- Smith, P.C., Karpowich, N., Millen, L., Moody, J.E., Rosen, J., Thomas, P.J., Hunt, J.F., 2002. ATP binding to the motor domain from an ABC transporter drives formation of a nucleotide sandwich dimer. *Mol Cell* 10, 139–49.
- Sohi, M., Alexandrovich, A., Moolenaar, G., Visse, R., Goosen, N., Vernede, X., Fontecilla-Camps, J.C., Champness, J., Sanderson, M.R., 2000. Crystal structure of *Escherichia coli* UvrB C-terminal domain, and a model for UvrB-uvrC interaction. *FEBS Lett* 465, 161–4.
- Spivak, G., 2015. Nucleotide excision repair in humans. *DNA Repair* 36, 13–18. <https://doi.org/10.1016/j.dnarep.2015.09.003>
- Stelter, M., Acajjaoui, S., McSweeney, S., Timmins, J., 2013. Structural and mechanistic insight into DNA unwinding by *Deinococcus radiodurans* UvrD. *PLoS One* 8, e77364. <https://doi.org/10.1371/journal.pone.0077364>
- Stivers, J.T., 2008. Extrahelical damaged base recognition by DNA glycosylase enzymes. *Chem. Weinh. Bergstr. Ger.* 14, 786–793. <https://doi.org/10.1002/chem.200701501>
- Stivers, J.T., Jiang, Y.L., 2003. A mechanistic perspective on the chemistry of DNA repair glycosylases. *Chem. Rev.* 103, 2729–2759. <https://doi.org/10.1021/cr010219b>
- Stracy, M., Jaciuk, M., Uphoff, S., Kapanidis, A.N., Nowotny, M., Sherratt, D.J., Zawadzki, P., 2016. Single-molecule imaging of UvrA and UvrB recruitment to DNA lesions in living *Escherichia coli*. *Nat. Commun.* 7, 12568. <https://doi.org/10.1038/ncomms12568>
- Sun, B., Wei, K.J., Zhang, B., Zhang, X.H., Dou, S.X., Li, M., Xi, X.G., 2008. Impediment of *E. coli* UvrD by DNA-destabilizing force reveals a strained-inchworm mechanism of DNA unwinding. *EMBO J* 27, 3279–87. <https://doi.org/10.1038/emboj.2008.240>
- Tanaka, M., Earl, A.M., Howell, H.A., Park, M.J., Eisen, J.A., Peterson, S.N., Battista, J.R., 2004. Analysis of *Deinococcus radiodurans*'s transcriptional response to ionizing radiation and desiccation reveals novel proteins that contribute to extreme radioresistance. *Genetics*

168, 21–33. <https://doi.org/10.1534/genetics.104.029249>

- Tanaka, M., Narumi, I., Funayama, T., Kikuchi, M., Watanabe, H., Matsunaga, T., Nikaido, O., Yamamoto, K., 2005. Characterization of pathways dependent on the *uvrE*, *uvrA1*, or *uvrA2* gene product for UV resistance in *Deinococcus radiodurans*. *J Bacteriol* 187, 3693–7.
- Tark, M., Tover, A., Koorits, L., Tegova, R., Kivisaar, M., 2008. Dual role of NER in mutagenesis in *Pseudomonas putida*. *DNA Repair Amst* 7, 20–30. <https://doi.org/10.1016/j.dnarep.2007.07.008>
- Tchou, J., Bodepudi, V., Shibutani, S., Antoshechkin, I., Miller, J., Grollman, A.P., Johnson, F., 1994. Substrate specificity of Fpg protein. Recognition and cleavage of oxidatively damaged DNA. *J. Biol. Chem.* 269, 15318–15324.
- Thayer, M.M., Ahern, H., Xing, D., Cunningham, R.P., Tainer, J.A., 1995. Novel DNA binding motifs in the DNA repair enzyme endonuclease III crystal structure. *EMBO J.* 14, 4108–4120.
- Theis, K., Chen, P.J., Skorvaga, M., Van Houten, B., Kisker, C., 1999. Crystal structure of UvrB, a DNA helicase adapted for nucleotide excision repair. *Embo J* 18, 6899–907.
- Thomas, D.C., Morton, A.G., Bohr, V.A., Sancar, A., 1988. General method for quantifying base adducts in specific mammalian genes. *Proc. Natl. Acad. Sci. U. S. A.* 85, 3723–3727. <https://doi.org/10.1073/pnas.85.11.3723>
- Timmins, J., Gordon, E., Caria, S., Leonard, G., Acajjaoui, S., Kuo, M.S., Monchois, V., McSweeney, S., 2009. Structural and mutational analyses of *Deinococcus radiodurans* UvrA2 provide insight into DNA binding and damage recognition by UvrAs. *Structure* 17, 547–58. <https://doi.org/10.1016/j.str.2009.02.008>
- Timmins, J., Moe, E., 2016. A decade of biochemical and structural studies of the DNA repair machinery of *Deinococcus radiodurans*. *Comput. Struct. Biotechnol. J.* 14, 168–176.
- Travers, A., Muskhelishvili, G., 2015. DNA structure and function. *FEBS J.* 282, 2279–2295. <https://doi.org/10.1111/febs.13307>
- Truglio, J.J., Croteau, D.L., Skorvaga, M., DellaVecchia, M.J., Theis, K., Mandavilli, B.S., Van Houten, B., Kisker, C., 2004. Interactions between UvrA and UvrB: the role of UvrB's domain 2 in nucleotide excision repair. *Embo J* 23, 2498–509. Epub 2004 Jun 10.
- Truglio, J.J., Croteau, D.L., Van Houten, B., Kisker, C., 2006a. Prokaryotic nucleotide excision repair: the UvrABC system. *Chem Rev* 106, 233–52.
- Truglio, J.J., Karakas, E., Rhau, B., Wang, H., DellaVecchia, M.J., Van Houten, B., Kisker, C., 2006b. Structural basis for DNA recognition and processing by UvrB. *Nat Struct Mol Biol* 13, 360–4. Epub 2006 Mar 12.
- Truglio, J.J., Rhau, B., Croteau, D.L., Wang, L., Skorvaga, M., Karakas, E., DellaVecchia, M.J.,

Wang, H., Van Houten, B., Kisker, C., 2005. Structural insights into the first incision reaction during nucleotide excision repair. *EMBO J* 24, 885–94. <https://doi.org/10.1038/sj.emboj.7600568>

- Tubbs, A., Nussenzweig, A., 2017. Endogenous DNA Damage as a Source of Genomic Instability in Cancer. *Cell* 168, 644–656. <https://doi.org/10.1016/j.cell.2017.01.002>
- Tubbs, J.L., Tainer, J.A., 2010. Alkyltransferase-like proteins: Molecular switches between DNA repair pathways. *Cell. Mol. Life Sci. CMLS* 67, 3749–3762. <https://doi.org/10.1007/s00018-010-0405-8>
- Van Houten, B., 1990. Nucleotide excision repair in *Escherichia coli*. *Microbiol. Rev.* 54, 18–51.
- Van Houten, B., Croteau, D.L., DellaVecchia, M.J., Wang, H., Kisker, C., 2005. “Close-fitting sleeves”: DNA damage recognition by the UvrABC nuclease system. *Mutat Res* 577, 92–117.
- Van Houten, B., Gamper, H., Hearst, J.E., Sancar, A., 1988. Analysis of sequential steps of nucleotide excision repair in *Escherichia coli* using synthetic substrates containing single psoralen adducts. *J. Biol. Chem.* 263, 16553–16560.
- Van Houten, B., Gamper, H., Sancar, A., Hearst, J.E., 1987. DNase I footprint of ABC excinuclease. *J. Biol. Chem.* 262, 13180–13187.
- Veaute, X., Delmas, S., Selva, M., Jeusset, J., Le Cam, E., Matic, I., Fabre, F., Petit, M.A., 2005. UvrD helicase, unlike Rep helicase, dismantles RecA nucleoprotein filaments in *Escherichia coli*. *EMBO J* 24, 180–9. <https://doi.org/10.1038/sj.emboj.7600485>
- Venkateswaran, A., McFarlan, S.C., Ghosal, D., Minton, K.W., Vasilenko, A., Makarova, K., Wackett, L.P., Daly, M.J., 2000. Physiologic Determinants of Radiation Resistance in *Deinococcus radiodurans*. *Appl. Environ. Microbiol.* 66, 2620–2626. <https://doi.org/10.1128/AEM.66.6.2620-2626.2000>
- Verhoeven, E.E., van Kesteren, M., Moolenaar, G.F., Visse, R., Goosen, N., 2000. Catalytic sites for 3' and 5' incision of *Escherichia coli* nucleotide excision repair are both located in UvrC. *J. Biol. Chem.* 275, 5120–5123. <https://doi.org/10.1074/jbc.275.7.5120>
- Verhoeven, E.E., van Kesteren, M., Turner, J.J., van der Marel, G.A., van Boom, J.H., Moolenaar, G.F., Goosen, N., 2002. The C-terminal region of *Escherichia coli* UvrC contributes to the flexibility of the UvrABC nucleotide excision repair system. *Nucleic Acids Res* 30, 2492–500.
- Verhoeven, E.E., Wyman, C., Moolenaar, G.F., Hoeijmakers, J.H., Goosen, N., 2001. Architecture of nucleotide excision repair complexes: DNA is wrapped by UvrB before and after damage recognition. *Embo J* 20, 601–11.
- Visse, R., de Ruijter, M., Ubbink, M., Brandsma, J.A., van de Putte, P., 1993. The first zinc-

binding domain of UvrA is not essential for UvrABC-mediated DNA excision repair. *Mutat Res* 294, 263–74.

- Wagenknecht, H.-A., 2006. The search for single DNA damage among millions of base pairs: DNA glycosylases trapped at work. *Angew. Chem. Int. Ed Engl.* 45, 5583–5585. <https://doi.org/10.1002/anie.200602387>
- Wang, H., Yang, Y., Schofield, M.J., Du, C., Fridman, Y., Lee, S.D., Larson, E.D., Drummond, J.T., Alani, E., Hsieh, P., Erie, D.A., 2003. DNA bending and unbending by MutS govern mismatch recognition and specificity. *Proc. Natl. Acad. Sci. U. S. A.* 100, 14822–14827. <https://doi.org/10.1073/pnas.2433654100>
- Wang, J., Grossman, L., 1993. Mutations in the helix-turn-helix motif of the *Escherichia coli* UvrA protein eliminate its specificity for UV-damaged DNA. *J Biol Chem* 268, 5323–31.
- Wang, J., Mueller, K.L., Grossman, L., 1994. A mutational study of the C-terminal zinc-finger motif of the *Escherichia coli* UvrA protein. *J. Biol. Chem.* 269, 10771–10775.
- Waters, T.R., Eryilmaz, J., Geddes, S., Barrett, T.E., 2006. Damage detection by the UvrABC pathway: crystal structure of UvrB bound to fluorescein-adducted DNA. *FEBS Lett* 580, 6423–7. Epub 2006 Nov 3.
- Weller, G.R., Kysela, B., Roy, R., Tonkin, L.M., Scanlan, E., Della, M., Devine, S.K., Day, J.P., Wilkinson, A., d'Adda di Fagagna, F., Devine, K.M., Bowater, R.P., Jeggo, P.A., Jackson, S.P., Doherty, A.J., 2002. Identification of a DNA nonhomologous end-joining complex in bacteria. *Science* 297, 1686–1689. <https://doi.org/10.1126/science.1074584>
- Welsh, K.M., Lu, A.L., Clark, S., Modrich, P., 1987. Isolation and characterization of the *Escherichia coli* mutH gene product. *J. Biol. Chem.* 262, 15624–15629.
- White, M.A., Azeroglu, B., Lopez-Vernaza, M.A., Hasan, A.M.M., Leach, D.R.F., 2018. RecBCD coordinates repair of two ends at a DNA double-strand break, preventing aberrant chromosome amplification. *Nucleic Acids Res.* 46, 6670–6682. <https://doi.org/10.1093/nar/gky463>
- White, O., Eisen, J.A., Heidelberg, J.F., Hickey, E.K., Peterson, J.D., Dodson, R.J., Haft, D.H., Gwinn, M.L., Nelson, W.C., Richardson, D.L., Moffat, K.S., Qin, H., Jiang, L., Pamphile, W., Crosby, M., Shen, M., Vamathevan, J.J., Lam, P., McDonald, L., Utterback, T., Zalewski, C., Makarova, K.S., Aravind, L., Daly, M.J., Fraser, C.M., et al, 1999. Genome sequence of the radioresistant bacterium *Deinococcus radiodurans* R1. *Science* 286, 1571–7.
- Wirth, N., Gross, J., Roth, H.M., Buechner, C.N., Kisker, C., Tessmer, I., 2016. Conservation and Divergence in Nucleotide Excision Repair Lesion Recognition. *J. Biol. Chem.* 291, 18932–18946. <https://doi.org/10.1074/jbc.M116.739425>
- Xiao, G., Tordova, M., Jagadeesh, J., Drohat, A.C., Stivers, J.T., Gilliland, G.L., 1999. Crystal structure of *Escherichia coli* uracil DNA glycosylase and its complexes with uracil and

glycerol: structure and glycosylase mechanism revisited. *Proteins* 35, 13–24.

- Xu, W., Shen, J., Dunn, C.A., Desai, S., Bessman, M.J., 2001. The Nudix hydrolases of *Deinococcus radiodurans*. *Mol. Microbiol.* 39, 286–290. <https://doi.org/10.1046/j.1365-2958.2001.02267.x>
- Yang, W., 2010. Lessons learned from UvrD helicase: mechanism for directional movement. *Annu Rev Biophys* 39, 367–85. <https://doi.org/10.1146/annurev.biophys.093008.131415>
- Yang, W., 2008. Structure and mechanism for DNA lesion recognition. *Cell Res.* 18, 184–197. <https://doi.org/10.1038/cr.2007.116>
- Yeung, A.T., Mattes, W.B., Oh, E.Y., Grossman, L., 1983. Enzymatic properties of purified *Escherichia coli* uvrABC proteins. *Proc. Natl. Acad. Sci. U. S. A.* 80, 6157–6161. <https://doi.org/10.1073/pnas.80.20.6157>
- Yin, Y., Yang, L., Zheng, G., Gu, C., Yi, C., He, C., Gao, Y.Q., Zhao, X.S., 2014. Dynamics of spontaneous flipping of a mismatched base in DNA duplex. *Proc. Natl. Acad. Sci. U. S. A.* 111, 8043–8048. <https://doi.org/10.1073/pnas.1400667111>
- Ylihonko, K., Tuikkanen, J., Jussila, S., Cong, L., Mantsala, P., 1996. A gene cluster involved in nogalamycin biosynthesis from *Streptomyces nogalater*: sequence analysis and complementation of early-block mutations in the anthracycline pathway. *Mol Gen Genet* 251, 113–20.
- Yokota, H., Chujo, Y.A., Harada, Y., 2013. Single-molecule imaging of the oligomer formation of the nonhexameric *Escherichia coli* UvrD helicase. *Biophys J* 104, 924–33. <https://doi.org/10.1016/j.bpj.2013.01.014>
- Zhang, Q.M., Miyabe, I., Matsumoto, Y., Kino, K., Sugiyama, H., Yonei, S., 2000. Identification of repair enzymes for 5-formyluracil in DNA. Nth, Nei, and MutM proteins of *Escherichia coli*. *J. Biol. Chem.* 275, 35471–35477. <https://doi.org/10.1074/jbc.M006125200>
- Zou, Y., Bassett, H., Walker, R., Bishop, A., Amin, S., Geacintov, N.E., Van Houten, B., 1998a. Hydrophobic forces dominate the thermodynamic characteristics of UvrA-DNA damage interactions. *J Mol Biol* 281, 107–19.
- Zou, Y., Crowley, D.J., Van Houten, B., 1998b. Involvement of molecular chaperonins in nucleotide excision repair. DnaK leads to increased thermal stability of UvrA, catalytic UvrB loading, enhanced repair, and increased UV resistance. *J. Biol. Chem.* 273, 12887–12892. <https://doi.org/10.1074/jbc.273.21.12887>
- Zou, Y., Luo, C., Geacintov, N.E., 2001. Hierarchy of DNA damage recognition in *Escherichia coli* nucleotide excision repair. *Biochemistry* 40, 2923–2931. <https://doi.org/10.1021/bi001504c>
- Zou, Y., Ma, H., Minko, I.G., Shell, S.M., Yang, Z., Qu, Y., Xu, Y., Geacintov, N.E., Lloyd, R.S.,

2004. DNA damage recognition of mutated forms of UvrB proteins in nucleotide excision repair. *Biochemistry* 43, 4196–205. <https://doi.org/10.1021/bi035992a>

- Zou, Y., Van Houten, B., 1999. Strand opening by the UvrA(2)B complex allows dynamic recognition of DNA damage. *EMBO J.* 18, 4889–4901. <https://doi.org/10.1093/emboj/18.17.4889>
- Zou, Y., Walker, R., Bassett, H., Geacintov, N.E., Van Houten, B., 1997. Formation of DNA repair intermediates and incision by the ATP-dependent UvrB-UvrC endonuclease. *J Biol Chem* 272, 4820–7.

La voie de réparation par excision nucléotidique (NER) est responsable de l'élimination de lésions très distinctes structuellement et chimiquement. Ces lésions qui sont généralement volumineuses peuvent provoquer des distorsions de la double hélice de l'ADN. Elles sont introduites dans le génome par des facteurs exogènes comme l'irradiation UV ou divers cancérogènes. La reconnaissance de substrats aussi diversifiés par les protéines Uvr dans les bactéries, est encore en grande partie inconnue. Pour répondre à cette question, nous avons développé un test d'incision *in vitro* utilisant le système NER de la bactérie résistante aux radiations, *Deinococcus radiodurans*, composé de 4 protéines : UvrA1, UvrB, UvrC et UvrD. L'hélicase UvrD n'est pas essentielle pour l'incision. Contrairement aux études antérieures qui utilisaient des protéines Uvr de bactéries thermophiles, la reconstitution de ce système UvrABC repose sur l'utilisation de protéines purifiées à partir d'une même bactérie mésophile. L'activité d'incision a été évaluée soit sur des oligonucléotides d'ADN courts contenant des bases modifiées, soit sur de l'ADN plasmidique traité avec différents agents génotoxiques.

Dans cette étude, nous avons optimisé le test d'incision et déterminé les composants minimaux et leurs concentrations optimales nécessaires pour une réparation efficace des lésions volumineuses. Ce test a permis d'explorer la spécificité de substrat du NER bactérien notamment en déterminant la nature et l'abondance des lésions réparées par les protéines Uvr par HPLC-MS/MS, la cinétique de réparation et la nature du produit libéré résultant du clivage du substrat. Nos données révèlent des différences nettes dans la réparation des différents substrats. Le test d'incision a également été utilisé pour mieux appréhender le rôle des différents domaines de la protéine UvrC dans le processus de réparation, qui reste l'une des étapes les plus énigmatiques du NER. Dans l'ensemble, ces études ont éclairci plusieurs aspects de cette voie de réparation et fournissent à la communauté scientifique un outil puissant pour de futures études.

Mots clés : UvrABC, Réparation par Excision de Nucléotides, lésions de l'ADN, *Deinococcus radiodurans*, agents génotoxiques, HPLC-MS/MS.

The Nucleotide Excision Repair (NER) pathway is responsible for the removal of a wide range of structurally and chemically variable bulky lesions causing minor to important distortions to the DNA helix. These lesions can be introduced by exogenous factors like UV-irradiation or diverse carcinogens. How such a diverse set of lesions are recognized and removed by just a small set of proteins, the Uvr proteins in bacteria, remains largely misunderstood. To address this question, we have developed an *in vitro* incision assay using the NER system from the radiation resistant bacterium, *Deinococcus radiodurans*, composed of 4 proteins: UvrA1, UvrB, UvrC and the DNA helicase UvrD, which is dispensable for the incision activity. In contrast to earlier studies that have made use of Uvr proteins from thermophilic bacteria, the reconstitution of the UvrABC system relied on the use of purified proteins from a single, mesophilic bacterium. The incision activity was evaluated on either short DNA oligonucleotides containing modified bases or on plasmid DNA treated with a number of damaging agents.

In this study, we have optimized the incision assay and determined the minimal components and their optimal concentrations needed for efficient repair of bulky lesions. This assay has enabled us to explore the substrate specificity of bacterial NER notably by determining the nature and abundance of lesions repaired by the Uvr proteins by HPLC-MS/MS, the kinetics of repair and the nature of the released product resulting from the dual cleavage reaction. Our data reveal clear differences in the extent of processing of different substrates. The incision assay was also used to decipher the role of the different domains of UvrC in the repair process, which remains one of the most enigmatic steps of NER. Overall, these studies have shed light on several aspects of this repair pathway and provide the scientific community with a powerful tool for future studies.

Keywords: UvrABC, Nucleotide Excision Repair, DNA lesions, *Deinococcus radiodurans*, damaging agents, HPLC-MS/MS.